

DOCTORAL THESIS

---

**SOFT TISSUE GROWTH & REMODELLING: APPLICATION  
IN LEFT VENTRICLE POST MYOCARDIAL INFARCTION**

---



The  
University  
Of  
Sheffield.

Shaktidhar Dandapani

Supervisor - Dr. Paul Watton

Department of Computer Science

The University of Sheffield

*A thesis submitted in partial fulfilment of the degree of  
Doctor of Philosophy in Computer Science*

June 2, 2020

This page has been intentionally left blank.

## Abstract

Cardiovascular diseases (CVDs) are the leading cause of mortality and morbidity today, myocardial infarction (MI) an effect of Ischaemic Heart Disease (IHD) contributes to the majority of such cases, accounting for upto 31 % of global mortality. Advancements in medical diagnostics, interventions, therapies and prognosis are hindered by the complex dynamics within tissue micro-structure due to observed changes after the onset of a disease. Modelling and simulation of soft tissue growth and remodelling proves to be a significant tool to simulate instances of disease progression and provide results helpful towards the medical field.

A 1D novel constrained mixture model of the left ventricular myocardium is presented using an incompressible, isotropic, elastic, spherical membrane approximation, taking into consideration the micro-structural constituents i.e. ground matrix, cardiomyocytes and collagen fibres. The constituents are assigned strain energy functions, along with mass density terms to account for their quantitative presence in the tissue. Collagen fibre stretches are represented with a distribution function accounting for their existence in different stretches in the tissue. Scenarios are presented where the homoeostatic state of the collagen fibres adapt via evolution of the distribution function, which provide understanding on the configurations and mass changes that could be simulated to understand their implications on the structure and function of the tissue. It was observed that the model simulates plausible changes in the tissue function when collagen fibres are configured in the load bearing configuration rather than in the crimped form.

A soft tissue growth and remodelling framework (STGRF) developed in Python, around the finite element simulation package (ANSYS ® Mechanical APDL) provides us with tools to develop biomechanical problems pertaining to the built-in fibre-reinforced, hyperelastic, incompressible soft tissue material model; employing stress-based differential equations for simulating tissue remodelling and growth. A key feature is the abstraction of the underlying coding using high level Python scripts, to ease the end-user into focussing on their research problem rather than be encumbered by programming ideologies. The STGRF, sees it's applications in two distinct problems in this thesis. **(A)** An idealised LV subjected to myocardial infarction, using stress-based formulations to simulate tissue extra-cellular matrix adaptation to the progression of the disease. A fibroblast field, mediated by the collagen fibre stretches is introduced to regulate growth/ atrophy of the collagen mass density in the myocardium. Two cases are explored to understand the impact of evolving homoeostatic Cauchy stresses for each volume element, versus, a constant homoeostatic Cauchy stress state which the tissue attempts to maintain throughout the time period of the disease. Lower dilatations in the wall structure and lower mass deposition is observed when evolving the homoeostatic stress. **(B)** A finite element model of the medial gastrocnemius muscle subjected to sustained overstretch is considered and remodelling of the muscle and tendinous regions is observed. The novelty lies in the definition of the muscle, tendon

and aponeurosis regions, reflected in the material parameter ascription to said regions. Using stress-based differential equations, remodelling of the muscle and tendinous regions are observed with varying rate constants. The model is purely exploratory in terms of remodelling of the distinct regions in the gastrocnemius muscle and future sophistications could aid in better understanding rehabilitation therapies, surgical techniques involved in muscle extension or purely adaptation to a variety of external mechanical stimuli and environments.

Mathematical and computational modelling enables us replicate models based on specific elements in disease which are difficult to capture experimentally or clinically. This sheds light on the possible mechanisms in play and delineate the processes in order to better understand the changes in tissue structure and function.

# Statement of Originality

I, Shaktidhar Dandapani, declare that this thesis titled, 'Soft Tissue Growth & Remodelling: Application in Left Ventricle post Myocardial Infarction' and the work presented in it are my own. I confirm that:

- This work was done wholly or mainly while in candidature for a research degree at this University.
- Where any part of this thesis has previously been submitted for a degree or any other qualification at this University or any other institution, this has been clearly stated.
- Where I have consulted the published work of others, this is always clearly attributed.
- Where I have quoted from the work of others, the source is always given. With the exception of such quotations, this thesis is entirely my own work.
- I have acknowledged all main sources of help.
- Where the thesis is based on work done by myself jointly with others, I have made clear exactly what was done by others and what I have contributed myself.

Signed: \_\_\_\_\_



Ph.D Student, Department of Computer Science.

Dated: \_\_\_\_\_

02.06.2020

This page has been intentionally left blank.

# Dissemination

## Posters

1. Soft Tissue Growth & Remodelling Framework in Commercial Finite Element Software, INSIGNEO Showcase, Sheffield, UK, (May 2019).
2. Shaktidhar Dandapani, Namrata Gundiah, Xiaoyu Luo, and Paul Watton, "*Applications of an ANSYS© Based Soft Tissue Growth & Remodelling Framework*", VPH2018, Virtual Physiological Human Conference, Zaragoza, Spain, (September, 2018).
3. Shaktidhar Dandapani, Namrata Gundiah, Xiaoyu Luo, and Paul Watton, "*Soft tissue growth and remodelling framework: Application in myocardial infarction*", Multi-scale Hard and Soft Tissue Modelling Workshop, Sheffield, UK, (June 2018).
4. Valentina Pacifico, Shaktidhar Dandapani, Paul Watton, "*Soft Tissue Growth & Remodelling Framework in Commercial Finite Element Software*", INSIGNEO Showcase, Sheffield, (May 2018).
5. Shaktidhar Dandapani, Namrata Gundiah, Xiaoyu Luo, and Paul Watton, "*A CONSTRAINED MIXTURE MODEL OF THE LEFT VENTRICLE AND ITS APPLICATION TO SIMULATING MYOCARDIAL INFARCTION*", Pittsburgh, USA, (April, 2018).
6. Shaktidhar Dandapani, Namrata Gundiah, Xiaoyu Luo, and Paul Watton, "*A CONSTRAINED MIXTURE MODEL OF THE LEFT VENTRICLE AND ITS APPLICATION TO SIMULATING MYOCARDIAL INFARCTION*", St Andrews, Scotland, (March, 2018).
7. Shaktidhar Dandapani, Namrata Gundiah, Xiaoyu Luo, and Paul Watton, "*Soft Tissue Growth & Remodelling Framework in Commercial Finite Element Software*", Joint Mechanobiology/ CMIAD Workshop, Sheffield, UK, (July 2017), **First Prize**.
8. Shaktidhar Dandapani, Namrata Gundiah, Xiaoyu Luo, and Paul Watton, "*A CONSTRAINED MIXTURE MODEL OF THE LEFT VENTRICLE AND ITS APPLICATION TO SIMULATING MYOCARDIAL INFARCTION*", SoftMech, Glasgow, (June, 2017).
9. Shaktidhar Dandapani, Namrata Gundiah, Xiaoyu Luo, and Paul Watton, "*A CONSTRAINED MIXTURE MODEL OF THE LEFT VENTRICLE AND ITS APPLICATION TO SIMULATING*

*MYOCARDIAL INFARCTION*", ECCOMAS Congress, Island of Crete, Greece, (June, 2016).

### **Presentations**

Presentations each year were given based on the progress made during such periods in the following locations:

1. Indian Institute of Science, Bangalore, India, (2016, 2017).
2. INSIGNEO and MultiSim research groups, Sheffield, UK , (2015-2018).
3. Research Group under Professor Xiaoyu Luo, Glasgow, Scotland, UK, (2015 - 2018).
4. Summer School on Biomechanics and Modeling in Mechanobiology, Graz, Austria , (July, 2016) - One minute presentation.

### **Conference Papers**

1. Dandapani, S., Gundiah, N., Luo, X. and Watton, P., 2017, April. "A constrained mixture model of the left ventricle and its application to simulating myocardial infarction." In Proceedings of the 5th International Conference on Computational & Mathematical Biomedical Engineering (pp. 1273-1276). CMBE.

# Contents

<b>1</b>	<b>Introduction</b>	<b>1</b>
1.1	Research Motivation & Contribution . . . . .	2
1.1.1	Contributions to Research . . . . .	4
1.2	Thesis Structure . . . . .	5
<b>2</b>	<b>Background &amp; Literature Review</b>	<b>7</b>
2.1	The Heart . . . . .	8
2.1.1	Anatomy . . . . .	8
2.1.1.1	The Pericardium . . . . .	9
2.1.1.2	Layers of the Myocardial Wall . . . . .	9
2.1.1.3	Chambers of the Heart . . . . .	10
2.1.1.4	Myocardial Tissue Micro-structural Composition and Structure . . . . .	11
2.1.2	Physiology . . . . .	14
2.1.2.1	The Cardiac Cycle . . . . .	14
2.1.3	Left Ventricle . . . . .	17
2.1.3.1	Left Ventricular Biomechanics . . . . .	17
2.1.3.2	Frank Starling Mechanism . . . . .	19
2.1.3.3	Myocardial Extra-Cellular Matrix Biomechanics . . . . .	19
2.1.4	Myocardial Infarction . . . . .	21
2.1.4.1	Biomechanics of the Infarcted Myocardium . . . . .	23
2.1.5	Treatment and Medical Intervention . . . . .	24
2.1.5.1	Pharmacological Intervention . . . . .	24
2.2	Pertinent Concepts in Continuum Mechanics . . . . .	25
2.2.1	Motion of a Continuum Body . . . . .	25
2.2.2	Deformation . . . . .	26
2.2.3	Strain Measures . . . . .	26
2.2.4	Polar Decomposition . . . . .	26
2.2.5	Volume Changes in Continuum body . . . . .	27
2.2.6	Stress Measures . . . . .	28
2.3	Soft Tissue Constitutive Models . . . . .	29

---

2.4	Soft Tissue Growth and Remodelling . . . . .	33
2.4.1	Remodelling of ECM constituents . . . . .	34
2.4.2	Growth Formulations . . . . .	35
2.4.2.1	Finite Growth . . . . .	35
2.4.2.2	Constrained Mixtures . . . . .	37
2.5	State of Art Growth & Remodelling Left Ventricular Biomechanical Models . . . . .	39
2.6	Inferences . . . . .	41
<b>3</b>	<b>Novel Constrained Mixture Model of the Left Ventricle: Growth &amp; Remodelling Application in Myocardial Infarction</b>	<b>43</b>
3.1	Introduction . . . . .	44
3.2	Aims and Objectives . . . . .	46
3.3	Continuum Basis . . . . .	47
3.3.1	Reference Configuration $\Omega_0$ . . . . .	48
3.3.2	Current Configuration $\Omega_t$ . . . . .	48
3.3.3	Attachment Stretch $\lambda_X^{AT}$ . . . . .	49
3.3.4	Recruitment Stretch $\lambda_X^R$ . . . . .	49
3.4	Left Ventricular Constrained Mixture Model . . . . .	51
3.4.1	Strain Energy Density Function . . . . .	51
3.4.1.1	Governing Equation . . . . .	52
3.4.2	Elastin and other ground substances . . . . .	54
3.4.3	Cardiac Myocytes . . . . .	55
3.4.4	Collagen . . . . .	56
3.4.4.1	Collagen Undulation Distribution . . . . .	57
3.4.5	Material Parameter Estimation . . . . .	60
3.4.6	Growth & Remodelling of the Myocardial Wall . . . . .	61
3.4.6.1	Remodelling of the Recruitment Stretch Distribution . . . . .	62
3.4.6.2	Growth in the ECCM mass density . . . . .	63
3.4.6.3	Attachment Stretch Distribution Specification . . . . .	64
3.4.6.4	Parameter Values . . . . .	66
3.4.6.5	Evolution of the Attachment Stretch Distribution . . . . .	67
3.4.6.6	Remodelled Volumetric Thickness . . . . .	69
3.5	Results . . . . .	70
3.5.1	Model performance with Experimental Data . . . . .	76
3.5.1.1	CMM Results for (Fishbein et al. (1978)) . . . . .	78
3.6	Discussions . . . . .	84
3.6.1	Comparison with (Fishbein et al. (1978)) . . . . .	86
3.6.2	Terminal Points . . . . .	87
3.7	Conclusions . . . . .	88

---

<b>4</b>	<b>Novel Soft Tissue Growth &amp; Remodelling Finite Element Framework</b>	<b>89</b>
4.1	Introduction . . . . .	90
4.2	Motivation for Framework Development . . . . .	91
4.3	Framework Overview . . . . .	93
4.3.1	Framework Development . . . . .	93
4.3.2	Design . . . . .	95
4.3.3	Soft Tissue Growth & Remodelling Framework Code Library . . . . .	97
4.3.3.1	Execution Files . . . . .	98
4.3.3.2	Preprocessing . . . . .	98
4.3.3.3	Postprocessing . . . . .	99
4.3.3.4	GenericOperations . . . . .	99
4.3.4	Customised Visualisation Toolkit . . . . .	101
4.3.5	Custom Workflow Creation . . . . .	103
4.3.6	Parallels to Template Method Design Pattern . . . . .	105
4.3.7	Workflow Execution . . . . .	106
4.3.8	Documentation of Code Library . . . . .	109
4.4	Discussions . . . . .	112
4.4.1	Capabilities . . . . .	112
4.4.2	Applications . . . . .	113
4.4.3	Framework Updates . . . . .	114
4.4.3.1	GUI Implementation . . . . .	114
4.4.4	Limitations of the Framework . . . . .	115
4.5	Conclusions . . . . .	117
<b>5</b>	<b>Verification of Soft Tissue Growth &amp; Remodelling Framework</b>	<b>119</b>
5.0.1	Anisotropic Exponential Hyperelastic Material Model . . . . .	119
5.0.1.1	Penalty Function . . . . .	120
5.0.2	Verification of Material Model . . . . .	120
5.1	Growth & Remodelling on Cube . . . . .	125
5.1.1	Growth Hypotheses . . . . .	125
5.1.2	Remodelling Hypotheses . . . . .	126
5.1.3	Reference Configuration . . . . .	128
5.1.4	Test Cases for Hypotheses . . . . .	129
5.1.4.1	Sustained Over-Stretch of Cubic Element . . . . .	129
5.2	Conclusions . . . . .	134
<b>6</b>	<b>Applications of STGRF I: Stress Based Growth &amp; Remodelling of the Left Ventricle Post Myocardial Infarction</b>	<b>135</b>
6.1	Aims and Objectives . . . . .	136

6.2	Novel Finite Element Analysis for the Growth & Remodelling of a Fibre-reinforced Passive Myocardial Tissue Post MI . . . . .	137
6.3	Methodology . . . . .	137
6.3.1	Fibre reinforced Material Model for Myocardial Tissue . . . . .	137
6.3.1.1	Difference between 1D and FE material model . . . . .	138
6.3.2	Model Configuration Assumptions . . . . .	139
6.3.3	Mesh Generation . . . . .	139
6.3.4	Boundary Conditions . . . . .	142
6.3.5	Collagen Fibre Directions . . . . .	143
6.3.6	Growth & Remodelling . . . . .	145
6.3.6.1	Collagen Remodelling Hypotheses . . . . .	145
6.3.6.2	Collagen Growth Hypotheses . . . . .	146
6.3.6.3	Infarct Zone Elements . . . . .	147
6.3.6.4	Material Parameter Values . . . . .	148
6.3.6.5	Model Parameter Values . . . . .	150
6.3.6.6	Result Cases . . . . .	151
6.4	Results . . . . .	152
6.4.1	Case 1: Growth & Remodelling with out evolution of homoeostatic collagen fibre Cauchy stress . . . . .	152
6.4.1.1	Collagen Fibre Cauchy Stresses . . . . .	154
6.4.1.2	Material Parameter Remodelling . . . . .	157
6.4.1.3	Collagen Fibres Stretch Invariants . . . . .	159
6.4.1.4	Fibroblast Stretches . . . . .	161
6.4.1.5	Collagen Fibre Matrix Mass Density Changes . . . . .	163
6.4.2	Case 2: Growth & Remodelling with evolution of homoeostatic collagen fibre Cauchy stress . . . . .	165
6.4.2.1	Collagen Fibre Cauchy Stresses . . . . .	166
6.4.2.2	Material Parameter Remodelling . . . . .	169
6.4.2.3	Collagen Fibres Stretch Invariants . . . . .	171
6.4.2.4	Fibroblast Stretches . . . . .	173
6.4.2.5	Collagen Fibre Matrix Mass Density Changes . . . . .	175
6.5	Discussion . . . . .	177
6.5.1	Comparison with relevant studies . . . . .	180
6.5.2	Model Limitations in the representation of the LV Tissue . . . . .	182
6.6	Conclusions . . . . .	183
<b>7</b>	<b>Applications of STGRF II: Gastrocnemius Skeletal Muscle Remodelling in Response to Sustained Stretch</b> . . . . .	<b>185</b>
7.1	Introduction . . . . .	186
7.1.1	Gastrocnemius Muscle . . . . .	187

---

7.1.2	Motivation	189
7.1.3	WorkContribution	189
7.2	Methods	190
7.2.1	Mesh Generation	190
7.2.2	Regional Volume Fraction Definition	192
7.2.2.1	Workflow Description	192
7.3	Volume Fractions Assignment Algorithm	194
7.3.1	Strain Energy Function	197
7.3.2	Fibre Orientation	197
7.3.3	Remodelling Assumption	197
7.3.4	Boundary Conditions	199
7.3.4.1	Single-Step Displacement Function	199
7.4	Parameter Set up	201
7.4.1	Rationale for Parameter Values	202
7.5	Results	203
7.6	Test Case	204
7.6.1	Cross-sectional Views of Gastrocnemius Muscle	204
7.6.1.1	Fibre Stretch Invariants values	205
7.6.1.2	$k_2^M$ values	207
7.6.1.3	$k_2^T$ values	209
7.6.1.4	$\sigma_M^{diff}$ values	211
7.6.1.5	$\sigma_T^{diff}$ values	213
7.6.2	Four Distinct Cases	215
7.6.2.1	Averaged $I_4$	215
7.6.2.2	Averaged $\sigma_M^{diff}$	216
7.6.2.3	Averaged $\sigma_T^{diff}$	217
7.6.2.4	Averaged $k_2^M$	218
7.6.2.5	Averaged $k_2^T$	219
7.7	Discussions	220
7.7.1	Relevance in Muscle Remodelling	221
7.7.2	Limitations	223
7.8	Conclusions	223
<b>8</b>	<b>Discussions &amp; Conclusions</b>	<b>225</b>
8.1	Summaries of the Study	225
8.2	Limitations of the Study	228
8.3	Future Considerations	230
8.4	Concluding Remarks	233
	<b>Appendix A</b>	<b>249</b>

---

A.1 Execution Files . . . . .	249
A.2 Preprocessing Code . . . . .	251
A.3 Postprocessing Files . . . . .	278
A.4 Custom Workflow Creation . . . . .	285
<b>Appendix B</b>	<b>311</b>
B.1 STL file . . . . .	311
B.2 Code For Volume Fraction Assignment Algorithm . . . . .	312
B.3 Tecplot Macro . . . . .	328
<b>Appendix C</b>	<b>331</b>
C.1 Modification of Material Model . . . . .	331

# List of Figures

2.1	<i>The heart's location within the human body, behind the mediastinum. (Betts et al. (2018))</i>	8
2.2	<i>The structure of the heart wall, details of the multi-layered tissue are shown (Betts et al. (2018))</i>	9
2.3	<i>Chambers of the heart. (Betts et al. (2018)).</i>	10
2.4	<i>The configuration of collagen fibres within a cardiomyocyte fibre (Weber et al. (1987)).</i>	12
2.5	<i>The electrical propagation fibre system architecture in the heart (Betts et al. (2018)).</i>	15
2.6	<i>The cardiac cycle showing various configurations of the heart during each phase (Betts et al. (2018)).</i>	16
2.7	<i>Pressure Volume Loop, adapted from Guyton &amp; Hall (2006)</i>	18
2.8	<i>The effect of a myocardial infarction on a region of myocardium. Dilatation and thinning due to cardiomyocyte necrosis and pathological adaptation by collagen fibrosis is observed (Awada et al. (2016)).</i>	21
2.9	<i>The various phases involved after the onset of a myocardial infarction in the myocardial tissue. It can roughly be divided into an early phase and late remodelling phase where the inflammation constitutes the early phases and wound healing, fibrosis reflects the late phase of remodelling (Fraccarollo et al. (2012), Sutton &amp; Sharpe (2000)). There could be proliferation could overlap between the early and late phases as well, thus they are shown as a distinct section.</i>	22
2.10	<i>The image displays the material particle <math>\mathbf{X}</math> in the unloaded reference configuration (<math>\Omega_0</math>) and its position after deformation in the current reference configuration (<math>\Omega_t</math>), denoted by <math>\mathbf{x}</math>. The deformation is a result of mechanical stimuli acting either externally or internally in the continuum body.</i>	25
2.11	<i>Finite growth schematic is displayed showing the multiplicative decomposition <math>\mathbf{F} = \mathbf{F}^e \cdot \mathbf{F}^g</math>. The reference configuration (<math>\Omega_0</math>) deforms based on <math>\mathbf{F}(s)</math> into the current or loaded configuration (<math>\Omega_t</math>), <math>s</math> denoting the current time. The growth part (<math>\mathbf{F}^g</math>) leads to an incompatible configuration whose physical significance leads to pieces of a physical body which might be incompatible and consists of overlapping elements and holes. This is transformed into the final deformed configuration <math>\Omega_t</math> by the elastic load dependant transformation (<math>\mathbf{F}^e</math>).</i>	35

---

3.1	<i>Pressure Volume Loop with a depiction of the configurations assumed for the constrained mixture model, adapted from Guyton &amp; Hall (2006)</i> . . . . .	47
3.2	<i>The relation between the attachment stretch and the recruitment stretches in the constituents of the myocardial tissue, shown as a function of lengths for motivating the idea behind the tissue stretch derivations.</i> . . . . .	50
3.3	<i>Configurations of the constrained mixture model: <math>\Omega_0</math> represents the stress free unloaded myocardial tissue and its current loaded configuration at end-diastole is denoted by <math>\Omega_t</math>. The tissue stretch <math>\lambda</math> in <math>\Omega_t</math> is calculated with respect to <math>\Omega</math>, however, the reference configurations for the cardiac myocytes and collagen fibres are defined relative to a recruitment stretch at which they partake in the stress response to applied internal blood pressure. These reference configurations are titled recruitment configuration for the cardiac myocytes and collagen fibres respectively as <math>\Omega_R^M</math> and <math>\Omega_R^C</math>, (Dandapani et al. (2017)).</i> . . . . .	51
3.4	<i>The length-tension graph of a sarcomere is shown, adapted from (Boron &amp; Boulpaep (2016)). The formulations shown in Equations [3.17, 3.16], aim to capture these behaviours. The active response is associated with activated acto-myosin cross-bridges by intra-cellular <math>Ca^{2+}</math> ions and the passive response with the resting tension, where the sarcomeres are not activated.</i> . . . . .	55
3.5	<i>The arrangement of collagen fibres in the myocardium, depicting the endomysial collagen struts and perimysial collagen fibres running parallel amongst the cardiac myocytes (source: (Fomovsky et al. (2010))).</i> . . . . .	56
3.6	<i>The attachment (<b>left</b>) and recruitment(<b>right</b>) stretch distributions for the myocardial and epicardial collagen fibres. The myocardial collagen attachment stretch distribution ranges from a minimum of 0.95 to a maximum of 1.05 and the recruitment stretch ranges from 1.1 to 1.095 to 1.21. Given that the tissue stretch at <math>t=0</math> is prescribed to be 1.15 the collagen fibres in the myocardial tissue, with stretches below 1.15 bear load. However, the attachment stretch distribution for the epicardial collagen fibres ranges from 0.9 minimum to 1.0 maximum and the recruitment stretch distribution ranges from 1.15 minimum to 1.27 maximum, and therefore, none of the epicardial collagen fibres bear load at time <math>t=0</math>. This reflects the epicardial collagen fibres acting as a protective sheathe, while the myocardial collagen fibres partake in the force-balance of the LV wall due to the internal diastolic blood pressure.</i> . . . . .	65
3.7	<i>Evolution of epicardial attachment stretch distributions for cases 2 to 5. Case 1 involves no change in the attachment stretch distribution and therefore is not represented in the figure.</i> . . . . .	68
3.8	<i>The cardiomyocytes mass density is degraded to <math>m_{min}^M = 0.01</math> over a period of 4 days to initiate the onset of myocardial infarctions in the constrained mixture model. This is true for all cases considered.</i> . . . . .	71

---

3.9	<i>The myocardial collagen fibres present within the myocardium are prescribed to degrade over a period of 14 days, depicting the inflammation phase of the extra-cellular matrix. True for all cases considered. . . . .</i>	72
3.10	<i>The circumferential stretch of the left ventricular myocardium, also referred to as the ground matrix stretch in the model. The rates of mass density changes are kept the same for each case. In case 1 the tissue stretch increases exponentially, whereas cases 2 to 4 <math>\lambda</math> continues to increase slightly by the end of the simulation, the slowest growth observed in case 4. Case 5 observes stabilisation by the end of the simulation. . . . .</i>	72
3.11	<i>The mass density changes in the epicardial collagen is shown, Case 1 observes an exponential rise in mass density reaching values beyond 100 after day 15. Cases 2, 3 and 4 observe a terminal mass density of <math>\approx 76</math>, <math>\approx 26</math> and <math>\approx 16</math> respectively rising at decreasing rates from Case 2 to Case 4 at <math>t=100</math> days. In case 5 the epicardial collagen mass density reaches <math>\approx 8</math> with a stabilising trend from day 60 to the end of the simulation. . . . .</i>	73
3.12	<i>The maximum epicardial collagen fibre stretch for the various cases. The values all tend towards the attachment stretch by the end of the 100th day. For Case 1, since the attachment stretch distribution is constant the maximum stretch tends towards the original value of 1.05 but fails to reach homoeostatic levels. The other cases the maximum collagen stretch reaches the evolved attachment stretch distribution by the end of day 100. . . . .</i>	74
3.13	<i>The remodelled LV wall thickness shown, takes into account the volumetric growth of the micro-structural constituents, denoted by (<math>h_{rem}</math>). Starting from a value of 7.78 mm the remodelled wall thickness attaining a final value of 13342.5 mm, 4.96 mm, 2.86 mm and 2.0 mm for Cases 1, 2, 3, and 4 respectively. In Case 5, where the tissue stabilises without enlarging further the remodelled thickness at day 100 is about 1.75 mm. . . . .</i>	75
3.14	<i>The remodelled thickness (<math>h_{rem}</math>) to remodelled radius is shown. An initial value of <math>\approx 0.22</math> at <math>t=0</math> is observed, reducing to around <math>\approx 0.35</math> at <math>t=5</math> days after which each case sees a variation in behaviour. Case 1 rises exponentially beyond 0.30 at <math>t=30</math> days. cases 2, 3, 4 observe slightly increasing values till <math>t=100</math> days at <math>\approx 0.057</math>, <math>\approx 0.04</math>, and <math>\approx 0.033</math> respectively. Case 5 stabilises at a value of <math>\approx 0.031</math> at <math>t=100</math> days. . . . .</i>	75
3.15	<i>Changing myocardial thickness, based on the observed evolution of myocardial infarction in rat hearts (six out of seven rats, (Fishbein et al. (1978)) measure at the thinnest point of the infarction. This image has been created using the data provided in aforementioned paper. . . . .</i>	76
3.16	<i>The myocardial collagen fibre mass density is degraded to 1 % of original value (1) from day 1 to day 4, representation for all cases are the same. . . . .</i>	78
3.17	<i>The cardiac myocyte mass density (<math>m^M</math>), is degraded from 1.0 to 0.10 through 4 days for each case. . . . .</i>	78

---

3.18	<i>The remodelled volumetric thickness (<math>h_{rem}</math>), decreases from 1.4 mm over time to a value of <math>\approx 0.36</math> at Day 4 due to the degradation regime of cardiac myocytes, but decreases only till about 0.415 for Case 1. While Case 1 exponentially rises, Cases 2 to 5 stabilise around <math>\approx 0.4</math>.</i>	79
3.19	<i>The remodelled thickness due to the degradation of cardiac myocytes to 10 % of original mass density till day 4 is observed. Initial value of 1.4mm and final values of around 0.4 for cases 2 to 5 are observed. Case 1, as noted in the CMM model analysis results proves to provide inconsistent results. The trajectory does not follow that of (Fishbein et al. (1978)) and the reasons are discussed in Section[3.6].</i>	79
3.20	<i>The circumferential tissue stretch (<math>\lambda</math>) is depicted in this Figure. All cases follow a common trend up until Day 1. Case 1 sees a continuous increase up until day 21 at a value of <math>\approx 2.23</math>. Cases 2 to 5 appear to have a reduction in stretch around day 4. Post day 4, Case 2 increases slightly till day 21 possessing a value around <math>\approx 1.51</math>. Cases 3,4 and 5 reach values around 1.415, 1.375 and 1.35 respectively at day 21.</i>	81
3.21	<i>The changes in the epicardial mass density in the infarcted tissue are shown in this Figure. Case 1 increases exponentially. Cases 2 to 5 observe an interesting trend, with an initial increase till day 1 followed by a decrease, and rising again after day 3. Case 2 shows an increasing trend and continues to increase at day 21 at a value of <math>\approx 4.35</math>. Cases 3, 4 and 5 show plateauing after day 15 with terminal values at day 21 being <math>\approx 3.2</math>, <math>\approx 2.2</math> and <math>\approx 1.96</math> respectively.</i>	81
3.22	<i>The maximum collagen fibre stretch variations are seen in Figure[3.22]. a rise in the values continues till day 3 for Case 1 and day 4 for the remaining cases. Thereafter, Case 1 remodels towards the original maximum attachment stretch attaining a value of 1.037 at day 21. The remaining cases 2, 3, 4 and 5 attain values close evolved maximum attachment stretch, at <math>\approx 1.105</math>, 1.1032, 1.1015 and 1.10 at day 21, with only cases 4 and 5 attaining stabilising behaviour with no upward or downward trend.</i>	83
4.1	<i>The diagram indicates the various components involved to enable finite element analysis of desired soft tissue models. This helped motivate the generation of a code library (shown as STGRF), which facilitates the interaction between these components and creation of independent workflow scripts.</i>	95
4.2	<i>Package diagram of the soft tissue growth &amp; remodelling framework, portraying the various packages involved which can be utilised to set up workflows or scripts for finite element simulations in ANSYS® MAPDL.</i>	97
4.3	<i>Figure depicting nodal numbering in ANSYS Mechanical APDL and VTK file formats (ANSYS (2013), File Formatsfor VTK Version 4.2 (2002)), for a hexahedral element.</i>	102
4.4	<i>Figure depicting nodal numbering in ANSYS Mechanical APDL and VTK file formats (ANSYS (2013), File Formatsfor VTK Version 4.2 (2002)), for a tetrahedral element.</i>	102

---

4.5	<i>Execution of the custom workflow routine. Perl manages the execution of ANSYS® Mechanical APDL and Python scripts for structural analysis and for post processing, respectively. An initial setup of APDL scripts is setup via the Python framework execution file. The Parameters File is used to setup rate constants, time periods, number of steps and other relevant parameters ,pertinent to each biomechanical problem. . . . .</i>	103
4.6	<i>Folder view of the STGRF code library, detailing the organisation of various python modules and packages. . . . .</i>	107
4.7	<i>The sequence diagram detailing the execution of the framework to create output files to be read in by ANSYS® Mechanical APDL Solver for structural analysis. . . . .</i>	108
4.8	<i>The README file listing the requisite soft ware to be installed, setting up the programming environment and installation of the framework. Also, contains an example of growth and remodelling on a unit cube to help motivate the user to set up their own models from pre-processing to post processing as well as establishing their own custom work flows. . . . .</i>	110
4.9	<i>A standardised documentation of the Python code library, containing information about the modules, packages, classes, objects and functions according to PEP-8 standard. (<a href="https://www.python.org/dev/peps/pep-0008/">https://www.python.org/dev/peps/pep-0008/</a>) . . . . .</i>	111
4.10	<i>Simple Schematic . . . . .</i>	115
5.1	<i>The stress responses for the isotropic (green) and anisotropic (blue) components are shown in this figure. In soft tissues, the collagen fibre response is modelled as with a strain stiffening effect (blue line) and a Neo-Hookean response for the isotropic component (green line), usually associated with ground matrix tissue. . . . .</i>	121
5.2	<i>Single unit cube element using a SOLID185 8-Node brick element type in ANSYS MAPDL. . . . .</i>	121
5.3	<i>The Degree of Freedom Solution for deformation of a cube under uniaxial stretch with <math>\lambda = 2.0</math>. . . . .</i>	122
5.4	<i>Verification of the anisotropic exponential hyperelastic material model in ANSYS®, analytical solution written in python and the red dots indicate the values obtained for subsequent displacement based solutions with each stretch value being the boundary condition for uniaxial stretching in the x-direction. . . . .</i>	123
5.5	<i>Verification of the anisotropic exponential hyperelastic material model in ANSYS®, under the effect of multiple <math>d</math> parameters attributed to the volumetric potential(Gong &amp; Riyad (2002)) . . . . .</i>	123
5.6	<i>Remodelling of the material parameter <math>c_2</math> or <math>e_2</math> represented by <math>k_2</math> shows the right ward shift in the stress-strain profile of the anisotropic contribution in the strain energy density function(Equation [5.4 for decreasing values of <math>k_2</math> as per Equations [5.10, 5.11]. Blue line indicates the initial profile with <math>k_2 = 10</math> and the right-most cyan line displays the final remodelled profile. . . . .</i>	127

---

5.7	<i>The initial reference configuration, remains unchanged the subsequent steps in the growth and remodelling workflow. This is because the reference configuration <math>\Omega_0</math> is not updated after each step and modifications are done via external scripts which affect the input material parameters for the mesh in consideration. This is reflected in the figure, where the loaded configurations <math>\Omega_t</math> for various steps from 0 to n are portrayed on the right having the same reference configuration <math>\Omega_0</math>.</i>	128
5.8	<i>The stretch invariants are shown for the fibres in directions <math>I_4</math> and <math>I_6</math>. The blue line and green lines overlap as both the fibres are subjected to same levels of stretch.</i>	131
5.9	<i>The material parameters <math>k_2, k_4</math>, associated with <math>I_4, I_6</math> fibre directions respectively are depicted. The <math>k_2</math> values remodel quicker due to having a higher rate constant <math>\alpha = 0.002</math> reaching stabilisation at <math>t=70</math> days at 0.1 % of atriaits original value, as compared to <math>k_4</math> which remodels at a slower rate. The analytical and numerical solutions are consistent.</i>	132
5.10	<i>The Cauchy stresses experienced by the <math>I_4, I_6</math> fibre families are shown. It can be seen that both the fibre families remodel with a similar trend, however a quicker remodelling is observed in terms of the fibres in the <math>I_4</math> direction, due to a higher rate constant <math>\alpha &gt; \beta</math>. The analytical and numerical solutions are consistent</i>	132
5.11	<i>Snapshots of the cube experiencing sustained stretch, the Cauchy stresses <math>\sigma_{\text{aniso}, I_4}</math> and <math>\sigma_{\text{aniso}, I_6}</math> are shown.</i>	133
5.12	<i>Snapshots of the cube experiencing sustained stretch, the remodelled material parameters <math>k_2</math> and <math>k_4</math> are shown.</i>	133
6.1	<i>The dimensions of the idealised left ventricle as considered in our model, adapted from (Hassaballah et al. (2013)).</i>	139
6.2	<i>The element type used to create the LV mesh, identified as SOLID185 (ANSYS (2013)), is an 8-Node hexahedral brick element.</i>	140
6.3	<i>(Left) The lines generated in ANSYS © Mechanical, approximated dimensions of the LV from (Hassaballah et al. (2013)), <b>Right</b> Surfaces generated by using the lines as a guiding construct, prepared for meshing.</i>	140
6.4	<i>The hexahedral mesh geenerated for the LV mesh, with an element edge size of 5 mm.</i>	141
6.5	<i>The left ventricle is held in place with a fixed support at the base of the ventricle, and an internal pressure of 1.3 kPa i.e. (<math>\approx 10</math> mm Hg) is defined. These conditions are employed to simulate the passive deformation of the LV wall during its passive filling phase due to the blood entering into it via the mitral valve from the left atrium.</i>	142
6.6	<i>The three myofibre axis directions as defined by (Nash &amp; Hunter (2000)), which are the fibre axis (<math>f</math>), sheet axis (<math>s</math>) and sheet-normal axis(<math>n</math>)</i>	143
6.7	<i>The fibre orientations in our model defined w.r.t the fibre and sheet-normal axis directions for the two collagen families in the <math>I_4</math>&amp;<math>I_6</math> directions respectively. We define the <math>I_4</math> family of collagen fibres as circumferential and the <math>I_6</math> fibres as longitudinal fibres.</i>	144

---

6.8	<i>The infarct zone is prescribed, by selecting a spherical region with a centre (<math>i_c</math>) and providing a radius. We define a radius of 20 mm i.e. a 2cm infarct and selected hexahedral elements are subjected to degradation of the ground matrix. . . . .</i>	147
6.9	<i>Nodal displacements for days 0 and 55 post-MI, for case considered with constant homoeostatic Cauchy stress for the collagen fibre families. . . . .</i>	152
6.10	<i>Degradation of the ground matrix over a period of 14 days, reflecting tissue necrosis due to ischaemia, marking the onset of a myocardial infarction. . . . .</i>	153
6.11	<i>The averaged circumferential (<math>I_4</math>) collagen fibre Cauchy Stress is shown. An initial increase from <math>2.6 \times 10^{-3}</math> MPa at <math>t=0</math> day, to a maximum of <math>4.36 \times 10^{-3}</math> MPa at <math>t=10</math> days and stabilising at a value of <math>3.67 \times 10^{-3}</math> MPa from <math>t=45</math> days to the end of the simulation. . . . .</i>	154
6.12	<i>The averaged longitudinal collagen fibre Cauchy stress is shown. An initial increase from <math>0.576 \times 10^{-4}</math> MPa at <math>t=0</math> day is observed upto <math>1.5 \times 10^{-3}</math> MPa at <math>t=6</math> days, diving in value at <math>t=13</math> days to <math>1.48 \times 10^{-3}</math> MPa and oscillating upwards again at <math>t=32</math> days to <math>4.6 \times 10^{-3}</math> MPa reaching a terminal value of <math>4.53 \times 10^{-3}</math> MPa at <math>t=55</math> days indicating further decline after day 55. . . . .</i>	155
6.13	<i>The Cauchy stresses experienced by the collagen fibre families are depicted. (Top), Circumferential fibre Cauchy stresses are shown, at <math>t=0</math> day it ranges from <math>\approx 0.0015</math> MPa to <math>\approx 0.05</math> MPa, varying to <math>\approx 0.03</math> MPa to <math>0.07</math> MPa in the infarcted to at <math>t=13</math> days, and subsequently to <math>\approx 0.01</math> MPa to <math>\approx 0.13</math> MPa at <math>t=27</math> days. Terminally at <math>t=55</math> days, the remodelled infarcted zone observes a Cauchy stress distribution in the range of <math>\approx 0.005</math> MPa to <math>0.05</math> MPa with a few elements in the higher range of <math>\approx 0.07</math> to <math>\approx 0.11</math> MPa. (Bottom) The longitudinal collagen fibres Cauchy stress is shown, observing an initial distribution at <math>\approx 0.0005</math> MPa to <math>\approx 0.001</math> MPa at <math>t=0</math> days. The stress range varies slightly between <math>\approx 0.01</math> MPa to <math>0.02</math> MPa at <math>t=13</math> days. An increase upto a range of <math>\approx 0.05</math> MPa to <math>1.1</math> MPa is seen around <math>t=27</math> and <math>t=55</math> days, as seen a few elements at the bottom of the infarct experience higher stresses than other regions. . . . .</i>	156
6.14	<i>The remodelling of averaged material parameters <math>k_2, k_4</math> occurs to maintain a preferred homoeostatic collagen fibre Cauchy stress (here, at <math>t=0</math>). (Blue line) Averaged values of <math>k_2</math>, associated with the collagen family of fibres oriented in the <math>I_4</math> direction, over the infarct region show a steady decline from <math>3.45</math> at <math>t=0</math> to about <math>0.42</math> at <math>t=55</math> days, seeing a slight rise from <math>0.36</math> to <math>0.42</math> at <math>t=37</math> days. (Purple line) Averaged values of <math>k_4</math>, associated with the collagen family of fibres oriented in the <math>I_6</math> direction, over the infarct region show a steady decline from <math>3.45</math> at <math>t=0</math> to about <math>1.89</math> at day 55, observing a slow increase beyond day 55. . . . .</i>	157

- 6.15 *Material Parameter changes due to remodelling are shown in this figure. (Top) Circumferential collagen fibre material parameter  $k_2$  is shown, with an initial distribution of 3.45 as prescribed at  $t=0$ . Post 13 days, the value ranges from  $\approx 0.035$  in the outer boundary to  $\approx 3$  going inwards. The range is more or less similar at  $t=27$  days and  $t=55$  days, with majority elements in the range of 0.035 i.e. the lower limit for  $k_2$  for  $k_2 > 0$  with a few elements in the range of  $\approx 3$  to 5 and 10 at  $t=27$  and  $t=55$  days respectively. The increase can be associated to compression which leads to a reduction in the Cauchy stress experienced, thereby reversing the effect of remodelling formulation seen in Equation[6.6]. **Bottom** The longitudinal collagen fibre material parameter  $k_4$  are shown, with an initial prescribed value of 3.45 at  $t=0$  days. The ranges vary from 0.035 to  $\approx 7$  at  $t=13$  days, consequently the maximum reducing to  $\approx 3.7$  at  $t=27$  days and rising again to a maximum value of  $\approx 6.8$  at  $t=55$  days, which again can be attributed to the reversal of behaviour in the remodelling formulation, Equation [6.7] due to reduced Cauchy stress experienced by the volume element at  $t=55$  days. . . . . 158*
- 6.16 *The averaged circumferential ( $I_4$ ) and longitudinal ( $I_6$ ) collagen fibre stretch invariants are displayed over a the simulation period of 56 days. (Black line) The value for  $I_4$  rises from  $\approx 1.012$  at  $t=0$  day to a maximum of 1.228 at  $t=16$  days, before stabilising at 1.184 at  $t=55$  days. (Red line) The  $I_6$  value rises from  $\approx 1.005$  at  $t=0$  day, to  $\approx$  value of 1.136 at  $t=15$  days before stabilising at a value of 1.12 by  $t=55$  days. . . . . 159*
- 6.17 *The stretch invariants experienced by the collagen family of fibres is shown in this figure. (Top) The circumferential collagen fibre stretch invariants  $I_4$  are displayed. At  $t=0$  the  $I_4$  values range from  $\approx 1$  to  $\approx 1.105$ , increasing to 1.1 to  $\approx 1.4$  in the infarcted region at  $t=13$  days. The values at  $t= 27$  days attain a range of  $\approx 1.16$  to  $\approx 1.38$  in the infarcted region and terminally at  $t=55$  days, it varies from  $\approx 1.16$  to  $\approx 1.3$ . (Top) The longitudinal collagen fibre stretch invariants  $I_6$  are displayed. At  $t=0$  day the  $I_6$  values range from 0.97 to  $\approx 1.05$ , post-MI at  $t=13$  days the  $I_6$  values in the infarct range from  $\approx 1.12$  to  $\approx 1.6$  (seen in only one volume element at the bottom). At  $t= 27$  days and  $t= 55$  days the range remains similar however, there is a slight increase in the  $I_6$  values through the infarcted region from  $\approx 1.12$  at  $t= 13$  days to  $\approx 1.26$  at  $t=55$  days. . . . . 160*
- 6.18 *The averaged fibroblast stretch experienced due to the stretch invariant variations of the circumferential ( $I_4$ ) and longitudinal ( $I_6$ ) collagen fibres are shown. For circumferential fibres ( $I_4$ ), fibroblast stretch ( $\lambda_{F,I_4}$ ) increases from a value of 1.05 at  $t=0$  day to a maximum of 1.124 at  $t=15$  days, before coming back to a value of 1.05 steadily at  $t=55$  days. A similar behaviour is observed for  $\lambda_{F,I_6}$ , where in an increase from 1.05 at  $t=0$  day to a maximum of 1.09 at  $t=15$  days is reached before coming back to a value of 1.05. . . . . 161*

---

6.19	<p>The fibroblast stretches experienced with respect to the two collagen family of fibres are shown. <b>(Top)</b> The fibroblasts associated with the maintenance of circumferential collagen fibres are displayed. At <math>t=0</math> the prescribed value of 1.05 is seen throughout the myocardium, increasing to a range of <math>\approx 1.0581</math> to 1.1 in the infarcted zone. At <math>t=27</math> days the range is similar to <math>t=13</math> days however, in the inner regions of the infarct the stretches reduce to a range of <math>\approx 1.052</math> to <math>\approx 1.058</math>. Terminally at <math>t=55</math> days the fibroblast stretches reduce to a range of <math>\approx 1.051</math> to <math>\approx 1.052</math>. <b>(Bottom)</b> The fibroblast stretches with respect to the longitudinal collagen fibre family are shown. An initial prescribed value of 1.05 is seen at <math>t=0</math> day. At <math>t=13</math> days the fibroblast stretches are in the higher range of 1.1 near the bottom centre of the infarcted region and the centre, also a reduction upto <math>\approx 1.0</math> is seen. At <math>t=27</math> days, the range varies from <math>\approx 1.04</math> to <math>\approx 1.1</math>, with higher stretches seen at the upper region. Terminally, the fibroblast stretches reach reduced range of <math>\approx 1.048</math> to <math>\approx 1.053</math>. . . . .</p>	162
6.20	<p>The averaged mass densities of circumferential and longitudinal collagen fibres are shown. <b>(Orange Line)</b> The circumferential fibre mass densities (<math>m^{C,I_4}</math>) increase from a value of 1 at <math>t=0</math> day steadily to a value of <math>\approx 4.5</math> at <math>t=55</math>, seeing a continued rise thereafter. For longitudinal fibre mass density (<math>m^{C,I_6}</math>), a lower rise is observed in comparison, from 1 at <math>t=0</math> day to a maximum of 4.03 at <math>t=37</math> days to a final value of <math>\approx 4</math> at <math>t=55</math> days. . . . .</p>	163
6.21	<p>The mass density variations for the collagen fibre families are shown in this Figure. <b>(Top)</b> The mass densities for the circumferential collagen fibres (<math>m^{C,I_4}</math>) is shown. An initial value of 1 at <math>t=0</math> days is seen, with an increase to <math>\approx 1.0</math> to <math>\approx 5.1</math> in the infarcted region at <math>t=13</math> days. A further increase is seen to a range of <math>\approx 3.5</math> to <math>\approx 9.6</math> is seen with a few elements nearing 11. Terminally at <math>t=55</math> days a range of <math>\approx 3</math> to a maximum of 10.5 is seen with only a few elements in the higher range of values. <b>(Bottom)</b> The mass densities associated with longitudinal collagen fibres are shown. Initially, at <math>t=0</math> day the <math>m^{C,I_6}</math> values are at unity. Subsequently, a minimum rise is observed upto a range of 1.0 to 3.5 at <math>t=13</math> days, and a rise to a maximum of <math>\approx 20</math> is seen at <math>t=27</math> days and <math>t=55</math> days, with one element exhibiting a high value of 42. . . . .</p>	164
6.22	<p>Nodal displacements for days 0 and 55 post-MI, for case considered with evolving homoeostatic Cauchy stress for the collagen fibre families. . . . .</p>	165
6.23	<p>The circumferential collagen fibre Cauchy stress is displayed. <b>(Purple Line)</b> Homoeostatic stresses evolve as per Equation [6.14 and reach a maximum of <math>\approx 3.72 \times 10^{-3}</math> MPa at <math>t=14</math> days from an initial value of <math>\approx 2.558 \times 10^{-3}</math> MPa at <math>t=0</math> day. <b>Blue Line)</b> The Cauchy stress experienced by the <math>I_4</math> collagen fibre family increases from <math>\approx 2.558 \times 10^{-3}</math> MPa to a maximum of <math>\approx 4.82 \times 10^{-3}</math> MPa at <math>t=12</math> days, subsequently decreasing below the homoeostatic stress levels post <math>t=24</math> days reaching a final value of <math>\approx 3.39 \times 10^{-3}</math> MPa at the end of the simulation. . . . .</p>	166

6.24 The longitudinal collagen fibre( $I_6$ ) stress is plotted. (**Black Line**) depicts the evolution of the homoeostatic stress ( $\sigma_{CH,I_6}(X, k_3, k_4, I_6, t)$ ) from an initial value of  $\approx 0.8 \times 10^{-3}$  MPa to  $\approx 1.65 \times 10^{-3}$  MPa at  $t=9$  days. (**Orange Line**) The longitudinal collagen fibre stress observes an increase from the homoeostatic value at  $t=0$  day to an increase of  $\approx 2.35 \times 10^{-3}$  MPa at  $t=9$  days, with a trough at  $t=19$  days, with a minimum value of  $\approx 1.46 \times 10^{-3}$  MPa at  $t=19$ . Another peak is observed at  $t=38$  days steadily declining till  $t=55$  days from  $\approx 3.25 \times 10^{-3}$  MPa to  $\approx 2.7^{-3}$  respectively, with a downward trend after the simulation ends. . . . . 167

6.25 The Cauchy stresses for collagen family of fibres are displayed. (**Top**) The circumferential collagen fibre Cauchy stresses are displayed, with an initial distribution at time  $t=0$  day ranging from  $\approx 0.002$  MPa to  $\approx 0.02$ . At  $t=13$  days an increase is seen due to myocardial infarction to a range of  $\approx 0.005$  MPa to  $0.025$  MPa, with a further increase of the maximum value to  $\approx 0.035$  MPa, and the minimum reducing to  $\approx 0.005$  MPa at  $t=27$  days. Terminally while majority of the infarcted zone is well below  $\approx 0.01$  MPa, a few elements experience a higher maximum of  $\approx 0.013$  MPa. (**Bottom**) The Cauchy stress distribution for the longitudinal collagen fibres ( $\sigma_{C,I_6}$ ) are displayed. An initial distribution of  $\approx 0.0003$  MPa to  $0.001$  MPa is seen at  $t=0$  day. Increasing to a maximum of  $\approx 0.005$  in the infarcted zone at  $t=13$  days. At  $t=27$  days a few elements experience higher stresses around the range of  $\approx 0.02$  MPa to  $0.032$  MPa with majority of the infarcted region experiencing stresses at about  $\approx 0.007$  MPa. Terminally at  $t=55$  days the stresses range from  $0.003$  MPa to a maximum of  $0.038$  MPa (skewing the average due to a few elements in the higher range). . . . . 168

6.26 (**Blue Line**)  $k_2$  material parameter remodelling, associated with circumferential collagen family of fibres ( $I_4$ ), declines from an initial value of  $3.45$  at  $t=0$  day, stabilising at  $0.5$  by the end of the simulation at  $t=55$  days. (**Purple Line** The longitudinal collagen fibres' material parameter ( $k_4$ ) remodels with an initial decrease from  $3.45$  to  $2.25$  from  $t=0$  day to  $t=8$  days, peaking at  $\approx 4.5$  at  $t=18$  days and lastly reaching a maximum of  $5.49$  at  $t=55$  days.) . . . . . 169

6.27 The material parameter remodelling over the course of the myocardial infarction in the left ventricle is shown in this figure. **(Top)** The circumferential collagen family of fibres' material parameter is displayed. An initial distribution of 3.5 is seen at  $t=0$ . Note: 3.5 has been set to be the maximum to see better distribution of the material values in the later stages. At  $t=13$  days, the  $k_2$  value ranges from  $\approx 1.2$  to  $\approx 2.5$ . Further at  $t=27$  days the values decrease further to a range of 0.035 to  $\approx 1.5$  with a few elements exhibiting higher values around 2. Terminally at  $t=55$  days, most of the infarct region  $k_2$  values have remodelled to a value of 0.035. **(Bottom)** The longitudinal collagen family of fibres material parameter  $k_4$  is shown in here. An initial distribution of values at 3.5 is seen at  $t=0$  day. At  $t=13$  days, the values range from  $\approx 0.04$  to  $\approx 1.7$  with a few elements reaching  $\approx 2.7$ . Further at  $t=27$  days, the  $k_4$  values range from 0.035 to  $\approx 1.6$  with a few elements on the outer boundary and inner region of the infarct at  $\approx 2.5$ . Terminally, at  $t=55$  days, the range of values goes from 0.035 to 3.5 and above, with the maximum seen in a few elements. . . . . 170

6.28 **(Black Line)** The circumferential collagen fibre stretch invariant ( $I_4$ ), increases gradually from an initial value of 1.01 at  $t=0$  days to a maximum of 1.165 at  $t=27$  days, with another peak at  $t=35$  days with a value of 1.17, reaching a value of 1.173 by  $t=55$  days with an upward slope. **(Red Line)** The longitudinal collagen fibre stretch invariant ( $I_6$ ) increases from  $\approx 1.0065$  at  $t=0$  day to a maximum of 1.085 at  $t=25$  days decreasing to 1.076 at  $t=45$  days, terminally attaining a value of 1.08 at  $t=55$  with an upward trend. 171

6.29 The stretch invariants experienced by the collagen fibres are shown in this figure. **(Top)** The invariant ( $I_4$ ) associated with the circumferential family of collagen fibres is seen. Initially, at  $t=0$  day a range of 0.99 to  $\approx 1.1$  is observed. Consequently, at  $t=13$  days the maximum increases to  $\approx 1.2$ , as the infarction progresses at  $t=27$  days,  $I_4$  values reach a higher range from 1.15 to 1.4+. Terminally at  $t=55$  days, the stretch invariants range reduces to a range between 1.2 to  $I_4$  1.35. **(Bottom)** The stretch invariant ( $I_6$ ) associated with the longitudinal collagen fibres are shown. At  $t=0$  a range of 0.98 to  $\approx 1.05$  is observed, increasing to a range of 1.01 to  $\approx 1.18$  at  $t=13$  days. At  $t=27$  days, the value range increases to a maximum of 1.4+ and terminally at  $t=55$  days, higher values are seen in a few elements whereas the majority of the infarcted region observes a range of 1.05 to  $\approx 1.25$ . . . . . 172

6.30 **(Red Line)** The circumferential fibroblast stretch ( $\lambda_{F,I_4}$ ) increases from 1.05 to a maximum of 1.089 at  $t=25$  days reaching a minimum with a downward trend at  $t=55$  days with a value of 1.056. **(Blue Line)** The longitudinal fibroblast stretch ( $\lambda_{F,I_6}$ ) increases from an initial value of 1.05 at  $t=0$  day, to a maximum value of 1.0652 at  $t=23$  days, thereafter stabilising at 1.053 at  $t=52$  days to the end of the simulation. . . . . 173

---

6.31	<i>The stretches experienced by the fibroblast cells are displayed in this figure. (Top) An initial prescribed value of 1.05 is seen at t=0 day. The values increase to a range of 1.058 to 1.1 at t=13 days, seeing a further increase in stretch in the infarcted zone elements to 1.1, with an increase in the minimum to <math>\approx 1.6</math>. Terminally, at t=55 days, the values for <math>\lambda_{F,I_4}</math> in the infarcted zone attain a range of 1.05 to <math>\approx 1.057</math>, with a few elements possessing higher values upto 1.1. (Bottom) The fibroblast cells maintaining the longitudinal collagen fibres, have their stretches displayed here. An initial prescribed distribution of 1.05 is seen at t=0 days. An increase to a range of 1.05 to 1.1+ is seen at t=13 days, with a reduction in the minimum seen at t=27 days to values around 1.046. Terminally, at t= 55 days, majority of the infarcted volume elements attain a value range of 1.001 to <math>\approx 1.057</math> with a few elements exhibiting higher <math>\lambda_{F,I_6}</math> values of around <math>\approx 1.09</math>.</i>	174
6.32	<i>(Orange Line) The circumferential collagen fibre mass density changes are seen to rise from 1 at t=1, with an upward slope from time t=5 days to a maximum of 4.25 at t=55 days. (Brown Line), In a similar trend but with a slightly faster increase in mass deposition the longitudinal collagen fibre mass density increases from 1 at t=0 day to a maximum of 2.76 at t=40 days and stabilises from t=50 days to the end of the simulation with a value of 2.7.</i>	175
6.33	<i>The collagen fibres mass densities are displayed in this figure. (Top) An initial mass density of 1.0 is observed at t=0 day for circumferential collagen fibres (<math>m^{C,I_4}</math>), a slight increase of the maximum upto <math>\approx 2.1</math> is observed in the infarcted region at t=13 days. AT t=27 days, the (<math>m^{C,I_4}</math>) values rise to a range of 2 to <math>\approx 8</math> in the infarcted zone and terminally at t=55 days an increase value range is seen from 4.3 to <math>\approx 10+</math>. (Bottom) For longitudinal collagen fibres, mass density changes are shown. An initial distribution of unity is observed at t=0 day, with a minor increase to a range of 1 to 1.5 are seen at t=13 days. At t=27 days the range of (<math>m^{C,I_6}</math>) the range rises from a minimum of 4 to upto 14, with higher values observed in a few volume elements at the bottom of the infarct. Terminally, at t=55 days a range of <math>\approx 4</math> to <math>\approx 22+</math> is observed, again with maximum values restricted to a few elements.</i>	176
7.1	<i>Skeletal Muscle Taxonomy (Betts et al. (2018))</i>	186
7.2	<i>Sarcomere Macroscopic Structure (Betts et al. (2018))</i>	187
7.3	<i>Gastrocnemius muscle anatomy (Britannica (2015)). It is located in the upper region of the calf region (boxed in image).</i>	188
7.4	<i>The diagram depicts the steps taken for the generation a volume mesh for finite element simulations, and a separate .vtk file to compute muscle-tendon volume fractions to incorporate with the volume mesh to define material parameters.</i>	190
7.5	<i>A flowchart, describing the methods employed for generating volume fraction demarcation, for the gastrocnemius muscle.</i>	193

---

7.6	<i>The assignment of <math>f_T(X)</math> based on the Volume Fraction Assignment Algorithm (Civisilli (2019)), where <math>f_T(X)=1.0</math> indicates tendon region (TR), <math>f_T(X) = 0</math> indicates muscle region (MR) and <math>f_T(X)</math> values between 0-1 are interpolated to indicate the tendinous aponeurosis region (AR). <b>(Top)</b>: shows the X-Z view of the gastrocnemius muscle mesh and <b>(Bottom)</b>: displays the sliced X-Z view clearly displaying the different regions. <b>(Centre)</b>: The slices show a cross-sectional view in the Y-Z plane showing the sliced-through variation in the <math>f_T(X)</math> parameter indicating depth-wise assignment.</i>	194
7.7	<i>Figure depicting the surfaces obtained after partitioning algorithm. The outer surface is shown in lightest shade of red, surface a i.e. the middle layer is shown with light red and finally the inner surface b is shown with a solid color red.</i>	196
7.8	<i>The prescribed fibre directions for both the muscle and tendon fibres, i.e. in the direction of the major axis of the gastrocnemius muscle.</i>	198
7.9	<i>The prescribed boundary conditions for extension of the gastrocnemius muscle, the proximal end is fixed in all directions while the distal end is allowed to be free in all degrees of freedom and an extension is applied in the positive x-direction over time with a ramp function (from a <math>\lambda_i = 1.05</math> to <math>\lambda_f = 1.1</math>).</i>	199
7.10	<i>The extension boundary condition, for stretching the muscle beyond the initial value (<math>\lambda_i</math>) to a maximum stretch (<math>\lambda_f</math>) from an initial time <math>t_i</math> to a final time point <math>t_f</math> is based on a linear ramp function shown.</i>	199
7.11	<i>The regions demarcated based on the <math>f_T</math> volume fraction variable and the volume fraction assignment algorithm (Appendix B). The regions are abbreviated as: <b>(a)</b> Tendon Region (TR), <b>(b)</b> Aponeurosis Region and <b>(c)</b> Muscle Region (MR).</i>	203
7.12	<i>The stretch invariant <math>I_4</math> is shown, where it ranges from 1.0 to <math>\approx 1.35</math> at <math>t=1</math> day to a range of <math>\approx 1.0</math> to <math>1.7</math> at <math>t=3</math> days, owing to the prescribed stretching of the gastrocnemius muscle. The values thereon remain constant till <math>t=10</math> days indicating a sustained stretch of the gastrocnemius muscle.</i>	205
7.13	<i>The prescribed stretch to the gastrocnemius muscle from <math>t=2</math> days to <math>t=3</math> days from 1.05 to 1.1 is reflected in the fibre stretch invariant <math>I_4</math>, from <math>\approx 1.116</math> to <math>\approx 1.246</math> between the same time steps and remains constant till the end of the simulation.</i>	206
7.14	<i>The <math>k_2^M</math> values are displayed, having a value of 0.5 <math>t=2</math> days with <math>\lambda = 1.05</math>. At <math>t=3</math> days, the <math>k_2^M</math> values reduce to a range of 0.26 to 0.325 for an increased stretch <math>\lambda = 1.1</math>. Terminally at <math>t=10</math> days, <math>k_2^M</math> values remodel and settle between a range value of <math>\approx 0.18</math> to 0.25.</i>	207
7.15	<i>The averaged <math>k_2^M</math> value decreases from 0.5 at <math>t=1</math> day to about <math>\approx 0.234</math> at <math>t=6</math> days and stabilises till the end of the simulation at <math>t=10</math> days.</i>	208
7.16	<i>The <math>k_2^T</math> values are shown, having a uniform value of 1 at <math>t=1</math> day with <math>\lambda = 1.05</math>. At <math>t=3</math> days when the gastrocnemius is stretch to <math>\lambda = 1.1</math> the <math>k_2^T</math> values remodel to a range of <math>\approx 2.5</math> to 3.4 and terminally at <math>t=10</math> days to a range of <math>\approx 2.0</math> to <math>\approx 2.4</math>.</i>	209

---

7.17	The averaged $k_2^T$ value is shown. After an initial value of 5 at $t=1$ days, it declines slowly compared to $k_2^M$ (7.15), from 5 to a value of around $\approx 4.54$ by the end of the simulation. . . . .	210
7.18	The difference between the muscle region Cauchy stress at a given time $t$ and the Cauchy stress at $t=1$ day i.e. before stretching the muscle, is shown. Initially at $t=1$ days $\lambda = 1.05$ and therefore there is no difference between the stress levels from $t=0$ days. However, a maximum difference of $\approx 0.25$ to $0.43$ is seen at $t=3$ post stretching to $\lambda = 1.1$ . Terminally the difference is 0 at $t=10$ days throughout the gastrocnemius muscle. . . . .	211
7.19	The muscle Cauchy stress difference is shown between stress values at time $t$ days to time $t=0$ days, initial difference increases at $t= 1.0$ days, peaking at $0.356$ at $t = t=2$ days and thereafter a downward trend is seen until $t=6$ days after which the difference remains at $0.0$ till the end of the simulation. . . . .	212
7.20	The Cauchy stress value differences for the tendon region are displayed here i.e. the values at time $t=0$ days to $t=0$ days. No difference is observed at $t=1$ days due to the muscle not being stretched beyond $\lambda_0$ . at $t=3$ days the differences observed range from $\approx 0.23$ to $\approx 0.341$ . Terminally at $t=10$ days, the stress differences are 0 across the gastrocnemius muscle. . . . .	213
7.21	The averaged difference in tendon Cauchy stress levels from a time $t$ days to $t=0$ days. An increase from $0.0$ to $0.591$ is seen till $t=2$ days and reaches an averaged value of $0$ by $t=10$ days. . . . .	214
7.22	The averaged $I_4, I_6$ values increase from $\approx 1.137$ at $t=1$ day to a maximum of $1.286$ for the Control Case and Case 1, while a maximum of $1.284$ is reached in Case 3 by $t=3$ days. While consistent for other cases the value drops to $1.2832$ and $1.2827$ for Cases 2 and 3 till $t=10$ days respectively. . . . .	215
7.23	The averaged muscle Cauchy stress difference $\sigma_M^{diff}$ are displayed. The control case rises from $0.0$ to $1.4$ from $t=1$ day to $t=3$ days, whereas over the same period Case 2 increases upto $1.41$ and slightly increases to $1.42$ after $t=4$ days. Case 1 and Case 3 observe a similar rising pattern between $t=1$ day to $t=2$ days and a descent until $t=6$ days and stabilises, with Case 3 stabilising at a slightly lesser rate. . . . .	216
7.24	The averaged tendon Cauchy stress difference is shown, with the Control Case increasing from $0.0$ to $0.182$ at $t=3$ days. Case 1 rises in the same time period upto $0.167$ and decreases slightly to $0.163$ after $t=4$ days. Cases 2 and 3 observe a similar rise till $t=2$ days at $\approx 0.0627$ and $0.0624$ respectively, thereafter declining to stabilisation post $t=6$ days. . . . .	217
7.25	The averaged $k_2^M$ material parameter values are depicted. No remodelling occurs in the Control Case and Case 2. Case 1 the value decreases sharply from $0.5$ to $\approx 0.25$ and stabilises at $\approx 0.23$ at $t=3$ days and $t=6$ days respectively. . . . .	218

7.26	<i>The averaged <math>k_2^T</math> values are shown here, with no changes observed in the Control case and Case 1. Case 2 observes a sharp decrease to <math>\approx 4.56</math> and stabilises around 4.503 at <math>t=3</math> days and <math>t=6</math> days respectively. Likewise, for Case 3 the value declines to <math>\approx 4.58</math> and <math>\approx 4.527</math> at <math>t=3</math> days and <math>t=6</math> days respectively.</i>	219
8.1	<i>Geometries from patient MRI-data, provided by (Luo (2019)).</i>	230
B.1	<i>A block or cube, represented as an stl file where each surface comprises of two triangles providing an idea about how stl surface geometries are generated.</i>	311
C.1	<i>A right-ward shift is observed based on the remodelling of <math>k_2</math> material parameter (<b>left</b>) For the original HGO model, adapted in an ANSYS® hyperelastic fibre-reinforced material subroutine. (<b>right</b>) Modified HGO model, based on post-processed material parameters after each simulation step to mimic the changes as would be obtained in an analytical solution for the strain energy function considered. The right-ward shift is greater in the modified HGO model and therefore, allowing the soft tissue model to dilate further than would be possible with the original strain energy formulation. The same applies for the collagen fibre strain energy with <math>k_4</math> remodelling.</i>	332

This page has been intentionally left blank.

# List of Tables

2.1	Constituent populations and volume fractions present in the myocardial tissue. . .	11
2.2	List of constitutive models developed for the myocardium. Where in $W$ and $\Psi$ represent notations used to define the Strain Energy Density Function in each constitutive model. . . . .	30
3.1	The various parameters, values and constants in the constrained mixture model and their associated values used in the 1D LV growth and remodelling simulation. . . . .	66
3.2	Parameter values for constrained mixture model, to capture the results observed in (Fishbein et al. (1978)). . . . .	77
5.1	Parameter set up for simulating sustained over-stretch of a cubic element. . . . .	130
6.1	List of constitutive models developed for the myocardium. $W$ and $\Psi$ represent notations used to define the Strain Energy Density Function in each constitutive model. The values used for the parameters in these models are listed on the far right column, to identify parameter values for our model. . . . .	149
6.2	Material parameter values identified for the left ventricular myocardium using the HGO hyperelastic material model from table [6.1]. . . . .	150
7.1	Material parameter values assigned for the muscle (superscript <sup>M</sup> ) and tendon (superscript <sup>T</sup> ) for representing a fibre reinforced hyperelastic material, based on the aponeurosis algorithm (Civisilli (2019)) for the volume fractions. . . . .	201

*Dedicated to my grandparents.*

# Chapter 1

## Introduction

Cardiovascular Diseases (CVDs) in particular Ischaemic Heart Diseases(IHDs) ([Finegold et al. \(2013\)](#)) are the major contributors to mortality and morbidity worldwide. The number of deaths due to CVDs are estimated around 17.9 million in 2016 ([Organisation \(2017\)](#)) accounting for upto 31 % of global mortality. Out of the various diseases which can be categorised from CVDs and IHDs, myocardial infarction and stroke contribute to about 85 % of the deaths. It was observed that the "risk-standardized hospital mortality rate" in patients under Medicare ([Krumholz et al. \(2009\)](#)) displayed a significant reduction, indicating the decreases in mortality due Acute Myocardial Infarction. However, even with a reduction in mortality due to better availability of treatment options, sophisticated surgical procedures and medicinal drug therapies, MI still remains one of the major contributors to deaths caused by CVDs. Current methods to provide diagnosis, stratify disease risks and complete prognostic analysis of myocardial infarction and heart diseases in general continue to be complex, with increasing challenges being faced. It is therefore necessary to adopt a new perspective in the utilisation of knowledge acquired in cardiology to better understand the heart, aetiology of diseases and better equip ourselves with tools to alleviate the risks, pain and ultimately death caused ([Chabiniok et al. \(2016\)](#)).

The study of cardiac biomechanics can be seen in the early works of ([Woods \(1892\)](#)), where in the left ventricle was approximated as a thin-walled spherical membrane to approximate the heart wall stresses. Since then, a number of models based on constitutive have been developed ranging from treating the heart wall as isotropic to having a non-linear anisotropic or orthotropic response. As the cardiac function is not only restricted to the mechanical stimuli the left ventricle experiences, other factors such as the electrophysiology due to the activation potential from the heart's natural pacemaker cells (Sino Atrial node) and the fluid dynamics involved due to the transient changes in wall stresses as a consequence of transient blood flow during the cardiac cycle. A growing body of knowledge with respect to each of these fields and multi-physics, multi-scale models are available today to help decipher the various pathologies of the heart as well as understanding the mechanisms involved in cardiac function from the cellular scale to the

tissue level. Not only has the field of biomechanics, computational modelling and theoretical frameworks progressed, but the tools at our disposal for imaging the cardiac tissue and diagnostic tools have provided us with a rich repository of data sets to model and test various hypotheses. This allows us to better understand the dynamics involved in cardiac function as well to suggest stratification methods, new procedures, experimental methods as well as develop tools to help in disease management. An important goal is to provide clinically usable tools for decision making, which is the focus of translational cardiac modelling (TCM) (Chabiniok et al. (2016)). TCM as a paradigm remains in its infancy due to the complexity and volume of medical data available, with a need to assimilate and refine them into usable data sets from various sources, however, there is a potential to achieve significant scientific impact and help the medical field as whole as a reliable tool.

Given the complexity involved in modelling the heart and understanding the various intricacies involved in its function, structure, rheology, physiology and pathophysiology focus is narrowed to understanding the mechanics of the heart wall. Particularly, the cardiac extra-cellular matrix protein collagen, the cardiomyocytes and the ground substances in the myocardial tissue, their contribution to the mechanical stress response and how they affect the structure and function of the left ventricle in the event of a myocardial infarction.

### **1.1 Research Motivation & Contribution**

Currently, clinical imaging techniques like Magnetic Resonance Imaging (MRI), Computed Tomography Scans (CT) and in vivo imaging equipment vis a vis Electron Microscopy, Atomic Force Microscopy provide data for histological sections of tissues as well as the changes in their structure and function owing to adaptation to variations in mechanical stimuli. These variations in mechanical stimuli could be due to physiological remodelling maintaining dynamic homeostasis, maladaptation due to disease progression or adaptive remodelling due to prolonged changes in forces acting internally or externally on the soft tissue.

Even though sophistication in acquiring data from patients has increased our understanding on the physiology and pathophysiology of soft tissues, there are still difficulties in understanding the fundamental characteristics due to the limitations of in vitro experiments as in vivo extraction of data to utilise in scientific laboratories would involve high cost, time consuming and invasive techniques to be used on patients. Due to this overhead which is difficult to clearly manage, mathematical modelling provides a means to bridge the gap. Mathematical modelling of biological systems allows us to gain a deeper understanding depending on the context of application, i.e. a mechanobiological model would help us understand the effect of physical forces on an organs tissue, molecular or whole-organ level dynamics. In contrast to in vivo and in vitro experiments, on the accurate set up of the model, experiments can be virtually performed while maintaining three key aspects i.e. repeatability, reproducibility and provide a better understanding of the

underlying mechanisms of the target biological component (cellular, molecular, tissue-level or whole-organ).

Modelling of the left ventricular soft tissue and the heart-chamber as whole has received tremendous interest over the past 50 years, following the inception of utilising mathematical as well as computational modelling of soft tissues (Humphrey (2003)). An effort to further add to the body of research with tools to supplement biological understanding of soft tissues, is made through the research undertaken. A list of goals and extended targets are outlined below.

Two major goals of the research introduced are:

- Novel Constrained Mixture Model of the LV, adapted from arterial models (Watton et al. (2009)) to model the myocardium and understand extra-cellular matrix growth and remodelling.
- Soft Tissue growth and remodelling framework packaged around ANSYS® to enable workflows to be made for soft tissue simulations, using in-built fibre-reinforced soft tissue material models.

A list of secondary targets are enumerated below:

### **Extended Research Goals**

1. To understand how the mass turnover of the structural protein collagen, in the cardiac extra-cellular matrix, and its material remodelling post-MI affects the stability of the infarction.
2. Provide a framework around a commercial finite element software package (ANSYS®), to simulate soft tissue growth and remodelling. To provide evidence of its usefulness.
3. Test various applications and hypotheses affecting surrounding the soft tissue characteristics in disease progression, maladaptation and prolonged exposure to stretch.
4. Introduce a means to include cellular modelling via the framework developed.
5. Gain insight into the model behaviour using various input parameter combinations. Thereby, understanding the range of input parameters and rate constants for cases which reflect experimental observations qualitatively, whereas draw conclusions from cases which don't and how such scenarios can affect structure and function of the soft tissue.

### 1.1.1 Contributions to Research

1. A novel one-dimensional constrained mixture model of the left ventricle, modelling extra-cellular matrix collagen fibres with a stretch distribution function allowing us to capture the complex behaviour of the collagen fabric with generalised triangular distribution function. Additionally, modelling myocardial infarction and its impact of extra-cellular matrix via growth and remodelling.
2. A novel framework to define soft tissue growth and remodelling simulations centred around an available material model ([Holzapfel et al. \(2000\)](#)) in the ANSYS ® Mechanical Finite Element commercial package. Including a range of functionality for pre-processing and post-processing of relevant mechanical quantities as well as the ability to create custom workflows for a desired soft tissue simulation.
3. An implementation of a finite element model for the left ventricle based on the ANSYS ® Soft Tissue Growth and Remodelling Framework (STGRF), undergoing myocardial infarction. Mass densities, stress profiles and the extra-cellular matrix remodelling to achieve homoeostasis post-MI are the features of this application. A notable feature is the incorporation of a cellular model for fibroblasts which regulate the growth of the extra-cellular collagen matrix.
4. Another application of the STGRF applied to the gastrocnemius skeletal muscle with defined aponeurosis regions. This involves a preliminary study based on the effect of sustained over-extension on the remodelling of the muscle and tendinous regions of the muscle.

## 1.2 Thesis Structure

- **Chapter 1:**

Provides a brief introduction about Cardiovascular diseases, an understanding of the importance of biomechanical research, outlining the research motivations. Important contributions to research from the work done are detailed as well.

- **Chapter 2:**

A two part literature review is over viewed, with *Part I* providing an understanding of the physiology, anatomy and pathophysiology of the myocardium, specifically the left ventricular myocardium along with the micro-structural ramifications of the same. *Part II* provides a description of basic mechanical formulations, constitutive models in literature to model soft tissues (focussed on the myocardium), remodelling and growth of extra-cellular matrix collagen and an overview about finite growth and constrained mixture models.

- **Chapter 3:**

A novel constrained mixture model of the left ventricle is introduced, to understand growth and remodelling of the left ventricle. The left ventricle is modelled as a elastic, spherical membrane composed of microstructural constituents, namely, ground matrix, cardiomyocytes and collagen fibres. Each constituents possesses its own natural reference configuration and mass density terms, and a myocardial infarction is simulated via the degradation of the cardiomyocyte mass density. Growth and adaptation/ remodelling of the collagen fibres occurs via stretch-based differential equations which aim to maintain a preferred state of stretch (homoeostasis). The collagen fibre stretches are represented using a distribution function, encapsulating the fact that not each collagen fibre in the extra-cellular matrix would possess the same stretch. Different cases are considered where the homoeostatic stretch distribution of collagen fibres is prescribed to evolve and the resultant effect on the tissue thinning and collagen mass density is analysed.

- **Chapter 4:**

A novel framework for soft tissue growth and remodelling developed around ANSYS® Mechanical APDL is introduced. It is based on the built-in passive, anisotropic, fibre-reinforced, hyperelastic material model. The language employed for the code library is Python. It is highly customisable, and contains a core set of modules containing functions and methods, which could be used to create customised workflows. Using these customisable workflows, with inputs for finite element analysis such as mesh information, material parameter specification and parameters for growth and remodelling simulation, the framework can be adapted to multiple soft-tissues. We illustrate the applicability to a cubic element to test the growth and remodelling hypotheses, introduced in this research, based on the material model. External workflows developed are tailored for a particular biomechanical problem and the interaction between Python and the ANSYS® Mechanical APDL solver is

orchestrated via PERL scripts. A list of capabilities and limitations are further assessed and discussed in this chapter.

- **Chapter 5:**

The finite element model for the left ventricle introduces the first application of the Soft Tissue Growth and Remodelling Framework (STGRF). An idealised left ventricular geometry, meshed with hexahedral elements is assigned material parameters is subjected to an internal diastolic pressure and the strain energy function is multiplied by mass densities for each constitutive term. These mass densities terms are assigned to the ground matrix (isotropic component), and two families of collagen fibres (anisotropic components). A myocardial infarction is simulated by degradation of the ground matrix mass density and remodelling of collagen fibres along with growth formulations are implemented using stress-based and stretch-based partial differential equations respectively. A key assumption introduced is the growth of collagen fibres is mediated by a fictitious fibroblast recruitment field, which is governed only by the collagen fibre stretches. Two cases are considered, with **(a)** adaptation of the homoeostatic Cauchy stresses of collagen fibres and **(b)** no change in the homoeostatic Cauchy stress. Results and implications are further discussed.

- **Chapter 6:**

The second application of the STGRF is shown in this chapter. A gastrocnemius skeletal muscle geometry is considered and using a volume fraction assignment algorithm, regions of muscle, tendon and aponeurosis have been defined. Remodelling of the tissue is implemented using Cauchy stress-based partial differential equations for the muscle and tendon fibres, which factor into the aponeurosis region scaled according to their volume fraction value. The stresses in the regions are observed for the muscle experiencing a sustained overstretch and remodelling equations attempt to maintain a preferred state of homoeostatic stretch. Implications and applications of this model are then discussed.

- **Chapter 7:**

The research introduced in the previous chapters are summarised in this Chapter, along with limitations of each study, potential future work in pertinence and concluding remarks.

## Chapter 2

# Background & Literature Review

---

*In this chapter, important concepts, definitions and background information are summarised. This will provide foundations underpinning the research outlined in the rest of the thesis. A literature review comprises the second part of this chapter, where in recent developments, state-of-art models are reviewed and the influence, impact, guidance and inferences in current research is outlined.*

*The two parts are divided as follows:*

***Part I:***

*Background about the heart, left ventricle and myocardial soft tissue. Implications of a myocardial infarction in the left ventricle, alterations in the biomechanics and the importance of understanding the growth and remodelling of the extra-cellular matrix.*

***Part II:***

*Past research, literature on which the current research, proposed models and ideas are based on. Recent state-of-art models, their contribution in the medical field and an insight into how mathematical models can help us understand the growth and remodelling of myocardial soft tissue in response to disease and further guide disease stratification, intervention techniques and therapies.*

---

## 2.1 The Heart

The perfusion of all the tissues in the human body with nutrients and oxygen by supply of fresh oxygenated blood is done by the heart. Unlike other organs, it can never be at rest. The flow of blood needs to be maintained in order to transport nutrients to every cell in the body, if there is an interruption or no flow there would be insufficient nutrition being absorbed by cells from the interstitial fluid. The heart's pumping function takes care of this need and is the core component of the circulatory system. It beats approximately 100, 000 times each day, pumping close to 8000 litres of blood through the circulatory system. Therefore, the cardiac muscles are thick and have a high pressure generating capacity due to the high demands of the human body's blood circulation demand (Martini et al. (2006)). Especially the left ventricular wall is thicker compared to the other chambers, bearing the primary role of supplying oxygenated blood from the lungs (pulmonary circulatory system), to perfuse all the tissues in the body.

### 2.1.1 Anatomy

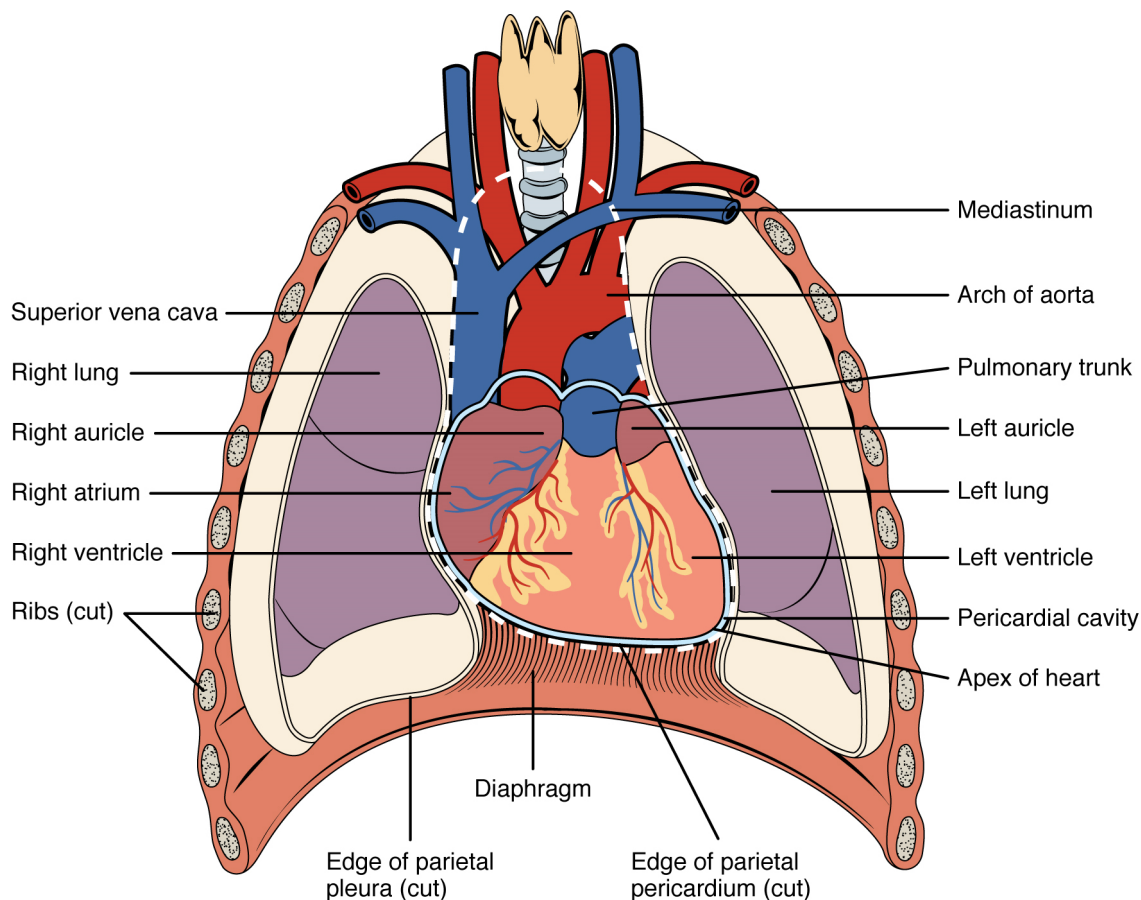


**Figure 2.1:** The heart's location within the human body, behind the mediastinum. (Betts et al. (2018))

The heart is located behind the sternum i.e. mediastinum within the thoracic cavity, with the

majority of its bulk, approximately two-thirds and its apex resting in the left side of the chest ( Figure [2.1], [Wilcox et al. \(2005\)](#)). The heart's mass is enclosed in a fibrous structure known as the pericardial sac, it is a layer consisting a dense mesh of collagen fibres and stabilises the position of the heart along with that of the associated blood vessels in the mediastinum.

### 2.1.1.1 The Pericardium

The pericardium encompasses the pericardial sac, the pericardial cavity is usually filled with a small amount of serous/ pericardial fluid which lubricates the heart walls. The outer lining of the heart wall is known as the visceral layer of the pericardium and is termed as the epicardium. The inner lining of the pericardial sac is known as the parietal layer.

### 2.1.1.2 Layers of the Myocardial Wall

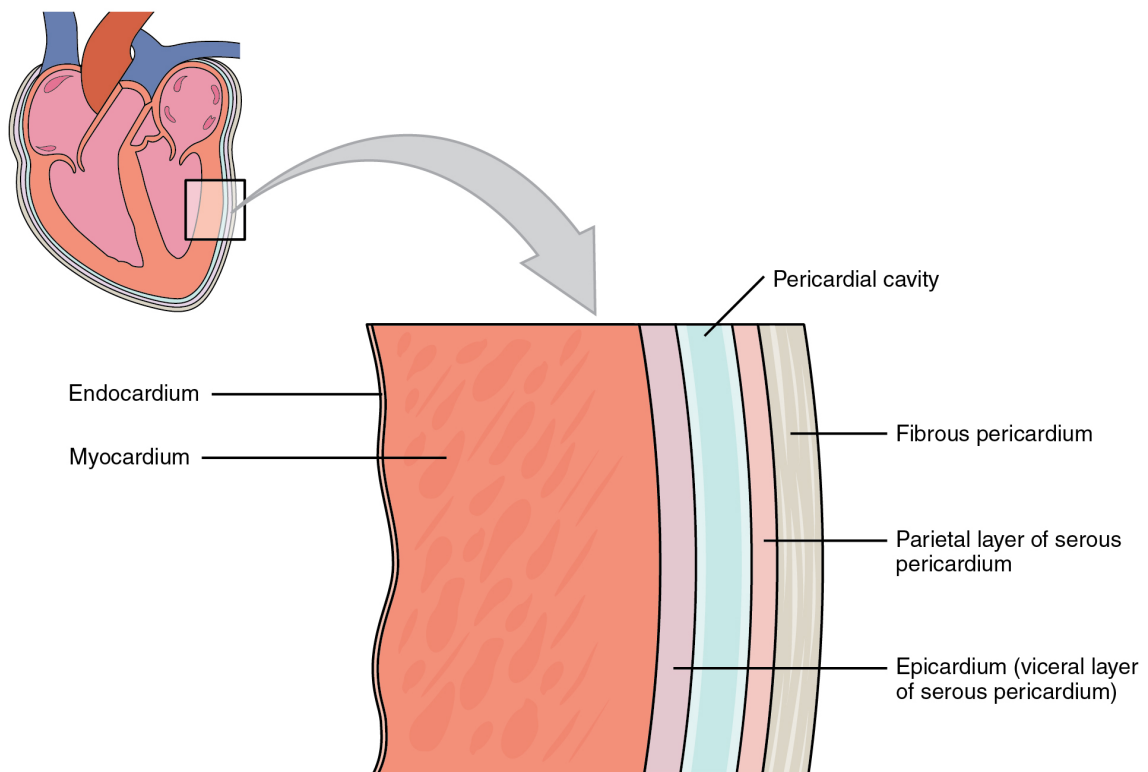


**Figure 2.2:** The structure of the heart wall, details of the multi-layered tissue are shown ([Betts et al. \(2018\)](#))

The heart wall is a composite structure, decomposed into three important layers apart from the pericardium described above. It consists of connective tissue containing collagen, elastin proteoglycans and other constituents, and the cardiac muscle bundle which is arranged in a helical pattern from the apex to the base with varying degrees of rotation in the three layers ([Anderson et al. \(2005\)](#)). These layers in are described in brief as follows, (Figure [2.2]):

**Endocardium:** The innermost layer of the heart is covered by the endocardium. It is a simple

layer of epithelial cells which is continuous with the endothelium of the attached blood vessels.

**Myocardium:** The middle layer of the heart wall, it is the thick and muscular, mainly composed of cardiac muscle (cardiomyocytes) fibres bundled together in concentric layers arranged in a helical pattern from the base to the apex. It also consists of the coronary blood vessels which perfuse the heart muscle for optimum functioning and nerves.

**Epicardium:** The epicardium as stated above is the visceral pericardium, which surrounds the outer wall of the heart. It is a serous membrane and consists of loose areolar connective tissue which is attached to the myocardium .

### 2.1.1.3 Chambers of the Heart

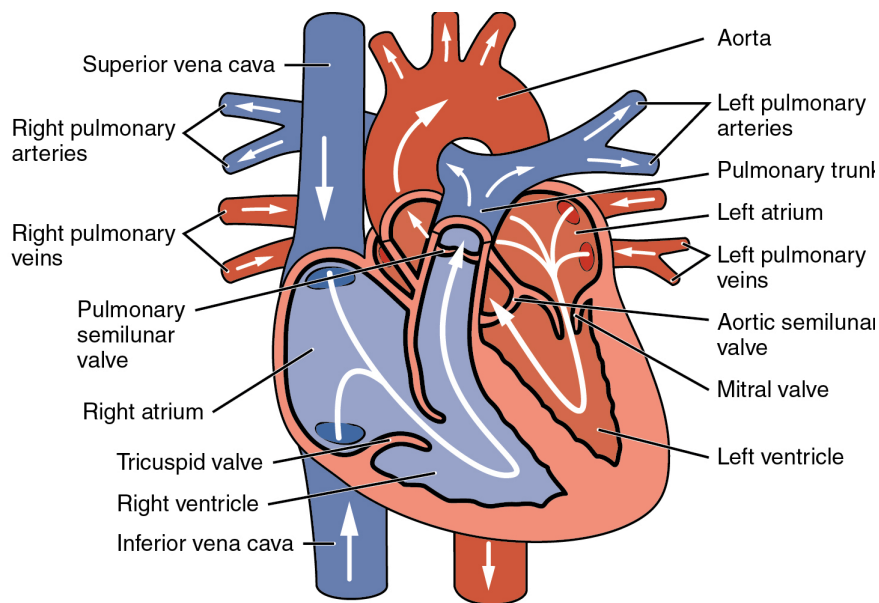


**Figure 2.3:** Chambers of the heart. (Betts et al. (2018)).

The human heart is divided into four distinct chambers, working in tandem to provide the body with oxygenated blood through the arteries, while purifying the de-oxygenated blood it receives from the veins. There are two atria forming the upper half of the heart, and the ventricles composing the lower half. The right atrium is connected by the superior and inferior vena cavae, which bring in de-oxygenated blood from the veins in the human body. The right atrium is connected to the right ventricle via a tricuspid valve. The right ventricle forms the lower right section of the heart and has a thicker wall compared to the atria. The right ventricle is connected to the lungs by the pulmonary arteries via the pulmonary valves in order to circulate the blood to be oxygenated. The lungs provide oxygenated blood via the pulmonary veins to the right atrium through, which is connected to the right ventricle with a bicuspid/ mitral valve. The right ventricle has the thickest wall structure in the heart and pumps blood out into the body at high pressures through the aorta, to which it is connected by the aortic valve. The left and right ventricle are

separated by a thick inter-ventricular septum. An important thing to observe is the atria have walls which are thinner than the ventricular walls given their specific function in the cardiac cycle. This briefly describes the anatomy of the heart and can be seen in the Figure[2.3].

#### 2.1.1.4 Myocardial Tissue Micro-structural Composition and Structure

The myocardial tissue is a complex ensemble of micro-structural constituents, cells and water content. It is important to understand their quantification in the healthy tissue, to guide our assumptions in computational and mathematical modelling. Various experimental studies have attempted to quantify the measurements of these constituents and are summarised in the table below. From various literature as in the table, approximate the averages and provide a final tally

Constituent	Volume Fraction	Population	Source
Cardiomyocytes	$\approx 67 - 75 \%$	$\approx 25 - 35\%$	<a href="#">Miner &amp; Miller (2006)</a>
Non-myocytes	-	$\approx 67 - 75\%$	-
Collagen Types (I/III)	$\approx 5\%$	-	<a href="#">Jugdutt (2005)</a>
Fibroblasts	$\approx 33\%$	-	<a href="#">Jugdutt (2003)</a>

**Table 2.1:** Constituent populations and volume fractions present in the myocardial tissue.

of the composition

#### Cardiomyocyte

The myocardium muscle cells (Cardiomyocyte), are  $\approx 100 \mu m$  long and approximately around  $10-25 \mu m$  in diameter ([Göktepe, Abilez, Parker & Kuhl \(2010\)](#), [Olivetti et al. \(1996\)](#)). The cardiac muscle fibre is composed of bundles of fibrils, which in turn are composed of serially linked cardiomyocytes, the cellular unit. These cells are connected with each other by end-to-end gap junctions which allow the conduction of electrical activation potential producing cyclic contraction-relaxation cycles via the up and down regulation of intra-cellular  $Ca^{2+}$  ions, due to the depolarisation of the sarcolemma, and sustained by the sarcoplasmic reticulum ([Woodcock & Matkovich \(2005\)](#)). They account for upto  $\approx 67 - 75 \%$  of the volume and their numbers are far less than the other extra-cellular components. Post birth the cardiomyocytes are terminally differentiated cells and adapted to any mechanical changes by hypertrophy ([Olson & Schneider \(2003\)](#), [van Empel & De Windt \(2004\)](#)) rather than hyperplasia due to its limited regenerative capacity.

#### Collagen

The concentration of collagen according to a study in ([Oken & Boucek \(1957\)](#)), for a normal human heart (weighing 250 g), approximately 1.15 g in the left ventricle is occupied by the extra-cellular collagen matrix ( $\approx 0.5\%$ ). Whereas, other major non-cardiac myocyte cell types include majorly endothelial cells and fibroblasts based on studies done in adult mouse and rat hearts ([Banerjee](#)

et al. (2007), Pinto et al. (2016)). The fundamental structural unit of collagen fibres are about 300 nm in length and diametrically measure around 1.5 nm. When placed together to form fibrils they attain a diameter of about 50-200 nm (Lodish et al. (2000)).

Below the endothelium of the endocardium and the myocardium the collagenous matrix termed as the epimysium is present. These are aligned with the muscle cells in a parallel fashion with stretching found by (Robinson et al. (1983), Weber (1989), Figure[2.4]). Therefore, the epimysium is responsible for preventing sarcomeric unit of the cardiac myocyte from excessive and disruptive stretching. Along with the epimysium, tendon-like extensions weave around myocytes to form myofibers. They are located in the spaces between the muscle bundles and provide support between myocytes and prevent misalignment or slippage which would lead to remodelling of the myocardium

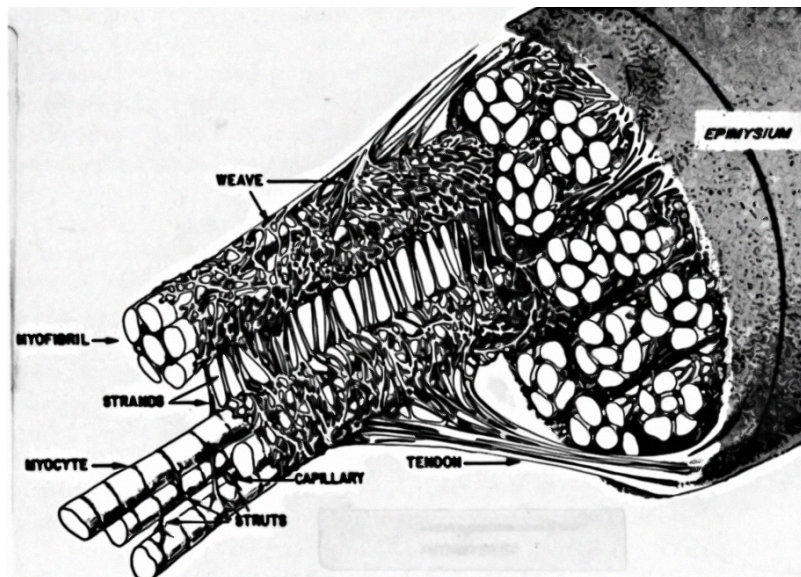


**Figure 2.4:** The configuration of collagen fibres within a cardiomyocyte fibre (Weber et al. (1987)).

Apart from the collagen fibre present in the myocardium, the extra-cellular matrix in the epicardium is recognised to play an important role in ventricular mechanics as well (Tidball (1992)). Wherein, the observations suggested collagen fibres of types I and III which are pertinent with respect to structural stiffness and mechanical strength of the collagen ECM, are concentrated more in the sub-epicardial layer than the myocardium itself. This is important to consider during our modelling assumptions in order to develop hypotheses of the collagen fibres present in various layers and delineate their roles. The extra-cellular collagen matrix is therefore, a crucial component of the myocardial ECM, and provides the tensile strength to the tissue to maintain homeostasis in such a high pressure environment for the left ventricle.

#### **Ground Substance and other constituents**

Fibroblasts are the most widely present soft tissue constituents in the myocardium, accounting

for upto  $\approx 33\%$  of the myocardium volume. They are embedded within the collagen extra-cellular matrix and attach themselves to this network via surface proteins namely integrins, which not only act as attachment facilitators but also mechano-receptors, thereby conveying information about deformation in the ECM to the fibroblast. This in turn leads to the initiation of enzymatic secretion by chemical signalling molecules in the fibroblasts, consequently synthesising new collagen fibres for deposition or the digestion of the extant matrix in response to the varying mechanical stimuli.

Elastin fibres are long and thin in appearance with a diameter of around  $1-6 \mu\text{m}$  (Green et al. (2014)). These elastic fibres are composed of a central core which are surrounded by proteins known as microfibrils (Shadwick (1999a)). The contribution of elastin to the myocardium in its mechanical function is not well known, due to limited studies that have been done. Similar to the giant protein titin, elastin has a similar elastic stress-strain profile (Fomovsky et al. (2010), Linke et al. (1994)).

Proteoglycans and glycosaminoglycans (GAGs) are important in the retention and regulation of water content in the myocardium (Fomovsky et al. (2010)). However, little is known about their exact role in the myocardial mechanical response, but studies have suggested its involvement in affecting the stiffness and residual stresses of the tissue as well as variation in collagen fibre structure leading to alterations in tissue mechanics post-MI (Campbell et al. (2008), Weber et al. (1994)).

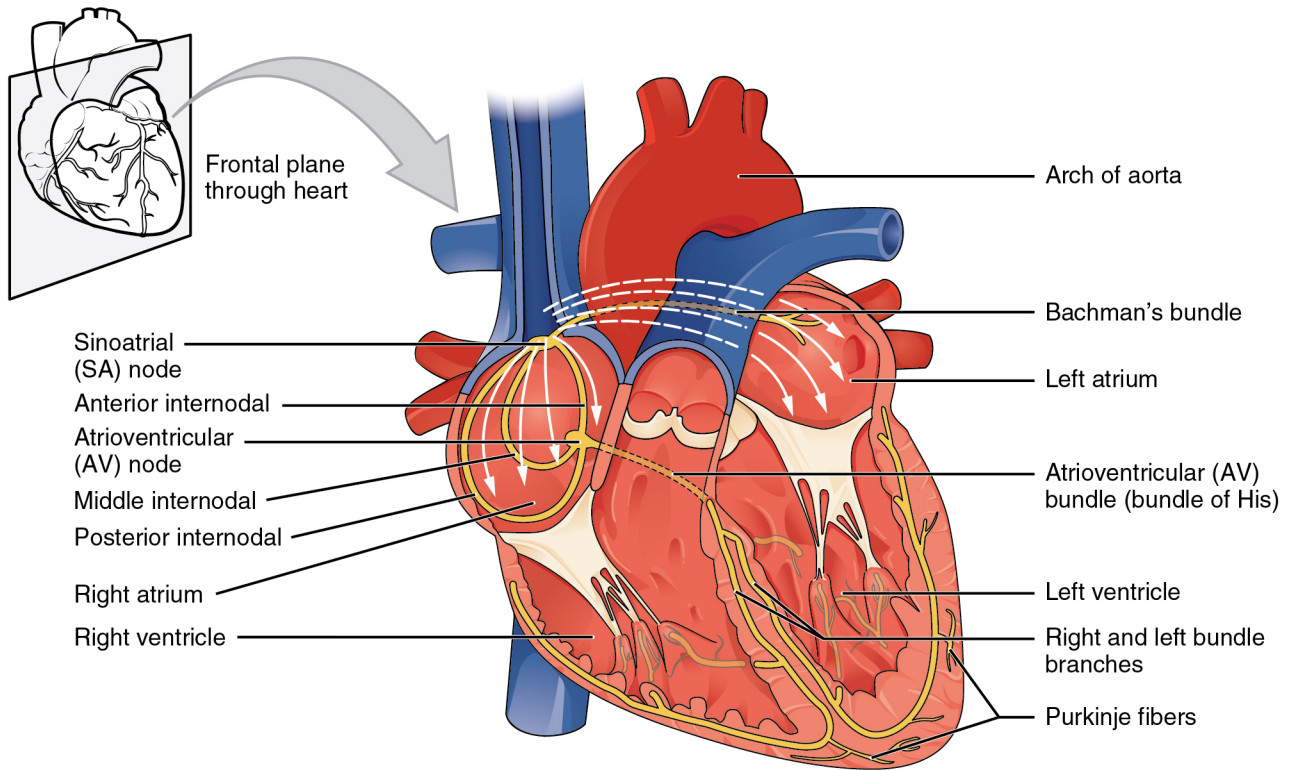
## 2.1.2 Physiology

Physiology is the field of medicine which aims to understand the underlying mechanisms and functions of the human body, which drive its survival (Guyton & Hall (2006)). The heart muscle's physiology is complex owing to the coupling between electrical excitation of the cardiac muscle, the mechanical stresses induced due to the pressure gradients and haemodynamic load caused by blood flow as well as the chemical signalling via the neurotransmitters, cells within the heart wall etc. functioning in tandem to maintain a constant rhythm and healthy flow of blood within the pulmonary and systemic circulatory systems. Given this broad range of factors, focus is narrowed to the mechanical aspects in this system, while briefly touching upon the other aspects involved in describing the cardiac cycle.

### 2.1.2.1 The Cardiac Cycle

A group of cells located in the right atrium, known as the sino atrial node (SA) are the source of the cardiac action potential Figure [2.5]. These cells depolarise spontaneously and at regular time intervals fire off action potentials usually between 60 to 100 times per minute for an individual at rest (Boron & Boulpaep (2016)). The cardiac cells are connected via gap junctions which allows the action potential to propagate from cell-to-cell. The action potential travels from the SA node to the right atrium and after about a 10th of a second arrives at the Atrio-ventricular node (AV). Due to the presence of the AV ring there is a discontinuous spread of the electrical impulse between the atrium to the ventricles and has to travel from the His-Purkinje fibre system. It is a specialised fibre system which branches out into both the ventricles and allows the electrical impulse or action potential to be carried to the ventricles.

In tandem with the electrical propagation system, the flow of blood within the heart sets up pressure gradients owing to which the chambers suction and expel blood. The superior and inferior vena cavae transport the de-oxygenated blood from the body carrying waste products collected back to the right atrium indicating atrial diastole, at the same time oxygenated blood from the lungs are transferred to the left atrium via the pulmonary veins. The increase in pressure in the atria opens up the atrio-ventricular valves (tricuspid and mitral) to eject the blood into the respective ventricles. The electrical action potential assists with the contraction i.e. the systolic phase of the atria, therefore contracting the atrial muscles to perform their function and work. The ventricles are in diastole during the systolic phase of the atria and at this point the pressure in the ventricles rise due to the filling action of the blood. The pressure between the pulmonary arteries and the right ventricle are in imbalance, with ventricular pressure being higher. Likewise, the pressure in the aorta is less than the pressure in the left ventricle at end-diastole. This leads to the opening up of the pulmonary valve in the right ventricle, and given the action potential the cardiac muscle cells contract ejecting blood into the lungs through the pulmonary arteries. The left ventricular muscle is also activated given the delayed action potential and pumps blood out through the aorta to perfuse the tissues in the body. This entire cycle occurs for about 0.8 seconds



Anterior view of frontal section

**Figure 2.5:** *The electrical propagation fibre system architecture in the heart (Betts et al. (2018)).*

and continues with slight variations depending on the needs of the body for the entire life cycle of the human being. The Figure [2.6] encapsulates this entire process showing the various phases. The walls of the ventricles are comparatively thicker than those of the atria as they have to work against the force of gravity to pump blood outwards to the lungs and the aorta, while also allowing for the blood to reach every cell and tissue. This needs a high pressure to be generated which is allowed by the thick muscle walls shaped helically with varying angles of orientation to allow for maximal force generation during ejection.

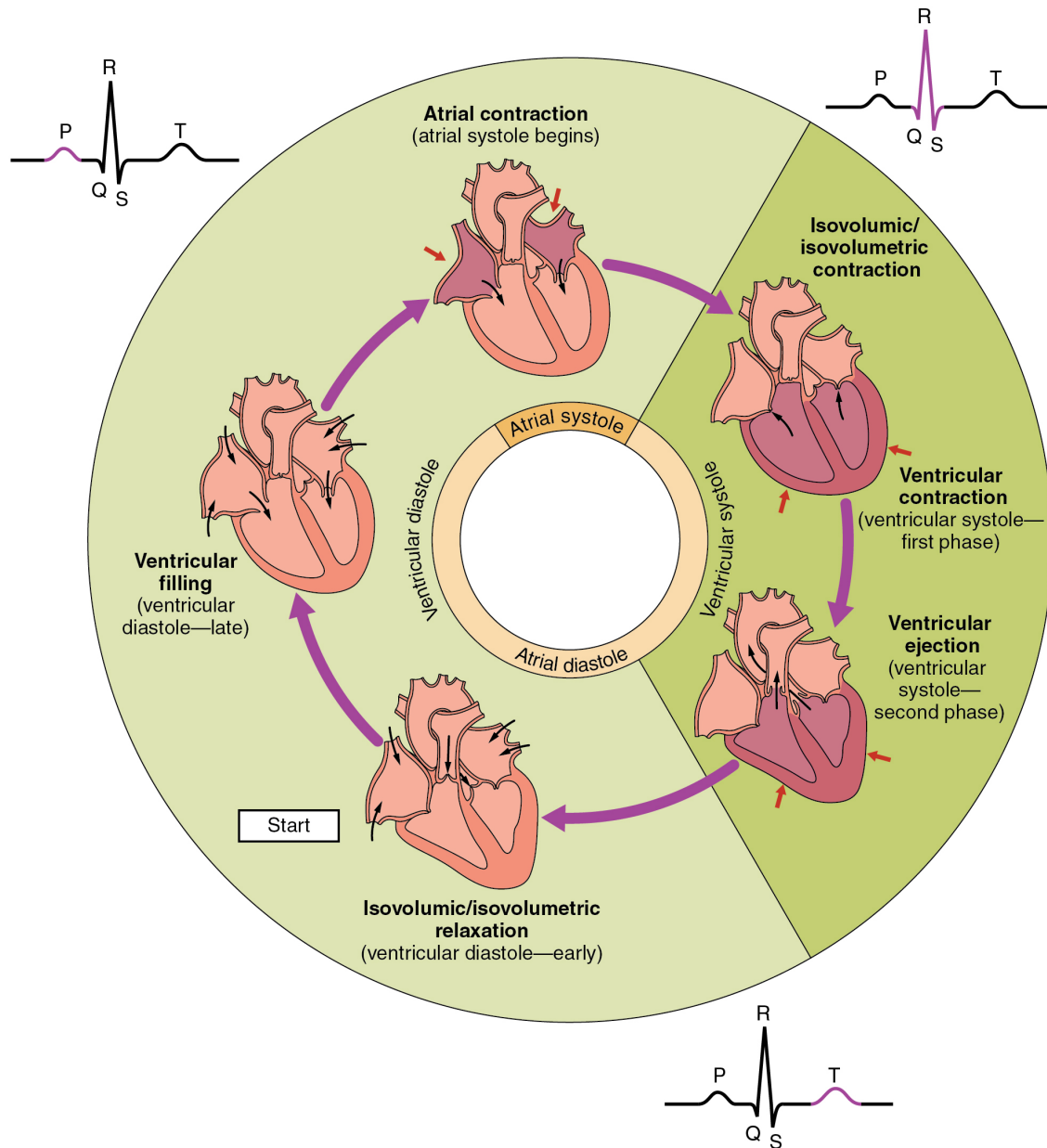


**Figure 2.6:** The cardiac cycle showing various configurations of the heart during each phase (Betts et al. (2018)).

### 2.1.3 Left Ventricle

The left ventricle is responsible for the perfusion of tissues in the human body, having the highest mechanical load amongst the other chambers of the heart. In this high pressure environment, it is important that all the biochemical, electro-physiological and biomechanical processes work in tandem while maintaining a state of homeostasis. Any alterations in these processes could impact the performance, function and structure of the ventricle which consequently impacts the body as a whole. Not all changes in these processes would have deleterious implications, but the ones which do negatively impact health lead more often than not to death or severely impaired survival conditions. Interest lies in the growth and remodelling of the myocardial tissue of the left ventricle in response to a myocardial infarction, and understand the changes in the structure and function on the global organ scale due to changes in the micro-structural extra-cellular matrix. These concepts are discussed briefly below.

#### 2.1.3.1 Left Ventricular Biomechanics

The primary role of the LV is to supply blood to every cell and tissue in the human body. It works on the principle of pressure gradients between blood pressures between itself and the left atrium for diastole; and the aorta for systole. The performance of the LV is dependant on factors such as the size and shape of LV, the contractile capabilities of the myocardium, valve function and the ventricular loading (Voorhees & Han (2011)).

The mechanics of the left ventricle is encapsulated succinctly by the depiction of the pressure-volume relationship diagram (Figure [2.7]). Particularly, the cardiac cycle or a heart beat is divided into two phases i.e. systole, where in the cardiac muscles contract actively to generate enough force to pump blood into the circulatory systems and diastole the period in which the ventricular wall relaxes followed by the filling of the LV via inflow of blood from the left atrium. Using the Figure[2.7] as a reference tissue biomechanics are described in conjunction with each phase in the PV relationship.

1. Filling Phase:

As the right atrium contracts undergoing systole, the left ventricle is filled with blood at a pressure of about 8 mmHg, abnormalities are observed if the pressure exceeds 16mm Hg (Paulus et al. (2007), Peterson et al. (1978)). As the filling continues upto point point A, the mitral valve and the aortic valves are closed shut. This terminates the filling phase and the ventricle is prepared to undergo contraction and towards the ejection phase.

2. Isovolumetric Contraction Phase:

After the filling phase ends, the valves being shut the electric activation potential propagates through the cardiomyocyte bundles in the LV and on the inter-linking of acto-myosin protein bonds within the cells they collectively undergo isovolumetric contraction. This works towards raising the fluid pressure against the aortic valve and once the pressure in the

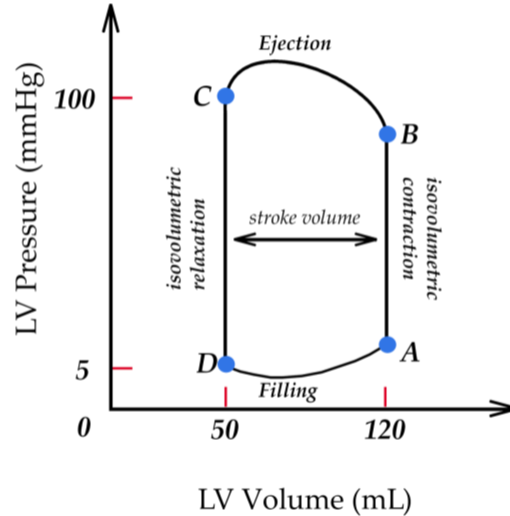


**Figure 2.7:** Pressure Volume Loop, adapted from *Guyton & Hall (2006)*

aorta is lower than the LV cavity pressure the ejection of the blood can begin. The increase in pressure is drastic, from around 8 mmHg to 80 mmHg.

### 3. Ejection Phase:

The pressure difference in the LV cavity and aortic vessel causes the aortic valve to open up and blood gushes out from the LV into the circulatory systems. During this period the cardiac muscle contracts in a helical pattern, and the contraction in the endocardium differs from the epicardium owing to the orientation of the myo fibres. This causes the pressure to increase upto 120 mmHg and after the ejection of blood the muscle starts to relax and the end of systole is marked by point C known as End Systolic Pressure, around 100 mmHg.

### 4. Isovolumetric Relaxation Phase:

At the end of systole the LV muscle, the cardiomyocytes begin a relaxation phase, due to the valves being closed the volume in the LV is preserved and the phase is termed as isovolumetric relaxation. There is a sharp drop in pressure as the cardiomyocytes get depolarised and no longer exert a high pressure which was needed to eject the blood into the circulatory system. This drop goes from about 100 mmHg to about 5 mmHg. Thus, the LV is ready to begin the cycle again from filling to ejection.

A few important concepts which can be derived from the PVR loop, useful for clinical purposes are defined below:

#### 1. Stroke Volume:

The difference between the end-diastolic volume (EDV) and the end-systolic volume (ESV)

is the stroke volume.

$$SV = EDV - ESV$$

. For a healthy individual the optimum stroke volume is around 50-70 mL.

2. Ejection Fraction:

It is defined as the amount of blood ejected from the left ventricle during systole, mathematical formulation is as:

$$EF = \frac{SV}{EDV} \times 100\%$$

3. Potential Energy:

The total area bounded under the End Systolic Pressure Volume Relationship curve (ESPVR) and above End Diastolic Pressure Volume Relationship curve (EDPVR), represents the potential energy in the left ventricle.

4. Work Done:

The area bounded by the pressure volume loop itself accounts for the stroke work done by the left ventricle in the ejection of the blood into the circulatory systems.

### 2.1.3.2 Frank Starling Mechanism

The principle behind the Frank-Starling mechanism states that "within physiological limits, the force of heart contraction is directly proportional to the initial length of the fibre", ([Betts et al. \(2018\)](#), [Boron & Boulpaep \(2012\)](#)). Indicating that greater the stretch of the left ventricular muscle architecture at end diastole, results in a higher magnitude of contraction terminally increasing the stroke volume (SV) and blood supply to the circulatory systems. If there is an increase in the venous return of blood to the heart, due to sympathetic stimulation or increase in body demand; would result in a greater distension of the left ventricle in the filling phase. Thereby, increasing its contractility. Though Otto Frank and Ernest Starling worked as independent physiologists, their similar conclusions have been together termed as the "Frank-Starling mechanism" ([Betts et al. \(2018\)](#)).

### 2.1.3.3 Myocardial Extra-Cellular Matrix Biomechanics

In mechanical terminology, the cardiac pressure-volume diagram is again the best depiction, to help understand the configurations of the cardiomyocytes, the collagen extra-cellular matrix, elastin and the various other constituents present in the myocardium. The pressure-volume loop is read in the anti-clockwise direction as can be observed in the description provided above. The area within the loop represents the work done by the LV i.e. the stroke work, showing the amount of energy imparted to the blood within LV by the myocardial wall.

The myocardium is a composite material, primarily made up of cardiac muscle cells (cardiomyocytes), the extra-cellular matrix. The mechanical characteristics, properties and behaviour of the

myocardial tissue are determined by the properties of its constituents. During the loading of the myocardium by intra-ventricular filling, the intracellular cardiomyocyte protein titin is responsible for the passive mechanical response/ characteristic of the tissue. this is due to the stiffness of a titin molecule helps maintain structural integrity of cardiomyocytes against excessive extension and the high population of cardiomyocytes in the myocardium. Therefore, under small deformations in the LV it is considered the primary determinant of LV mechanical properties (Hein et al. (2002)). The active contractile function of the myocardium is ascribed to the actin-myosin motor filaments interaction, due to the activation by the electric potential the  $Ca^{2+}$  ions (either through the ion gates or from the endoplasmic reticulum depending on the effect of noripinephrine, or neurotransmitters) molecules bind with the actin-myosin complex. This causes the attachment of the myosin heads to the actin filaments and they slide against each other depending on the load experienced by the cardiomyocyte and the amount of  $Ca^{2+}$  ions molecules. This is in part described by the Frank-Starling mechanism which states the amount passive filling stretch the cardiomyocyte experience causes an equal amount of contractile force during systole. Therefore, while the passive properties are determined by the titin molecule majorly, the active properties are described by the acto-myosin interaction within the cardiomyocyte (Guyton & Hall (2006)).

Other than the cardiomyocytes, the extra-cellular matrix also contributes to the mechanical function of the LV. Elastin, a structural protein existing as long, thin fibres and are encased within a layer of microfibrils, a class of proteins (Shadwick (1999b)). The elastic fibres have a similar elastic behaviour as that of the titin and therefore share a similar stress-strain profile, however knowledge on elastin's contribution to the healthy myocardial stress response is limited and needs further studies to be done. Another important constituent i.e. the proteoglycans which regulate the water content in tissues their function in the myocardium is still not well understood (Fomovsky et al. (2010), Linke et al. (1994)).

Apart from elastin, proteoglycans; the collagen extra-cellular matrix provides structural integrity, binding sites for cells supporting their proliferation, migration and signalling mechanisms. The primary role of the collagen fibres is to prevent the overstretch of the cardiomyocytes in the healthy myocardium and to provide attachment sites for them to enable transmission of the contractile forces to the tissue (Voorhees & Han (2011)).

### 2.1.4 Myocardial Infarction

If a coronary artery's lumen is partially or completely occluded, it results in the disruption of oxygenated blood required by the myocardial region perfused by it for healthy functioning, leading to a condition known as ischaemia. In situations where the nutrients and oxygen supply is interrupted, cardiac myocytes undergo necrosis as early as in under 30 minutes (Turillazzi et al. (2014)). If not reperfused well within the critical time window, the myocytes would undergo permanent necrosis culminating in a scar tissue. The scar tissue is passive in nature, as myocardium lacks the ability to regenerate in order to replace lost cells. This triggers a cascade of overlapping events which can be delineated into the inflammation phase, proliferation phase and the maturation/fibrosis phase. Though they occur in a particular order, clear distinctions is difficult between the phases as some stages may overlap with others(Chen & Frangiannis (2013), Czubryt (2012), Talman & Ruskoaho (2016)).

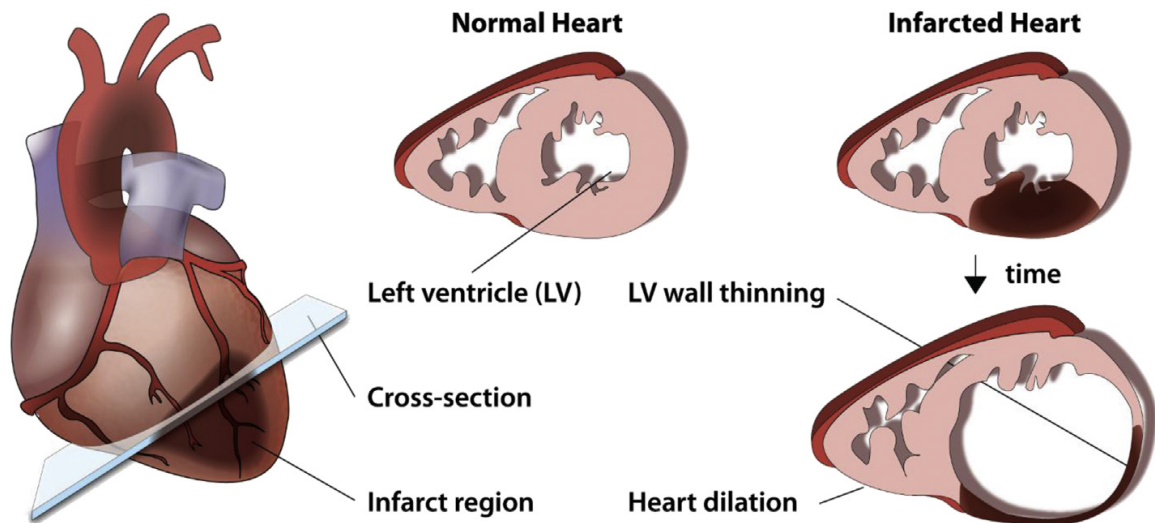


**Figure 2.8:** *The effect of a myocardial infarction on a region of myocardium. Dilatation and thinning due to cardiomyocyte necrosis and pathological adaptation by collagen fibrosis is observed (Awada et al. (2016)).*

Eventually the infarcted myocardium dilates over the progression of the disease, forming a stiff collagenous scar tissue and thinning of the myocardium affects not only the infarcted region but the non-infarcted region as well [Figure2.8]. (Awada et al. (2016)).

The Figure [2.9], attempts to detail the phases involved in the tissue remodelling post myocardial infarction. According to (Fraccarollo et al. (2012), Sutton & Sharpe (2000)), the phases are arbitrarily divided into an early phase which occurs within 72 hours post-MI, and a late remodelling phase (after 72 hours).

#### Early Remodelling Phase

Injured myocytes due to ischaemic conditions, trigger the infiltration of immune cells i.e. neutrophils, macrophages and proteolytic enzymes such as Matrix-metalloproteinases (MMPs) which

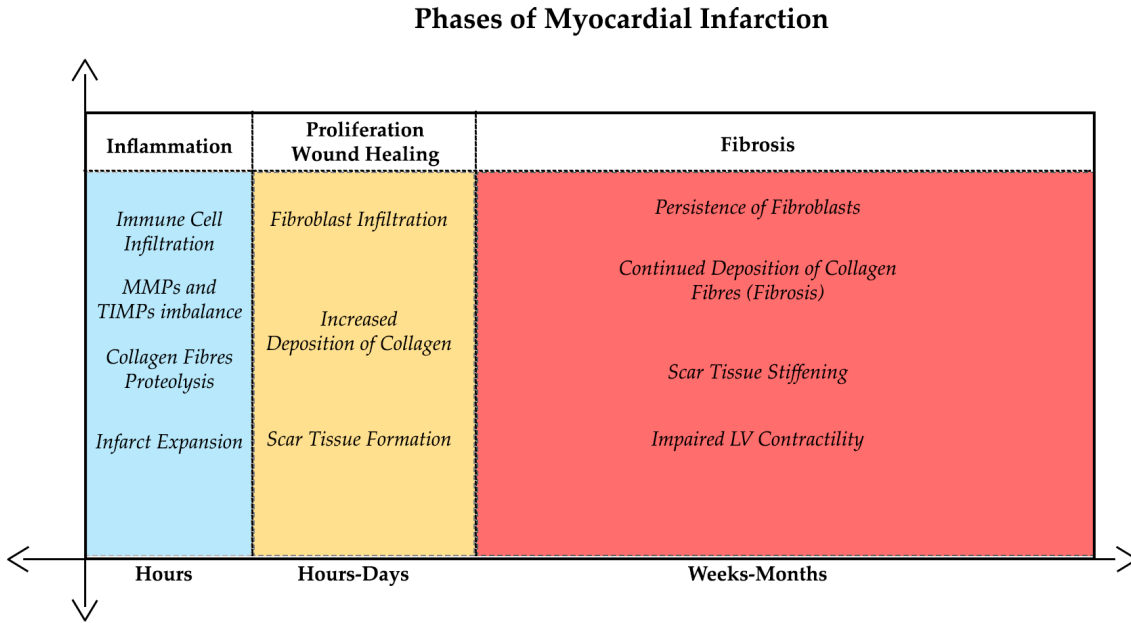


**Figure 2.9:** The various phases involved after the onset of a myocardial infarction in the myocardial tissue. It can roughly be divided into an early phase and late remodelling phase where the inflammation constitutes the early phases and wound healing, fibrosis reflects the late phase of remodelling (Fraccarollo et al. (2012), Sutton & Sharpe (2000)). There could be proliferation could overlap between the early and late phases as well, thus they are shown as a distinct section.

causes the degradation of the collagen struts between myocytes, within 3 hours of infarction. This leads to cardiomyocyte slippage resulting in wall thinning, dilatation of the ventricle and increased wall stresses from internal blood pressure variations in the cardiac cycle. Elevated wall stresses disrupt the performance and function of the ventricle, causing the viable (surviving) myocardium to undergo hypertrophy in order to compensate for the loss in myocardial contractile ability. Wall stress is an important factor for determination of structure and function of the LV. This initial dilatation and thinning of the myocardial wall after the onset of infarction is known as infarct expansion, which is well documented in humans known to occur within hours after the onset of myocardial infarction (Sutton & Sharpe (2000)). This initial event can be classified as the inflammation phase wherein due to the action of immune cells, and proteolytic enzyme up-regulation the strength of the myocardial wall is reduced.

### Late Remodelling Phase

The early phase of remodelling is followed by a proliferation of fibroblast cells in the infarcted region (also termed as infarcted zone - IZ), in an effort to re-adjust the lost tissue integrity and structure. The time period between proliferation of fibroblasts and excess collagen deposition occurs, the infarcted myocardium is particularly prone to distorting forces from internal blood pressure. Infarct expansion is said to occur in this time period (Hochman & Bulkley (1982), Kass et al. (1988)). Given the heart's inability/ limited regenerative capacity of cardiomyocyte synthesis, the infarcted tissue matures into a non-cellular extensively cross-linked collagenous

scar tissue which is relatively stiffer than the tissue stiffness during infarct expansion. Fibroblasts transdifferentiate into myofibroblasts(myoFb) which have an increased deposition rate of collagen fibres and proliferate not only in the infarcted region but throughout the left ventricle. The stiff scar tissue interferes with systolic function, because of the loss in contractility of the tissue and therefore it fails to generate adequate force to maintain a healthy ejection fraction (fraction of blood pumped out of the heart through the aorta). Moreover, diastolic filling may lead to secondary volume overload and due to the tissues reduced overall strength post infarction the internal blood pressure might produce stress on the LV wall which exceeds its capability to compensate with adequate cardiomyocyte stiffness, contributing to a possible pressure-overload as well. Fibroblasts are known to exist in the myocardial tissue long after the scar tissue has been formed and healed, leading to progressive fibrosis years after the event of myocardial infarction. Therefore, not only is the infarcted zone affected but the ventricle stiffens overtime leading to complications which could result ultimately in heart failure.

#### **2.1.4.1 Biomechanics of the Infarcted Myocardium**

Given the mechanical contributions of the cardiomyocytes, collagen fibres and ground matrix, it is important that these tightly coupled microstructural constituents maintain a balance in their function to achieve healthy heart function throughout the cardiac cycle. Implying the cardiomyocytes achieve optimum contractility during systole and muscle relaxation to facilitate diastolic filling in response to changing physiological needs per beat, the ground matrix maintain the 5-10 % volume change (reference-bodhjugdutts paper) during wall deformation and the collagen fibres in its balanced continual state of synthesis/ degradation due to enzymatic action of chemicals, fulfil their role of protecting the cardiac muscle from abrupt deformations. However, during ischaemic disease, the necrosis of cardiomyocytes impacts the active and passive mechanical properties of the myocardial wall. Loss of contractility is observed due to loss in functioning cardiac cells, it triggers the proteolytic action of MMPs which degrades the collagen matrix and leads to edema of the tissue causing interstitial fluids to enter the cardiac chamber and the muscular wall.

Leading to infarct expansion early on post-MI causes the myocardium to be susceptible to rupture or incessant dilatation due to loss in stiffness. This in turn causes increased diastolic blood volume, as well as increased pressure on the myocardial wall by the action of atrial systole. This high pressure needs to be compensated, thereby causing the surviving myocytes to undergo hypertrophy either by thickening or thinning by parallel/ serial addition of sarcomeres due to a secondary pressure overload or consequent volume overload respectively. Importantly, systolic dysfunction is a major outcome of such infarct expansion as the ejection fraction is reduced even though stroke volume is maintained and the weak infarcted tissue is prone to develop aneurysms or in high risk cases rupture. Over time due to proliferation of fibroblasts, transdifferentiation to myofibroblasts causing increased deposition of collagen, there is an inverse change in the myocardial tissue stiffness. A stiff scar tissue causes complications in the filling of the ventricle due to reduced compliance, result of cross-linked highly fibrous collagenous tissue. In turn the

ejection of blood is hampered due to the passive scar tissue, forcing other cardiomyocytes to be restricted in terms of active contraction and extension during diastole. These complications therefore, interfere with the mechanical output of the left ventricle leading to Congestive Heart Failure (CHF), cardiac arrhythmia or ultimately death.

### **2.1.5 Treatment and Medical Intervention**

Therapy and treatment of myocardial involves either surgery or prescription of drugs, both of which focus heavily on the re-perfusion of the scar tissue, in order to save healthy cardiomyocytes which in turn help retain some (or all) of the hearts' functionality. The atheroma(plaque deposition) within the coronary blood vessels of the heart majorly cause ischaemic, leading to cardiomyopathy. Pharmacological intervention aims at thrombolysis of the atheroma and increase re-perfusion to the ischaemic myocardium; resulting in the salvage of the cardiomyocytes within the ischaemic region([Sutton & Sharpe \(2000\)](#)) .

#### **2.1.5.1 Pharmacological Intervention**

The several pharmacological intervention techniques are listed below in some detail.

1. *Nitroglycerin*: Intravenous nitroglycerin is beneficial for limiting infarct size, expansion and other complications as well as mortality for upto 1 year. However, nitrate therapy is not recommended after the first 24 hours following a myocardial intervention except for persistent ischaemic, hypertension or heart failure.
2. *ACE Inhibition*: Angiotensin Converting Enzyme Inhibition is related to peripheral vasodilation, ventricular unloading and the attenuation of chamber dilatation. This may have a direct effect on the myocardial tissue, helping prevent inappropriate growth and hypertrophy simulated by Angiotensin II and other growth factors. This treatment is recommend for patients with left ventricular dysfunction or heart failure without delay after an infarction.
3.  *$\beta$  Blockade*: Little has been studied about the effects of Blockades on post infarction left ventricular remodelling. However, preliminary results suggest it may attenuate remodelling, with a significant decrease in subsequent adverse cardiac events.
4. *Statins*: Statistically, statins have proved in a small but significant reduction in in-hospital mortality, given their administration to patients in the early hours following a myocardial infarction. The beneficial effects that are thought to be responsible for the stabilisation of atherosclerotic plaque induced by statins, include its influence on the endothelial function and impact on the inflammatory response ([Martínez et al. \(2013\)](#)).

Other than pharmacological intervention, surgical techniques such as Percutaneous Coronary Intervention (PCI) and Coronary Angiography Bypass Grafts (CABG) are employed to improve re perfusion to the ischaemic cardiac tissue to help restore cardiac function ([Thygesen et al. \(2012\)](#)).

## 2.2 Pertinent Concepts in Continuum Mechanics

The requisite information about non-linear continuum mechanics, are discussed, for utility in our modelling purposes. The concepts have been referred from the textbook (Chapter 4, [Bonet & Wood \(1997\)](#)) and can be consulted for detailed derivations.

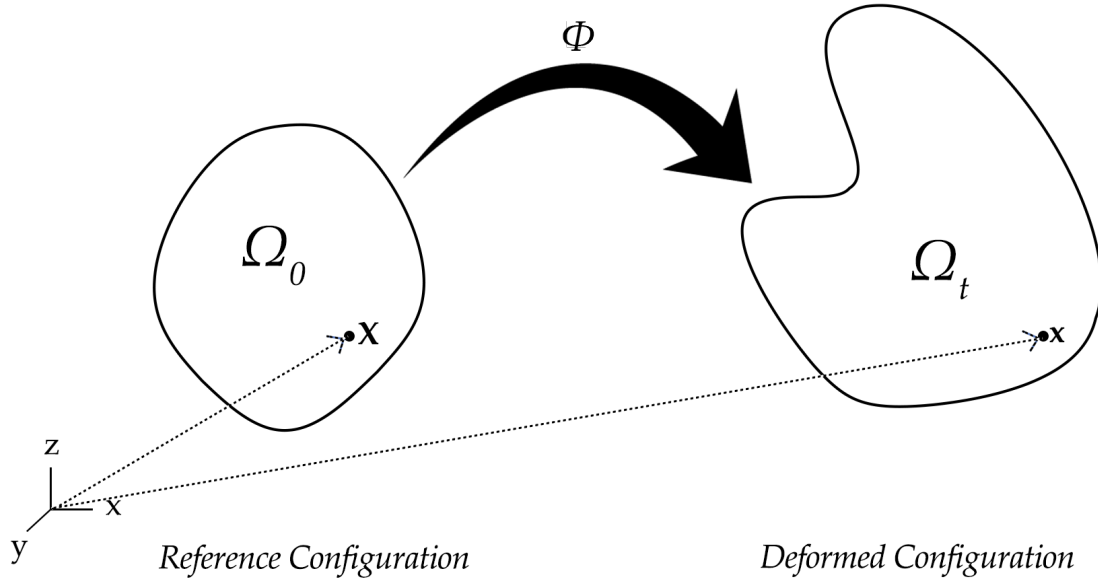


**Figure 2.10:** The image displays the material particle  $\mathbf{X}$  in the unloaded reference configuration ( $\Omega_0$ ) and its position after deformation in the current reference configuration ( $\Omega_t$ ), denoted by  $\mathbf{x}$ . The deformation is a result of mechanical stimuli acting either externally or internally in the continuum body.

### 2.2.1 Motion of a Continuum Body

A continuum body is considered to be an assembly of continuous material points or particles, without any gaps in the continuity. These particles in their initial state are denoted by  $\mathbf{X}$  with respect to a Cartesian basis vector  $E_1$ , at an initial time ( $t = 0$ ). The material particle at a time point ( $t$ ) is represented by the variable  $\mathbf{x}$  with respect to an alternate Cartesian basis  $e_i$ . The change in position of the material particle between the two time points (Figure[2.10]) is shown as:

$$\mathbf{x} = \phi(\mathbf{X}, t) \quad (2.1)$$

The body in the initial time ( $t = 0$ ) and a further point in time ( $t$ ) where the material particles are displaced, is called the undeformed body/ configuration ( $\Omega_0$ ) and deformed body/ configuration ( $\Omega_t$ ). The mapping between the two material points is shown as  $\mathbf{u} = \mathbf{x} - \mathbf{X}$ , known as the displacement.

### 2.2.2 Deformation

A key component in mechanical analysis of continuum bodies is the deformation gradient ( $\mathbf{F}$ ). It enables the spatial position of two neighbouring material particles or points after deformation to be mapped to their relative positions in the body prior to deformation i.e. from  $(\Omega_t)$  to  $(\Omega_0)$ . It is involved in the derivation of strains and hence stresses experienced by the body. As defined in (Bonet & Wood (1997)) the formulation is as:

$$F = \frac{\partial \phi}{\partial \mathbf{X}} = \nabla_0 \phi = \sum \frac{d\mathbf{x}_i}{d\mathbf{X}_I} e^i E^I \quad (2.2)$$

The deformation gradient in essence provides an understanding of the displacement of a material point between the two configurations  $(\Omega_0)$  and  $(\Omega_t)$ . This is mathematically shown as the

$$\mathbf{x} = \phi(\mathbf{X}, t) = \mathbf{X} + \mathbf{u}(\mathbf{X}, t)$$

### 2.2.3 Strain Measures

The right Cauchy Green material deformation tensor  $\mathbf{C}$  is given in terms of  $F$ , it provides us with a quantity which is a square of the deformation of an element in the reference (undeformed) to the current(deformed) configuration.

$$\mathbf{C} = \mathbf{F}^T \mathbf{F} \quad (2.3)$$

An alternative representation is the left Cauchy Green deformation tensor.

$$\mathbf{b} = \mathbf{F} \mathbf{F}^T \quad (2.4)$$

These quantities help us derive the Green-Lagrange strain measure, which is calculated as:

$$\mathbf{E} = \frac{1}{2}(\mathbf{C} - \mathbf{I}) \quad (2.5)$$

### 2.2.4 Polar Decomposition

The deformation between material points  $\mathbf{X}$  to  $\mathbf{x}$  involves both stretch and rotational components which completely defines the movement of the material points. Therefore, the deformation gradient can be decomposed into the rotational stretch tensor ( $\mathbf{R}$ ) multiplied with a stretch tensor ( $\mathbf{U}$ ).

$$\mathbf{F} = \mathbf{R} \mathbf{U} \quad (2.6)$$

A few important derivations from the above quantities are defined in the following equations, which will find use in our growth and remodelling algorithms discussed in Chapters [4, 6, 7].

$$\mathbf{C} = \mathbf{F}^T \mathbf{F} = \mathbf{U}^T \mathbf{R}^T \mathbf{R} \mathbf{U} \quad \mathbf{C} = \mathbf{U}^2 \quad (2.7)$$

### 2.2.5 Volume Changes in Continuum body

On considering an infinitesimal unit volume with edges parallel to the Cartesian axes, given by  $dX_1 = dX_1 E_1$ ,  $dX_2 = dX_2 E_2$ ,  $dX_3 = dX_3 E_3$ , where  $E_I$ ,  $I = 1, 2, 3$  are the orthogonal unit vectors. The scalar triple product gives us the volume of the material element. Note: the edge vectors  $dX_i$  can be understood as the vector obtained by the formulation  $\mathbf{X} - \mathbf{O}$ , where  $\mathbf{X} = \{X_1, X_2, X_3\}$  and  $\mathbf{O}$  is the origin  $\{0, 0, 0\}$  with  $dX_1 = X_1 - O_1$ ,  $dX_2 = X_2 - O_2$  and  $dX_3 = X_3 - O_3$ . This may not necessarily be the case for a continuum body, and the edge vectors can be an infinitesimal volume within that body in 3D space.

$$dV = dX_1 dX_2 dX_3. \quad (2.8)$$

The deformed elements in  $\Omega_t$  can be calculated as:

$$dx_i = F dX_i \quad i = 1, 2, 3 \quad (2.9)$$

The corresponding volume in the ( $\Omega_t$ ) is mapped to undeformed volume (in  $\Omega_0$ ) as  $dv = J dV$  where,  $dv = dx_1 \cdot (dx_2 \times dx_3)$ . This leads to the formulation of the Jacobian of the deformation gradient, which gives us an idea about the deformed volume to the initial undeformed volume.

$$J = \det[\mathbf{F}] \quad (2.10)$$

In the context of compressible and nearly incompressible materials, the deformation gradient is separated into a multiplicative decomposition of a volumetric component and an isochoric (distortional) component.

$$\begin{aligned} \mathbf{F} &= \mathbf{F}_{vol} \cdot \mathbf{F}_{dev} \\ \mathbf{F}_{vol} &= \mathbf{J}^{1/3} \mathbf{I} \\ \mathbf{F}_{dev} &= \mathbf{J}^{-1/3} \mathbf{F} \end{aligned} \quad (2.11)$$

Wherein, the distortional or deviatoric component ( $\mathbf{F}_{dev}$ ) does not imply any volumetric changes dealing only with elastic deformations. Given the volume ratio is obtained by the determinant of  $F$ , an incompressible material must satisfy:

$$\det[\mathbf{F}_{dev}] = 1 \quad (2.12)$$

The quantities defined herein, and the incompressibility assumption allows us to proceed and formulate the necessary equations, stress measures and strain measures for our models.

### 2.2.6 Stress Measures

By the principle of virtual work, the equilibrium condition over a body is given as:

$$\delta W = \int_v (\text{div } \boldsymbol{\sigma} + \mathbf{f}) \cdot \delta \mathbf{v} dv = 0 \quad (2.13)$$

where,  $\boldsymbol{\sigma}$  is the Cauchy stress Tensor,  $\mathbf{f}$  is the force acting on a unit volume of the body,  $\delta W$  is the virtual work through the volume of body.  $v$  is the volume of the body while  $dv$  is a unit volume, and  $\delta \mathbf{v}$  is an arbitrary virtual velocity form a current position on the body.

The stress quantities relevant for our research, is derived from Equation[2.13] depending on the deformation gradient  $\mathbf{F}$ , for complete derivations please refer to (Bonet & Wood (1997)).

#### First Piola-Kirchhoff Stress Tensor

The first PK Tensor, is a two-point tensor as it is a measure of the force acting in the current/ deformed configuration ( $\Omega_0$ ), to the surface are in the undeformed/ reference configuration ( $\Omega_t$ ). Mathematically formulated as:

$$\mathbf{P} = J \boldsymbol{\sigma} \mathbf{F}^{-T} \quad (2.14)$$

#### Second Piola-Kirchhoff Stress Tensor

The first PK tensor is not completely related to the material configuration, and is an unsymmetric two-point tensor. The second Piola Kirchoff tensor is a measure of the force acting on the undeformed configuration to the surface area element in the undeformed configuration. This allows us to conveniently derive stress tensors with Cauchy Green Deformation gradients, while deriving stresses from strain energy functions, which are fundamental to our models discussed in Chapters [3, 4, 6, 7].

$$\boldsymbol{\sigma} = J^{-1} \mathbf{F} \mathbf{S} \mathbf{F}^T \quad (2.15)$$

The concepts introduced in this section will be utilised in the forthcoming chapters and any further derivation as necessary will be documented in pertinent sections. This has been done so that the general concepts for modelling a 1D constrained mixture model and finite element models have the same continuum basis, but their implementation differs due to the analytical and numerical nature of the two models.

### 2.3 Soft Tissue Constitutive Models

Soft tissues are treated as continuum bodies, i.e. bodies which have a continuous mass distribution without any holes or gaps. The myocardium undergoes large deformations due to the high pressure loading conditions in a non-linear, heterogeneous characteristic behaviour due to the composite material constituents. It's anisotropic nature has been identified and tested experimentally owing to its unique fibre architecture (Holzapfel & Ogden (2009)), although it has been modelled as an isotropic, transversely isotropic and orthotropic materials in past models. Also, owing to the water content within the wall and the relatively preserved tissue volume it is also considered to be incompressible. The theory of continuum mechanics is most appropriate to model such tissue behaviour and stress, strain formulations are based on general constitutive equations typically formulated as:

$$\sigma = \frac{2}{J} \mathbf{F} \frac{\partial W}{\partial \mathbf{C}} \mathbf{F}^T \quad (2.16)$$

where,

**F** - deformation gradient

**J** - Jacobian of the deformation gradient

**C** - Right Cauchy Green Tensor

**W** - Strain Energy Density Function

On perusing the equation above it can be seen that the stress-strain profile or behaviour of soft tissues can be described using various forms of strain energy density functions. (Fung et al. (1993)) originally proposed an exponential strain energy function to describe the non linear anisotropic stress-strain response of tissues and is the most widely employed function:

$$W = \frac{1}{2} c (e^Q - 1) \quad (2.17)$$

where in  $c$  is a material constant and  $Q$  is an equation which can be chosen to represent the anisotropic behaviour of the material tissue under consideration (Voorhees & Han (2011)). (show papers using different values for  $Q$ ) The Table [2.2] below details the various constitutive models that have been employed to represent the cardiac tissue, by no means exhaustive:

No.	Article	Strain Energy Density Function	Material Property
1	<a href="#">Humphrey et al. (1990)</a>	$W(I_1, \alpha) = c_1(\alpha - 1)^2 + c_2(\alpha - 1)^3 + c_3(I_1 - 3) + c_4(I_1 - 3)(\alpha - 1) + c_5(I_1 - 3)^2$	Transversely Isotropic
2	<a href="#">Holzapfel &amp; Ogden (2009)</a>	$\Psi(I_1, I_{4s}, I_{4f}, I_{8fs}) = \frac{a}{2b} \exp[b(I_1 - 3)] + \sum_{i=f,s} \frac{a_i}{2b_i} \exp\{[b_i(I_4 i - 1)^2] - 1\} + \frac{a_{fs}}{b_{fs}} \{\exp[b_{fs} I_{8fs}^2] - 1\}$	Transversely Orthotropic
3	<a href="#">Göktepe et al. (2011)</a>	$\Psi(I_1, I_{4s}, I_{4f}, I_{8fs}) = \frac{a}{2b} \exp[b(I_1 - 3)] + \sum_{i=f,s} \frac{a_i}{2b_i} \exp\{[b_i(I_4 i - 1)^2] - 1\} + \frac{a_{fs}}{b_{fs}} \{\exp[b_{fs} I_{8fs}^2] - 1\}$	Transversely Orthotropic
4	<a href="#">Wenk et al. (2011)</a>	$W_{passive} = \frac{\xi}{2} [\exp(b_f E_{11}^2 + b_t (E_{22}^2 + E_{33}^2 + E_{23}^2 + E_{32}^2) + b_{fs} (E_{12}^2 + E_{21}^2 + E_{13}^2 + E_{31}^2) - 1)]$	Transversely Isotropic
5	<a href="#">Kerckhoffs (2012)</a>	$W = \frac{1}{2} c_{pas} (e^Q - 1) + c_{comp} ((\det[\mathbf{F}] - 1) \ln(\det[\mathbf{F}])) / 2$ $Q = b_f E_{ff}^2 + b_c (E_{cc}^2 + E_{rr}^2 + E_{cr}^2) + b_f (2E_{fc}^2 + 2E_{fr}^2)$	Transversely Isotropic
6	<a href="#">Oomen et al. (2018)</a>	$\Psi = (1 - \phi_f) \Psi_m + \phi_f \Psi_f = \frac{k}{2} \ln^2(J_e) + \frac{\mu}{2} (I_{1,e} - 3 - 2 \ln(J_e))$ $\Psi_f^i = \frac{k_1}{2k_2} \{\exp[k_2 < (\lambda_e^i)^2 - 1 >] - 1\}$	Anisotropic
7	<a href="#">Zhuan et al. (2019)</a>	$\Psi = \Psi_m + \Psi_{cf}$ $\Psi_m = \frac{a}{2b} \{\exp[b(I_1 - 3)] - 1\}$ $\Psi_{cf} = \frac{a_{cf}}{2b_{cf}} \{\exp[b_{cf} (I_4(\theta) - 1)^2] - 1\}$	Transversely Orthotropic

**Table 2.2:** List of constitutive models developed for the myocardium. Where in  $W$  and  $\Psi$  represent notations used to define the Strain Energy Density Function in each constitutive model.

In (Humphrey et al. (1990)), the excised passive myocardial tissue is assumed to be nearly incompressible, pseudo elastic and transversely isotropic. The strain energy function is a function of four co-ordinate invariants of deformation  $W = W(I_1, I_2, I_4, I_5)$ , and on obtaining results from mechanical testing of excised tissue, the strain energy function of the following form has been formulated:

$$W(I_1, \alpha) = c_1(\alpha - 1)^2 + c_2(\alpha - 1)^3 + c_3(I_1 - 3) + c_4(I_1 - 3)(\alpha - 1) + c_5(I_1 - 3)^2 \quad (2.18)$$

where,  $\alpha > 0$ , is the stretch ratio in the muscle direction,  $c_{ij}$  are material parameters and  $I_1$  is the first invariant of deformation. The passive constitutive model of the myocardium, characterised in (Holzapfel & Ogden (2009)) the strain energy function is a function of the invariants in the fibre(f), sheet(s) and normal(n) directions (see (Nash & Hunter (2000))), formulated as:

$$\Psi(I_1, I_{4s}, I_{4f}, I_{8fs}) = \frac{a}{2b} \exp[b(I_1 - 3)] + \sum_{i=f,s} \frac{a_i}{2b_i} \exp\{[b_i(I_{4i} - 1)^2] - 1\} + \frac{a_{fs}}{b_{fs}} \{\exp[b_{fs} I_{8fs}^2] - 1\} \quad (2.19)$$

where  $a, b, a_f, a_s, b_f, b_s, a_{fs}$  and  $b_{fs}$  are eight positive material constants, with  $a$  parameters having units of stress while  $b$  parameters is a dimensionless quantities. The terms contributing to the isotropy of the strain energy is  $I_1$ , transversely isotropic invariants  $I_{4f}$  and  $I_{4s}$ , whereas the orthotropic term is in  $I_{8fs}$ . The strain energy function employed in (Göktepe et al. (2011)), is the same function introduced in (Holzapfel & Ogden (2009)), applied to a biventricular finite element model. The transversely isotropic strain energy function, with respect to the local fibre directions in the passive myocardium (Wenk et al. (2011)) has the form:

$$W_{passive} = \frac{C}{2} [\exp(b_f E_{11}^2 + b_t(E_{22}^2 + E_{33}^2 + E_{23}^2 + E_{32}^2) + b_{fs}(E_{12}^2 + E_{21}^2 + E_{13}^2 + E_{31}^2) - 1)] \quad (2.20)$$

where,  $C, b_f, b_t$  are material parameters of the myocardium, in diastolic configuration.  $E_{11}$ , fibre direction strain, the cross fibre in-plane strain  $E_{22}$  and radial strain transverse to the fibre direction is denoted by  $E_{33}$  while the remainder of terms are associated with shear strains experienced by the tissue. In the computational modelling of growth in a post-natal rat heart, using a strain-based law (Kerckhoffs (2012)), the slightly incompressible and transversely isotropic strain energy function was given to be:

$$W = \frac{1}{2} c_{pas}(e^Q - 1) + c_{comp}((\det[\mathbf{F}] - 1) \ln(\det[\mathbf{F}]))/2$$

$$Q = b_f E_{ff}^2 + b_c(E_{cc}^2 + E_{rr}^2 + E_{cr}^2) + b_f(2E_{fc}^2 + 2E_{fr}^2) \quad (2.21)$$

where,  $\mathbf{F}$  is the deformation gradient,  $E_{xx}$  for  $(xx = ff, rr, cc)$  are the strains in the muscle fibre direction ( $f$ ), transmural radial direction ( $r$ ) transverse to fibre direction and the cross-fibre direction ( $c$ ) perpendicular to radial and transmural direction. The other parameters associated with shear strains. material parameters are denoted by  $C_{pas}, C_{comp}, b_f, b_c$  and  $b_{fr}$ . The hyperelastic constitutive model to characterise a fibre reinforced material behaviour for heart valve is

composed of an isotropic matrix part ( $m$ ) and anisotropic fibrous part ( $f$ ), represented by the strain energy function:

$$\Psi = (1 - \Phi_f)\Psi_m + \Phi_f\Psi_f \quad (2.22)$$

with the individual strain energy functions described as:

$$\begin{aligned} \Psi_m &= \frac{\kappa}{2}\ln^2(J_e) + \frac{\mu}{2}(I_{1,e} - 3 - 2\ln(J_e)) \\ \Psi_f^i &= \frac{k_1}{2k_2}(\exp[k_2((\lambda_e^i)^2 - 1) - k_2((\lambda_e^i)^2 - 1) - 1]) \end{aligned} \quad (2.23)$$

Herein, the  $\Phi_x$  denotes the volume fractions for  $m$  and  $f$ , which are arbitrarily chosen as 0.5 and the subscript  $e$  is used to denote dependence on only the elastic deformation of the body.  $\kappa$  is the bulk modulus,  $\mu$  is the shear modulus and  $I_{1,e}$  is the first invariant of deformation. The strain energy function per individual fibre( $i$ ) is modelled with  $\Psi_f^i$ , where  $k_1, k_2$  are material parameters and  $\lambda_e^i$  are the fibre stretches. (Zhuan et al. (2019)), also applies an approach with volume fractions associated with a matrix ( $m$ ) component and fibrous ( $cf$ ) component, wherein the infarcted tissue's mechanical behaviour is described as:

$$\Psi = \Phi_{m,t}\Psi_m + \Phi_{cf,t}\Psi_{cf} \quad (2.24)$$

wherein the volume fractions are represented by  $\Phi_x$ , where  $x = m, cf$  for the matrix and fibrous components. The specific forms for the strain energy functions are given as:

$$\begin{aligned} \Psi_m &= \frac{a}{2b} \{\exp[b(I - 1 - 3)] - 1\} \\ \Psi_{cf} &= \frac{a_{cf}}{2b_{cf}} \{\exp[b_{cf}(I_4(\theta) - 1)^2] - 1\} \end{aligned} \quad (2.25)$$

where,  $a, b, a_{cf}, b_{cf}$  are material parameters and  $I_1, I_4$  are stretch invariants. This material model is further analysed in Section[2.5].

## 2.4 Soft Tissue Growth and Remodelling

Ranging from cells to tissues and thereafter the human body, there is an innate capability of maintaining a homoeostatic level in terms of temperature, circulatory flow, electrical conduction and mechanical responses. It implies that the body maintaining a healthy state is not a static phenomena but a complicated process of biological, biomechanical, electrical and biochemical factors which work in tandem to maintain a balance between positive and negative feedback cycles (Boron & Boulpaep (2016)). This can be understood by the body's rise and fall in temperature in concert with changing environmental temperatures at 35 °C.

Soft biological connective tissue are composed of cells, an extra cellular matrix and ground substances which have their own dynamic processes of maintaining individual homoeostasis and when observed as a unit tissue homoeostasis. In terms of the myocardium, its structure and function on observing the cardiomyocytes they are composed of contractile sarcomeric units which produce individual cell contraction and as a whole the ventricle to attain systole. For maintaining a homoeostatic level of cardiac output, the muscle adapts to the changes in pressure gradient, where in the amount of passive stretch experienced in diastole relates directly to the amount of pressure or work the cardiomyocyte can produces (also known as the Frank-Starling mechanism). The extra-cellular matrix is maintained by fibroblasts which adhere to the matrix surface via mechano receptors (Chiquet et al. (2003), MacKenna et al. (2000)), on experiencing increased stretch in the collagen fibres the fibroblasts sense this change via these feedback mechano receptors and produce proteolytic enzymes or protein formation catalysts in order to either digest or deposit new collagen fibres. A balance between synthesis and degradation maintains a level of homoeostasis which allows the ventricle to maintain its shape and function by preventing its over-distension in the cardiac cycle.

In relevance to research motive of current research, focus is narrowed to a few aspects in terms of soft tissue growth and remodelling,

1. Remodelling of the extra-cellular matrix constituent stretches in response to altered mechanical stimuli (increased stretch in case of myocardial infarction).
2. Growth of collagenous fibres in the ECM, as a direct consequence of increased fibroblast proliferation, transdifferentiation into myofibroblasts and collagen deposition.

### 2.4.1 Remodelling of ECM constituents

Growth and remodelling in soft tissues generally occur in tandem, i.e. occurring simultaneously in response to disease, adaptation to changing mechanical environments etc. The intrinsic microstructural constituents (collagen fibres, elastin fibres, cells and other components) can change their properties when new fibres replace the old fibres via deposition or removal due to the action of cells (fibroblasts for the extra-cellular matrix) and attain new orientations, geometric properties and configurations. This change in cytoskeleton or the extra-cellular matrix may be accompanied by mass changes or may not involve such modifications, being an important point to consider while proposing remodelling laws for soft tissues. Changes in the microstructure consequentially alter the properties of biological tissues such as strength, stiffness anisotropy etc, together these alterations have been described as the "remodelling" of the tissue [Ambrosi et al. (2011), Liu & Fung (1988)]. Cells also possess the properties to reconfigure themselves irrespective of regulation of mass of constituents by means of production of more contractile filaments within (Fletcher & Mullins (2010)). In remodelling of extra-cellular matrix components, especially collagen fibres, reconfiguration of the fibres based on the ECM deformation is of interest. This could be either strain-driven or stress-driven (Ambrosi et al. (2019)).

(Watton et al. (2009)), defines remodelling of arterial tissues microstructural collagen fibres based on the stretch they attain in their natural reference configurations, modelled in pertinence to cerebral aneurysms. This reference configuration ( $\Omega^R(t)$ ) is separate from the overall arterial tissues reference configuration ( $\Omega_0$ ), however its deformation is governed by the tissue stretch  $\lambda$  in the loaded configuration and collagen fibre stretch is related to the tissue stretch as :

$$\lambda_\gamma^C = \frac{\lambda_\gamma}{\lambda_\gamma^R} \quad (2.26)$$

where  $\lambda_\gamma^C$  is the collagen fibre stretch and  $\lambda_\gamma^R$  is the recruitment stretch which is attained in the natural reference configuration  $\Omega^R$  and  $\gamma$  defines the orientation of the collagen fibres, given for a cylindrical approximation of the arterial wall as  $\lambda_\gamma = \sqrt{\lambda_z^2 \sin^2 \gamma + \lambda^2 \cos^2 \gamma}$ , with  $\lambda_z$  being the stretch along the long axis of the cylinder and  $\lambda$  being the circumferential stretch.

The remodelling of the collagen fibres is formulated as:

$$\frac{d\lambda_\gamma^R}{dt} = \mathcal{F}(\lambda_\gamma^C, \lambda_{AT}^C) = \alpha_0 (E_\gamma^C - E_{AT}^C) \quad (2.27)$$

Here,  $E_\gamma^C$  denotes the Green-Lagrange strain ( $E_\gamma^C = \frac{1}{2}((\lambda_\gamma^C)^2 - 1)$ ) and  $E_{AT}^C$  is the Green-Lagrange Strain for collagen fibre attachment stretch, which is the stretch ( $\lambda_{AT}^C$ ) the collagen fibre attains in the loaded configuration in the healthy state of the artery prior to aneurysm formation. The functional form seen in Equation [2.27], is described so as to maintain the stretch of the collagen fibre to a preferred level of stretch, in the loaded configuration after tissue enlargement due to aneurysm formation, leading to increased fibre stretches.

## 2.4.2 Growth Formulations

Within the continuum mechanics community pertinent to biological soft tissues, growth as a change of form, based on the observations of organisms and their sub-parts attaining well-formed geometric structure and the idea of molecular interactions propelling biological processes has gained acceptance. Essentially, the growth phenomena as a consequence of changes in form and mass (Ambrosi et al. (2011)). The concept of "mass-stress" relation introduced by Fung, and the incorporation of a stress based mass density evolution, provide an understanding for the evolution of mass densities of the constituents in mixture formulations (Humphrey & Rajagopal (2002)). Two major approaches employed to define growth in soft tissues are detailed in the subsequent sections.

### 2.4.2.1 Finite Growth

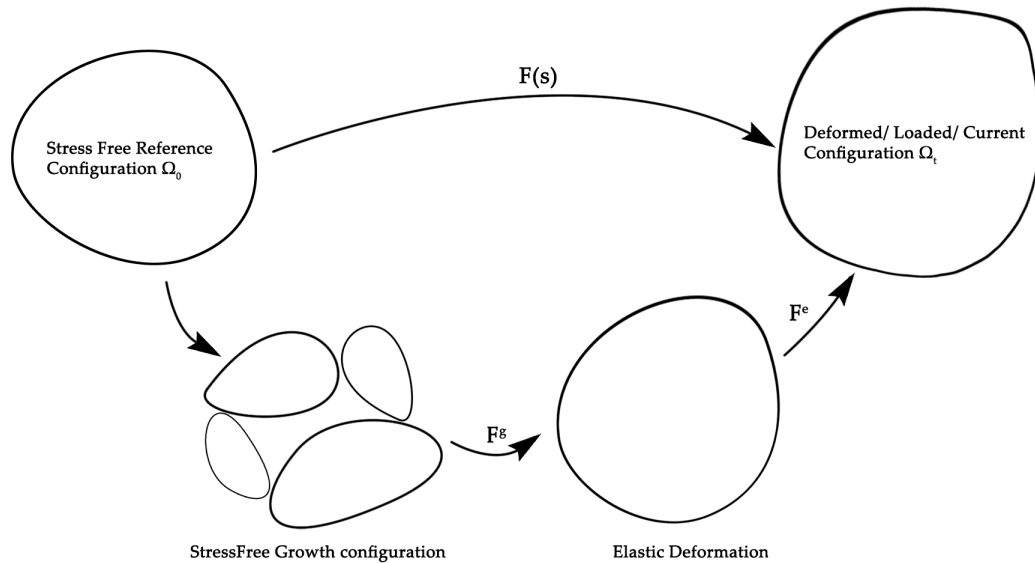


**Figure 2.11:** Finite growth schematic is displayed showing the multiplicative decomposition  $F = F^e \cdot F^g$ . The reference configuration ( $\Omega_0$ ) deforms based on  $F(s)$  into the current or loaded configuration ( $\Omega_t$ ),  $s$  denoting the current time. The growth part ( $F^g$ ) leads to an incompatible configuration whose physical significance leads to pieces of a physical body which might be incompatible and consists of overlapping elements and holes. This is transformed into the final deformed configuration  $\Omega_t$  by the elastic load dependant transformation ( $F^e$ ).

(Rodriguez et al. (1994)), introduced and formulated the concept of finite growth which was increasingly adopted with the use of computational methods. Additional equations are required to define finite kinematic growth and are prescribed with respect to the governing equations and are specific to the biomechanical problem or the physiological system which include the brain, the heart, lungs, skin, gut and so on (Ambrosi et al. (2019)). This theory is based on the multiplicative decomposition of the deformation gradient  $F$  into an elastic part  $F^e$  and a growth

part  $\mathbf{F}^g$  (Rodriguez et al. (1994)).

$$\mathbf{F} = \mathbf{F}^e \cdot \mathbf{F}^g \quad (2.28)$$

The removal or addition of mass to a local volume element in the finite element mesh is represented by the growth tensor  $\mathbf{F}^g$ , which is prescribed either directly or in rate form to encapsulate the growth evolution characteristic of the specific problem in consideration. The elastic tensor  $\mathbf{F}^e$  is the component which contributes in the generation of mechanical stresses. Therefore,  $\mathbf{F}^g$ , is considered to be a stress-free or traction-free configuration, by nature of which a series of incompatible configurations are mathematically introduced and the physical interpretation implies the growth from the initial parts of the body may be incompatible with each other resulting in overlapping or non-fitting body as a whole (Garikipati (2009)). This incompatibility is scaled into a continuum body with gaps or holes by the multiplication of  $\mathbf{F}^g$  with the elastic part of the deformation gradient  $\mathbf{F}^e$  to obtain the deformed configuration of the body post growth. An important aspect of growth-induced residual stresses arising in the body is neglected in this research. The schematic for the multiplicative decomposition is illustrated in Figure[2.11].

(Göktepe, Abilez, Parker & Kuhl (2010)), applied the finite deformation growth theory to a concept called "sarcomerogenesis", where in based on the growth tensor definition  $\mathbf{F}^g$  and rule sets for  $\vartheta$  which dictates serial (eccentric) or parallel deposition of sarcomeres in the cardiac muscle. The growth tensor  $\mathbf{F}^g$  is given as:

$$\mathbf{F}^g = \vartheta^f \mathbf{f}_0 \otimes \mathbf{f}_0 + \vartheta^s \mathbf{s}_0 \otimes \mathbf{s}_0 + \vartheta^n \mathbf{n}_0 \otimes \mathbf{n}_0 \quad (2.29)$$

where,  $\mathbf{f}_0, \mathbf{s}_0, \mathbf{n}_0$  are unit vectors in the reference configuration related to the orthotropic microstructural directions assumed.  $\boldsymbol{\vartheta} = [\vartheta^f, \vartheta^s, \vartheta^n]$  are growth multipliers and are defined with respect to the case considered, herein with eccentric or concentric hypertrophy of the myocardium in response to the tissue being subjected to either volume or pressure overload respectively. A mechanically driven growth criteria is defined as  $\phi^g$ , which is activated when a physical threshold is exceeded by a mechanical driving force. It can either be strain based or stress based, which correlate to eccentric and concentric hypertrophy respectively. For eccentric growth the growth criterion is given as :  $\phi^g = \lambda^e - \lambda^{crit}$ , which observes change when the elastic stretch  $\lambda^e$  exceeds a critical physiological stretch level  $\lambda^{crit}$ . Concentric growth scalar multiplier is given as  $\phi^g = tr(\mathbf{M}^e) - p^{crit}$ , where  $tr(\mathbf{M}^e)$  is the Mandel stress and  $p^{crit}$  is the threshold level. The growth multipliers  $\boldsymbol{\vartheta}^g = \mathbf{k}^g(\boldsymbol{\vartheta}^g \cdot \phi^g(\mathbf{F}^e))$  or  $\boldsymbol{\vartheta}^g = \mathbf{k}^g(\boldsymbol{\vartheta}^g \cdot \phi^g(\mathbf{M}^e))$  i.e either strain drive ( $\mathbf{F}^e$ ) or stress driven ( $\mathbf{M}^e$ ). To ensure there is no unbounded material growth a weight function is introduced as  $\mathbf{k}^g(\boldsymbol{\vartheta}^g)$ . Their results agree well with the studies (Bray et al. (2008), Geisse et al. (2009)), where in cardiomyocyte shape and intracellular sarcomeric architecture correlations are observed.

A technical note defined in (Cowin (1996)), introduces a strain driven finite growth formulation as an addendum to (Rodriguez et al. (1994)). They provide formulations using separate time scales, one for loading of the tissue ( $\tau$ ) and another for remodelling time scale ( $t$ ). Another stress based

finite growth formulation for elastic tissues based purely on strain energy functions is presented in (Ambrosi & Guana (2007))

#### 2.4.2.2 Constrained Mixtures

In comparison to finite growth, where constitutive relations are defined for the growth tensor, constrained mixture theory proposes an approach where in individual micro-structural components present in a tissue possess their own mass density term and turnover rates. Mechanically, each constituent has its own natural reference configuration but their overall mechanical behaviour is governed/ constrained by the deformation of the mixture as a whole. Introduced in (Humphrey & Rajagopal (2002)), where in mass-stress relations are used to formulate growth of constituent mass densities.

In each volume element of the continuum body, a mixture of  $n$  structurally important constituents are assumed to exist. In biological tissues, each constituent possesses a continuous turnover rate in the healthy tissue to maintain homoeostasis. For each constituent associated with  $i$ , where  $i = 1, 2, \dots, n$  a deposition function within the body is allowed at a time scale  $\tau \in [0, s]$ , where  $\tau$  is associated with the deposition of a constituent and  $s$  is the time scale associated with the loading of the tissue. Each constituent  $i$  has mass increments incorporated within the mixture at a time  $\tau$ , with a pre-stretch  $\mathbf{F}_{pre}^{i(\tau)}$ . This pre-stretch is associated with the independent natural reference configurations for each constituent. Given the body deforms between time  $\tau$  and  $s$ , such that  $\mathbf{F}(\tau)$  tends to  $\mathbf{F}(s)$ , then the mass increments of constituents will experience an elastic stretch i.e. a in a constrained behaviour.

$$\mathbf{F}_e^{i(\tau)}(s) = \mathbf{F}(s)\mathbf{F}^{-1}(\tau)\mathbf{F}_{pre}^{i(\tau)} \quad (2.30)$$

The mass density of the constituent  $i$  at a given time  $s$ , is derived via the mass balance relation for a mixture as:

$$\rho_0^i(s) = \rho_0^i(0)Q^i(s) + \int_0^s \dot{\rho}_{0+}^i(\tau)q^i(s-\tau)d\tau \quad (2.31)$$

where,  $\rho_0^i$  is the mass density per reference volume for a specific constituent, and  $\dot{\rho}_{0+}^i$  is the associated true mass production rate  $i$ -th constituent per unit reference volume for any given time  $s \geq 0$ .  $Q^i$  denotes the existing fraction of mass for at time 0 and still surviving at time  $s$   $Q^i(s) \in [0, 1]$ .

The strain energy of the continuum body is given by the sum of the strain energies of each individual constituent  $i$ , given by.

$$\Psi^i(s) = \sum_{i=1}^n \Psi^i(s) \quad (2.32)$$

Various constitutive relations exist to define the strain energy functions based on desired behaviour for each constituent.

A net mass production rate is formulated as:

$$\dot{\rho}_0^i = \dot{\rho}_{0+}^i - \dot{\rho}_{0-}^i \quad (2.33)$$

A net production rate  $\dot{\rho}_0^i = \dot{\rho}_{0+}^i - \dot{\rho}_{0-}^i$ , with production rates  $\dot{\rho}_{0+}^i$  and degradation rates  $\dot{\rho}_{0-}^i$ .

Consequently, on introduction of time ( $\tau$ ), the formulation for net mass production rate is as follows:

$$\dot{\rho}_0^i(\tau) = \dot{\rho}_0^i \mathbf{k}_\sigma^i : (\boldsymbol{\sigma}(\tau) - \boldsymbol{\sigma}_0) \quad (2.34)$$

where  $\boldsymbol{\sigma}(\tau)$ , is the Cauchy stress experienced at time  $\tau$  and  $\boldsymbol{\sigma}_0$ , is the equilibrium/ homoeostatic Cauchy stress experienced by the tissue.

Constrained mixture models therefore, are capable of accounting for multiple constituents present in soft tissues, having their own turnover rates and natural reference configuration. A downside to such models is the high utilisation of computational cost due to the tracking of a large number of variables, which depend on the number of constituents. But consideration of micro-structural constituents provides insights and clarity of several fundamental mechanisms upto the tissue level (Cyron & Humphrey (2017)).

## 2.5 State of Art Growth & Remodelling Left Ventricular Biomechanical Models

Understanding the key contributions in myocardial tissue growth and remodelling simulations, provides a sense of the contribution provided by the novel models introduced in this research, further sophistications, directions are discussed in the final Chapter [8].

### Points from (Lin & Taber (1995))

The pre-natal heart grows by means of hyperplasia i.e. cell-division and the mature heart has a dominative hypertrophic growth pattern (Burton (1972), Grossman (1980)). (Lin & Taber (1995)), studied the embryonic chick heart and suggested similarities between the growth behaviour in pre-natal and mature heart myocardium muscle. Embryonic chick studies provide results which can be acquired within hours rather than weeks associated with the results obtained from mature heart studies. They employ the finite growth model using a cylindrical assumption as an initial ideal geometry for the pre-natal chick heart. An important assumption they postulated is the reference configuration ( $\Omega_0$ ), evolves linearly with the Cauchy stress for the developing embryonic heart until it matures, after which point a constant homoeostatic state is assumed for the reference configuration. In the decomposition of the deformation gradient  $\mathbf{F} = \mathbf{F}_e \cdot \mathbf{F}_g$ , the growth is assumed to be  $\mathbf{F} = \mathbf{I}$  if no growth occurs for rates along each cylindrical axis  $\alpha_r = \alpha_\theta = \alpha_z = 1$ . However, Stress-dependent growth is induced via  $\dot{\mathbf{F}}_g = \dot{\mathbf{F}}_g(\boldsymbol{\sigma} - \boldsymbol{\sigma}^*)$ , where the growth tensor  $\dot{\mathbf{F}}_g$  evolves in accordance to the difference in the Cauchy stress tensor  $\boldsymbol{\sigma}$  and  $\boldsymbol{\sigma}^*$  an experimentally determined growth-equilibrium (homoeostatic) stress tensor (Rodriguez et al. (1994)).

### Points from (Taber (1998))

This paper proposes a set of biomechanical growth laws for muscle cells. Combining data of published results from experiments with simple theoretical models. In the formulations proposed, the rate of growth ( $\dot{\epsilon}_g$ ) at each material point also linearly depends on the local state of stress experienced. The formulation  $\dot{\epsilon}_g = D(\sigma - \sigma_0)$ , where  $\sigma$  is the Cauchy stress experienced and  $\sigma_0$  is the equilibrium (homoeostatic) stress. Growth is driven when  $\sigma > \sigma_0$ , and atrophy occurs for  $\sigma < \sigma_0$ . However, a small perturbation in the strain induced due to inflation of the body because of internal blood pressure might result in unbounded growth for which an alternative formulation is suggested. The major findings of the study is that known characteristics of biological structural growth containing muscle can be delineated using simple biomechanical growth laws. An additional insight was the need to formulate remodelling laws for isometric contractions of muscles. The conclusion that for the heart, is that regulation of circumferential growth can possibly be regulated by the End-Diastolic sarcomere length.

**Points from (Klepach et al. (2012))**

In this study, structural variations in response to mechanical overload is predicted using a mechanistic growth model, based on finite growth formulations. A patient specific ventricle is considered, and a case with an infarcted zone is considered, with the second case containing the left ventricle with the infarcted zone removed to indicate a post-operation situation due to surgical intervention. The growth tensor is based on the theory of sarcomerogenesis introduced earlier from (Göktepe, Abilez, Parker & Kuhl (2010)), with the formulation

$$\mathbf{F}^g = \vartheta \mathbf{f}_0 \otimes \mathbf{f}_0 + \frac{1}{\sqrt{\vartheta}} [\mathbf{I} - \mathbf{f}_0 \otimes \mathbf{f}_0] \quad (2.35)$$

where,

The growth formulation is given by  $\dot{\vartheta} = k(\vartheta)\phi(\sigma)$ , where  $k(\vartheta)$  - scaling function and  $\phi(\sigma)$  - growth criterion. Here,  $k = \frac{1}{\tau_\vartheta} \left[ \frac{\vartheta^{\max} - \vartheta}{\vartheta^{\max}} \right]^\gamma$ ,  $\phi = \max\{\text{tr}(J\sigma) - p^{\text{crit}}, 0\}$ . The growth is associated with eccentric remodelling of the cardiac muscle, due to the serial deposition of sarcomeres within the cardiac muscle due to volume overload.

**Points from (Zhuan et al. (2019))** A rat heart post-MI is studied, employing multiscale formulations introducing chemokine concentration, fibroblast migration and remodelling of the collagen fibre structure upto the tissue level. A 5 week study is done with a spherical infarct zone on the ventricular free-wall and collagen fibre degradation, deposition and remodelling is observed. A 2D agent based chemokine model is adapted from (Fomovsky & Holmes (2009)) to 3D domain. The fibroblasts regulation depends on the resultant of chemical, mechanical, structural, persistence (velocity) cues.

The local collagen fibre distributions remodel as per the actions of fibroblasts. The deposition and degradation of collagen fibres is given by a rate of change of number of collagen fibres  $N(\theta)$  in the  $\theta$  direction

$$\frac{\partial N(\theta)}{\partial t} = k_{\text{cf, gen}}(C)\beta\pi R_{\text{cell}}^2 \delta(\Theta - \theta) - k_{\text{cf, deg}}(C)N(\theta) \quad (2.36)$$

where,  $\beta$  - maximum collagen fibre number per unit area,  $R_{\text{cell}}$  - is the fibroblast cell radius,  $\delta$  function ensures the alignment of newly deposited fibres along the fibroblast cell migration direction, and  $k_{\text{cf, gen}}$ ,  $k_{\text{cf, deg}}$  regulate the generation and degradation of collagen fibres.

The collagen fibre angles change rotation i.e. remodel as per the following formulation:

$$\frac{\partial \theta}{\partial t} = \begin{cases} k_{\text{cf, rot}}(C) \|\sin(\Theta - \theta)\|, & \Theta - \theta \in (-\frac{\pi}{2}, 0) \cup (\frac{\pi}{2}, \pi) \\ -k_{\text{cf, rot}}(C) \|\sin(\Theta - \theta)\|, & \Theta - \theta \in (0, \frac{\pi}{2}) \cup (\pi, \frac{3\pi}{2}) \end{cases} \quad (2.37)$$

where,  $\theta$  - is the direction of the collagen fibre,  $\Theta$  - is the orientation of the fibroblast cell and  $k_{\text{cf, rot}}$  is the rate of rotation.

## 2.6 Inferences

Given the methods to model soft tissue growth and remodelling, inferences applied to the research introduced, listed below shed light on the methods implemented in the models described in the subsequent chapters.

- Based on the pressure volume loop for the left ventricle, states (points A, B, C, D, are identified; Figure [2.7] which are utilised in our models for definition of unloaded (undeformed) reference configuration( $\Omega_0$ ) and loaded (deformed) current configuration ( $\Omega_t$ ).
- The theory of constrained mixture models is applied in Chapter 3 where the mass densities of individual micro-structural constituents are defined and they retain an independent natural reference configuration as opposed to the mixture's reference configuration, and their stretches are functions of the tissue mixture's stretch in the loaded configuration.
- Mass growth formulations, where in mass density variables are multiplied to strain energy function constitutive relations, are utilised in Chapter 6, due to our choice of using an in-built material model (Holzapfel et al. (2000)) in the commercial ANSYS ® Mechanical APDL finite element package.
- It has been postulated in (Taber (1998)), that the equilibrium (homoeostatic) stresses in the mature heart have adapted to a preferred set of values and therefore even with changes in loading conditions, the growth-equilibrium stresses remain constant. This is contrast with the evolving equilibrium stress for the chick embryo which is postulated to achieve a homoeostatic state at a point where it attains maturity. Based on this assumption, the evolution of the equilibrium (homoeostatic) Cauchy stresses for the collagen fibres in the mature myocardium to investigate its effects on the growth and remodelling post-MI, are investigated.

In terms of model sophistication, the state-of-art models are capable of providing results for patient-specific data which provide guidance for clinical procedures, underlying mechanisms ranging from biomechanical to electrophysiological domains. Our models are purely mechanical and are driven by stretch or stress based growth and remodelling assumptions. The key difference in our finite element approach is the developed framework which is based around a commercial software (ANSYS ® Mechanical APDL), employed only for solving a finite element simulation. The entire process is controlled externally and can be further sophisticated with biochemical, electrophysiological and fluid dynamics model. The positive aspect about this framework is the aim to utilise industry-grade finite element solvers in comparison with custom in-house finite element code utilised in previous research. It is not claimed the work introduced herein to be better than previous research, but hope to synergise the advantages of both industrial and research aspects.

This page has been intentionally left blank.

## Chapter 3

# **Novel Constrained Mixture Model of the Left Ventricle: Growth & Remodelling Application in Myocardial Infarction**

---

*A novel 1D constrained mixture model of the left ventricle, modelled using a non-linear, elastic, isotropic, spherical membrane approximation is presented. The micro-structural constituents namely cardiomyocytes, ground substances and collagen fibre strain energy density functions provide the combined strain energy formulation for the myocardial tissue. Mass density variables are associated with each constituent and possess their own natural stress-free reference configurations. Myocardial infarction is simulated by degrading the mass density of cardiomyocytes. Collagen fibres are modelled using triangular distribution functions to represent their fibre stretches in the extra-cellular matrix and adaptation of their distributions is prescribed corresponding to their transition into load bearing components post-MI. Multiple adaptations of the homoeostatic stretch distribution of the collagen fibres are explored. It was observed that on evolving this distribution to include higher number of load bearing collagen fibres and in turn affecting their mass deposition rates based on growth and remodelling laws proposed, provides a plausible depiction of LV thinning post-infarction. Further sophistications for inclusion of chemical signalling pathways along with mechanical and biological cues along with consideration of the entire cardiac cycle is would provide a more complete mathematical model capable of enhancing the phenomenological predictive capabilities of the model.*

---

### 3.1 Introduction

Creating mathematical models of complex real-world problems helps us understand their fundamental working and associated behaviours, as well as patterns thereby providing predictive capabilities for future possibilities. The same can be applied to soft tissues, by applying simplified assumptions within reasonable boundaries, their fundamental structure and function can be delineated. It is difficult to replace experiments and clinical procedures with purely mathematical models, but insights can be obtained about a particular mechanism or phenomenon which would be sufficient to replicate or produce an observation in experiments or clinics ([Brodland \(2015\)](#)). Given our sense of space and time we can model problems in  $n$ -dimensions, where  $n = 1, 2, 3..$  and  $n=3$  being enough to capture realistic topographies, specifications and boundaries for a given soft tissue, organ or whole human body models. A wide acceptance is observed in terms of established one to three dimensional models. An important facet being even though 1D models can replicate sufficiently an observed phenomenon agreeing well with experiments, three dimensional models build on this knowledge and provide spatial understanding of resultant values. In soft tissue-biomechanics, this can mean a 1D model might predict the maximum stretch or stress a tissue experiences in a certain situation (disease, adaptation, growth etc) while an equivalent 3D model would allow us to understand the stress-strain profile over the entire tissue and if the tissue in 1D is modelled as a simplification of a whole organ, the 3D model can provide insight into spatial distribution of pertinent quantities, which are useful in comparison with clinical data or experiments. Therefore, this is not only useful in understanding fundamental mechanisms but modelled with enough complexity can help guide clinical procedures, therapies and discover novel therapeutic targets. ([Bhogal et al. \(2019\)](#)). In light of the utility of mathematical models, a soft tissue growth and remodelling model for the left ventricle following on the principles introduced in ([Aparício et al. \(2016\)](#), [Watton et al. \(2009\)](#)), is introduced herein.

We present a novel growth and remodelling formulation with a one-dimensional constrained mixture model for the left ventricle, post the onset of myocardial infarction. The left ventricular geometry and topography change drastically post-MI owing to the various processes which digest the extra-cellular matrix, cause the necrosis of cardiomyocytes leading to ventricular dilatation and thinning. The LV has been ideally is shaped as a prolate spheroid or ellipsoid, whereas the infarcted scar tissue causes the LV to attain a more spherical shape due to the dilatation and thinning caused by the infarction. Therefore, the LV wall is assumed to be an ideal sphere, to achieve simplicity in pertinent calculations. Moreover, in past research the LV being modelled as a spherical membrane provided results which agreed well with empirical data albeit qualitatively ([Bogen et al. \(1980\)](#)). Qualitative validation allows us to understand the mechanisms involved in the changing micro-structural constituents, cells and understand the macroscopic variations in the tissue as a whole in pertinent simulations which could be during disease progression, adaptation to increased blood pressure filling, cardiomyocyte hypertrophy to name a few.

The left ventricle is modelled as a spherical membrane subjected to internal pressure, the value of

which depends on the chosen configuration in the cardiac cycle i.e. the phases in the pressure-volume relationship (Figure [2.7]). The strain energy response of the constituents are modelled using non-linear elastic formulations. Moreover, the mechanical response of the tissue is assumed to be composed of the mechanical responses of its microstructural constituents namely elastin, proteoglycan and other water retaining elements forming the ground matrix, the cardiomyocytes and the collagenous extra-cellular matrix. A long term 1D simulation, is considered, to observe the changes in the myocardium post-MI by degrading the ground matrix and cardiomyocytes, whereas the collagen extra-cellular matrix (ECCM) adapts in response to the changing mechanical environment to maintain the mechanical equilibrium. The degradation of the ground matrix and cardiomyocytes as well as the regulation of collagenous fibres is attributed to a mass density term introduced to reflect the changes in mass density of each constituent with respect to their initial healthy concentration levels in the healthy myocardium.

The ECCM collagen fabric is considered to have its collagen fibres configured in the healthy myocardium, as a range of stretches using a triangular probability function (Aparício et al. (2016), Chen (2014)), and is termed as the attachment stretch distribution. After the onset of the disease as the collagenous fabric attains the role of primary load bearer from being a protective sheath which prevents over-distension of the ventricle, this is reflected by the changing mass density of the collagen fabric to help stabilise the infarcted tissue and the remodelling of the collagen stretch distribution as it tries to restore increased stretches to the attachment stretch distribution. An important assumption is the evolution of the attachment stretch distribution, which provides insights into the changing morphology, configuration and mass densities of the collagenous scar tissue post-MI. The functional forms for the degradation, stretch distributions, growth in mass densities and remodelling of the relevant constituents is dependent on the rate of change of stretches in the tissue constituents, the rate of degradation of the ground matrix and cardiomyocytes as well as the load borne by the individual constituents. Stabilisation and rupture of the left ventricle are the focus of the model's hypotheses, guiding result analysis and re-consideration of initial hypotheses.

## 3.2 Aims and Objectives

The mathematical model proposed for the left ventricle, allows us to test hypotheses and gain insight into the changes the ECM undergoes during the progression of a myocardial infarction. We model the necrotic myocardium and its progression into a scar tissue. Depending on the amount of damage to the myocardium i.e. the area of damage, size of the infarct and amount of cardiomyocytes undergoing necrosis, which are quantified by a mass density term in our uni-dimensional model, it can be aimed to predict the changes experienced by the collagen matrix and the consequent modulations in its mass density affecting the volumetric thickness of the ventricular wall in disease.

With an understanding of the possibilities the proposed mathematical model provides us, the aims and objectives of this study are enumerated as follows:

1. To understand the behaviour of constrained mixture model employed for the left ventricle after the onset of myocardial infarction based on the growth and remodelling hypotheses introduced in (Chen (2014), Watton et al. (2009))
2. To model the collagen extra-cellular matrix undulations with a triangular distribution function to account for the different stretch configurations in which the collagen fibres could be configured to the tissue, following (Aparício et al. (2016), Chen (2014)).
3. To understand the changes in the volumetric thickness of the infarcted left ventricular tissue in the scenario of assuming a constant homeostatic stretch distribution for collagen matrix and an evolving homeostatic stretch distribution.
4. With regard to the previous point, understand the mass density changes in the collagen fibre matrix leading to fibrosis of the infarcted tissue and qualitatively observe the plausibility of predicted values.

We discuss the model definition, the results obtained and the analyses done to understand constituent contributions to the tissue over time past disease progression.

### 3.3 Continuum Basis

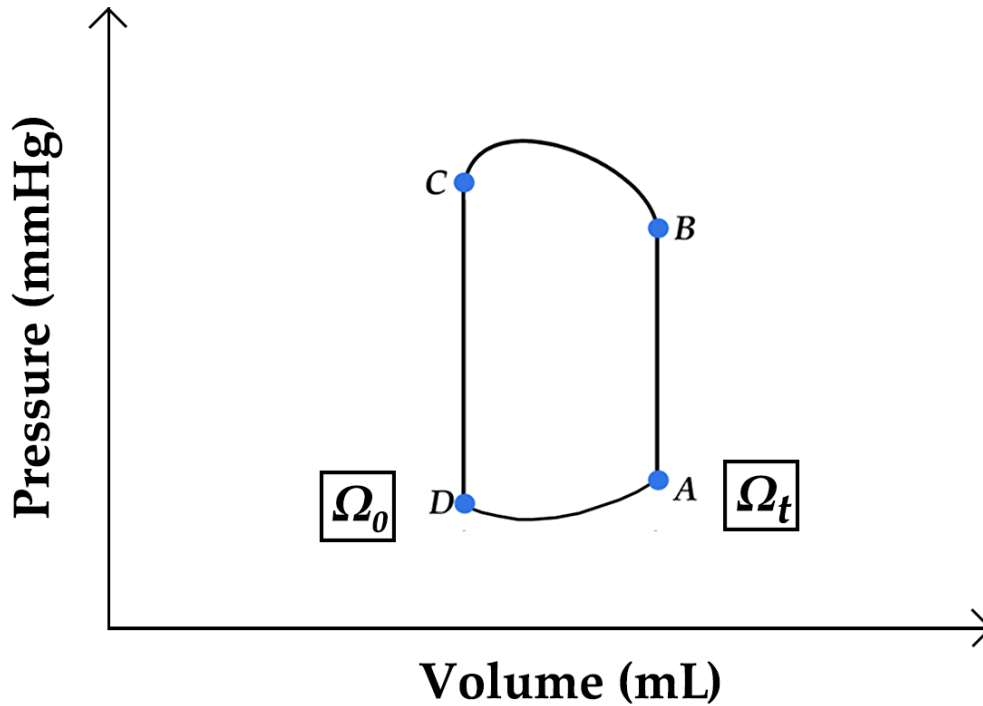


**Figure 3.1:** Pressure Volume Loop with a depiction of the configurations assumed for the constrained mixture model, adapted from [Guyton & Hall \(2006\)](#)

Every human individual has a unique shape, size of the heart, with respect to its overall dimensions and topography. Based on echocardiographic measurements from a study ([Kou et al. \(2014\)](#)) the End Systolic Volume and End Diastolic Volume dimensions provide an approximate value for the required tissue stretch measurements (discussed in further sections). We use an idealised LV measurement ([Hassaballah et al. \(2013\)](#)), with an approximation of sphere from the measurements with a radius of 31.075mm and a thickness of 10.3 mm. Post MI the ventricular wall thickness further reduces as the radius tends to increase. Therefore following the assumption in ([Watton et al. \(2009\)](#)) for cerebral aneurysms it is hypothesised that the infarcted LV wall to be modelled as a membrane. Understanding the configurations of the left ventricle in the cardiac cycle, from the view point of continuum mechanics will help us clearly define the problem statement. Moreover, the choice of the state in the PV relationship (Figure [2.7, 3.1]), will effect the stretches in the tissue and its micro-structural constituents. mechanical behaviour of constituents or contribution.

### 3.3.1 Reference Configuration $\Omega_0$

On observing the pressure volume relationship (Figure [2.7]), the left ventricle is never in a state of rest (in contrast to arteries) and therefore obtaining an unloaded configuration for mathematical calculations of deformation fields and mechanical quantities proves to be difficult. However, there are two (pseudo-rest states) possibilities which have been considered in past research to ascribe an unloaded configuration by analysing the pressure volume relationship along with clinical MR data. The first assumption is the instance after iso-volumetric relaxation (Figure [3.1]) and before the beginning of the filling of the LV by blood flowing in from the left atrium via the mitral valve i.e. point D can be considered as a rest state. The second assumption is there exists a state wherein there is zero variation in the pressure in the LV chamber and all the valves remain closed so that the net flow of blood within the ventricle and therein the pressure is zero. This point lies between points A and D, clinically identified as diastasis (Nikou et al. (2016)).

#### *Constituent Reference Configuration*

1. *Cardiomyocyte:*

The cardiomyocytes bear the passive load owing to the giant protein titin present within its contractile units structural assembly. On extension after systolic contraction it reaches a point where it is recruited to bear load for the next cardiac cycle. This point in time where they participate in the tissue's stress response is assumed to be the reference configuration for the cardiomyocyte by which its stretch is calculated in the loaded configuration.

2. *Collagen:*

Collagen fibres exist in a coiled configuration in the myocardial tissue, protecting the cardiomyocytes. During the filling phase of the cardiac cycle, some fibres uncoil and attain a certain level of stretch whereby they straighten bearing load thereafter. Combined with the responses of other constituents it contributes to the characteristic strain stiffening effect observed in soft tissues. The point in time at which the fibres straighten is assumed to be different in the loaded configuration and it is hypothesised to be its reference configuration.

We detail these independent reference configurations in our membrane model in later sections.

### 3.3.2 Current Configuration $\Omega_t$

The left ventricular mechanical function can be characterised by the pressure-volume relationship due to the transient flow of high-pressure blood between the chambers and vasculature. Four particular points on the PVR loop can be identified which describe discernible states in the cardiac cycle i.e. Points A, B, C and D. Out of these states the points A and C, which correspond to the end-diastolic state and end-systolic state can be identified using MRI, CT scans and other imaging techniques. Therefore, the loaded configuration can be quantified for the constrained mixture model configuration hypothesis. The end-diastolic state is chosen.

### 3.3.3 Attachment Stretch $\lambda_X^{AT}$

Introduced in [Watton et al. \(2004\)](#), the attachment stretch of a constituent is defined as the level of stretch attained when the constituent is configured to the tissue in the loaded configuration. In a spherical membrane approximation of the left ventricle, this stretch can be attributed to the collagen fibres, wherein they attain a certain level of stretch in the end diastolic loaded state ( $\Omega_t$ ). The collagen extra-cellular matrix is maintained continually via deposition, degradation mechanisms regulated by fibroblasts. They exert a compacting force during the deposition or re-organisation of collagen fibres into the extant matrix and might be the cause of the attachment stretch in the newly deposited constituents, this is observed in both experimental and computational models ([Chen \(2014\)](#), [Engler et al. \(2004\)](#), [Grinnell & Petroll \(2010\)](#), [Nagel & Kelly \(2012\)](#)).

Similarly, the cardiomyocytes are stretched to a certain value at the end of the filling phase (point A, [Figure 2.7](#)) to gain optimum configuration for the functioning of the ventricle. It is assumed that these stretches in the healthy homeostatic myocardial tissue in the left ventricle loaded configuration are referred to as the attachment stretch for the particular constituent. Mathematically they are represented as  $\lambda_X^{AT}$ , where the  $X$  denotes the constituent with respect to which the stretch is defined.

To summarise the attachment stretches for the cardiomyocytes and collagen fibres:

1. The cardiomyocytes are assumed to attain an attachment stretch  $\lambda_M^{AT} > 1$ , on being configured in the myocardial tissue at end-diastole to achieve optimum function and be capable of generating maximum active stress during ejection. This value can be inferred from the force-length relationship of a cardiomyocyte.
2. Collagen fibres behave as a protective sheath for the myocardium to prevent over-distension and or slippage of the cardiomyocytes. Particularly, the attachment stretch  $\lambda_C^{AT} > 1$ , is assumed to obtain a maximum attachment stretch, during the cardiac cycle.

### 3.3.4 Recruitment Stretch $\lambda_X^R$

The loaded (current) configuration  $\Omega_t$  of the LV allows us to describe the configurations of the collagen and cardiomyocytes to the myocardial tissue with a certain attachment stretch. Before, they are configured in the loaded configuration, owing to diastolic filling of the LV the collagen fibres and cardiomyocytes go through a deformation and partake in the mechanical response of the myocardium at different time points prior to  $\Omega_t$ . The distinct time points, at which the collagen fibres and the cardiomyocytes achieve a stretch so as to begin bearing the load of the internal blood pressure and provide mechanical response, are associated with a certain tissue configuration ( $\Omega_R^X$ ) at those respective time points for collagen ( $C$ ) and cardiomyocytes ( $M$ ) respectively ( $X = C, M$ ). The stretch in the configuration at which the individual constituents attain a role of partaking in the stress response of the tissue as a whole is termed as the recruitment stretch ( $\lambda_R^X$ ). The reference configurations for the collagen and cardiomyocytes in the tissue are distinct and differ

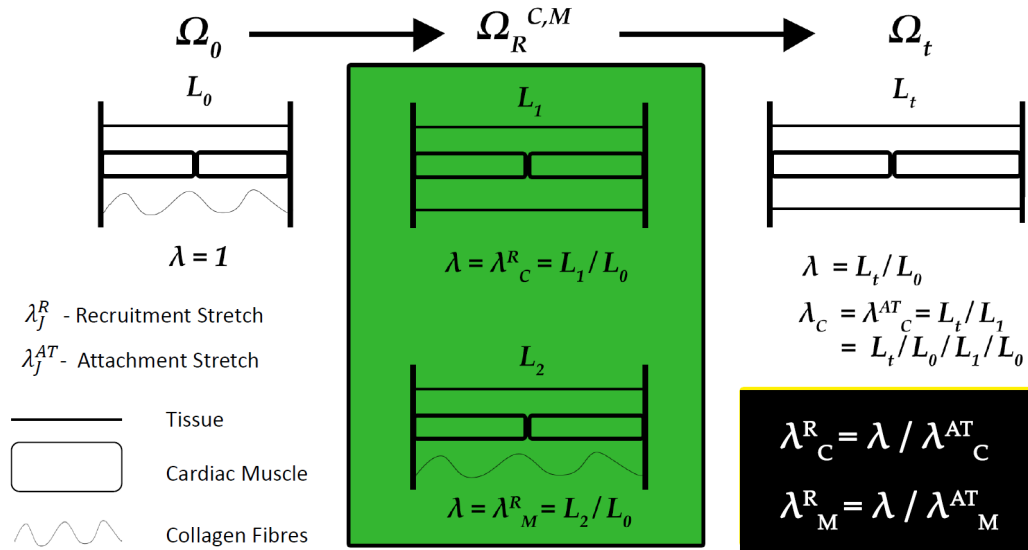


**Figure 3.2:** The relation between the attachment stretch and the recruitment stretches in the constituents of the myocardial tissue, shown as a function of lengths for motivating the idea behind the tissue stretch derivations.

from the loaded configuration of the tissue ( $\Omega_t$ ). We define these reference configurations as recruitment configurations (please refer Figure [3.3]).

The recruitment stretch and the attachment stretch can be mathematically related (as seen in the Figure [3.2]), as:

$$\lambda^R_X = \frac{\lambda}{\lambda^{AT}_X} \quad (3.1)$$

### 3.4 Left Ventricular Constrained Mixture Model

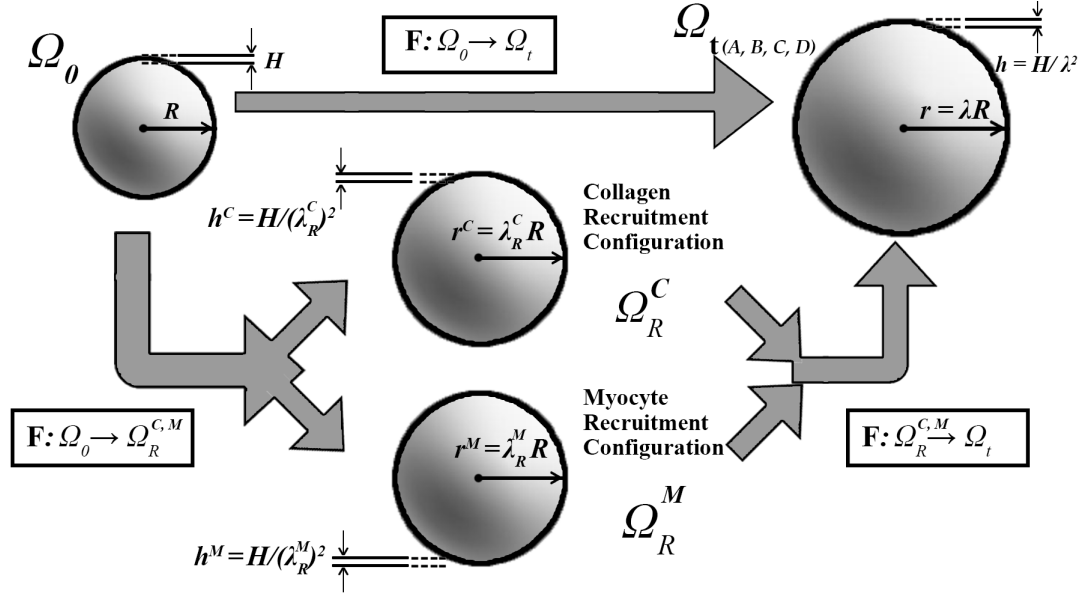


**Figure 3.3:** Configurations of the constrained mixture model:  $\Omega_0$  represents the stress free unloaded myocardial tissue and its current loaded configuration at end-diastole is denoted by  $\Omega_t$ . The tissue stretch  $\lambda$  in  $\Omega_t$  is calculated with respect to  $\Omega$ , however, the reference configurations for the cardiac myocytes and collagen fibres are defined relative to a recruitment stretch at which they partake in the stress response to applied internal blood pressure. These reference configurations are titled recruitment configuration for the cardiac myocytes and collagen fibres respectively as  $\Omega_R^M$  and  $\Omega_R^C$ , (Dandapani et al. (2017)).

The constrained mixture model approach allows us to not only model the LV cardiac tissue as whole and simulate biomechanical characteristics, but also define the corresponding constituent mechanical properties. Thereby, allowing individual constituent evolution in terms of mass densities and adaptation of mechanical characteristics. The deformation of the entire tissue as a whole governs the deformation of the micro-structural constituents as detailed in the previous section. The loaded configuration to be considered in our model, can be characterised by any of the four prominent states in the LV pressure volume relationship (Figure [2.7]). The micro-structural components present within the myocardium are taken into consideration and their natural reference configurations are defined as shown in Figure [3.3].

#### 3.4.1 Strain Energy Density Function

The energy acquired by a continuum body due to the deformation it experiences as a consequence the applied external force is known as the strain energy function. The energy per unit volume of the body is known as strain energy density function. This function is used to quantify constitutive equations to describe the mechanical behaviour of the soft tissue.

The strain energy function of the tissue is assumed to be an additive decomposition of the individ-

ual strain energy contributions of the tissue constituents, as employed in previous models[Watton et al. (2004) and a few more].

$$\tilde{\Psi} = \tilde{\Psi}_{GM} + \tilde{\Psi}_M + \tilde{\Psi}_{C,myo} + \tilde{\Psi}_{C,epi} \quad (3.2)$$

where,

$\tilde{\Psi}$  - Strain Energy Function of the entire tissue.

$\tilde{\Psi}_{GM}$  - Strain Energy Function of the ground matrix.

$\tilde{\Psi}_M$  - Strain Energy Function of the cardiac muscle.

$\tilde{\Psi}_{C,x}$  - Strain Energy Function of a collagen fibre, x denotes the layer, i.e. the myocardium(myo) or the epicardium(epi).

On analysing the equation the strain energy functions are related to a single unit of each constituent, i.e a single collagen fibre, a single muscle and a unit component of the ground matrix. To evaluate the strain energy over the entire scale of the tissue, particularly a collection of muscle fibres, the extant collagen matrix and the ground tissue components a normalised mass density variable ( $m^X$ ), is introduced, for each term in the strain energy function. It is formulated as:

$$\Psi = m^{GM}\tilde{\Psi}_{GM} + m^M\tilde{\Psi}_M + m^{C,myo}\tilde{\Psi}_{C,myo} + m^{C,epi}\tilde{\Psi}_{C,epi} \quad (3.3)$$

The term  $m^X$ , where X represents the particular constituent relating to the ground matrix (GM), cardiomyocytes (M) and collagen fibres (C). It denotes the ratio of the normalised mass densities of the constituent X at time t to the normalised mass density at time t=0.

### 3.4.1.1 Governing Equation

The law of Laplace is commonly applied to calculate the stresses in the left ventricle for a spherical membrane approximation and is formulated as:

$$t = \frac{pr}{2h} \quad (3.4)$$

where,

$t$  - Cauchy stress experienced by the tissue,

$p$  - Internal pressure due to inflow of blood after left atrial systole,

$r$  - Radius of the spherical membrane,

$t$  - Thickness of the spherical membrane.

On re-arranging the above equation, the pressure is related to the stress experienced by the myocardial wall.

$$p = \frac{2h}{r} t \quad (3.5)$$

We model the left ventricle as a non linear elastic spherical membrane, composed as a mixture of the micro-structural constituents present in the myocardium. The overall governing equation for a spherical membrane undergoing inflation is detailed in (Watton et al. (2009)). We adapt the same formulation, however, with a few changes in the terms considered for the stress responses based on the constituents present in the myocardium as opposed to the arterial micro-structural composition. The constrained mixture model theory suggests the stress experienced by the individual constituents provide the combined stress response of the tissue to the applied internal pressure (Bogen et al. (1980), Humphrey & Rajagopal (2002)). For a spherical membrane formulation, the deformed radius( $r$ ) is related to the undeformed radius( $R$ ) by the stretch of the whole tissue as  $r = \lambda R$ , and likewise the deformed thickness ( $h$ ) with the undeformed thickness ( $H$ ) as  $h = \frac{H}{\lambda^2}$ . On substituting these formulations in Equation [3.5]:

$$p = \frac{2H}{R\lambda^3} \left( \sum_{i=X} \sigma^X \right) \quad (3.6)$$

The  $X$  represents each constituent in the tissue. The Cauchy stress (represented by  $\tilde{\sigma}$  henceforth) is derived from the strain energy density function as follows:

$$\tilde{\sigma} = \lambda \frac{\partial}{\partial \lambda} (\tilde{\Psi}_X) \quad (3.7)$$

The governing equation is mathematically expressed as:

$$p = \frac{2H}{R\lambda^3} \left[ m^{GM} \frac{\partial}{\partial \lambda} (\tilde{\Psi}_{GM}) + \frac{\partial}{\partial \lambda} (\tilde{\Psi}_M) + \frac{\partial}{\partial \lambda} (\tilde{\Psi}_{C,myo}) + \frac{\partial}{\partial \lambda} (\tilde{\Psi}_{C,epi}) \right] \quad (3.8)$$

$$p = \frac{2H}{R\lambda^3} \left[ m^{GM} (\tilde{\sigma}_{GM}) + (\tilde{\sigma}_M) + (\tilde{\sigma}_{C,myo}) + (\tilde{\sigma}_{C,epi}) \right] \quad (3.9)$$

The inner pressure on the wall is reflected for the end diastolic wall pressure ( $\approx 5$  mmHg or  $\approx 1.3$  kPa), and this is counter balanced by the microstructural constituents, of the tissue. Each constituent gains energy due to the applied strain and their strain energy functions can be used to determine the overall stress response. This stress response is derived by obtaining the derivative of the strain energy function with respect to the stretch in the respective constituent as described in Equations [3.3, 3.7, 3.8].

The deformation gradient for a spherical membrane is as follows:

$$F = \begin{bmatrix} \lambda_{rr} & \lambda_{r\theta} & \lambda_{r\phi} \\ \lambda_{\theta r} & \lambda_{\theta\theta} & \lambda_{\theta\phi} \\ \lambda_{\phi r} & \lambda_{\phi\theta} & \lambda_{\phi\phi} \end{bmatrix} \quad (3.10)$$

where,  $r$  - radial direction,  $\theta$  - circumferential direction and  $\phi$  - azimuthal direction.

Considering a sphere with an unloaded reference thickness  $H$  and radius  $R$ , on undergoing pressure inflation, which forms the basis of filling of the left ventricle in the diastolic phase, in

the deformed current configuration  $\Omega_t$  the deformed thickness is calculated as  $h = \frac{H}{\lambda^2}$  and the deformed radius =  $r = \lambda R$ . (another figure for the deformed sphere configuration, slice of a sphere). The deformation gradient shown in Equation [3.10], takes the form of:

$$F = \begin{bmatrix} \frac{1}{\lambda^2} & 0 & 0 \\ 0 & \lambda & 0 \\ 0 & 0 & \lambda \end{bmatrix} \quad (3.11)$$

$$C = \begin{bmatrix} \frac{1}{\lambda^4} & 0 & 0 \\ 0 & \lambda^2 & 0 \\ 0 & 0 & \lambda^2 \end{bmatrix} \quad (3.12)$$

On inspecting the stretches denoted in Equation [3.11], they are denoted as  $\lambda$  in the circumferential and azimuthal direction which denote the principal direction of stretches for a hollow sphere undergoing pressure inflation. The principal invariant required for the constrained mixture model is  $I_1 = tr(C) = 2\lambda^2 + \frac{1}{\lambda^4}$ .

An important assumption is the incompressibility of the myocardial tissue, which implies  $J = det[F] = 1$ . This has been accounted for during the formation of the deformation gradient. This is due to the myocardial volume changes between 10% to 15 % during the cardiac cycle given isovolumetric contraction, by which the cardiomyocytes thicken and isovolumetric relaxation phases (Figure[2.7]) and due to the presence of ground substances (Jugdutt (2005)).

### 3.4.2 Elastin and other ground substances

In past research models for arteries, it has been commonly assumed to approximate the ground substance and elastin (here associated with the ground matrix) with a Neo-Hookean material (Holzapfel & Ogden (2010), Martufi & Gasser (2012), Watton et al. (2009)), experimental basis suggesting the same can be found in (Gundiah et al. (2007)). Drawing parallels from arterial models to describe the passive non-collagenous matrix materials present in the myocardial tissue, it is assumed to behave as a Neo-Hookean material and its strain energy function is defined as follows:

$$\tilde{\Psi}_{GM} = \frac{k_{GM}}{2} [I_1 - 3] \quad (3.13)$$

On deriving the Cauchy Stress response from the Neo-Hookean strain energy function:

$$\tilde{\sigma}_{GM} = \frac{\partial}{\partial \lambda} (\tilde{\Psi}_{GM}) = 2k_{GM}\lambda^2 \left[ 1 - \frac{1}{\lambda^6} \right] \quad (3.14)$$

In the above equations  $k_{GM}$  is the material parameter for the ground matrix,  $I_1$  is the first invariant of the deformation tensor  $F$  w.r.t  $(\lambda)$  and  $\tilde{\sigma}_{GM}$ , signifies the Cauchy stress response.

### 3.4.3 Cardiac Myocytes

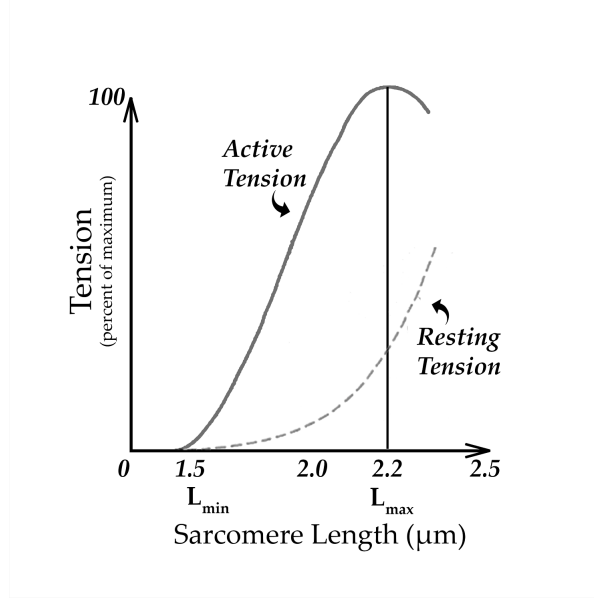


**Figure 3.4:** The length-tension graph of a sarcomere is shown, adapted from (Boron & Boulpaep (2016)). The formulations shown in Equations [3.17, 3.16], aim to capture these behaviours. The active response is associated with activated acto-myosin cross-bridges by intra-cellular  $Ca^{2+}$  ions and the passive response with the resting tension, where the sarcomeres are not activated.

The cardiomyocyte cells in the myocardial wall tissue have both a passive response to stress dominated by the giant protein titin in diastole, and an active response due to the contractile forces generated by the actin-myosin assembly (please refer Section [2.1.3.3], graphically realised as shown in Figure[3.4]). Therefore, the mechanical response of the cardiomyocyte, is modelled, to be a linear combination of a passive Neo-Hookean response, given its behavioural similarity to elastin fibres but being much more tensile and an active response as described in (Rachev & Hayashi (1999)). These are formulated as follows:

$$\tilde{\Psi}_M = \frac{k_M^{pass}}{2} [I_1 - 3] \quad (3.15)$$

$$\sigma_M^{pass} = \lambda_M \frac{\partial}{\partial \lambda_M} (\tilde{\Psi}_M) = 2k_M^{pass} \lambda_M^2 \left[ 1 - \frac{1}{\lambda_M^6} \right] \quad (3.16)$$

The passive behaviour of the cardiomyocyte passive response bears the same functional form as that for the ground matrix, with a key difference being the stretch calculations are defined with respect to the muscle stretch ( $\lambda_M$ ).  $k_M^{pass}$  defines the material parameter for passive cardiomyocyte behaviour.

$$\sigma_M^{active} = T(Ca^{2+}) \lambda_M \left[ 1 - \left( \frac{\lambda_M^{max} - \lambda_M}{\lambda_M^{max} - \lambda_M^{min}} \right)^2 \right] \quad (3.17)$$

Here, the  $T(Ca^{2+})$ , represents an activation function for active contraction assigned as 0 or 1 in this

model.  $\lambda_M^{max}$  is the maximum sarcomere stretch and  $\lambda_M^{min}$  is the minimum stretch configuration possible.

These equations represent the curves as observed in experimental observations on sarcomere stretching, which in turn is a measure for the cardiomyocyte due to parallel arrangement and stretching of the sarcomere unit within the cell (Boron & Boulpaep (2016)). The population of cardiomyocytes together describe the lengthening of the ventricular myocardium as a whole and therefore, the behaviour of the entire LV tissue can be defined based on the sarcomere Length-Tension curve.

### 3.4.4 Collagen

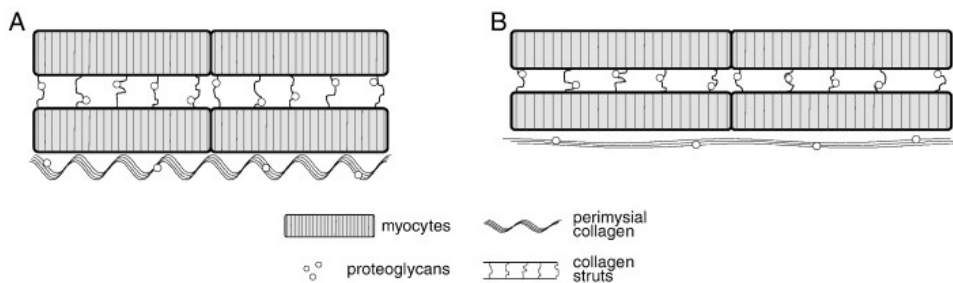


**Figure 3.5:** The arrangement of collagen fibres in the myocardium, depicting the endomysial collagen struts and perimysial collagen fibres running parallel amongst the cardiac myocytes (source: (Fomovsky et al. (2010))).

The mechanical response of collagen in the myocardium is assumed to be a function of the stretch it attains in the tissue during the cardiac cycle. The arrangement of the collagen fibres in the myocardium is complex as defined in the Section [2.1.1.4]. The cardiomyocytes are connected to each other by collagen struts which help in the transmission of forces and maintain the orientation of the myofibres in systole, whereas in diastole the perimysial collagen fibres which run parallel to the cardiomyocyte sheets help prevent them from over-stretching, thus serving as a protective sheath. This is shown in the Figure [3.5], adapted from (Fomovsky et al. (2010)). These collagen fibre types present within the myocardium are collectively referred to as myocardial collagen fibres in our model, using the subscript ( $_{myo}$ ). The second layer of collagen fibre matrix is derived from the extant matrix in the epicardial layer, which prevent the ventricular myocardium as whole from over-distension and maintain healthy physiological function. These fibres run parallel to the cardiac muscle fibres and their strain energy is accounted for the tissue in our model, with their quantities denoted with a subscript ( $_{epi}$ ). Given the uni-dimensional approximation of the myocardial tissue, it is assumed they are aligned circumferentially along with the other constituents as a simplification to focus majorly on the remodelling of fibre stretches and mass densities.

### 3.4.4.1 Collagen Undulation Distribution

In soft connective tissues, the fibrillar collagen network is composed of individual collagen fibrils, bundled together to form collagen fibres (use fibril/fibre interchangeably) which are not necessarily in the same state of stretch during the cardiac cycle. Depending on their location within the myocardial wall there could be recruitment of a certain number of fibres during loading in the cardiac cycle while the remaining fibres may still be uncoiled below the recruitment stretch. To account for this variation in the stretches in the existing collagen fibre matrix, it is important to represent them with a range of values rather than a single constant. This has been addressed in past research by considering various distribution functions in order to represent the collagen fibre undulation distribution i.e. attachment stretch distribution in excised soft tissues using various imaging techniques. Based on the observations in vivo (Schrauwen et al. (2012)) for collagen fibre undulation distribution of stretches, it can be understood that the recruitment stretch distribution ( $\Pr(\Lambda_C^R)$ ) occurs as a consequence of loading the tissue to the loaded configuration, at which the stretch distribution assumes an in vivo attachment stretch distribution ( $\Pr(\Lambda_C^{AT})$ ). We can therefore, redefine the Equation [3.1] for collagen undulation distribution as:

$$\Lambda_{C,x}^R = \frac{\lambda}{\Lambda_{C,x}^{AT}} \quad (3.18)$$

Examples can be seen in (Flynn et al. (2011), Gleason Jr & Humphrey (2005), Martufi & Gasser (2012), Wan et al. (2010)), based on these models follow their implementations seen in (Aparício et al. (2016), Chen (2014)) are followed to represent the myocardial and epicardial collagen fibre matrices with a triangular distribution function. We assume the attachment stretch distribution ( $\Pr(\Lambda_C^{AT})$ ) using a triangular approximation as follows:

$$f_{\Lambda_C^{AT}}(\lambda_C^{AT}) = \begin{cases} 0, & \lambda_C^{AT} < \lambda_C^{AT,min} \\ \frac{2(\lambda_C^{AT} - \lambda_C^{AT,min})}{(\lambda_C^{AT,max} - \lambda_C^{AT,min})(\lambda_C^{AT,mod} - \lambda_C^{AT,min})}, & \lambda_C^{AT,min} \leq \lambda_C^{AT} < \lambda_C^{AT,mod} \\ \frac{2(\lambda_C^{AT,max} - \lambda_C^{AT})}{(\lambda_C^{AT,max} - \lambda_C^{AT,min})(\lambda_C^{AT,max} - \lambda_C^{AT,mod})}, & \lambda_C^{AT,mod} \leq \lambda_C^{AT} < \lambda_C^{AT,max} \\ 0 & \lambda_C^{AT} \geq \lambda_C^{AT,max} \end{cases} \quad (3.19)$$

On closer inspection, it can be seen that the distribution function is characterised by three primary values, namely, minimum attachment stretch ( $\lambda_C^{AT,min}$ ), maximum attachment stretch ( $\lambda_C^{AT,max}$ ) and mode attachment stretch ( $\lambda_C^{AT,mod}$ ). Collagen fibres which have a minimum attachment stretch ( $\lambda_C^{AT,min}$ ), need to be stretched further compared to other collagen fibres in order to contribute to the tissue stress response and therefore are attributed with a maximum recruitment stretch ( $\lambda_C^{R,max}$ ). Whereas, collagen fibres which have a maximum attachment stretch ( $\lambda_C^{AT,max}$ ), are recruited prior to the straightening of other collagen fibres, attaining a minimum recruitment stretch ( $\lambda_C^{R,min}$ ). Terminally, fibres with ( $\lambda_C^{AT,mod}$ ) attain the same stretch in the loaded configuration therefore having a mode recruitment stretch ( $\lambda_C^{R,mod}$ ). An implication seen from the relation between the attachment and recruitment stretch is that due to the distributed undulated nature of

collagen fibres in the unloaded state ( $\Omega_0$ ), the recruitment stretch distribution ( $Pr(\Lambda_C^{AT})$ ) occurs as a natural consequence.

To determine the recruitment stretch in the initial loaded configuration of the left ventricular myocardium at time  $t=0$ ,  $e$  ( $\lambda_C^{R,min}$ ), ( $\lambda_C^{R,mod}$ ) and ( $\lambda_C^{R,max}$ ) from corresponding values in the attachment stretch distribution function, can be derived.

$$\lambda_C^{AT,min} \cdot \lambda_C^{R,max} = \lambda_C^{AT,max} \cdot \lambda_C^{R,min} = \lambda_C^{AT,mod} \cdot \lambda_C^{R,mod} = \lambda \quad (3.20)$$

As the attachment stretch distribution ( $Pr(\lambda_C^{AT})$ ) is a piecewise triangular distribution function, it implies the recruitment stretch distribution ( $Pr(\lambda_C^R)$ ) function is another piecewise triangular distribution function given as:

$$f_{\Lambda_C^R}(\lambda_C^R) = \begin{cases} 0, & \lambda_C^R < a \\ \frac{2(\lambda_C^R - a)}{(b-a)(c-a)} & a \leq \lambda_C^R < c \\ \frac{2(b - \lambda_C^R)}{(b-a)(b-c)} & c \leq \lambda_C^R < b \\ 0 & \lambda_C^R \geq b \end{cases} \quad (3.21)$$

In the above formulation, the variables  $a$ ,  $b$  and  $c$  represent  $\lambda_C^{R,min}$ ,  $\lambda_C^{R,max}$  and  $\lambda_C^{R,mod}$  respectively.

Given the definition of a triangular distribution function for collagen fibres recruitment and attachment with respect to the loaded configuration at end diastole ( $\Omega_t(t=0)$ ), the stress responses, can be derived, as a piecewise function following the triangular distribution function. We consider the strain energy function for both the myocardial and epicardial collagen fibres using a modified formulation from the approach in (Hill et al. (2012)), by using a quadratic function from (Chen (2014)). The strain energy function for an individual collagen fibre, in a layer  $x$ , is given as:

$$\tilde{\Psi}_{C,x} = \frac{k_{C,x}}{2} (\lambda_{C,x}^2 - 1) \quad (3.22)$$

where,  $k_{C,x}$  is the collagen material constant and  $\lambda_{C,x}$  is the stretch experienced by the collagen fibre measured from its natural reference configuration. It is related to the tissue stretch via its recruitment stretch  $\lambda_{C,x}^R$  through the relation shown in Equation [3.1].

Given, the distribution of stretches in the recruitment and attachment distributions in the collagen recruitment ( $\Omega_R^{C,x}$ ) configuration and loaded configuration ( $\Omega_t$ ), the stress response of the collagen fibres per unit volume of tissue at a stretch ( $\lambda$ ) can be calculated by integration over the range of recruitment stretches for a single collagen fibre strain energy density function ( $\tilde{\Psi}_{C,x}$ ) multiplied by the normalised mass density term  $m^{C,x}$ :

$$\Psi_{C,x}(\lambda) = m^{C,x}(t) \int_1^\lambda \tilde{\Psi}_{C,x} \left( \frac{\lambda}{\lambda_{C,x}^R} \right) f_{\Lambda_{C,x}^R}(\lambda_{C,x}^R) d\lambda_{C,x}^R \quad (3.23)$$

Here,  $\lambda_{C,x}^R$  is the recruitment stretch of the collagen fibre in the layer  $x = myo, epi$  and  $f_{\Lambda_{C,x}^R}$  is

the PDF for the recruitment stretch distribution  $Pr(\Lambda_{C,x}^R)$  and  $m^{C,x}(t)$  is the normalised mass density for the collagen fibre matrix at time t, and at  $t=0$ ,  $m^{C,x}(t=0) = 1$ . From Equations [3.21, 3.23] it follows that  $\Psi_{C,x}(\lambda)$  is a piece wise linear function. The 1st Piola-Kirchoff stress is therefore derived as:

$$P_{C,x}(\lambda) = \begin{cases} f(\lambda), & \lambda < a \\ g(\lambda), & a \leq \lambda < c \\ h(\lambda), & c \leq \lambda < b \\ i(\lambda), & \lambda \geq b \end{cases} \quad (3.24)$$

The explicit functional forms are as follows:

$$\begin{aligned} f(\lambda) &= 0 \\ h(\lambda) &= m_c k_c \zeta \left[ \frac{1}{(c-a)} \left( (a+\lambda) \ln\left(\frac{\lambda}{a}\right) + 2a - 2\lambda \right) \right] \\ h(\lambda) &= m_C k_c \zeta \left[ \frac{1}{(c-a)} \left( (a+\lambda) \ln\left(\frac{c}{a}\right) + a - c + \left(\frac{a-c}{c}\right) \lambda - \frac{1}{(b-c)} \left( (b+\lambda) \ln\left(\frac{\lambda}{c}\right) + b - c + \left(\frac{b+c}{c}\right) \lambda \right) \right) \right] \\ i(\lambda) &= m_C k_c \zeta \left[ \frac{1}{(c-a)} \left( (a+\lambda) \ln\left(\frac{c}{a}\right) + a - c + \left(\frac{a-c}{c}\right) \lambda - \frac{1}{(b-c)} \left( (b+\lambda) \ln\left(\frac{b}{c}\right) + b - c + \left(\frac{b-c}{c}\right) \lambda \right) \right) \right] \end{aligned} \quad (3.25)$$

From which the Cauchy stress is derived as  $\sigma_{C,x}(\lambda) = \lambda P_{C,x}(\lambda)$ . The variables a, b and c represent  $(\lambda_C^{R,min}, \lambda_C^{R,max}$  and  $\lambda_C^{R,mod}$ ) respectively.  $\zeta$  is used to replace  $(\frac{1}{b-a})$ .

### 3.4.5 Material Parameter Estimation

The material parameter variables described in the following sections are derived from the governing equilibrium equation for a spherical membrane. Specifically, in the given the ascribed time period for the simulation running over a number of steps, the material parameters are calculated at the initial time step i.e. ( $t = 0$ ), when the tissue is in the healthy loaded configuration ( $\Omega_t|_{t=0}$ ) with initial stretch values for each constituent ( $\lambda_x|_{t=0}$ ) and mass densities ( $m^x|_{t=0}$ ). The deformed and undeformed, radius and thickness for a spherical membrane as stated above are related as,  $r = \lambda R$  and  $h = \frac{H}{\lambda^2}$ , where  $\lambda$  is the stretch experienced by the tissue as a whole at ( $\Omega_t|_{t=0}$ ) with a pressure of  $\approx 5$  mmHg or 1.3 kPa. Consequently, on assuming the load borne by the constituents at different points in the cardiac cycle, following values, are assumed, given their contributions discussed in the section (biomechanics of ecm) at the end-diastolic point A (Figure [2.7]).

$$P_{GM}^{lb} = 0.1; \quad P_{M,pass}^{lb} = 0.8; \quad P_{M,act}^{lb} = 0; \quad P_C^{lb} = 1 - P_{GM}^{lb} - P_{M,pass}^{lb} - P_{M,act}^{lb} \quad (3.26)$$

where in *lb* - is an acronym for load-borne. Please note, unity represents the total load borne, and use fractions to describe the load borne by the respective constituents. This could be represented as a total 100 % but has been kept to 1 for simplicity.

Subsequently, the material parameters for each constituent are calculated as shown below:

#### Cardiomyocytes

During the passive filling of the LV in diastole, the giant protein titin is responsible for the mechanical properties of the myocardium as stated in Section [2.1.3.1]. From the the passive load borne at end-diastole, cardiomyocyte are assumed to bear to 80 % of the internal blood pressure. The material parameter for the active and passive responses can be individually accounted from the equilibrium condition (Equation [3.8]):

$$k_M^{pass} = \frac{pP_{M,pass}^{lb}R\lambda^3|_{t=0}}{2Hm^M|_{t=0}} \left[ 2\lambda_M^2|_{t=0} \left( 1 - \frac{1}{\lambda_M^6|_{t=0}} \right) \right]^{-1} \quad (3.27)$$

$$k_M^{act} = \frac{pP_{M,act}^{lb}R\lambda^3|_{t=0}}{2Hm^M|_{t=0}} \lambda_M|_{t=0} \left[ 1 - \left( \frac{\lambda_M^{max} - \lambda_M|_{t=0}}{\lambda_M^{max} - \lambda_M^{min}} \right)^2 \right]^{-1} \quad (3.28)$$

#### Ground Matrix

The elastin fibres and other ground substances within the myocardial tissue, have yet to be understood based on their function, quantification and role in the tissue mechanical response. Therefore, its contribution is taken to be 10 % of the total load borne by the constituents of the tissue. This is an assumption and needs to be quantified in further studies to obtain insight into

its mechanical role.

$$k_{GM} = \frac{pP_{GM}^{lb} R \lambda^3|_{t=0}}{2Hm^{GM}|_{t=0}} \left[ 2\lambda^2|_{t=0} \left( 1 - \frac{1}{\lambda^6|_{t=0}} \right) \right]^{-1} \quad (3.29)$$

### Collagen Fibre Network

Owing to the protective nature of the collagen fibre matrix in the cardiac extra-cellular matrix, preventing over distension and transmitting forces across the tissue, the load borne by the collagenous fibres, is assumed to be the difference between the total load borne by the other constituents and unity. Given the stress response of the collagen fibres is derived by employing the triangular distribution stresses, the material parameter is determined by the recruitment stretch distribution (see Section[3.4.4]). These are formulated as follows :

$$k_{C,x} = \begin{cases} \frac{pP_C^{lb} R \lambda^3|_{t=0}}{2Hm^C|_{t=0}} \lambda f(\lambda)^{-1} & \lambda < a \\ \frac{pP_C^{lb} R \lambda^3|_{t=0}}{2Hm^C|_{t=0}} \lambda g(\lambda)^{-1} & a \leq \lambda < c \\ \frac{pP_C^{lb} R \lambda^3|_{t=0}}{2Hm^C|_{t=0}} \lambda h(\lambda)^{-1} & c \leq \lambda < b \\ \frac{pP_C^{lb} R \lambda^3|_{t=0}}{2Hm^C|_{t=0}} \lambda i(\lambda)^{-1} & \lambda \geq b \end{cases} \quad (3.30)$$

Here again, do note that  $\lambda$  represents the circumferential tissue stretch, and the minimum ( $\lambda_C^{R,min}$ ), maximum ( $\lambda_C^{R,max}$ ) and mode ( $\lambda_C^{R,mod}$ ) recruitment stretches are denoted by  $a$ ,  $b$  and  $c$  respectively and the  $x$  represents *myo* or *epi*.

### 3.4.6 Growth & Remodelling of the Myocardial Wall

The cardiomyocytes are replete with mitochondrial structures, which essentially generates the power to actuate contraction in the muscle. This generation of energy needs to be supplemented by enough nutrition and oxygen supply to the cells by perfusion. The cardiomyocytes stay functional since inception in neo-natal hearts all the way upto death of the individual and have a life span of the individual in question and can be ascribed to the average survival rate of human beings. Therefore, with the passive constituents considered in healthy myocardial tissue elastin with a half-life of approximately 40 to 70 years (Langille (1993), Martyn & Greenwald (1997)), are one of the most stable proteins. Collagen fibres are being maintained by the action of fibroblasts eventuating deposition and degradation via chemical signalling pathways, having a shorter half-life of around 3 months. In the infarcted myocardium however, due to the necrosis of cardiomyocytes a cascade of biochemical and biomechanical processes are in play altering the composition and affecting the life span of the cells and the extra-cellular matrix constituents. Devoid of cardiomyocytes, the myocardial tissue contains an increased mass density of collagen fibres in the region of damage, however over the time period of disease progression damage by MMPs, loss of cross-linking between collagen fibres, cardiomyocyte slippage and degradation throughout the tissue results in a complex, stiff, almost isotropic scar tissue. Though the phases and damage to the myocardial wall is well understood post-MI, it still remains poorly understood

in terms of quantification of how each constituent mass density evolves. Therefore, with this knowledge necrosis of the cardiomyocytes is ascribed to simulate an infarcted tissue as follows:

$$m^M = m_d^{i/t} \quad (3.31)$$

where, in the cardiomyocytes normalised mass density ( $m^M$ ) is subject to a degradation to a minimum value ( $m_d$ ), over the a period of time ( $t$ ) to reach this minimum value. This is based on the current step in the simulation cycle which determines the division of the total time period considered by a certain number of steps. An example is considering the remodelling of the myocardium post-MI for upto 8 weeks and carried out over 100 steps per step time unit can be determined as:

$$dt = tp/n \quad (3.32)$$

where,  $dt$  is the time unit per step based on the total time period considered and  $n$  is the number of steps. Based on the example above 8 weeks translates to 56 days and a 100 steps would estimate  $dt = 0.56$  and  $\frac{x}{dt}$  would give us the value of  $t$  (Equation [3.31]) in terms of the days ( $x$  days) rather than steps, making it easier to set a degradation time based on experimental/ clinical observations or test scenarios as desired.

### 3.4.6.1 Remodelling of the Recruitment Stretch Distribution

The collagen fibre natural reference configuration stretch i.e. the recruitment stretch remodels according to a partial differential equation as employed in (Aparício et al. (2016), Chen (2014)). The recruitment stretch is assumed to evolve due to the changing tissue stretch, to maintain a preferred homoeostatic stretch in the loaded configuration ( $\Omega_t$ ) at end-diastole for the myocardial tissue. The evolution is driven by the deviations in the collagen fibre stretch from the attachment stretch, in our model this attachment stretch is calibrated at time  $t=0$ . The formulation for recruitment stretch remodelling is shown below:

$$\begin{aligned} \frac{d\lambda_C^{R,max}}{dt} &= \alpha \left[ \frac{\lambda_C^{min} - \lambda_C^{AT,min}}{\lambda_C^{AT,min}} \right] \\ \frac{d\lambda_C^{R,min}}{dt} &= \alpha \left[ \frac{\lambda_C^{max} - \lambda_C^{AT,max}}{\lambda_C^{AT,max}} \right] \\ \frac{d\lambda_C^{R,mod}}{dt} &= \alpha \left[ \frac{\lambda_C^{mod} - \lambda_C^{AT,mod}}{\lambda_C^{AT,mod}} \right] \end{aligned} \quad (3.33)$$

Since, the recruitment stretch distribution is defined by a triangular distribution (Equation [3.18]), defined by a minimum ( $\lambda_C^{R,min}$ ), maximum ( $\lambda_C^{R,max}$ ) and mode ( $\lambda_C^{R,mod}$ ) recruitment stretch, the remodelling equations apply to these three quantities.

### 3.4.6.2 Growth in the ECCM mass density

Fibroblasts and myofibroblasts are observed in the healthy myocardium but are engaged in the regulation of the synthesis, degradation of the collagen extra-cellular matrix to maintain homoeostasis. Due to the balance between the TIMPs and MMPs no disruption in the ECCM or fibrosis is observed. However, the disruption of this balance due to myocardial infarction leading to cardiomyocyte death and replacement with collagenous scar tissue is the results of proliferative behaviour of fibroblasts, and increased deposition of collagen due to multiple chemical signalling, biomechanical factors. There is no known functional form to describe the mechanical behaviour and cues which influences the up-regulated collagen fibre synthesis in the infarcted tissue. We therefore assume the deviatons in the maximum collagen fibre stretch from the maximum attachment stretch at  $t=0$  ((from the attachment stretch distribution,  $\rho(\lambda_C^{AT})$ )), is responsible for the synthesis and/or degradation of the collagen mass density. Mathematically it is represented as:

$$\frac{dm^C}{dt} = \gamma \left[ \frac{\lambda_C^{max} - \lambda_C^{AT,max}}{\lambda_C^{AT,max}} \right] \quad (3.34)$$

If there is an increase in the maximum collagen stretch, a positive net increase in the mass density is observed, leading to a decrease in the maximum collagen stretch ( $\lambda_C^{max}$ ) in an attempt to restore the maximum collagen stretch to the maximum attachment stretch ( $\lambda_C^{AT,max}$ ). Consequently, a decrease in the mass density can be interpreted as the degradation of collagen fibres as the maximum collagen stretch levels are lower than the maximum attachment stress level. Therefore, the dynamic process of synthesis and degradation of the collagen fibres by the action of fibroblasts in response to mechanical cues (here collagen fibre stretch) is encapsulated in the differential equation, this has been derived from past research on aneurysms ([Aparício et al. \(2016\)](#), [Watton et al. \(2009\)](#)).

### 3.4.6.3 Attachment Stretch Distribution Specification

The specification of the stretch distributions  $\Pr(\Lambda_{C,myo}^{AT})$  and  $\Pr(\Lambda_{C,epi}^{AT})$  for the myocardial and epicardial collagen fibres respectively, are calibrated with respect to the maximum attachment stretch ( $\lambda_{C,x}^{AT,max}$ ), minimum attachment stretch ( $\lambda_{C,x}^{AT,min}$ ) and mode attachment stretch ( $\lambda_{C,x}^{AT,mod}$ ) values. The values for collagen attachment stretches vary from 1 to 1.10 across various models in the past (please refer (Chen (2014)) for a full list). We assume the myocardial collagen attachment distribution has a maximum attachment stretch ( $\lambda_{C,myo}^{AT,max}$ ) of 1.05 at time  $t=0$ , based on its participation of preventing overstretch between cardiomyocyte muscle bundles during diastole. For the epicardial collagen attachment stretch distribution, a maximum attachment stretch ( $\lambda_{C,epi}^{AT,max}$ ) of 1.0 is assumed, to indicate its presence as a protective sheath in the healthy myocardium. Both these triangular distributions are assumed to have a width ( $w$ ) of 0.1 and skew ( $s$ ) of 0.5, providing us with a univariate attachment distribution, given the circumferential arrangement of fibres assumed.

The triangular distribution is formulated with the minimum, maximum and mode values (taken as  $\lambda_{C,x}^{AT,min}$ ,  $\lambda_{C,x}^{AT,max}$ ,  $\lambda_{C,x}^{AT,mod}$  respectively). We define a width w.r.t the maximum attachment stretch for collagen fibres, as this helps us calculate the minimum attachment stretch and mode attachment stretch via Equation [3.35]. These distributions are plotted in the Figure [3.6]. In parallel to biological assumption, it can be observed as the range of stretches the collagen fibres in the myocardium are configured at time  $t=0$ .

The values for the attachment stretch distribution are calculated based on the width ( $w$ ) and skew ( $s$ ) as mentioned, they are derived by defining a maximum attachment stretch ( $\lambda_{C,x}^{AT,max}$ ) and the minimum ( $\lambda_{C,x}^{AT,min}$ ), mode ( $\lambda_{C,x}^{AT,mod}$ ) are calculated as follows:

$$\begin{aligned} \lambda_{C,x}^{AT,min} &= \lambda_{C,x}^{AT,max} - w \\ \lambda_{C,x}^{AT,mod} &= \lambda_{C,x}^{AT,min} + s(\lambda_{C,x}^{AT,max} - \lambda_{C,x}^{AT,min}) \end{aligned} \quad (3.35)$$

where  $x$  denotes the layer in which the collagen fibres are present i.e.  $x = myo, epi$ .

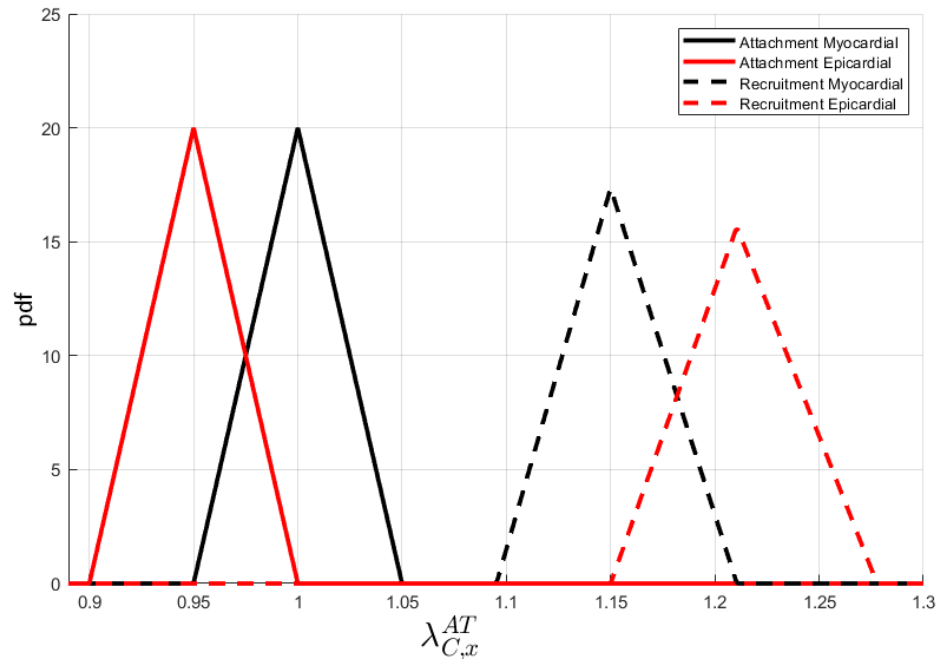


**Figure 3.6:** The attachment (**left**) and recruitment(**right**) stretch distributions for the myocardial and epicardial collagen fibres. The myocardial collagen attachment stretch distribution ranges from a minimum of 0.95 to a maximum of 1.05 and the recruitment stretch ranges from 1.1 to 1.095 to 1.21. Given that the tissue stretch at  $t=0$  is prescribed to be 1.15 the collagen fibres in the myocardial tissue, with stretches below 1.15 bear load. However, the attachment stretch distribution for the epicardial collagen fibres ranges from 0.9 minimum to 1.0 maximum and the recruitment stretch distribution ranges from 1.15 minimum to 1.27 maximum, and therefore, none of the epicardial collagen fibres bear load at time  $t=0$ . This reflects the epicardial collagen fibres acting as a protective sheathe, while the myocardial collagen fibres partake in the force-balance of the LV wall due to the internal diastolic blood pressure.

### 3.4.6.4 Parameter Values

Here, parameter values are summarised and appropriate justification is provided for values not covered previously in the Table [3.1].

Parameter	Value
R (undeformed radius)	31.0175 mm (Hassaballah et al. (2013))
H (undeformed thickness)	10.3 mm (Hassaballah et al. (2013))
p (diastolic pressure)	1.3 kPa (Boron & Boulpaep (2016))
$\lambda$	1.15
$\lambda_M^{AT}$	1.05
$\lambda_M^{max}$	1.26
$\lambda_M^{min}$	0.89
$\lambda_{C,myo}^{AT,max}$	1.05
$\lambda_{C,myo}^{AT,mod}$	1.00
$\lambda_{C,myo}^{AT,min}$	0.95
$\lambda_{C,epi}^{AT,max}$	1.00
$\lambda_{C,epi}^{AT,mod}$	1.95
$\lambda_{C,epi}^{AT,min}$	0.9
width ( $w$ )	0.1
skew ( $s$ )	0.5
time period ( $t$ )	100 days
simulation steps ( $n$ )	1000 steps
$dt$	$\frac{t}{n} = 0.1$
$\alpha$	0.5
$\beta$	0.5
$\gamma$	2.65

**Table 3.1:** The various parameters, values and constants in the constrained mixture model and their associated values used in the 1D LV growth and remodelling simulation.

#### Rationale for parameter values

The undeformed radius (R) and undeformed thickness (H) considerations are based on the data from studies as described in Section [3.3], and pressure 1.3 kPa refers to the internal pressure on the LV wall at end-diastole. The tissue stretch  $\lambda = 1.15$ , is inferred from echocardiographic reference from the NORRE study (Kou et al. (2014)), where the average Left Ventricular End Diastolic Diameter (LVEDD) is 44.3 mm and the average Left Ventricular End Systolic Diameter (LVSD) is calculated from the data with the value 29.9 mm. Given our assumption for the stress free reference configuration ( $\Omega_0$ ), to be at point D (3.1) the diameter at said point is calculated as  $(\frac{LVEDD+LVSD}{2})$  and a value of 37.1 mm is obtained. On considering the LV diameter at reference configuration ( $\Omega_0$ ) and loaded configuration ( $\Omega_t$ ) at end diastole, the stretch obtained by the data above is  $\lambda = \frac{44.3}{37.1} = 1.19$ . Given our dimension for LV radius and thickness obtained from (Hassaballah et al. (2013)), 1.15 is assumed to be the stretch of the tissue at loaded configuration ( $\Omega_t$ ), as a

test case. The constituent stretches are based on the assumptions provided in Section [3.4.6.3] for collagen fibre stretches ( $\lambda_{C,x}^{AT,max}$ ), where  $x = myo, epi$ . The cardiomyocyte stretches ( $\lambda_M^{AT}$ ),  $\lambda_M^{max}$  and  $\lambda_M^{min}$  are derived via the length-tension or force-length curve for sarcomeres shown in Figure [3.4], as the maximum physiological length for sarcomeric stretch is  $2.2 \mu\text{m}$  (0), and assumed resting length to be  $1.9 \mu\text{m}$  the muscle stretch at  $\Omega_t|_{t=0}$  is taken to be  $\lambda_M^{AT} = \frac{2.2}{1.9} = 1.15$ , whereas the maximum is taken to be  $\lambda_M^{max} = \frac{2.3}{1.9} = 1.26$  and minimum around  $\lambda_M^{min} = \frac{1.5}{1.9} = 0.89$ , where minimum sarcomeric length is  $L_{min} = 1.5 \mu\text{m}$  and maximum muscle stretch is taken to be a little above maximum length ( $L_{max}$ ) at  $2.3 \mu\text{m}$ , see Figure [3.4], (Flitney & Hirst (1978), Krueger & Pollack (1975)). The width and skew of the collagen undulation distribution are taken to be  $w = 0.1$  and  $s = 0.5$ , respectively as the collagen fibres in soft connective tissues, especially the myocardial tissue are stiff and resist lengthening beyond a certain limit (Holzapfel & Ogden (2009)), in order to maintain structural integrity of the organ. The skew maintains the attachment stretch distribution so that half of the collagen fibres are in crimped  $\lambda_C^{AT} < 1$ , whereas the other half  $\lambda_C^{AT} > 1$  are in load bearing configuration. This captures the collagen fibres existing in a varied state of stretch rather than possessing a single stretch configuration (Aparício et al. (2016), Chen (2014)). The maximum attachment stretch of myocardial collagen in the healthy LV is considered to be 1.1 due to its role as contributing to primary load bearing role in end-diastole along with ground matrix and cardiac myocytes, whereas 1.0 for the maximum attachment stretch of epicardial collagen fibres due to its role as a protective sheathe. Clinical studies and experiments pertaining to the left ventricular myocardium undergoing infarction is usually carried out for a period of 1 to 8 weeks i.e. 7 to 56 days. Therefore, a time period ( $t$ ) of 100 days,  $\approx 14$  weeks, is chosen, to understand the changes in collagen mass densities and structural changes, i.e. tissue stretch and thickness beyond those days to understand model behaviour. The simulation steps ( $n$ ) depict the division of the time period( $t$ ), into a number of simulation steps and greater the number provides a smoother curve owing to more plotting points which are computed at each step,  $n = 1000$ . Terminally, the rate parameters  $\alpha = 0.5, \beta = 0.5$  and  $\gamma = 2.65$ , were selected to observe perceivable dilatation and thinning of myocardium post-MI and their calibration can be based on empirical data (Sections [3.5.1], [3.6.1] and Table [3.2]).

### 3.4.6.5 Evolution of the Attachment Stretch Distribution

The epicardial collagen fibres in a healthy LV, act as a protective sheathe to prevent over-distension of cardiomyocytes. However, after cardiomyocyte necrosis post-MI, they are assumed to bear a primary load bearing role leading to their uncoiling and stretching as a consequence of increased load experienced due to the internal diastolic blood pressure. To mathematically assume the evolution the maximum attachment stretch for epicardial collagen fibres ( $\lambda_{C,epi}^{AT,max}$ ) undergo an adaptation/ evolution regime. This in turn causes a translational shift in the attachment stretch distribution function, wherein the minimum ( $\lambda_{C,epi}^{AT,min}$ ) and mode ( $(\lambda_{C,epi}^{AT,mod})$ ) attachment stretches are derived from the maximum attachment stretch, the width and the skew of the distribution (Section [3.4.6.3]). We adapt the attachment stretch distribution with a few cases to

understand the impact of amount of uncoiled collagen fibres on the overall tissue composition and stretch post-MI. These formulations have been adapted from (Chen (2014)).

$$\lambda_{C,epi}^{AT,max}(t) = \lambda_{C,epi}^{AT,max}(0) + \frac{\lambda_{C,epi}^{AT,max}|_f - \lambda_{C,epi}^{AT,max}(0)}{1 + e^{-B(t-n/5)}} \quad (3.36)$$

where, B is the growth rate of the curve (taken as 3), n is the duration of cardiomyocyte degradation/gm, t is the current time step in the simulation.  $\lambda_{C,epi}^{AT,max}|_f$  is the maximum final stretch of the epicardial collagen, after the cardiomyocytes have undergone complete necrosis.

Based on the triangular attachment distribution function considered, a number of cases can be identified for the method of evolving it based on its skew and width. The cases in Figure [3.7], are

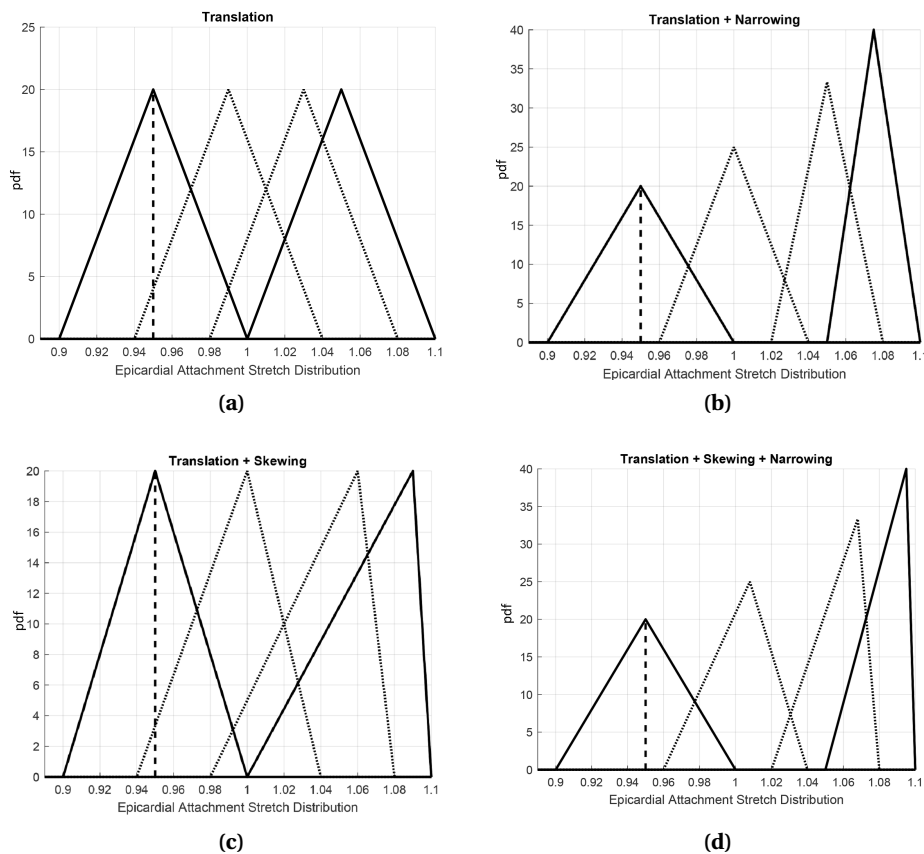


**Figure 3.7:** Evolution of epicardial attachment stretch distributions for cases 2 to 5. Case 1 involves no change in the attachment stretch distribution and therefore is not represented in the figure.

detailed below:

- *Case 1* The attachment stretch distribution for the epicardial collagen fibres is considered to be constant.
- *Case 2* (Figure [3.7] (a)), assumes the translation of the attachment stretch distribution ( $\rho(\lambda_C^{AT})$ ) with the initial width ( $w$ ) and skew ( $s$ ) (refer Equation [3.35]).

- *Case 3* (Figure [3.7] (b)), involves the translation of the  $\rho(\lambda_C^{AT})$  by 0.1 units, a decrease in width from 0.1 to 0.05.
- *Case 4* (Figure [3.7] (c)), assume the  $\rho(\lambda_C^{AT})$  to translate by 0.1 units for maximum attachment stretch ( $\lambda_C^{AT,max}$ ) and a skew from an initial 0.5 to 0.9.
- *Case 5* (Figure [3.7] (d)), involves the translation, skewing and width decrease of 0.1, 0.9 and 0.05 respectively.

### Rationale for Cases

Given the limited amount of biological data, describing the collagen undulation distribution in the infarcted scar tissue post-MI in a specific form as hypothesised (Section[3.4.6.3]) the role change of the epicardial collagen fibres is represented by evolving the distribution maximum attachment stretch ( $\lambda_{C,epi}^{AT,max}$ ). The initial epicardial collagen distribution function maximum attachment stretch is  $\lambda_{C,epi}^{AT,max} = 1.0$ , and the corresponding minimum, mode attachment stretches are  $\lambda_{C,epi}^{AT,min} = 0.9$ ,  $\lambda_{C,epi}^{AT,mode} = 0.95$ . Since, all these stretch values are less than 1 they typically bear no load in the healthy myocardial tissue in the CMM. Therefore, a translation is applied, to shift its role from a protective sheathe to a primary load bearer to compensate for tissue necrosis post-MI. The maximum value  $\lambda_{C,epi}^{AT,max}$  is limited to 1.1 for every case, as collagen fibres are known to be highly resistant to stretch, resulting in the steep slope in its stress-stretch response [Holzapfel (2006)]. The five different cases are considered as a set of combinations can be applied to a triangular distribution function based on its width and skew, along with translation.

#### 3.4.6.6 Remodelled Volumetric Thickness

The deformed thickness  $h$  changes in the simulation would reflect variations due to our assumption of the myocardium being an incompressible soft tissue. However, if the myocardial wall is considered to be composed of volume fractions ( $\mathbf{v}_f$ ) of each constituent, it is possible to calculate the volumetric changes in wall thickness based on the assumptions introduced in (Chen (2014)), where the volumetric thickness changes are  $h_{rem}$ . In this case the remodelled thickness for the myocardial wall is taken to be as follows:

$$h_{rem} = \mathbf{v}_f^{GM} m^{GM} + \mathbf{v}_f^M m^M + \mathbf{v}_f^{C,myo} m^{C,myo} + \mathbf{v}_f^{C,epi} m^{C,epi} \quad (3.37)$$

where,

$\mathbf{v}_f^x$  - volume fraction of constituent x.

The values assumed here are grossly based on the volume occupied by each constituent taken as:  $\mathbf{v}_f^{GM} = 0.2$ ,  $\mathbf{v}_f^M = 0.7$ ,  $\mathbf{v}_f^{C,myo} = 0.05$ ,  $\mathbf{v}_f^{C,epi} = 0.05$ .

### 3.5 Results

Python scripts were employed to run the model. The cases displayed in the result sets are as follows:

1. *Case 1*: Maintaining a constant attachment stretch distribution.
2. *Case 2*: The translation of the epicardial attachment stretch distribution.
3. *Case 3*: The translation and width reduction of the epicardial attachment stretch distribution.
4. *Case 4*: The translation and skewing of the epicardial attachment stretch distribution.
5. *Case 5*: The translation, skewing and width reduction of the epicardial attachment stretch distribution.

The results detail the evolution of epicardial collagen mass density, circumferential tissue (ground matrix) stretch, cardiomyocyte mass density degradation, maximum in vivo epicardial collagen stretch, remodelled volumetric thickness and the ratio of the remodelled thickness over remodelled radius illustrated over a span of 100 days. We observed the model behaviour for these 5 cases using the rate constants for growth and remodelling parameters as follows:

1. Collagen fibre recruitment stretch distribution remodelling rate ( $\alpha = 0.5$ ).
2. Collagen fibre mass density rate of change ( $\beta = 2.65$ )
3. Cardiomyocyte recruitment stretch ( $\gamma = 0.5$ )

Figure [3.8], shows the mass density degradation for the cardiomyocytes and myocardial collagen fibres until day 4, after which it maintains a minimum mass density ( $m_{min}^X = 0.01$ ) and remains the same for all cases considered.

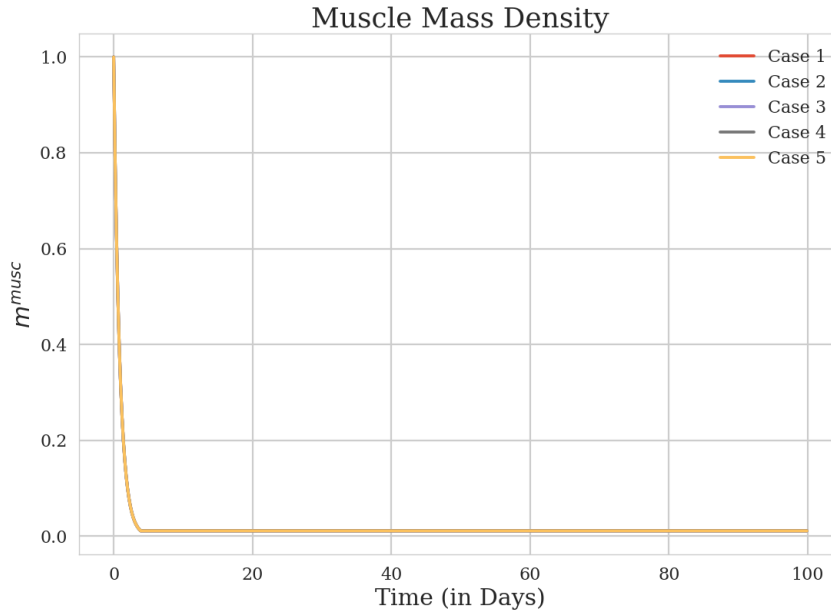


**Figure 3.8:** The cardiomyocytes mass density is degraded to  $m_{min}^M = 0.01$  over a period of 4 days to initiate the onset of myocardial infarctions in the constrained mixture model. This is true for all cases considered.

Figure [3.9], depicts the degradation of collagen fibres over a period of 14 days, indicating the disruption of the collagen extra-cellular matrix due to the infiltration of immune cells.

The change in circumferential tissue stretch ( $\lambda$ ) of the LV myocardium is shown in Figure [3.10]. In every case the stretch increases from 1.15 to 1.275, after which a deviation in their behaviour is observed. For Case 1 there is a rapid rise in  $\lambda$ , rising well above 3 at day 17 and reaching 29.92 at day 100. Cases 2, 3 and 4 continue to enlarge at the end of the simulation, with case 4 showing the least rise at day 100, reaching a stretch of 2.88, 2.36 and 2.004. Case 5 sees stabilisation of the infarction at a stretch of 1.85. Comparatively, even though the infarction stabilises in Case 5, the enlargement is small compared to the other cases for the infarcted LV tissue. The increase in stretches for Cases 1,2,3,4 and 5 is 26.0, 2.5, 2.05, 1.74 and 1.6 respectively from an initial value of 1.15.

The growth of epicardial collagen mass density is captured in Figure[3.11]. Given the mass density of collagen ( $m^{C,epi}$ ) is proportional to the cube of the tissue stretch ( $\lambda^3$ ), a large increase is required to help stabilise the tissue post-MI. This is observed prominently in Case 1, where the mass density goes well beyond 100 at day 17, and reaches a target value of  $2.3 \times 10^7$ . In case 2, ( $m^{C,epi}$ ) increases upto 75.58 times the initial value. Cases 3, 4 and 5 subsequently see a rise of

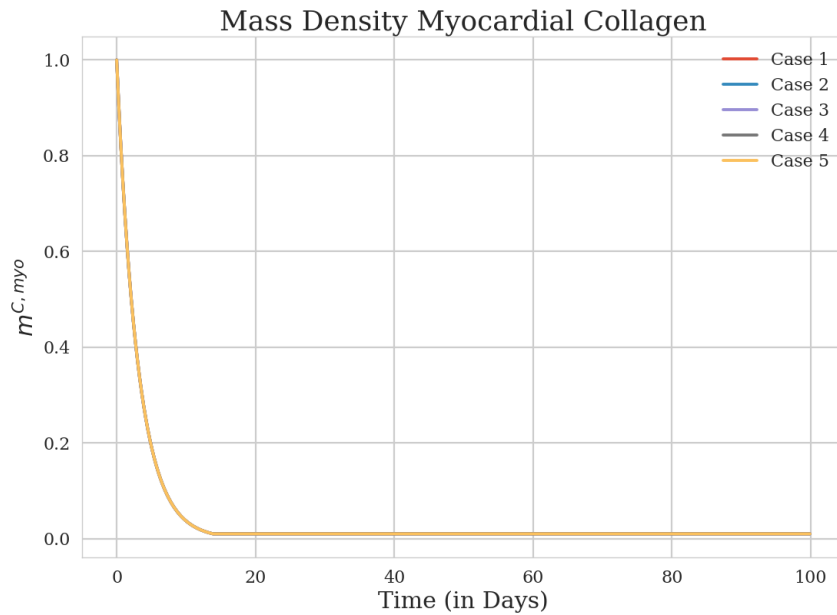


**Figure 3.9:** The myocardial collagen fibres present within the myocardium are prescribed to degrade over a period of 14 days, depicting the inflammation phase of the extra-cellular matrix. True for all cases considered.

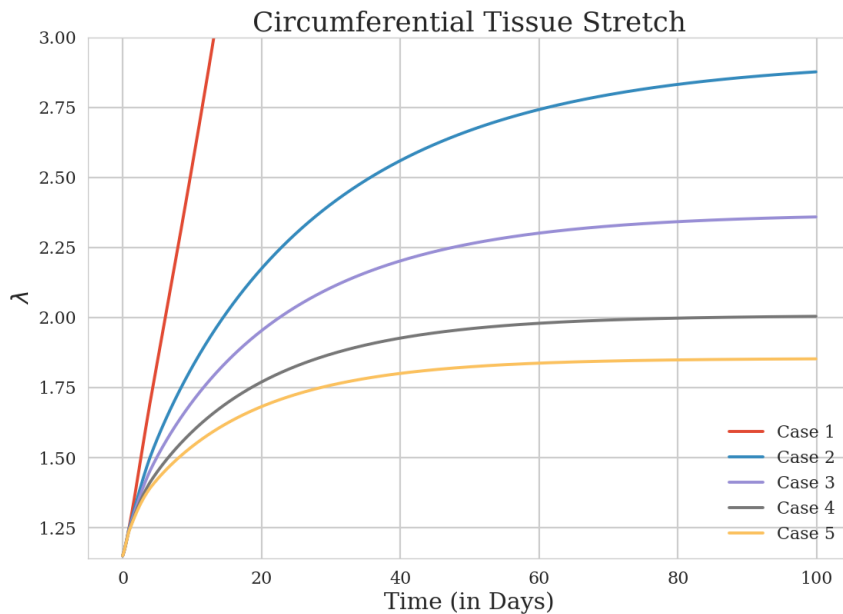


**Figure 3.10:** The circumferential stretch of the left ventricular myocardium, also referred to as the ground matrix stretch in the model. The rates of mass density changes are kept the same for each case. In case 1 the tissue stretch increases exponentially, whereas cases 2 to 4  $\lambda$  continues to increase slightly by the end of the simulation, the slowest growth observed in case 4. Case 5 observes stabilisation by the end of the simulation.

26.75, 11.36 and 7.5 at the end of the simulation from an initial mass density of 1 at time  $t=0$ .

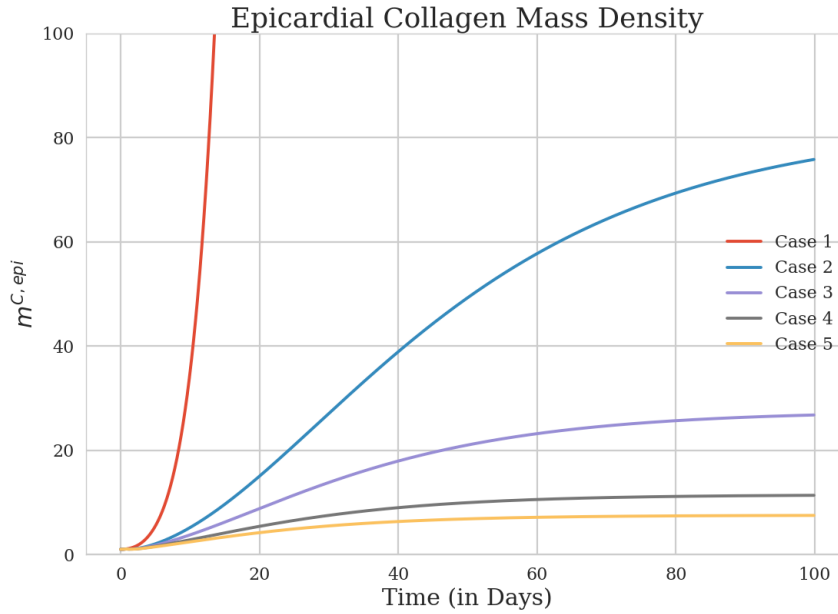


**Figure 3.11:** The mass density changes in the epicardial collagen is shown, Case 1 observes an exponential rise in mass density reaching values beyond 100 after day 15. Cases 2, 3 and 4 observe a terminal mass density of  $\approx 76$ ,  $\approx 26$  and  $\approx 16$  respectively rising at decreasing rates from Case 2 to Case 4 at  $t=100$  days. In case 5 the epicardial collagen mass density reaches  $\approx 8$  with a stabilising trend from day 60 to the end of the simulation.

The maximum stretch experienced by an epicardial collagen fibre is shown in Figure[3.12]. In Case 1 the maximum collagen stretch reaches a value of about 1.033 from an initial value of 1.00. In the other cases, owing to the evolution of the attachment stretch distribution to a final maximum stretch of value of 1.1 it can be seen that the collagen fibres tend towards this new homeostatic stretch value albeit at slower rates from Case 2 to Case 5, where in Case 5 homeostatic attachment stretch levels are obtained i.e the tissue stabilises.

The remodelled volumetric thickness ( $h_{rem}$ ), is shown in Figure [3.13]. The remodelled thickness takes into account the micro-structural constituent mass densities in the constrained mixture model multiplied with the deformed incompressible thickness (see Section[3.4.6.6]). Case 1 shows the a rapid increase in the remodelled thickness following the steep rise in the epicardial collagen mass density ( $m^{C, epi}$ ) in Case 1, starting from an initial 7.78 mm to 13342.5 mm at day 100. Subsequently, Cases 2 and 3 are still relatively thicker compared to Cases 4 and 5, however lower than the initial remodelled thickness of 7.78mm. At day 100, the remodelled thickness reduces to 4.96 mm, 2.86 mm, 2.0 mm and .175 mm from an initial value of 7.78 mm for cases 2, 3, 4 and 5 respectively. The remodelled thickness stabilises in Case 5, where as it continues to enlarge at increasing rates from Case 4 to Case 1.

Terminally, the ratio of the remodelled thickness ( $h_{rem}$ ) to the remodelled radius ( $r_{rem}$ ), repre-

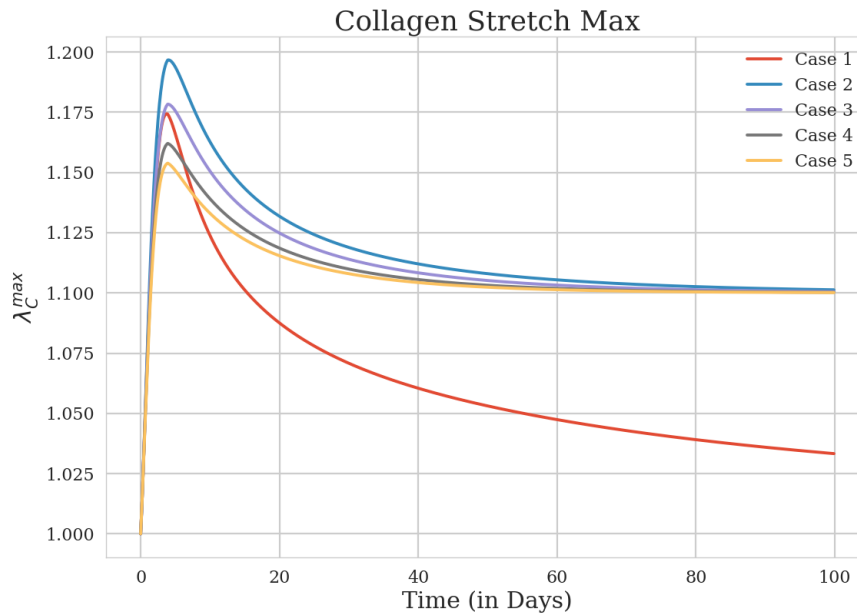


**Figure 3.12:** The maximum epicardial collagen fibre stretch for the various cases. The values all tend towards the attachment stretch by the end of the 100th day. For Case 1, since the attachment stretch distribution is constant the maximum stretch tends towards the original value of 1.05 but fails to reach homeostatic levels. The other cases the maximum collagen stretch reaches the evolved attachment stretch distribution by the end of day 100.

sented as ( $\chi$ ) is shown in Figure [3.14]. It follows the remodelled thickness graph, where in, at day 100, a  $\chi$  value of 14.36 is reached in Case 1, a ratio of  $\approx 0.057$  is attained for Case 2,  $\approx 0.039$  for Case 3 and  $\approx 0.032$  for case 4. In Case 5, where the tissue stabilises a value of  $\approx 0.03$  is seen at day 100.

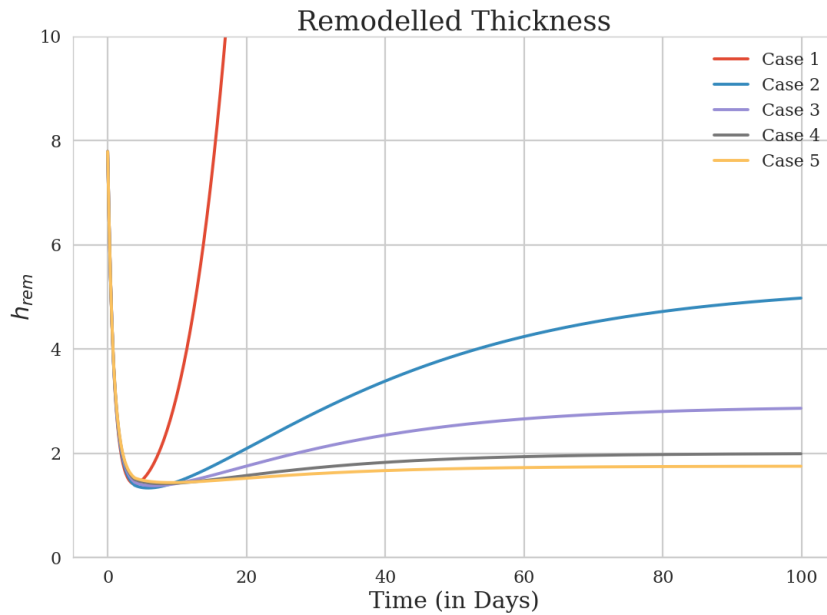


**Figure 3.13:** The remodelled LV wall thickness shown, takes into account the volumetric growth of the micro-structural constituents, denoted by ( $h_{rem}$ ). Starting from a value of 7.78 mm the remodelled wall thickness attaining a final value of 13342.5 mm, 4.96 mm, 2.86 mm and 2.0 mm for Cases 1, 2, 3, and 4 respectively. In Case 5, where the tissue stabilises without enlarging further the remodelled thickness at day 100 is about 1.75 mm.

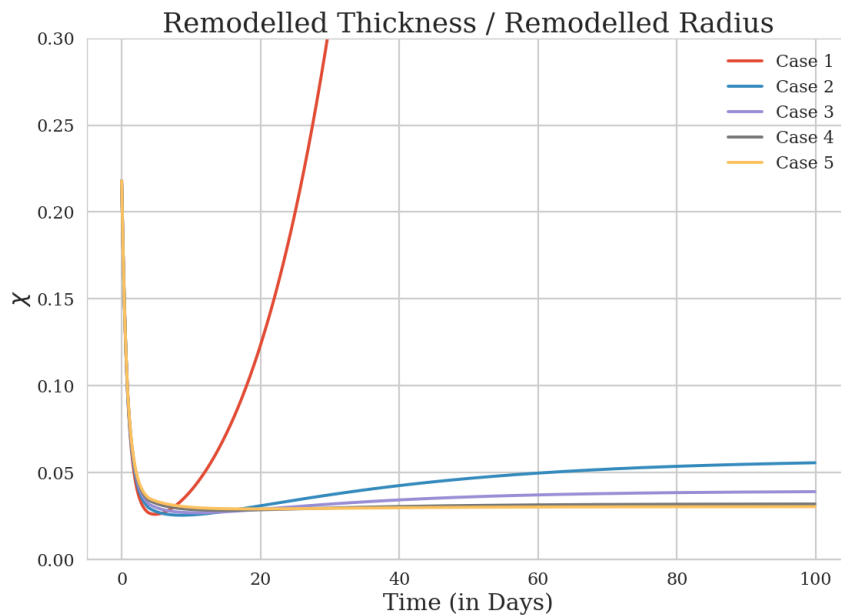


**Figure 3.14:** The remodelled thickness ( $h_{rem}$ ) to remodelled radius is shown. An initial value of  $\approx 0.22$  at  $t=0$  is observed, reducing to around  $\approx 0.035$  at  $t=5$  days after which each case sees a variation in behaviour. Case 1 rises exponentially beyond 0.30 at  $t=30$  days. cases 2, 3, 4 observe slightly increasing values till  $t=100$  days at  $\approx 0.057$ ,  $\approx 0.04$ , and  $\approx 0.033$  respectively. Case 5 stabilises at a value of  $\approx 0.031$  at  $t=100$  days.

### 3.5.1 Model performance with Experimental Data

Experimental data from (Fishbein et al. (1978)), provides information about the change in structure and morphology of the rat left ventricle post-MI induced via ligation of the left coronary artery. The occlusion of the said artery, led to histologic changes which provides us with comparable data for the 1D constrained mixture model. Based on the data reproduced as a graph in Figure[3.15], model input parameters are calibrated and rates tabulated as seen in Table[3.2]. This study observed the infarcted tissue for a period of 21 days post ligation, and healed necrotic tissue were excised for calculating its dimensions, structure and morphology. apart from the dimensions and time steps, which are derived from existing literature, the attachment stretches have been considered from hypotheses presented in Section[3.4.6.3]. Remodelling and deposition rate parameters ( $\alpha, \beta, \gamma$ ) have been tuned so as to capture the thickness changes observed in (Fishbein et al. (1978) in the model variable  $h_{rem}$ . This allows model validation with experimental results, and infer data which have not been accounted for in the paper, namely the collagen mass density changes, tissue stretch and maximum collagen stretch configurations as a result of the growth and remodelling regime.

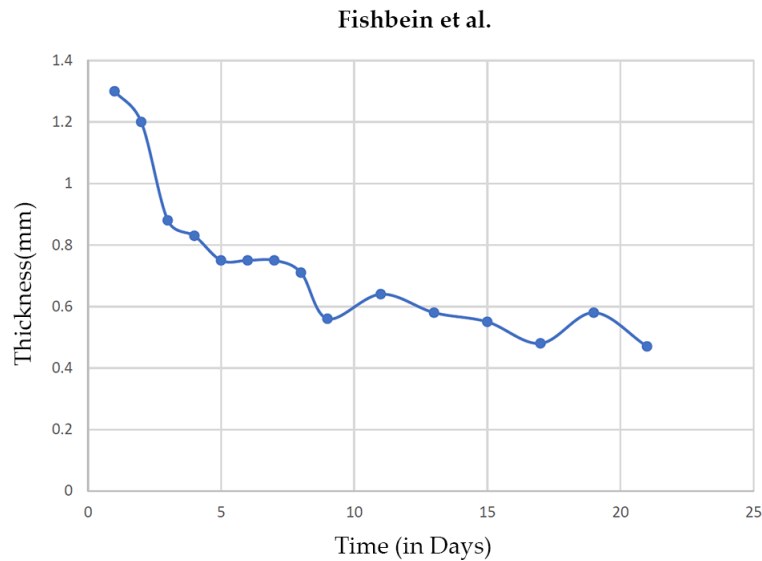


**Figure 3.15:** Changing myocardial thickness, based on the observed evolution of myocardial infarction in rat hearts (six out of seven rats, (Fishbein et al. (1978)) measure at the thinnest point of the infarction. This image has been created using the data provided in aforementioned paper.

An important consideration is the degradation ascription for the cardiac myocyte mass density ( $m^M$ ). Observing the thickness changes in (Fishbein et al. (1978)), multiple degradation regimes can be employed however since it was not quantified in the data observed. Assumptions can be made on continuous degradation, non-continuous degradation or a mix of both. A simplistic degradation function is used by degrading  $m^M$  to 10 % of it's original value ( $m_0^M$ ) and other cases are further discussed in latter Section[3.6], indicating a need to sophisticate degradation criteria

Parameter	Value
R (undeformed radius)	3.5 mm (Pawlush et al. (1993))
H (undeformed thickness)	1.4 mm (Fishbein et al. (1978))
p (diastolic pressure)	0.53329 kPa (Fletcher et al. (1981))
$\lambda$	1.15
$\lambda_M^{AT}$	1.05
$\lambda_M^{max}$	1.26
$\lambda_M^{min}$	0.89
$\lambda_{C,myo}^{AT,max}$	1.05
$\lambda_{C,myo}^{AT,mod}$	1.00
$\lambda_{C,myo}^{AT,min}$	0.95
$\lambda_{C,epi}^{AT,max}$	1.00
$\lambda_{C,epi}^{AT,mod}$	1.95
$\lambda_{C,epi}^{AT,min}$	0.9
width ( $w$ )	0.1
skew ( $s$ )	0.5
$\alpha$	0.5
$\beta$	0.5
$\gamma$	5.0
time period ( $t$ )	21 days
simulation steps ( $n$ )	1000 steps
$dt$	$\frac{t}{n} = 0.021$

**Table 3.2:** Parameter values for constrained mixture model, to capture the results observed in (Fishbein et al. (1978)).

for  $m^M$  from empirical data.

3.5.1.1 CMM Results for (Fishbein et al. (1978))

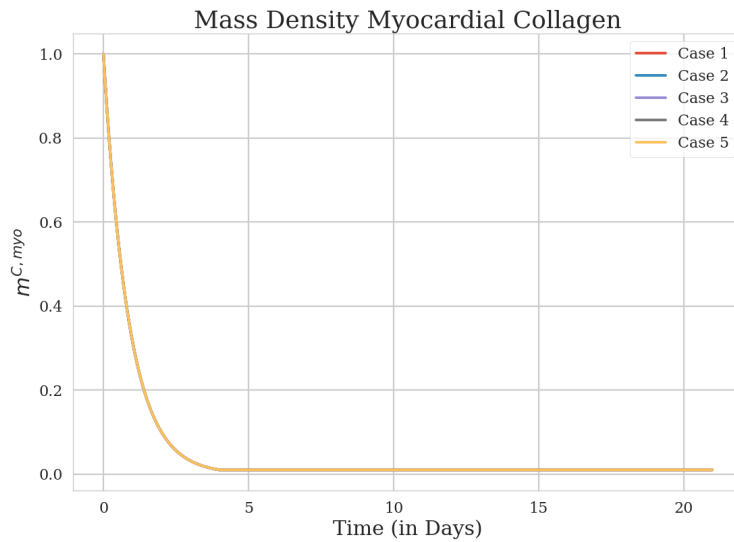


**Figure 3.16:** The myocardial collagen fibre mass density is degraded to 1 % of original value (1) from day 1 to day 4, representation for all cases are the same.

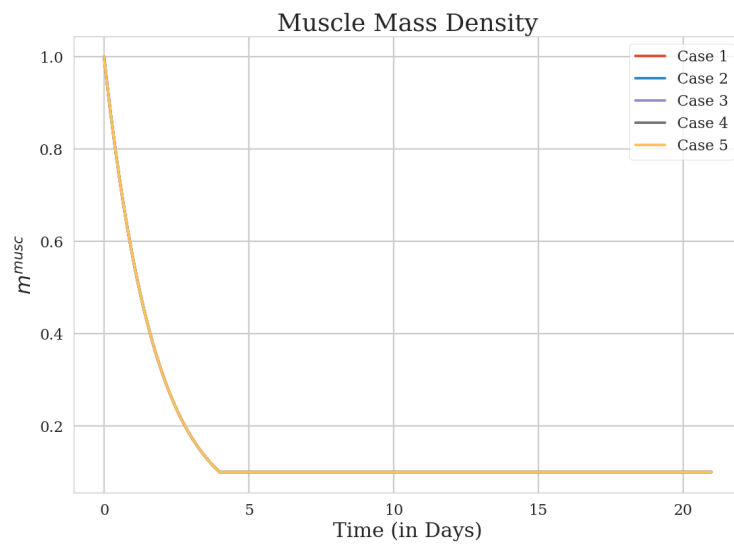


**Figure 3.17:** The cardiac myocyte mass density ( $m^M$ ), is degraded from 1.0 to 0.10 through 4 days for each case.

The cardiac myocyte mass density ( $m^M$ ), is degraded from 1.0 to 0.10 through 4 days for each case, shown in Figure[3.17] and likewise 0.01 for myocardial collagen mass density ( $m^{c,epi}$ , Figure[3.16]).

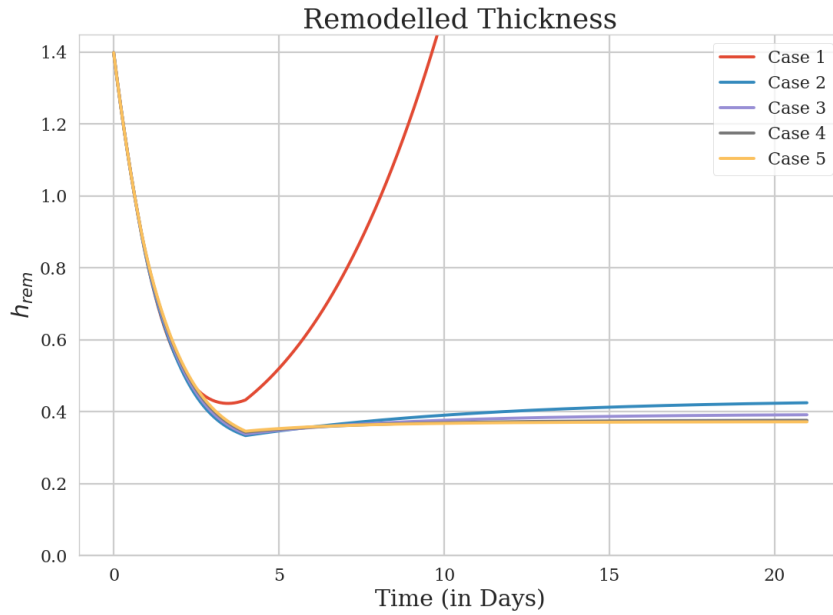


**Figure 3.18:** The remodelled volumetric thickness ( $h_{rem}$ ), decreases from 1.4 mm over time to a value of  $\approx 0.36$  at Day 4 due to the degradation regime of cardiac myocytes, but decreases only till about 0.415 for Case 1. While Case 1 exponentially rises, Cases 2 to 5 stabilise around  $\approx 0.4$ .

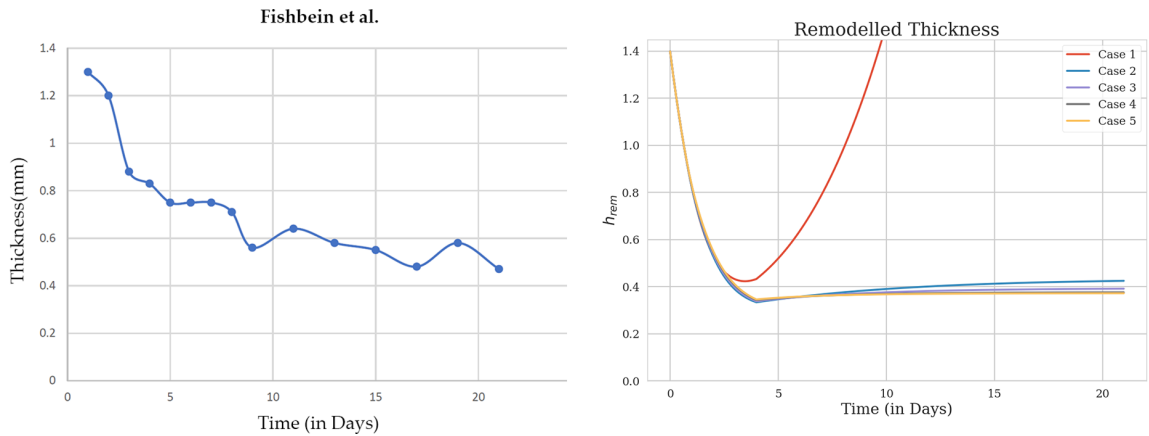


**Figure 3.19:** The remodelled thickness due to the degradation of cardiac myocytes to 10 % of original mass density till day 4 is observed. Initial value of 1.4mm and final values of around 0.4 for cases 2 to 5 are observed. Case 1, as noted in the CMM model analysis results proves to provide inconsistent results. The trajectory does not follow that of (Fishbein et al. (1978)) and the reasons are discussed in Section [3.6].

The remodelled volumetric thickness ( $h_{rem}$ , Figure[3.18]), decreases from 1.4 mm over time to a value of  $\approx 0.36$  at Day 4 due to the degradation regime of cardiac myocytes, but decreases only till about 0.415 for Case 1. As expected, Case 1 depicts an unrealistic increase in the thickness post-MI, whereas Cases 2 to 5 thin upto Day 4 and gradually thicken over time with varying trends by Day 21. There is a slight increasing trend in Case 2, whereas the Cases 3 to 5 show stabilising infarcts.

The remodelled thickness due to the degradation of cardiac myocytes to 10 % of original mass density till day 4 is observed, in comparison to data from (Fishbein et al. (1978)) in Figure[3.19]. Initial value of 1.4mm and final values of around 0.4 for cases 2 to 5 are observed. Case 1, as noted in CMM model analysis results proves to provide inconsistent results. The trajectory does not follow that of (Fishbein et al. (1978)) and the reasons are discussed in Section[3.6].

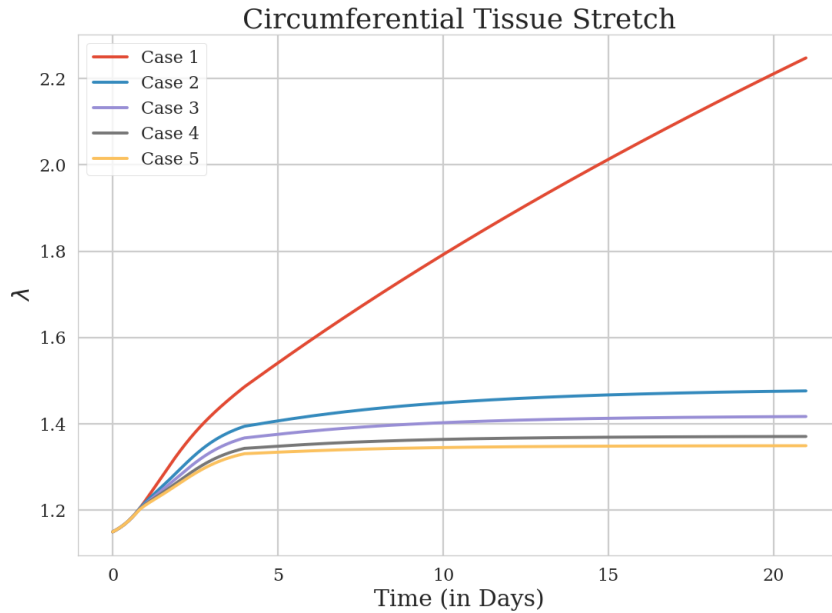


**Figure 3.20:** The circumferential tissue stretch ( $\lambda$ ) is depicted in this Figure. All cases follow a common trend up until Day 1. Case 1 sees a continuous increase up until day 21 at a value of  $\approx 2.23$ . Cases 2 to 5 appear to have a reduction in stretch around day 4. Post day 4, Case 2 increases slightly till day 21 possessing a value around  $\approx 1.51$ . Cases 3,4 and 5 reach values around 1.415, 1.375 and 1.35 respectively at day 21.

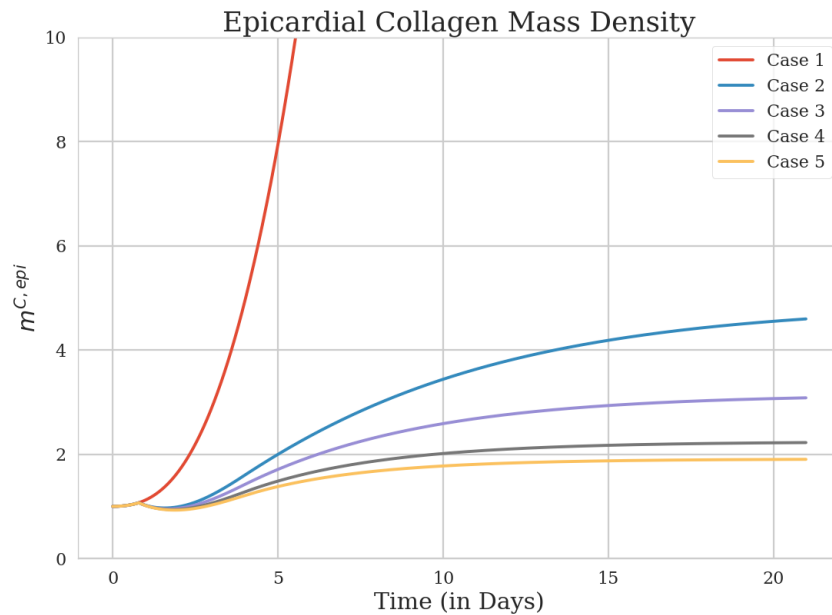


**Figure 3.21:** The changes in the epicardial mass density in the infarcted tissue are shown in this Figure. Case 1 increases exponentially. Cases 2 to 5 observe an interesting trend, with an initial increase till day 1 followed by a decrease, and rising again after day 3. Case 2 shows an increasing trend and continues to increase at day 21 at a value of  $\approx 4.35$ . Cases 3, 4 and 5 show plateauing after day 15 with terminal values at day 21 being  $\approx 3.2$ ,  $\approx 2.2$  and  $\approx 1.96$  respectively.

The circumferential tissue stretch, for our spherical membrane approximation for the rat heart model is depicted in Figure [3.20]. All cases follow a common trend up until Day 1 and their behaviours diverge forthwith. Case 1 sees a continuous increase up until day 21 at a value of  $\approx 2.23$ . Cases 2 to 5 appear to have a reduction in stretch around day 4. Post day 4, Case 2 increases slightly and retains this trend at day 21 with a value around  $\approx 1.51$ . Cases 3,4 and 5 show stabilising infarcts with values around 1.415, 1.375 and 1.35 respectively at day 21. The changes in the epicardial mass density in the infarcted tissue are shown in Figure[3.21]. Case 1 increases exponentially leading to unrealistic depositions of collagen fibres. Cases 2 to 5 observe an interesting trend, with an initial increase till day 1 followed by a decrease, and rising again after day 3 as cardiac myocytes degrade until day 4. Case 2 shows an increasing trend and continues to increase at day 21 at a value of  $\approx 4.35$ . Cases 3, 4 and 5 show plateauing after day 15 with terminal values at day 21 being  $\approx 3.2$ ,  $\approx 2.2$  and  $\approx 1.96$  respectively.

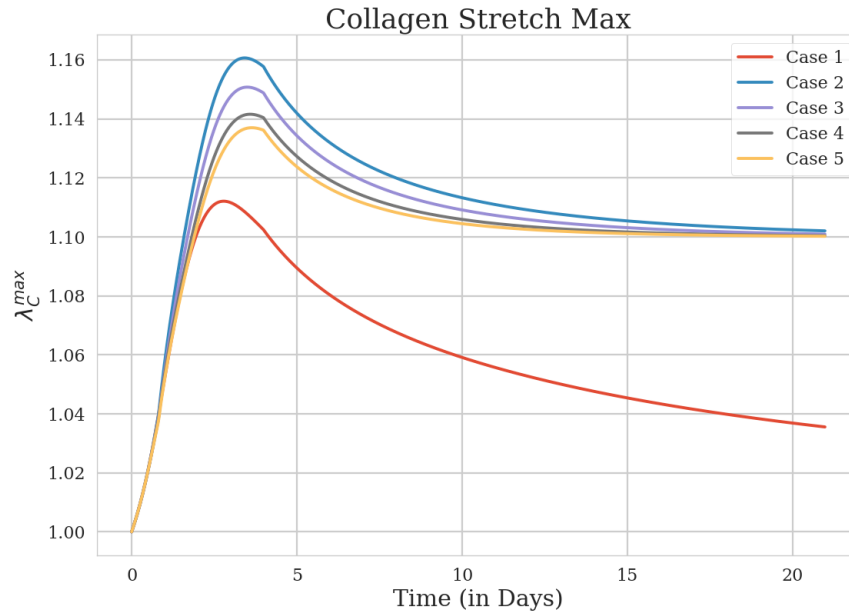


**Figure 3.22:** The maximum collagen fibre stretch variations are seen in Figure[3.22]. a rise in the values continues till day 3 for Case 1 and day 4 for the remaining cases. Thereafter, Case 1 remodels towards the original maximum attachment stretch attaining a value of 1.037 at day 21. The remaining cases 2, 3, 4 and 5 attain values close evolved maximum attachment stretch, at  $\approx 1.105, 1.1032, 1.1015$  and  $1.10$  at day 21, with only cases 4 and 5 attaining stabilising behaviour with no upward or downward trend.

The maximum collagen fibre stretch variations are seen in Figure[3.22]. The stretches in epicardial collagen fibres rise as a consequence of compensating for the loss in myocardial collagen and cardiac myocyte muscle fibres. This trend continues till day 3 for Case 1 and day 4 for the remaining cases. Thereafter, Case attempts to reach the initial homeostatic maximum value via remodelling Equations[3.33] attaining a value of 1.037 at day 21. The remaining cases 2, 3, 4 and 5 attain values close evolved maximum attachment stretch, at  $\approx 1.105, 1.1032, 1.1015$  and  $1.10$  at day 21, with only cases 4 and 5 attaining stabilising behaviour with no upward or downward trend.

### 3.6 Discussions

A membrane model of the left ventricle as a spherical membrane approximation including the micro-structural constituents has been developed to simulate a myocardial infarction over a period of 100 days, due to the necrosis of cardiac muscle cells and myocardial collagen fibres. Specifically, the effect of evolution or adaptation temporally of the epicardial collagen attachment distribution on the growth and remodelling of an infarcted myocardial tissue, is investigated. Due to the consideration of the passive diastolic cardiac cycle in our simulation, the active contribution of the cells is neglected as per our configuration considerations being in the filling phase i.e. ventricular diastole, moreover given the degradation of the cardiomyocytes within the initial 4 days, the cardiomyocytes only affect the remodelling of the tissue with minor significance. Biological information on the assumptions based on the load bearing behaviour of the various micro-structural constituents and deposition of new collagen fibres is lacking and therefore, a few scenarios, are tested, for the evolution of the collagen attachment stretch distributions via translation, skewing and width reduction.

Cardiomyocytes are known to undergo necrosis as early as 30 minutes after ischaemic event occurs, depending on the coronary blockage. We model the degradation over 4 days for the cardiomyocytes up to a minimum 1 % of the original mass density. This is not realistic as it assumes a complete degradation of the cardiac muscle which would ultimately not be suitable for recovery post MI. However, the aim was to understand the impact of the degradation of the cardiomyocytes on the extra-cellular collagen matrix remodelling and growth in response to the increased tissue stretch, due to the dilatation and thinning of the left ventricle. Further investigations can be carried out by limiting the degradation of the cardiomyocytes towards a plausible level of damage, possibly coupled with a coronary occlusion model which drives the necrosis of a certain mass density of cardiomyocytes depending on the oxygen supply or nutritional requirements. To concisely state the reason, it is aimed to understand the phenomenological consequence of cardiomyocyte degradation in a constrained mixture model and understand the compensation against the internal diastolic blood pressure by the collagen extra-cellular matrix by simulating the natural response of growth and remodelling with a stretch or strain based model, resulting in a scar tissue.

Clinically it has been observed an immediate effect of tissue necrosis causes myocyte slippage, and edema. Edema is associated with an elevated papillary muscle stiffness([Detwiler et al. \(1994\)](#)) and increased fibrosis due to interstitial collagen deposition ([Laine & Allen \(1991\)](#)). This could account for an initial increase in stiffness, due to the cardiomyocyte swelling induced by interstitial fluid retention and also fluid accumulation within the interstitial space of the myocardium. We however, considered the ground matrix mass density which represents the elastin and other ground substances to be constant and provided fluid constituent, is not modelled, in the constrained mixture it is currently not accounted for.

The major points to illustrate as seen in the figures of the results section the following aspects in accordance to the 5 cases, in which evolution of  $\rho(\lambda_{C,epi}^{AT})$  is hypothesised, are discussed.

1. Circumferential tissue stretch ( $\lambda$ ).
2. Maximum epicardial collagen stretch ( $\lambda_{C,epi}^{max}$ ).
3. Epicardial collagen mass density ( $m^{C,epi}$ ).
4. Remodelled thickness ( $h_{rem}$ ).

An initial degradation of the cardiomyocytes due to necrosis until  $t = 4$  days, and a consequent degradation in myocardial collagen due to increased expression of proteolytic enzymes by infiltration of immune cells until day 14 was assumed. This results in the increase of the circumferential tissue stretch  $\lambda$  beyond the homoeostatic value at  $t=0$  days.

The cardiomyocytes bear the most load as assumed (refer Equation [3.26]) at  $t=0$  but becomes negligible at day  $t=4$  due to necrosis up to 1 % of the original. The load is therefore, borne by the other constituents i.e. the ground matrix, myocardial collagen and epicardial collagen fibres. The myocardial collagen fibres are degraded upto 14 days to simulate proteolytic activity which leads to digestion of the myocardial collagen fibres and the load is borne by the ground matrix and epicardial collagen fibres. Due to the degradation of the two constituents and given the  $m^{C,epi}$  changes due to the implemented growth law (6.13) the membrane enlarges in an almost linear fashion, whereas in Case 2,3 and 4 the  $\lambda$  increases proportionally to the loss of cardiomyocytes and myocardial collagen fibres until day 14 but decreases over time but continue to enlarge by the end of the simulation. Case 5 observes stabilisation.

The differences in the stretches is due to the fact that the  $m^{C,epi}$  growth is driven by the maximum stretch differences for the collagen fibres throughout the cardiac cycle given by  $\frac{\lambda_{C,epi}^{max} - \lambda_{C,epi}^{AT,max}}{\lambda_{C,epi}^{AT,max}}$  as seen in Equation [3.34]. The evolution of the attachment stretch distributions according to the 5 cases considered (Figure [3.7]) causes the difference to vary and therefore affects the rate of increase of  $\lambda$  based on the degradation of myocardial collagen fibres and cardiomyocytes. Therefore, in comparison to Case 1 having a constant attachment stretch distribution ( $\Pr(\Lambda_C^R)$ ), the difference between the collagen fibre maximum attachment stretch and the maximum stretch at time  $t$  is vast and a large amount of collagen mass growth is needed to stabilise the infarcted tissue's enlargement, however, due to the evolution of distribution function to include more load bearing collagen fibres as seen in Cases 4, 5 a reduced amount of collagen mass growth is required achieving stabilisation quicker. This implies for a reduced amount of collagen fibre mass growth their configuration in the infarcted tissue assumes a load bearing state rather than a crimped configuration. It is therefore, seen that the mass density  $m^{C,epi}$  increases are unrealistic in Case 1, relatively large in Case 2 whereas Cases 3, 4 and 5 are acceptable as per clinical observations (Fishbein et al. (1978), Lieberman et al. (1981)). However, on consideration of the remodelled thickness changes  $h_{rem}$ , which considers the thickness to be a function of the mass density

changes in the tissue constituents it can be seen that cases 2 to 5 have  $h_{rem}$  at the end of the simulation to be lower than the initial thickness, which is acceptable. Infarcts are known to cause dilatation and thinning in the ventricular wall and due to the internal blood pressure it continues to be thin almost a fraction of the original thickness ( papers as many exp sutides dude !). With this in view Case 4 and 5 provide the most realistic predictions of the remodelled thickness  $h_{rem}$  and could be considered useful as the basis for a spherical membrane approximation of the left ventricle post-MI.

The trajectory for change in thickness follows the degradation of the cardiomyocytes and collagen fibres, taken to degrade upto 1 % of their original mass densities by day 4 and day 14 respectively. This however, does not reflect the necrosis of the myocardial tissue in experimental/ clinical observations (Jugdutt & Amy (1986), Jugdutt et al. (1996)) but provides insight into the growth and remodelling of the cardiac extra-cellular matrix post-MI. The rate constants for growth & remodelling laws, as well as modification of degradation rates would allow us to achieve comparable data with experimental and clinical observations.

### 3.6.1 Comparison with (Fishbein et al. (1978))

As observed in Section[3.5.1.1], it is possible to calibrate the model to reflect experimental data, where thinning of myocardial tissue post-MI due to coronary ligation in rats is seen. Though the trajectory represented as a continuous curve calculated by the constrained mixture model compared to discontinuous thinning observed in experiemtal observations (Figure[3.19]), the initial and final values between the experimental data and Cases 2 to 5 are similar. This can be attributed to the degradation of  $m^{C,myo}$  and  $m^M$  i.e the myocardial collagen and cardiac myocytes respectively, suggesting an improvement in the degradation regime considered in the model which is quite simplistic based on a final value to degrade the constituents to. Sophistications to include better degradation functional forms for constituents, would allow the model to reflect realistic necrosis from empirical data. The study (Fishbein et al. (1978)), did not provide the muscle mass density and therefore the exponential degradation function was employed. However, given the target thinning of infarcted tissue thickness is similar for Cases 2 to 5, it can be fairly assessed and other quantities can be inferred from the model.

On observing the circumferential tissue stretch (Figure[3.20]), Cases 3 to 5 show stabilising infarcts, with Case 2 showing slight increasing trend at the end. Please note Case 1 is dismissed due to its unrealistic thickness predictions. On that account, epicardial collagen mass density (Figure[3.21]) can be observed to initially decrease for Cases 2 to 5, and increasing over time possibly alluding to the initial degradation of collagen due to increase in Matrix-metallo proteinases and cardiac myocyte degradation, after day 3 however increases are observed with from a value of  $\approx 0.19$  to  $\approx 4.25$  from Cases 5 to 2 respectively. This captures proliferation of collagen fibres due to deposition by fibroblast and increased fibrosis as is typically observed in infarcted tissues.

Therefore, it is clear that insights can be obtained for quantities which were possibly not quanti-

fied in experiments to understand the collagen configuration, structural changes, dimensional variations and shed light on the integrity as well as functioning of infarcted scar tissue. Furthermore, it would be beneficial to model chemical signalling pathways in future iterations, so as to be able to identify markers for structural changes in protein, cellular as well as extra-cellular components. This provides testing grounds for various scenarios and can be modelled to obtain useful predictions to stratify disease outcomes and prognosis.

### 3.6.2 Terminal Points

An important aspect that has been neglected is the active contribution of cardiomyocytes as the passive filling of the left ventricle and the end-diastole to be the loaded configuration ( $\Omega_t$ ), is taken into account, it is important from a physiological stand point and it is necessary to consider for complete realisation of cardiomyocyte response to MI. Previous models proposed ([Guccione et al. \(1993\)](#)) provide a basis to incorporate complex dynamics of active contraction of the actin-myosin complex within sarcomeres of the cardiac muscle fibre.

Provided the assumptions of allowing a mass density variable to be associated with each constituent in the mixture model, another physiological response of the left ventricular myocardium can be modelled i.e. hypertrophy of the myocardium. This is based on either parallel or serial deposition of sarcomeres which result in thickening or thinning of the muscle respectively and has been demonstrated in models proposed by ([Göktepe, Abilez & Kuhl \(2010\)](#)), ([Göktepe, Abilez, Parker & Kuhl \(2010\)](#)).

Fibroblasts regulate the collagen extra-cellular matrix configuration and mass density in soft tissues. In a diseased tissue post inflammation phase, fibroblasts proliferate in the damaged tissue and transition into myofibroblasts which have a greater deposition capability of collagen ([Ma et al. \(2014\)](#)) to help stabilise the injury. Inclusion of the chemical signalling pathways involved in terms of the Matrix-metallo-proteinases and Tissue Inhibitors of metallo-proteinases, is required to garner an understanding from a molecular level therefore, allowing for multi-scale modelling. This has been achieved in ([Aparício et al. \(2016\)](#)), wherein a novel chemo-mechano-biological model has been developed to simulate chemical variations and causes in terms of arterial tissue growth and remodelling.

### 3.7 Conclusions

A novel constrained mixture model for the left ventricle, approximated as a spherical membrane using non-linear continuum approach is presented. The ground matrix, cardiac myocytes and collagen fibre matrix have been encapsulated and allow for tracking results for changes in their mass densities and stretch configurations. Collagen fibre undulation distribution allows for understanding the variations in the stretches of the extra-cellular collagen matrix providing insight into the configuration of the fibres in the infarcted myocardium and its effect on the mechanical function at end-diastolic configuration. Cardiac myocyte active stress response though not modelled directly, allows for future sophistications with intra-cellular calcium models and modelling the entire cardiac cycle for each step in the simulation rather than be bound to a single configuration. Evolution of collagen attachment stretch distribution is key to obtaining realistic modelling in the collagen mass densities and volumetric thinning. Qualitative consistency with observed phenomenon in the myocardium post-MI has been modelled and comparison with experimental data provides confidence in the modelling hypotheses undertaken. Further work in validating the model with a greater body of empirical, experimental and clinical studies could prove useful in shedding light on the extra-cellular matrix configurations as well as collagen mass density variations in the infarcted myocardium. A chemo-mechano-biological model is the next logical step to understand chemical signalling pathways and fibroblast proliferation in the infarcted myocardial tissue.

## Chapter 4

# Novel Soft Tissue Growth & Remodelling Finite Element Framework

---

*In the past 50 years, the utilisation of Finite Element Analysis in the Biomechanics domain has seen a surge allowing insights into fundamental mechanisms, design progression patterns, delineating novel therapeutic techniques. With the advancement of technologies in the medical field as well as the computational domain has made it difficult to select an appropriate method to implement designs for computational models. Implementations in various styles and languages prove difficult for knowledge translation, dissemination of results and collaborations between research groups. Efforts have been taken to standardise the implementation of research methodologies to address biomechanical problems, but lack of tailored finite element software or frameworks towards biomechanics still proves to be a challenge. This project aims to address this issue by developing a framework around the FE software ANSYS® structured around the fibre-reinforced material model available, allowing users to create automated workflows. Primarily, based on the research focus, the growth and remodelling of passive fibre-reinforced hyperelastic and incompressible soft tissue are considered. Results have been achieved for myocardial tissue undergoing infarctions, skeletal muscle adaptation to changes in mechanical stimuli and provide them as test cases to showcase the framework's utility and ease of use.*

---

## 4.1 Introduction

Computational modelling suited for analysis of biological phenomena, biomechanical, biochemical, electro-mechanical and fluid simulations have drawn attention as a useful alternative to supplement existing empirical knowledge by means of *in vivo*, *in vitro* testing as well as results from clinical data. The major draw being the non-invasive approach in understanding the fundamental mechanisms, complex changes in biological phenomena ranging from cellular scale to whole organ scales. Predicting outcomes for difficult to diagnose diseases for which prognosis depends on several factors that prove to be a challenge in the clinical setting have found a hypotheses test bed in computational models, which on accurate replication of the biological problem at hand can provide useful information to aid in the diagnosis, prognosis and possibly identify novel therapeutic techniques or even shed light on improved surgical interventions.

Finite element analysis has been applied to understand soft tissue growth and remodelling from times dating back to the 1970s ([Belytschko et al. \(1974\)](#), [Janz & Grimm \(1972\)](#)). Overtime, sophisticated models to understand the pathological changes, maladaptation due to biological environmental variations and reactive adaptation to physiological processes have been developed. The stress and strain data estimates obtained from such simulations can provide insight into the affected regions of interest in the human body, which may be difficult to image or diagnose due to technological barriers. Tissue imaging technologies have evolved remarkably providing nano-meter level information, allowing complex molecular, cellular, tissue level or organ level models from the most basic unit to be implemented and tested. Though there are standards that need to be solidified based on the invasive nature of certain procedures, there is surely a step in the direction to make possible modelling of extensively inclusive models for all levels of data in the human body, having great potential in medical applications ([Pinkert et al. \(2018\)](#)).

In terms of implementation and executing simulations for the aforementioned research and medical problems, the technology, hardware and software form the crux of the entire scenario. While hardware can be scale depending on availability, the software tools are the primary driving force to understand biological models. The verification of software in accordance with standards ([Morse et al. \(2002\)](#)) with respect to the language used, the mathematical solvers and their accuracy in analytical as well as numerical approximations have an impact on the quality of results and data obtained. The limitation that is faced in dissemination, access and acceptance of computational models is a vast abundance of said models but also the variation in the implementation standards. The lack of standardised or tailored FE software and approaches has proved to be a hurdle for integration of models and consistency between results obtained to share, thereby introducing complications in collaborations needing additional work to be undertaken to iron out these issues.

Originating from Auckland Bioengineering Institute, the CellML language has a vision to exchange mathematical models developed computationally between scientists and users inclined towards research in biological models. It is based on the XML markup language encouraging reuse of

components or code libraries generated. This not only saves time but allows the user to better utilise resources towards addressing the research problem than be encumbered by the knowledge, expertise required to tailor commercial FE software or learn a complete programming language to implement the desired biological model. It has a deep database of models ranging from cellular biomechanical to electrophysiology domains. Their attempt is to reduce the translational overhead between the proliferate biological models, where in "code-to-text-to-code" translations can produce human errors which can be alleviated by the proposed standard (Lloyd et al. (2008)).

In the case of finite element modelling of biomechanical simulations, FEBio presents tools with a view of providing useful implementations to aid computational biomechanics as well as set a standard for computer simulation software. The software provides a pertinent selection of element types, a range of material models and boundary condition applications along with test cases to simulate biomechanical problems. It is written in C++, and given the need for users to work around commercially available software on their limitations, it provides ways to tailor the software to those specific needs (Maas et al. (2012)).

## 4.2 Motivation for Framework Development

Given the aims of the CellML, FEBio projects along with others like (Delp & Loan (2000) and more), the standardisation of software and language element to implement biomechanical simulations would provide a efficient means of achieving integrative knowledge translation with less complications involved in translation of software and methods between research groups. Our intention is more along the lines of (Haddad & Samani (2017)), where in instead of implementing constitutive models in finite element software specific to the myocardial tissue, readily available off-the-shelf commercial solvers can be utilised by modelling the the myocardial tissue as a composite of a "background part" and "myofibres".

In the soft tissue growth and remodelling framework (STGRF in short), it is aimed to utilise available fibre-reinforced, exponential, hyperelastic material model (Holzapfel et al. (2000)) in ANSYS® (ANSYS (2013)) FE software in an effort to streamline the process of setting up models within a workflow from mesh setup, material model ascription to boundary conditions and post processing methods for that particular material model. Although, it may not be clear as to why an additional framework is required to create a workflow in an available FE software, the necessity is clarified forthwith. In terms of soft tissue growth and remodelling, there is an existing fibre-reinforced, anisotropic, hyperelastic material model in the ANSYS® commercial package for modelling passive soft tissues. This is implemented on the foundations provided in (Holzapfel et al. (2000)), known as the Holzapfel-Gasser-Ogden(HGO) model.

Functions are created in Python (Van Rossum & Drake Jr (1995)), to handle the mesh data input from a source into a common format, which includes information from mesh nodes to material model associated with each element. This makes it easier to translate data from various formats

into a framework which automatically produces the requisite format to be read into the FE solver and produce results. An additional use of the framework is the creation of modular FE execution scripts, which can be independently modified after creation. This allows for setting up time-integration schemes used to simulate growth & remodelling of soft tissues (in the vein of [Miller et al. \(2007\)](#)) by editing a single independent script without intervening in any other file or section in the framework code library. The advantage of this is that it allows the user to model a soft tissue mesh, provide values for material parameters and set boundary conditions which are automatically translated into FE solver readable input files. Thereafter, an independent script can then be created to handle the workflow and call the FE solver as a function within the script while modifying post-processed files as seen fit for the simulation in consideration.

The objective of our framework is to reduce time to set up a growth and remodelling workflow for fibre-reinforced soft tissues allowing the user to focus on the research problem rather than be encumbered by the numerous intricacies of programming and software development concepts.

### 4.3 Framework Overview

The finite element analysis process has a few steps in order to set up a simulation to be solved using the Newton-Raphson iteration. This involves the description of a mesh composed of points known as nodes and a certain type of a finite element, defined by shape functions and association with nodes. After the mesh is defined, a material model needs to be associated with the mesh either a homogeneous or heterogeneous material for all elements depending on the required model. Thereafter, boundary conditions need to be ascribed before proceeding to solve for stress and strain results, which involves making assumptions about the real life scenario taken in consideration so as to model the scenario as accurately as possible using the possible allowed assumptions that can be placed on the mesh in the given co-ordinate system. This entire process is broadly termed as pre-processing steps, which essentially tells us the definition of the problem and hypotheses placed on the model.

The solution is then executed by defining a pressure, displacement or force condition on desired elements or nodes and the stress-strain values are obtained. Thereafter, post processing is done on the results which includes but is not restricted to analysing the stress-strain profile, deformation of mesh from the undeformed configuration and understanding whether the results depict the scenario considered upto a required standard of accuracy.

On realising the steps involved, it becomes apparent that for different finite element software available commercially, open-source software or in-house solvers by different groups the need to understand how to utilise the particular tool becomes an overhead. It would be difficult to gain expertise in such technology if the user has a background unrelated to mechanics with an idea of basic programming. Therefore, bearing this in mind a code library is designed in Python to enable end-users to set up simulations for soft tissue growth and remodelling in ANSYS ®. Python is an simple to learn programming language without the added complexities of other statically typed languages as C++ or Java. Depending on the depth of programming required even Python can become quite complex to utilise as new method designs are introduced. However, as it allows for functional and object-oriented programming in an interpreted environment the level of engagement can be decided by the user. The code library for the framework intends to alleviate the need to delve too deep into Python programming by introducing modularity in the code structure and the need to modify only a single file which can be set up using developed functions to create workflows. Specifically, focus is on the workflow required to modify material parameters in the finite element script to run static structural analysis in ANSYS ® and is detailed in the following sections.

#### 4.3.1 Framework Development

There are two ways to setup a simulation in ANSYS ® mechanical, one is via the Graphical User Interface and the other is through scripting the model in FORTRAN. The upside of the GUI is the

ability to modify the mesh visually and have an understanding of the application of boundary conditions as desired. However, certain functions are only available through the commands provided in FORTRAN and becomes difficult to access advanced functionality. Even though the scripting method might be complex and unintuitive given the absence of graphical feedback, it gives more control over setting up the simulation given the mesh is already created or the correct functions are employed to get the desired mesh and quality.

Initially, only a finite element script was created for simulating a left ventricle undergoing myocardial infarction using the HGO model. On further analysing the code and the need to modify certain elements within the script like the parameters, rate constants and material values for growth and remodelling it became tedious to constantly modify a static script. It was more pragmatic to gain control over these elements by means of developing a script which would produce an input file for simulation in the FE solver. Therefore, any part of the code library could be modified to suit the needs of the required simulation on the given biomechanical problem. Thereafter, the structure was further broken down into atomic functions, classes and independent scripts which made it possible to not only set up a single simulation for the left ventricle but also for simulating other biomechanical problems. We detail this in the subsequent chapter on skeletal muscle remodelling. The entire simulation has been automated using an external perl script and the parameters, rate constants can be set in a text file which is read in by the framework and automatically fed into the input script for ANSYS ®. The complete description of the software design, ideologies and design patterns used are explained below.

### 4.3.2 Design

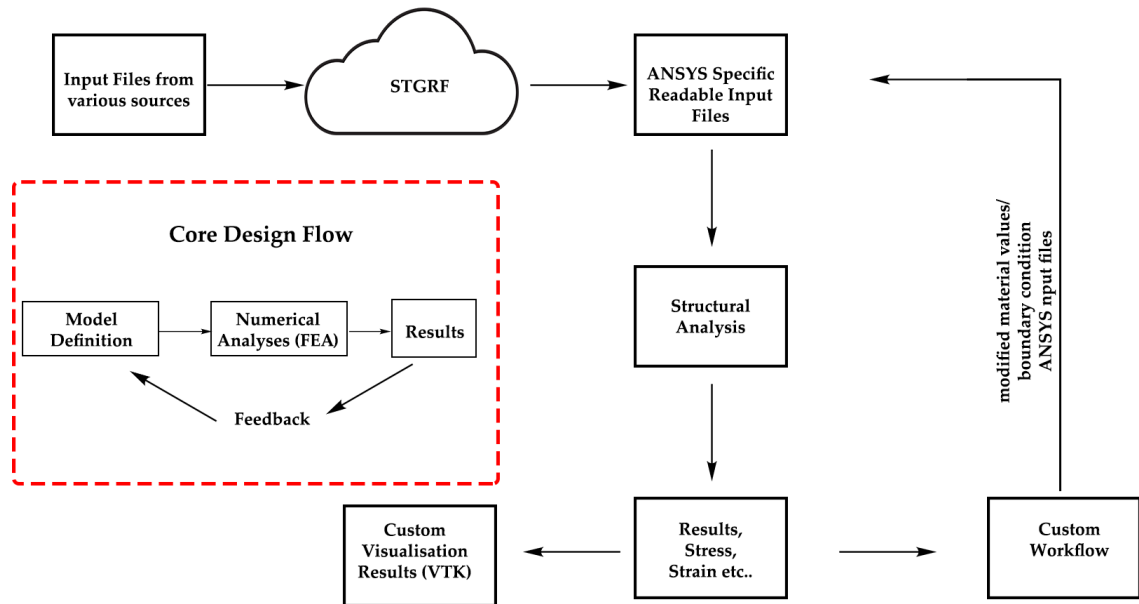


**Figure 4.1:** The diagram indicates the various components involved to enable finite element analysis of desired soft tissue models. This helped motivate the generation of a code library (shown as STGRF), which facilitates the interaction between these components and creation of independent workflow scripts.

The Figure [4.1], outlines the basic ideology behind the design of the framework. In particular, on observing the red box, it provides the basic design of work-flow based finite element analysis in our perspective. A model is defined with respect to mesh definition, material ascription, boundary conditions and requisite forces to be applied. Thereafter, it is made available to the finite element structural solver, mechanical static structural analysis in our case to produce results. These results act as an indicator for the next step to be performed by adjusting the material parameters or boundary conditions of the model with respect to the desired soft tissue simulation in consideration. On passing these modified input values as feedback to the model definition the next step is prepared to be executed. This loop continues until the desired time step is reached or expected results are obtained or until an error occurs which would indicate an adjustment to be made in one of the previous steps. On understanding these core steps involved, it becomes clear that the scripts to be setup to work with the FE software would prove to be cumbersome, in order to modify the model definition after each time step based on the results obtained in the previous step. A lot of overhead (time and effort) is wasted in terms of code modification and can be saved by constructing automated work flows which take care of these rudimentary aspects. Laws can be described to govern the modifications in the model definition based on the results of the previous step and the cycle can be kept continuous without abrupt intervention by the user. This not only saves time and effort for the end user but reduces human error during transitions between steps.

We now delve into the specifics of the various components involved in facilitating the functioning of the framework by observing the broader picture outside the dotted red-box in Figure[4.1]. Data for creation of the model mesh can be obtained from various sources, i.e. via segmentation of medical images from CT-scans, MRIs etc. which could be stored in multiple formats depending on the software used or via mesh generation software. Currently, the code library (STGRF) contains reader functions for ANSYS ® APDL output list files for mesh input, a material creation script based on the mesh input and a separate function to provide boundary conditions in Python. These input files are then assembled in the STGRF invocation and input files which are readable by the FE solver program are created. After the numerical solution is obtained via the solver, the results files are generated in accordance with the quantities required to carry out the steps defined in the workflow for the modelling problem. The custom workflow would then utilise these quantities to modify the material properties, rate parameters, applied boundary conditions or mesh properties as appropriate for the next step in the simulation based on the time integration procedure defined via a parameters file. These modifications are then carried out on the FE software readable format files which are updated and fed into the solver to obtain results for the next step. This loop continues till a desired criteria is fulfilled which is left to the user to decide. The Custom Visualisation Toolkit is based around the VTK standard ([File Formats for VTK Version 4.2 \(2002\)](#)), and automatically reads in the results file, mesh information and provides data which are not displayable in ANSYS ® MAPDL, which includes post-processing fibre-oriented specific strains, mass density terms introduced via custom workflows etc. Also, since the files are generated on the fly without interruption of the workflow, they can be reviewed separately even while the simulations are running for subsequent steps, allowing for intervention if necessary based on any errors spotted in these results.

The various components are inspired by FEBio ([Maas et al. \(2012\)](#)), which includes a Finite element solver as well as a pre processing package and post processing package. An obvious advantage can be observed, which is the complete independence from the unprocessed input files obtained from various sources at initiation. The only files modified are the ones readable by the finite element software, which is much easier given the strict format it needs to be built around causing a standardised procedure to be followed and reduces errors. Additionally, human intervention in any steps other than the initial set up is avoided and therefore saves up time which can be spent in analysing the results obtained and make changes to the model if any problems are encountered on perusal of the results.

The software design and the procedures involved in utilising the framework have been described, however, there are a few components which need to be elaborated to understand their specific roles in the entire framework and how they facilitate its functioning. Therefore, the core components in the framework's design are described in the following sections to clarify their roles and particular functions which they address in the core design flow.

### 4.3.3 Soft Tissue Growth & Remodelling Framework Code Library

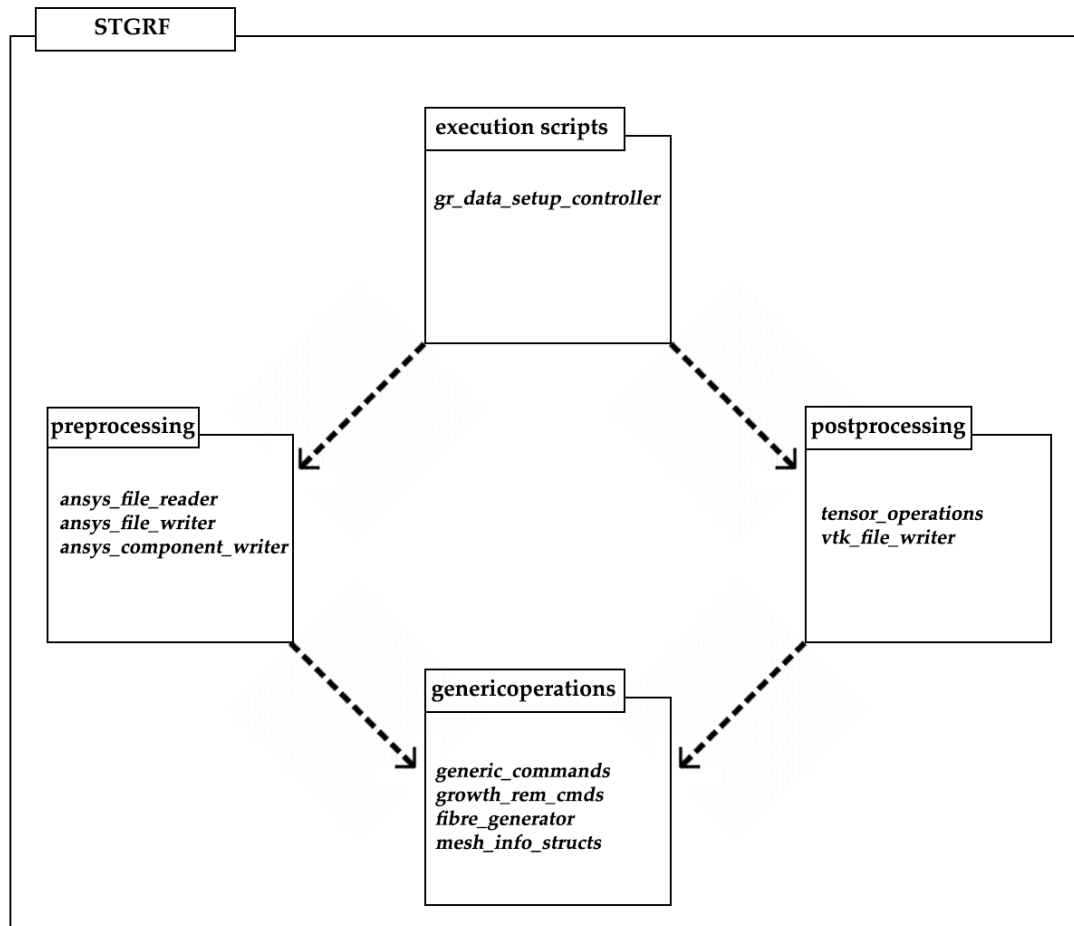


**Figure 4.2:** Package diagram of the soft tissue growth & remodelling framework, portraying the various packages involved which can be utilised to set up workflows or scripts for finite element simulations in ANSYS ® MAPDL.

The code library developed in Python (Van Rossum & Drake Jr (1995)), is the component due to which the generalised framework for soft tissue growth and remodelling can be utilised. The functional package is divided into three packages which consists multiple Python modules. It is not object-oriented in the strictest of sense, but borrows both from functional programming and object-oriented programming. Initially the functions and class structures procedurally came into being due to their need and were formulated into organised modules over time. Therefore, the code library has a structured format with a few modules consisting of classes as well as independent functions. This has been done due to the similarity in their application, for example the class *ListReader* in the reader module has class functions and methods associated with a particular input mesh. However, certain functions like reading strain outputs (*read\_strain\_output()*) in from ANSYS ® MAPDL generated files are included as their function belongs to reading a certain file. In a broad sense the Figure [4.2] describes the structure of the code library and the organisation of modules and packages.

It can be seen the pre-processing and post processing code packages are kept separate as it provides a clear distinction between their roles in the framework. The execution scripts act as a controller which utilises both *preprocessing* and *postprocessing* operations to set up the required Finite Element files. The role of controller is defined based on the design principle in Model-View-Controller pattern, this will be clarified in Section [4.4], where the translation of the framework from a command line based software to a Graphical User Interface (GUI) software, is discussed. The final package i.e. the *genericoperations* contains classes and methods which have utility in both *preprocessing* and *postprocessing* packages and is therefore in the third level in the Package Diagram. The dotted-arrows show dependencies of the packages on one another. The packages are designed with as described below: Please note, the code library for the components discussed below can be found in Appendix[A].

#### 4.3.3.1 Execution Files

The modules in this package are helpful in setting up individual controller scripts to modify the model definition as required for a particular biomechanical problem and calls in functions from the other packages to be processed and output FE software readable files.

1. *gr\_data\_setup\_controller*:

Currently, this module involves the steps to set up multiple simulation files using a conditional statement. These include a left ventricle model, skeletal muscle model and a cuboid model to test verification of material model as well as growth and remodelling assumptions. Though it is recommended to maintain individual scripts for each to avoid code mix up.

#### 4.3.3.2 Preprocessing

The various Python modules in this package deal with the set up of pre-processing steps in a finite element simulation, particularly input files (.inp) to be read into ANSYS® Mechanical structural solver. These modules include:

1. *ansys\_file\_reader*:

The class and method to create reader objects for a mesh are included in this module. Each mesh, if the FE model has more than one, can be defined as independent objects containing their own information which can be accessed and modified to suit the users needs. A key difference in this module is it also contains reader functions for post-processed stress strain results files from ANSYS® due to the function having a role of reading a file, it is an independent function not tied into the class.

2. *ansys\_file\_writer*:

Writing files in a file format readable by the FE software is done by using the functions in this module, the mesh data from the reader functions are stored in data structures known as *Dictionaries* in python and can be accessed, modified and written out as desired.

3. *ansys\_component\_writer*:

In ANSYS® Mechanical software, there exists an option to select a range of nodes, elements or other primitives like area, volume, lines etc. and provide them with a name. These are known as named selections and make it easier to define boundaries for application of displacement, force and support conditions without having to manually enter the numbers of each entity. This module contains functions to write out such named selections which can be included in other sections of the model for ease of access to a set of finite element entities.

#### 4.3.3.3 Postprocessing

On the completion of a simulation step, the results files obtained are to be processed and operations carried out by deducing various quantities from observations via post processing. This package addresses that need by providing independent methods to carry out pertinent functions as required during particular tensor transformations to either observe results or to help set up the next step in a work flow.

1. *vtk\_file\_writer*:

This module contains functions to create a graphical VTK file representation from the mesh data, either using the pre-processed mesh to understand fibre-direction definition or during post-processing the results and displaying quantities not shown in the FE software standard results display.

2. *tensor\_operations* :

The various operations involved in modifying the material properties or boundary conditions are dependent on the strain / stress tensors obtained as a result of a finite element simulation. They include conversion operations to obtain mechanical quantities which are necessary to carry out work flow operations by using transformations on resultant tensors of a simulation.

#### 4.3.3.4 GenericOperations

In the case of separation of tasks (or concerns) due to the logic involved in the packages set up, there remain some methods, functions and classes which are utilised by all other packages. Therefore, a separate package for generic functions is created to address this and having an independent package helps in code re-usability rather than repeating a set of instructions in every other package. This package includes:

1. *generic\_commands*:

A module containing functions to manage the file directory locations, used by other functions for reading or writing files.

2. *growth\_remoulding\_commands*:

Specific functions which deal with the equations and calculations involved in growth and remodelling laws are included in this module. Specifically the reading/ writing of parameter files which contain information about the rate constants, time ranges and in some cases displacements for boundary conditions.

3. *centroid\_fibre\_gen*:

This module contains mathematical formulations which help generate fibre directions for various meshes. It is made up of individual functions and not classes as different algorithms can be employed for different mesh structures for fibre-orientations to be defined.

4. *mesh\_information\_structures*:

This module contains a Mesh class that has objects of Point and Element classes. Here the object oriented approach becomes apparent as it helps in managing individual meshes and performing functions related to that particular mesh. This uses the concepts of encapsulation and inheritance from Object-Oriented Programming, using the ABC (Abstract Base Class) concept in Python. This allows for future implementations with other FE software where the class methods can be modified based on the read and write formats it encounters.

#### 4.3.4 Customised Visualisation Toolkit

An important component is the visualisation tools in the *postprocessing* module, which provides us a means of displaying and analysing results data without being dependent on the in-built results display in the FE software. Therefore, given the propriety of the material models and limited access to the strain energy functions, deformation gradient and invariants associated with the stress results formulation; the results based on respective transformations from strain and stress files, are post-processed, after an analysis is done. The data format used is VTK (see [[File Formats for VTK Version 4.2 \(2002\)](#)] for documentation). The standard format for a vtk output file is as below:

```
# vtk DataFile Version version_number
File_name
ASCII
DATASET UNSTRUCTURED_GRID
POINTS total_points_count float
x y z # point number 1
.
x y z # point number n

CELLS total_lines_count total_lines_count x 3
cell_no point_1 point_2

CELL_TYPES total_lines_count
3
```

As in the code snippet above, a vtk file contains a header line to define the vtk file name and version. The type whether it is in ASCII or Binary data format for description of the mesh. DATASET defines the type of mesh to be displayed which are derived from various options listed in ([File Formats for VTK Version 4.2 \(2002\)](#)), of which an UNSTRUCTURED\_GRID is suitable for our needs. The points define the nodes in a serial fashion and the cells depending on the type of element and number of nodes associated are listed below using the node numbers described under points. Finally the CELL\_TYPES option defines the type of cell/ element that is being described by the connectivity matrix defined under CELLS, be it a tetrahedron, hexahedron or other structure types ([File Formats for VTK Version 4.2 \(2002\)](#)).

An important point to note is during the conversion of various types of elements into their equivalent types between the vtk file format and ANSYS® generated mesh definitions is the ordering of the vertices/nodes for an element need to be thoroughly verified to produce accurate result output and the numbering for points/vertices/nodes in the vtk file start with 0, in contrast to 1 in ANSYS® Mechanical The following Figures [4.3, 4.4] shows equivalence between a few

element types in ANSYS® and its equivalent processing in vtk using the *postprocessing* package.

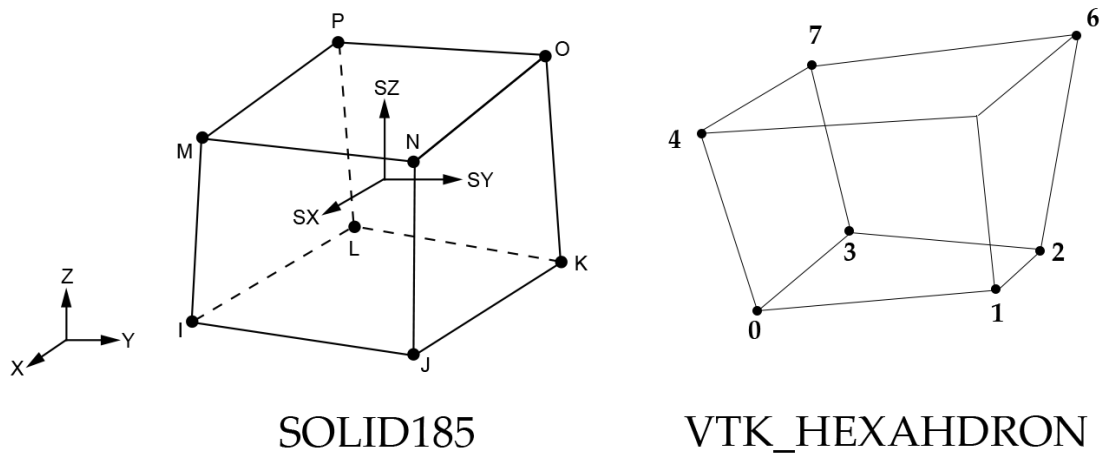


**Figure 4.3:** Figure depicting nodal numbering in ANSYS Mechanical APDL and VTK file formats (ANSYS (2013), *File Formats for VTK Version 4.2* (2002)), for a hexahedral element.

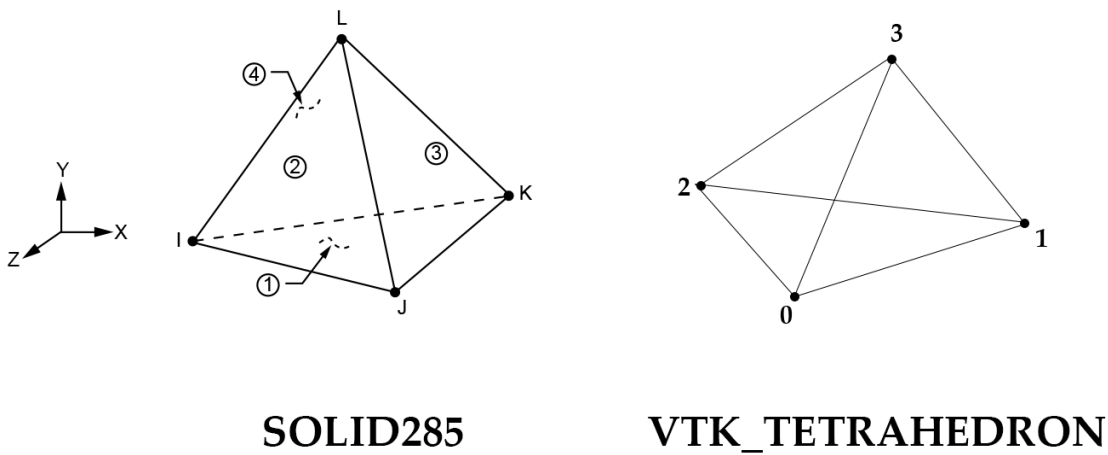


**Figure 4.4:** Figure depicting nodal numbering in ANSYS Mechanical APDL and VTK file formats (ANSYS (2013), *File Formats for VTK Version 4.2* (2002)), for a tetrahedral element.

The generation of this file format is done using functions in the *vtk\_file\_writer* module in the *postprocessing* package and can be visualised using Paraview (Ayachit (2015)) or other available software. The standard implementations provide results based on the invariants, Cauchy stresses for each constituent, material parameters including mass densities, material constant changes and stretches experienced by individual fibre directions. This however can be customised to fit the needs of the user, by creating a new function, external scripts or extending existing functions. This brings us to the concept of modularity in the framework design and will be discussed in Section[4.4].

### 4.3.5 Custom Workflow Creation

The tools provided by the code library allows the set up of ANSYS® Mechanical readable input script files to perform analysis on a defined model. The analysis of a simulation accounts for one step performed in the growth & remodelling of the pertinent soft tissue model and to obtain subsequent analyses on further time steps there is a need to create an additional work flow on top of the existing translation between source input files and structural analysis for the biomechanical model. This issue is addressed by utilising the code library developed to create one off external scripts, employing a combination of PERL and Python scripts to create a time dependent growth & remodelling structure for simulation over a specified period of time. We discuss the generic procedure to create work flows tailored to cater the needs of the requisite need in terms of the soft tissue model in consideration.

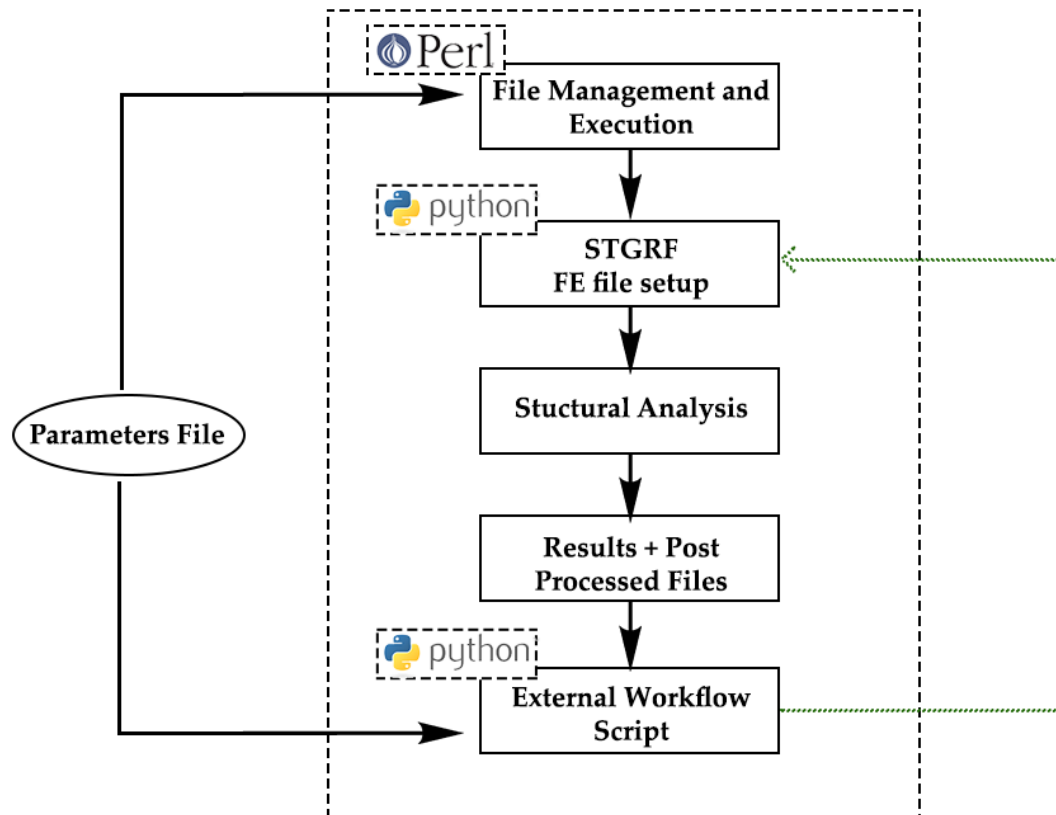


**Figure 4.5:** Execution of the custom workflow routine. Perl manages the execution of ANSYS® Mechanical APDL and Python scripts for structural analysis and for post processing, respectively. An initial setup of APDL scripts is setup via the Python framework execution file. The Parameters File is used to setup rate constants, time periods, number of steps and other relevant parameters, pertinent to each biomechanical problem.

1. *Parameters File:*

This file defines the time period, no of steps required, rate parameters for growth, remod-

elling equations, and any boundary condition changes as needed. In the presence of such a file, it becomes easier to have one source which contains all the information related to time integration scheme, and values which would be read in by multiple scripts in the work flow. Thereby, it avoids modification of each file and reduces human effort in book keeping and managing basic parameter values.

2. *PERL Script:*

The PERL language is used as the root controller of the entire workflow, acting as the manager of the system. It is used to deploy calls to various scripts, update the parameters file and execute ANSYS ® Mechanical via the command line. A basic template is shown [4.5] and the execution sequence is shown below.

- (a) Execute STGRF root (main) Python execution file to create ANSYS ® readable input scripts (.inp).
- (b) Execute ANSYS ® MAPDL via command line passing the root .inp file (ansys\_job.inp) issuing the command  
"ansysXXX -i ansys\_job.inp" -j job\_name (XXX - refers to version number).
- (c) Save results obtained from (a), (b) as homoeostatic step results, i.e. corresponding to time ( $t = 0$ ).
- (d) Initiate growth and remodelling loop by calling the custom workflow script, taking input from post-processed files in the previous step. This results in the updating of material properties and/or boundary conditions depending on the work flow.
- (e) Execute ANSYS ® MAPDL scripts again to obtain updated results. Also, vtk visualisation results are produced for current time step.
- (f) Re-iterate steps (d) and (e) until time ( $t = n$ ), where  $n$  is the final simulation step obtained by dividing a time period into a number of simulation steps.

### 3. *Python Script:*

Given that the PERL script manages the files, target directories and execution of scripts and the solver, the task of carrying out the actual task of running the growth and remodelling laws is delegated to a secondary python script. There are two reasons for this, (1) To keep the functionality of PERL script to strictly only for execution and file management and (2) Already developed functions for reading, writing and modifying python data structures exists in the STGRF code library. This also holds with the idea of separation of concerns and modularity of code functions.

The basic flow of the Python work flow algorithm is shown below:

- (a) Read in Hencky/ Logarithmic strain output from ANSYS ® Mechanical and material files obtained from simulation.
- (b) Calculate requisite mechanical quantities (stretch invariants, Cauchy stresses) involved in growth and remodelling laws.
- (c) Remodel material parameters based on laws considered with a given time step increment (calculate using a defined time period and number of steps)..
- (d) Update material files and applicable boundary conditions for the next step.
- (e) Create visualisation files in .vtk format to observe results using the post-processing package (in STRGF).

This Python script falls into step (d) of the PERL script thereby being strictly involved in only the growth and remodelling whereas, the file management and code execution is left to the PERL script.

#### **4.3.6 Parallels to Template Method Design Pattern**

The concept of template method design pattern was identified by (Gamma et al. (1995)), where in a template is defined with the intent of being a skeleton of the algorithm. In this algorithm, classes can have modifiable subclasses allowing for the behaviour of the subclasses to be varied as desired. However, regardless of the behavioural shift in the subclasses the original intent of the class does not change therefore, in a sense an algorithm suited to a particular problem is defined and its steps can be modified producing variations in the results but not in the problem which is to be addressed. On drawing parallels with our framework, our intent is to address the issue of setting up simulations for soft tissue growth and remodelling with a commercial software based on the stress-based remodelling assumptions, adapted from (Watton et al. (2009)). The components in the framework and the workflow (please see Figure [4.1, 4.5]) are independent of each other and can be customised to suit the needs of the user. This however, does not deviate the focus of the framework therefore offering modularity in the framework components, separation of functions (concerns) as individual components address separate aspects of our problem statement. This

proves useful in maintaining the code libraries and work flows as the framework matures into a complete software.

An example is the applications of STRGF presented further in following chapters (refer chapter), which include (1) Application to the Left Ventricle post Myocardial Infarction and (2) Application to skeletal muscle adaptation to sustained stretch.

#### 4.3.7 Workflow Execution

The starting point of the work flow is the PERL script which is tailored to a particular problem using the steps shown in (Section [perl script pseudo code]). Currently, a command line execution is performed by running the PERL file using the command

```
"perl gr_perl_script arguments"
```

This initiates the custom workflow, and produces results after each simulation step is completed and requires no user intervention apart from a few steps which need to be addressed prior to calling this command. We describe the directory structure of the framework and detail the initial steps which need to be carried out by the user for their particular growth & remodelling case study.

The directory structure shown in Figure [4.6], displays the organisation of the modules and packages in the STGRF code library. This provides us with an idea of importing relevant code functions based on the users needs as one would expect from a standard PyPi Python package library(Van Rossum & Drake Jr (1995)) installed on their systems. This would follow as "*ansys-total.package\_name.module\_name.object\_name*". This clarifies the need for packaging of the STGRF code library for use in external scripts by re-using fundamental code functions without the need for rewriting them. The workflow is described in Section[4.3.5]

Please note: all the function calls code is presented in Appendix A. The creation of input files for the structural analysis solver is shown in the sequence diagram (Figure[4.7]). The user executes the command to begin the simulation run. The main script `gr_hgo_model` along with an argument for the relevant simulation i.e. myocardium, cube, muscle is executed. It calls on the `gr_data_setup_controller.py` script to organise the input files and perform file writing operations by calling in `ansys_file_reader.py` via `read_nodes()`, `read_elements()` and `read_hgo_material()` functions. Further the `ansys_file_writer.py` and `ansys_component_writer.py` modules are executed via `inp_writer_name_model()` function call, where "name" correlates to the type of simulation as called by the command line argument (myocardium, cube, muscle), and subsequent commands are executed. This creates files for one simulation run in the structural solver. It continues for each step provided in the parameters file and until the PERL wokflow terminates.

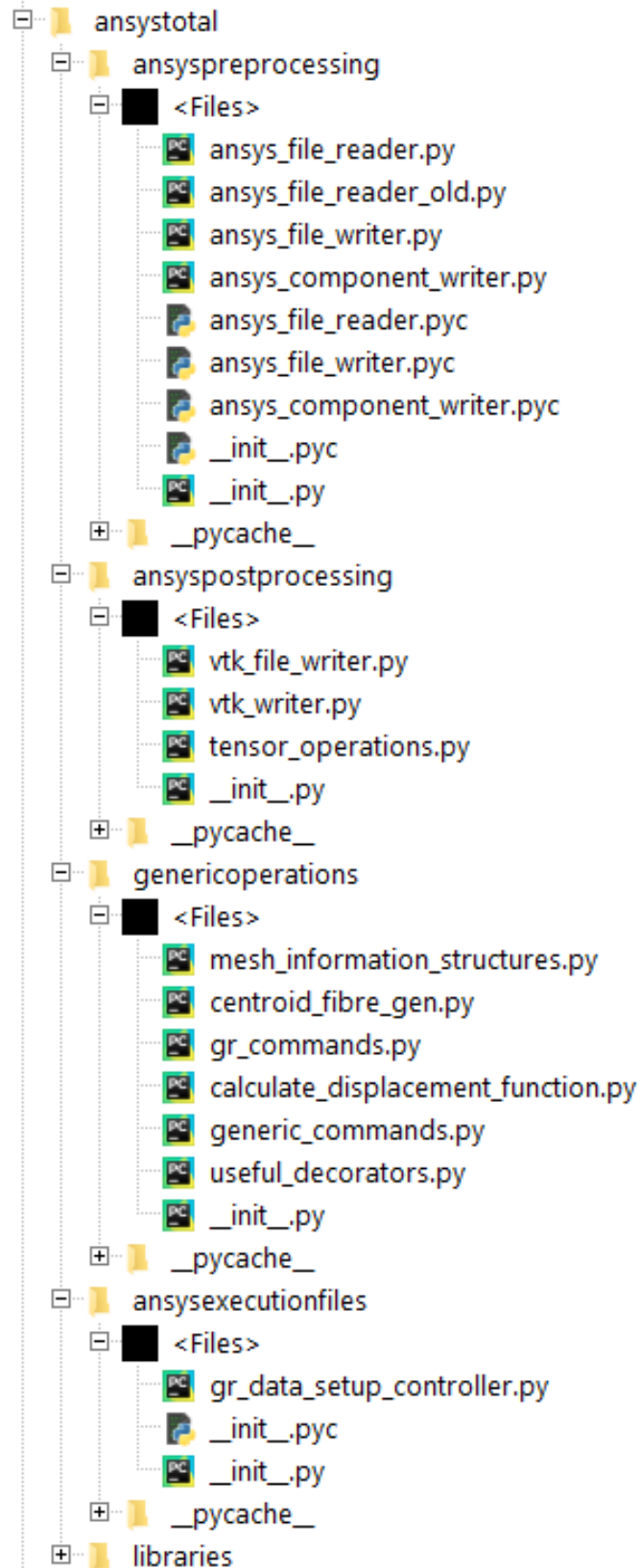


**Figure 4.6:** Folder view of the STGRF code library, detailing the organisation of various python modules and packages.

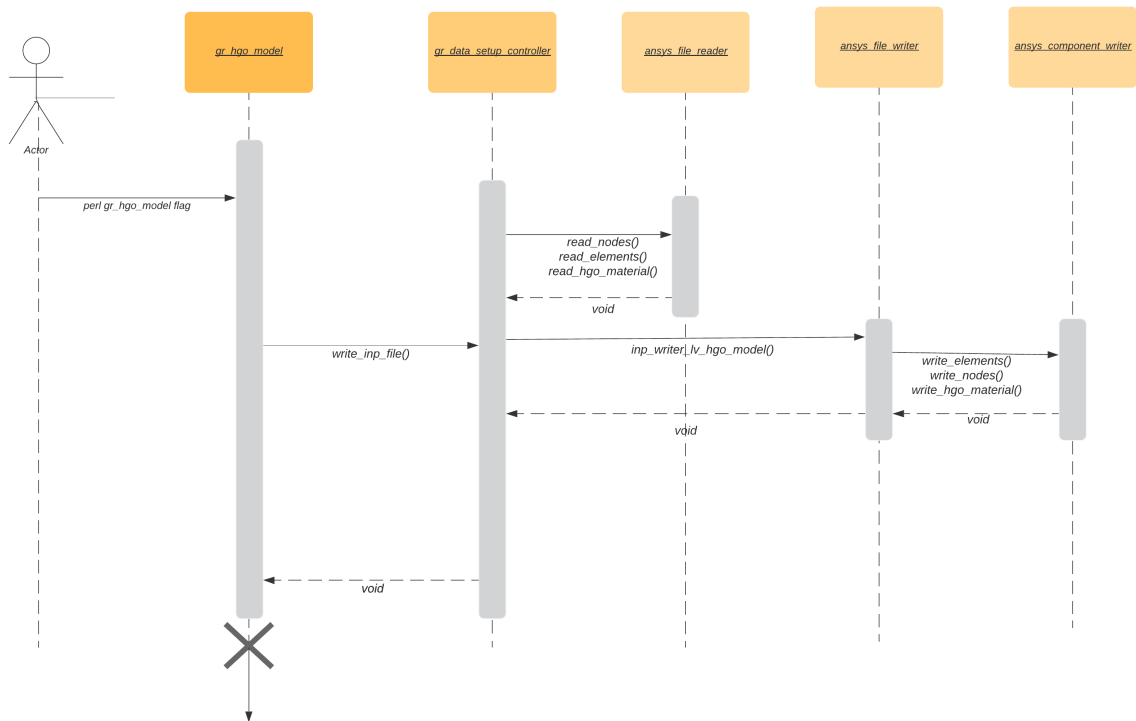


**Figure 4.7:** The sequence diagram detailing the execution of the framework to create output files to be read in by ANSYS® Mechanical APDL Solver for structural analysis.

### 4.3.8 Documentation of Code Library

Requisite documentation has been created to help the end-user utilise the framework and be aware of the core functionality. This includes a complete descriptive documentation of the Python library of packages and modules using standard format, created using Sphinx (A Python documentation library, *Sphinx* (2019)). A readme has been included as well which describes how to execute an example cubic simulation and modifying required files to suit a particular growth and remodelling scenario. The figures [4.8, 4.9] show snippets of the aforementioned documentation.

The snippets shown in Figures[4.8], [4.9], show a glimpse of the documentation as it currently stands. The readme (Figure[4.8]) file contains instructions on how to develop work flows using the libraries provided in the framework and execution commands. The Python documentation (Figure [4.9]), provides an understanding of the code library, modules and packages upto the function level with in-depth definitions and examples. The documentation is an effort to build a user manual when the software matures into a full GUI based system following an Model-View-Controller pattern.

# Soft Tissue Growth & Remodelling Framework(STGRF)

This python package has been developed as an add-on or more aptly a tool to create ANSYS scripts for growth and remodelling simulations of soft tissues. A host of basic functions have been implemented to simplify the creation of ANSYS MAPDL scripts and can be modified as desired. The code base has been kept modular and is not restricted by any inherent hard-coded boundaries.

A folder-wise organisation has been adopted to keep the growth and remodelling scripts distinguishable from the core package. These too again can be changed and modified to suit different needs.

Perl - the file manager and controller of the simulation cycle has been implemented in an independent perl script per simulation. As it helps keep the workings of the simulation loop away from the FEM set-up oriented nature of the python package. A simple implementation of a cube has been included to understand the cycle and simulations can be built on top of it for various soft tissue growth and remodelling problems.

## Pre-requisites

**Figure 4.8:** *The README file listing the requisite software to be installed, setting up the programming environment and installation of the framework. Also, contains an example of growth and remodelling on a unit cube to help motivate the user to set up their own models from pre-processing to post processing as well as establishing their own custom work flows.*

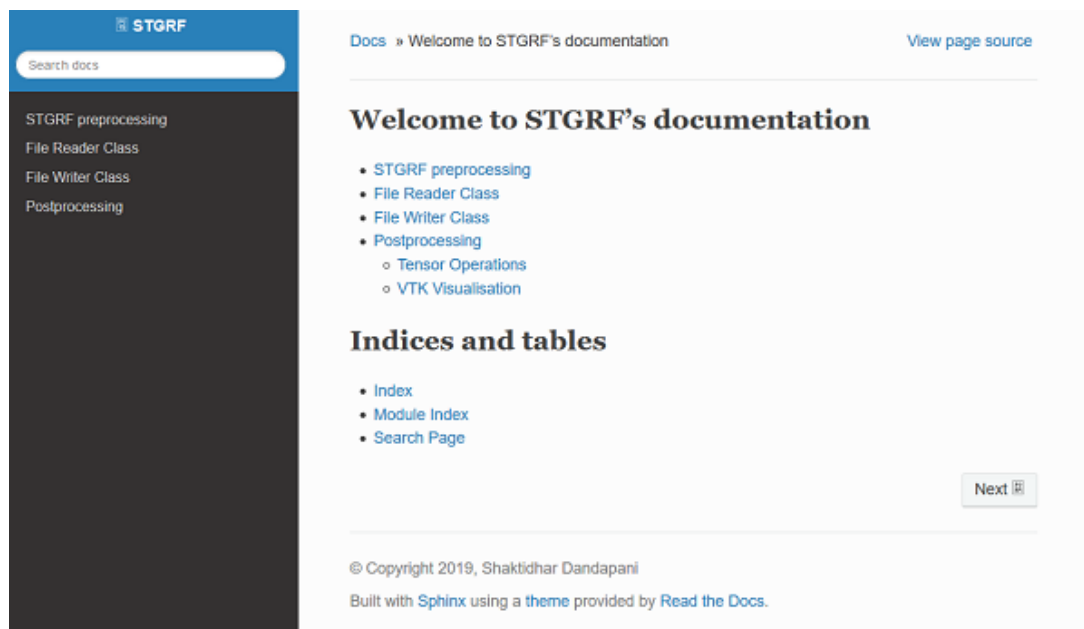


**Figure 4.9:** A standardised documentation of the Python code library, containing information about the modules, packages, classes, objects and functions according to PEP-8 standard. (<https://www.python.org/dev/peps/pep-0008/>)

## 4.4 Discussions

Establishing a framework around ANSYS® Mechanical is important in order to automate common tasks involved for a particular engineering, biomechanical or other simulations in focus, in order to minimise time and effort spent on setting up a model. With pertinence to the research objective of soft tissue growth and remodelling, simulation needs vary depending on the soft tissue in consideration. For example, in an application to understand degradation of soft tissue ground matrix, cellular components and the remodelling of anisotropic collagen fibres, mass density terms need to be introduced into the strain energy function which are taken care of by multiplying the respective material parameter and providing it as an input to the HGO fibre-reinforced constitutive model. Thereafter, the growth and remodelling equations take charge and on initiating the custom work flow produce results as desired. This is applied to the left ventricle experiencing diastolic blood pressure on its inner surface and prescribe degradation of the isotropic component to simulate a myocardial infarction and observe how the extra-cellular matrix remodels to compensate for the loss in functionality of the healthy tissue.

Another example, is to understand remodelling of skeletal muscles which undergo lengthening due to sustained mechanical stretch. Herein, the work flow would consist of only remodelling the anisotropic fibre material parameters and in contrast to our ventricular example are free of the mass density term in its current form.

Therefore, though the applications differ, the primary pipeline or algorithm from the setting up of ANSYS® readable scripts to post processing and execution of custom workflows by PERL scripts remains the same. The changes in the workflow can be modified in the requisite components of the framework itself (Figure [4.1]) and execution remains the same. Therefore it enables the user to focus primarily on the research problem and model definitions specific to their needs rather than building the basic functionality for setting up the scripts from scratch.

A few points are discussed in terms of the framework including its advantages and limitations in its current state of implementation.

### 4.4.1 Capabilities

The framework and customisable work flow feature enables the user to achieve quite a few important targets with respect to simulating growth and remodelling of soft tissues over a period of time.

1. *Modularity*: To independently modify any aspect of the library without affecting other package components or modules due to modularity in package design.
2. *Custom Work flows*: To create their own customised work flow to suit their particular simulation need, incorporating scripts and models which are not included in the framework via the work flow component (Figure 4.5).

3. *Management*: To control the work flow using a singular parameter file, reducing the time and effort required to manually sift through the code by editing multiple files. This displays code reusability and encapsulation which are fundamental in Object Oriented design as the changes are made via objects derived from classes and passing arguments via overridden functions.
4. *Results*: Obtain results based on their needs, as each quantity can be separately displayed using vtk visualisation created by in-built functions in the framework. This helps in analysing results obtained and verifying if the output is according to desired conditions set.
5. *Code Modification*: Classes developed in the pre-processing and post-processing packages have interfaces or abstract methods which can be modified as desired by sub classes. An example is the *ANSYSInpWriter* class, which exists in the *preprocessing/ansys\_file\_writer* modules (Figure 4.2). Currently, its writer methods are tuned to output files in a format readable by ANSYS ® Mechanical, but can be extended to other sub classes to obtain outputs in formats readable by other FE software. The same can be said for classes existing in the *ansys\_file\_reader* module.
6. *Automation*: The automation of the steps required for a particular soft tissue remodelling scenario lessens user intervention during the simulation by setting up rule sets in their work flow scripts. This conserves effort on the user's side and can be better utilised for other priorities rather than focus on simple modifications for the next step in the simulation.

#### 4.4.2 Applications

The verification of the mathematical model as well as the growth and remodelling on a unit cube, provides confidence in the computational model in ANSYS ® Mechanical as well as its numerical solutions. During the course of research and framework development, these features have been applied to cases in particular, as follows:

##### *Left Ventricle*

The left ventricle undergoing myocardial infarction due to coronary artery occlusion, by considering a region of elements in the finite element mesh to be degraded. This causes the remodelling hypotheses to trigger and the collagen fibres to grow w.r.t their mass densities and remodel their mechanical properties in order to compensate for the loss in function. This is described in Chapter [6] with details about the adaptation of the framework to suit the hypotheses considered.

##### *Skeletal Muscle - Gastrocnemius*

An additional application has been undertaken to simulate the remodelling of skeletal muscle fibres in response to sustained stretching. This can be applied to understand the process of muscle lengthening in scenarios such as toe-walking, casting and even exercise. The details of the simulations, adaptation of framework with a customised work flow and key hypotheses are

introduced in Chapter [7].

### 4.4.3 Framework Updates

The framework is currently in a state where work flows are controlled via a parameters file and command line execution. The intention is to update the framework in terms of code standards as accepted by Open Source Initiative. This allows the code library to be of optimum quality to be published in the PyPi library, which exposes the code to the community and interested users can be invited to collaborate and modify the framework towards the future goal of developing a full-fledged software.

#### 4.4.3.1 GUI Implementation

The package design and modular components of the framework developed are organised in a manner to enable the development of a Graphical User Interface in future iterations in the software development cycle. There exists a model composed of the underlying mesh information, finite element analysis set up and parameters required in the pre-processing package. The setting up of the model, linking it with the execution script is taken care of by a controller file (*gr\_data\_setup\_controller.py*) and this controller file is called in as a function with command line arguments via a simple python scripts called (*main\_gr\_hgo\_model*) which acts as the call to the execution of framework components. With this in view the code library organisation makes it possible to separate the model from the view (GUI) due to the existence of an intermediate controller, therefore, adherence to the Model-View-Controller design pattern is observed. Moreover, the PERL script managing the entire workflow post the set up of simulation files along the custom work flow script can be considered as an additional function in the GUI. The major goals envisioned for the GUI on the framework wrapped around a fibre-reinforced soft tissue model is as follows:

1. *Visualisation*: Provide a display window, to define named selections via mesh entity selection and apply boundary conditions using vtk module within Python or by exporting the script to Paraview ([Ayachit \(2015\)](#)).
2. *Work flow Creation*: Provide graphical tools like buttons, fields to input file names to create workflows with provided rules.
3. *Modification of Parameters*: Allow varying values for the fibre-reinforced HGO model, work flow rate parameters, growth and remodelling rate constants.
4. *Import/Export*: Provide options to import mesh information from various formats or sources and convert using in-built classes and methods into framework readable format. Likewise, export information into various formats for post-processing thereby allowing freedom for the user to visualise results in their own desired software of the visualisation provided by the framework GUI.

A simple schematic for the GUI concept is shown below:

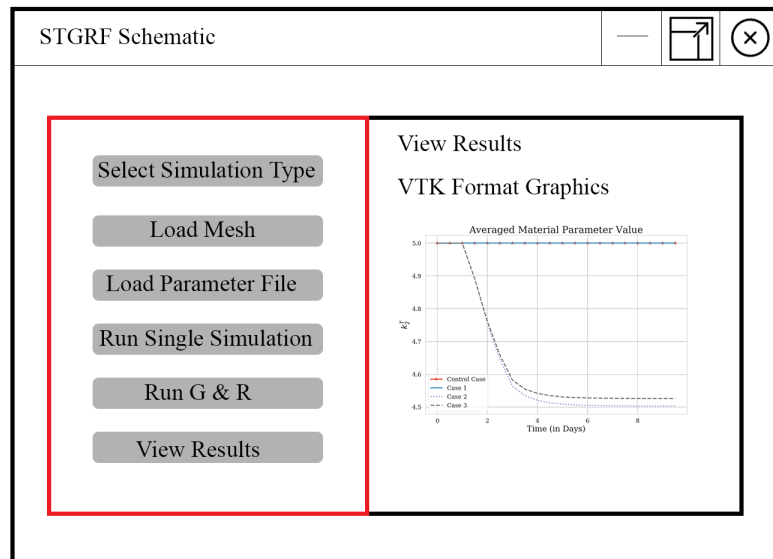


**Figure 4.10:** Simple Schematic

#### 4.4.4 Limitations of the Framework

Apart from the benefits of an ANSYS® oriented framework to address facilitation of soft tissue growth and remodelling models using commercial software, there are limitations which are identified and need to be addressed in future iterations. They are listed below:

1. *Error Checking:* While there are basic error checking procedures using try-except structures, a definite set of custom errors identified during development are still lacking. This would benefit during the development of a GUI and in general so that the end-user is aware of an error when an issue arises, therefore avoid confusion between framework related and language specific errors.
2. *Testing Suite:* No designated testing procedures have been implemented which is a crucial consideration to test every component of the code library behaves in accordance with its expected output for a given input. This includes white box and black box testing, being an important future consideration.
3. *Graphical User Interface:* A lack of GUI proves to be a challenge as the user still has to understand and execute command line instructions as well as modify certain aspects of script files, which need to be overhauled and provided as tool kits in a GUI environment. Not only would this make it easier to reach a wider target audience but facilitate smoother set up of biomechanical soft tissue models in ANSYS®.

4. *Optimisation*: Though the performance of the simulation depends on the FE solver, mesh properties and boundary problem complexity it is important to evaluate these procedures in a standardised way to make sure there are no bottlenecks between the framework and transitions between the FE software.
5. *Other Issues*: This point ties in with the points (1) and (2) as automatic reading in of files requires them to be in the ANSYS ® Mechanical format, and this needs to be modified to enable reading in of various file formats in order to provide an import functionality in the GUI. Also, the same applies for exporting the results, as currently vtk file format is supported and other commonly used formats need to be considered to develop export functions.

## 4.5 Conclusions

Apart from the issues identified, the framework has been useful in setting up a pipeline for soft tissue growth and remodelling for the myocardium and skeletal muscle [Civisilli (2019)]. The users or specifically PhD/ UG/ Masters students involved in projects requiring the use of STGRF adapted quickly to its workings by understanding the documentation and produced results. In finality, a framework has been developed in Python around the commercial finite element software ANSYS © Mechanical whose execution is facilitated by PERL. This has led to the effective set up of multiple soft tissue models around a fibre-reinforced, nonlinear, hyperelastic and incompressible material model (HGO model Holzapfel et al. (2000)) available in the FE software. The feature of creating external scripts provides a form independent biomechanical problem and model definition as seen fit by the user within reasonable boundaries with pertinence to the FE software, possibilities with available material model and functionality offered by the STGRF code library. Based on the models simulated during the term of research has built confidence in the frameworks utility, and though in its nascent stages proves to be promising in alluring the possibility of using industry-standard FE solvers to address soft tissue growth and remodelling domain of research. It is hoped that the framework translates into a full-fledged software, thereby, being useful not only for research, but see the light of day in teaching, medical practice and tool for interested users from all fields.

This page has been intentionally left blank.

## Chapter 5

# Verification of Soft Tissue Growth & Remodelling Framework

The framework introduced in the previous chapter needs to be verified to reliably apply in growth and remodelling simulations. Therefore, in this chapter the material model around which the framework is built (available in ANSYS ©Mechanical APDL library) is verified mathematically with a uni-axial cube extension simulation. Thereafter, a verification is performed for the growth and remodelling hypotheses presented further and the results between Finite Element Analysis and independent mathematical calculations for a cube undergoing sustained stretch for a period of time.

### 5.0.1 Anisotropic Exponential Hyperelastic Material Model

The ANSYS ® material model library has a set of hyper elastic materials which can be utilised to model non-linear material behaviour of soft tissues. However, the recommended material model in ANSYS® MAPDL for fibre-reinforced elastomers especially biomedical materials, is the anisotropic hyperelasticity formulation (ANSYS (2013)), of which the exponential strain energy function (Holzapfel et al. (2000)), see Equation [5.2], is selected. The specific forms employed are shown in Equations[5.3],[5.4].

The ANSYS documentation (ANSYS (2013)), describes the constitutive equation for the strain energy density function as:

$$W = W_v(J) + W_d(\hat{C}, A \otimes A, B \otimes B) \quad (5.1)$$

Wherein,  $W_v$  is related to the strain energy function related to volumetric changes and  $W_d$ , is a purely isochoric contribution accounting for the invariant stretches of the tissue. Please note from here on  $\Psi$  is utilised in place of  $W$  to represent the strain energy density function.

The specific strain energy functional form adapted from (Holzapfel et al. (2000)) to represent soft

tissues is assumed to be a composition of an isotropic and anisotropic component, resulting in a transversely isotropic material behaviour. It is represented as:

$$\tilde{\Psi}_d = \tilde{\Psi}_{iso} + \tilde{\Psi}_{aniso} \quad (5.2)$$

$$\tilde{\Psi}_{iso} = \sum_{i=1}^3 a_i (\bar{I}_1 - 1)^i \quad (5.3)$$

$$\tilde{\Psi}_{aniso} = \frac{c_1}{2c_2} \{\exp [c_2(\bar{I}_4 - 1)^2] - 1\} + \frac{e_1}{2e_2} \{\exp [e_2(\bar{I}_6 - 1)^2] - 1\} \quad (5.4)$$

The typical stress stretch profile for the anisotropic and isotropic strain energy formulations are depicted in Figure [5.1], reproduced using parameters for medial arterial wall from (Holzapfel et al. (2000)).

### 5.0.1.1 Penalty Function

Tissue incompressibility in our constitutive model is enforced by what is known as a penalty function. The mathematical form for the penalty function, which defines the volumetric potential (Equation [5.1]) as documented in (ANSYS (2013)) is:

$$W_v(J) = \frac{1}{d} [J - 1]^2 \quad (5.5)$$

where,  $J$  is the determinant of the deformation tensor, and  $d$  defines the volumetric potential. The bulk modulus( $K$ ) is related to  $d$  as:

$$K = \frac{2}{d} \quad (5.6)$$

The bulk modulus of a fully incompressible tissue would be infinite, which ensures  $J = 1$ . This mathematical simplification leads to theoretical simplifications for constitutive models and their formulations. However, it is not as straight forward in numerical formulations and therefore, a penalty function as in Equation[5.5] is introduced to enforce incompressibility. A large value is required for the bulk modulus to ensure this condition, by varying the volumetric potential there is a value which can be reached so that it does not affect the stress-strain relation of the constitutive model(Gong & Riyad (2002)). Therefore, we test this concept during the verification of the material model.

## 5.0.2 Verification of Material Model

The American Society for Mechanical Engineers defines verification as "The process of determining that a computational model accurately represents the underlying mathematical model and its solution." (Schwer (2009)). In our case the implication bears that we need to analytically solve the constitutive model for a certain scenario and compare the results for stresses, strains obtained mathematically either by hand calculation or by writing a programming script. Either

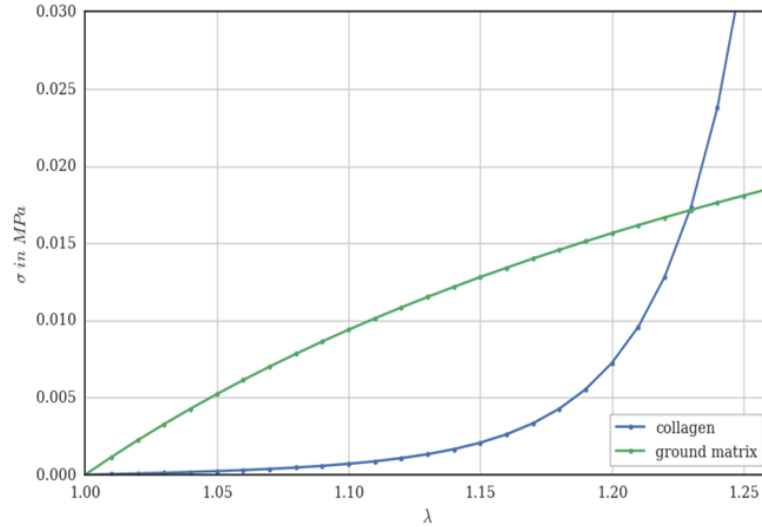


**Figure 5.1:** The stress responses for the isotropic (green) and anisotropic (blue) components are shown in this figure. In soft tissues, the collagen fibre response is modelled as with a strain stiffening effect (blue line) and a Neo-Hookean response for the isotropic component (green line), usually associated with ground matrix tissue.

way, the underlying mathematical implementation of the HGO (Holzapfel et al. (2000)) model in ANSYS® Mechanical APDL needs to be verified for us to be confident in furthering the model for understanding growth and remodelling of soft tissues.

### Uniaxial Extension of a Cube

A cubic model is generally used in finite element analysis to verify the underlying material model utilised in the software, to be sure about the numerical approximations are producing values which we are aware of. A cubic geometry is created using the element type SOLID185 a 8-Node brick element with an edge size of 1mm Fig[5.2]. The collagen fibre directions are both aligned along the x-axis.

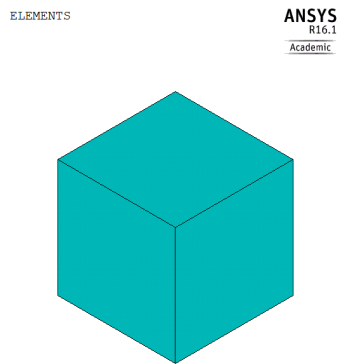


**Figure 5.2:** Single unit cube element using a SOLID185 8-Node brick element type in ANSYS MAPDL.

A displacement based boundary condition is applied, pulling the element in the x-direction i.e. a uni-axial extension regime commonly used to test the material strength of soft tissues atria(Freytes et al. (2008), Mohan & Melvin (1983), Woo et al. (1979) ). We provide test material parameters seen in Equation[5.4] as,  $c = 0.2362$  MPa,  $k_1 = 0.562 \times 10^{-3}$  MPa,  $k_2 = 0.7112$  and understand the values provided numerically by the finite element model. The resultant deformation is shown below in Fig[5.3].

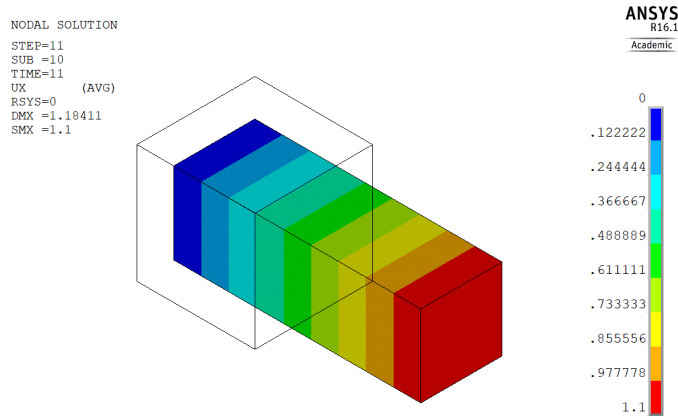


**Figure 5.3:** The Degree of Freedom Solution for deformation of a cube under uniaxial stretch with  $\lambda = 2.0$ .

The analytical solution is based on the Cauchy stress responses of the anisotropic and isotropic contribution in the material model and the number of collagen fibre families considered (for anisotropy). We compare the first principal Cauchy tissue stress experienced by the unit cube under uniaxial extension and compare this analytical solution with a corresponding equivalent setup with relevant boundary conditions in finite elements.

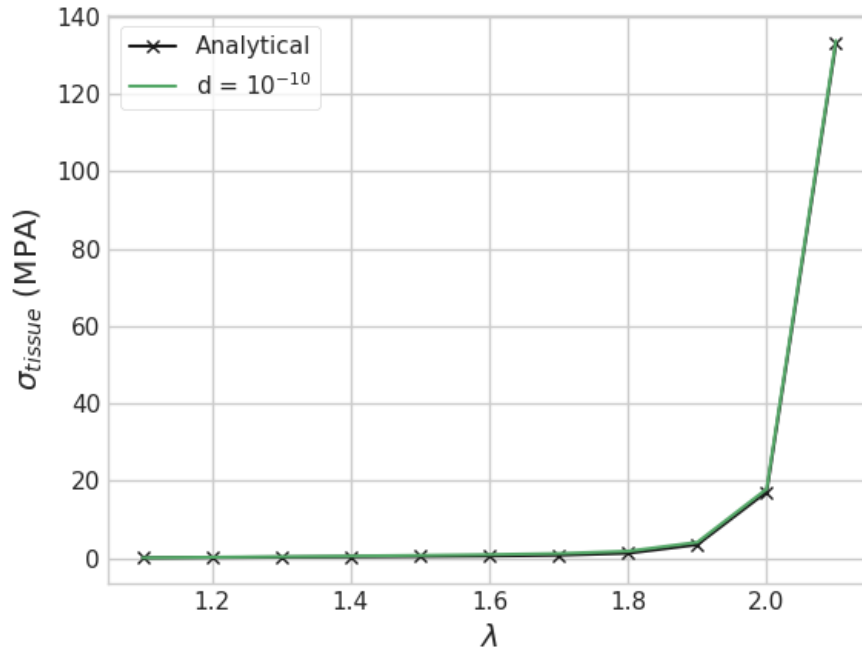


**Figure 5.4:** Verification of the anisotropic exponential hyperelastic material model in ANSYS®, analytical solution written in python and the red dots indicate the values obtained for subsequent displacement based solutions with each stretch value being the boundary condition for uniaxial stretching in the x-direction.

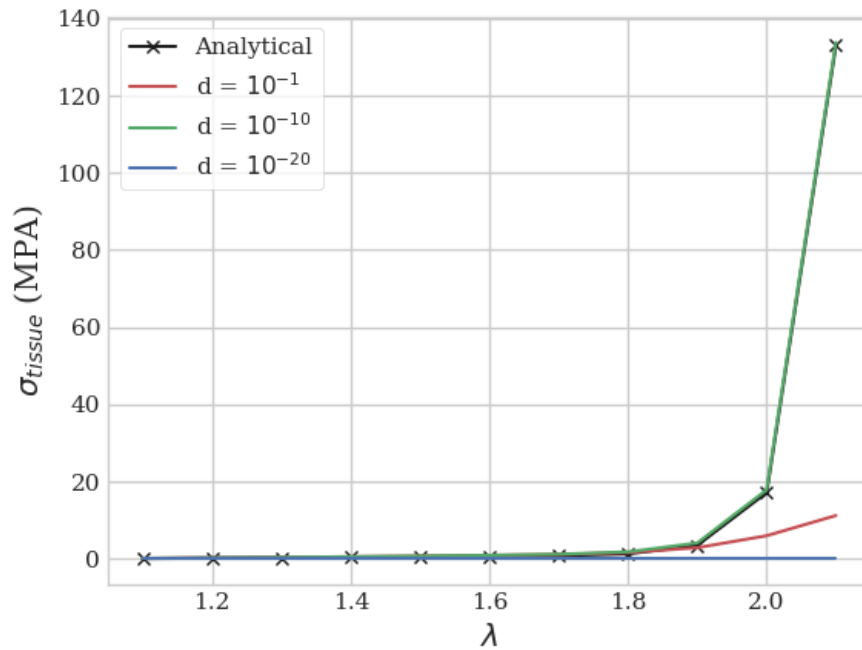


**Figure 5.5:** Verification of the anisotropic exponential hyperelastic material model in ANSYS®, under the effect of multiple  $d$  parameters attributed to the volumetric potential (Gong & Riyad (2002)).

The solutions obtained from numerical approximations in finite elements is comparable to the ones obtained analytically for the HGO material model. An important point is the consideration of the volumetric potential term involved in the material description for the input used in the finite element analysis. There exists a certain value for enforcing incompressibility and not affecting the stress strain relation of the material (Figure [5.5]). The plot in Fig [5.4] uses a value of  $10^{-10}$  for pvol in the TBCDATA code formulation for input in ANSYS.

Figure [5.5], provides results for uni-axial stretching of a cubic element for the HGO model (Holzapfel et al. (2000)). Varying values for  $d$ , seen in the penalty function are considered to observe the stress-stretch response and compared with the analytical solution to identify the value appropriate for our simulations as a step in mathematical verification. The purpose of introducing this plot, is that there exists a certain value for the bulk modulus for the hyperelastic model, which does not affect the mechanical response of the material, while obeying incompressibility constraint (i.e. nearly incompressible or quasi-incompressible). As an infinite bulk modulus would be ideal, it is far from feasible in realistic computation. There exists a particular value for each material parameter combination considered in the strain energy function(5.4)(Gong & Riyad (2002)). The value  $d = 10^{-10}$  is therefore considered as it closely follows the expected behaviour via our 1D analytical solution, for a cube in Finite Element Analysis (Figure [5.4]).

## 5.1 Growth & Remodelling on Cube

The verification of the material model enables us to be sure of the implementation of the fibre-reinforced hyperelastic assumption is accurately represented in the finite element software package. The next step is to test our hypotheses on growth and remodelling using said material model analytically as a 1-D model both mathematically using a Python script and numerically approximating the solution by means of the finite element method. This guarantees our ideas can be implemented on a single element of hyperelastic soft tissue model and enables us to move forward with simulating ideal shaped organ models, patient specific geometries and so forth.

### 5.1.1 Growth Hypotheses

The strain energy function representing the isotropic and anisotropic components (Equation [5.2]), is modified by the inclusion of mass densities for each component. This enables the representation of not only on individual unit of each component but a population of such entities, this has been adapted throughout past research (Wattton et al. (2004, 2009), Zhuang et al. (2019)) and therefore employed in our model. This allows us to model pathological conditions in soft tissues by either prescribing degradation of desired mass density or degradation based on a functional basis of mechanical stretch, stress etc. In our models we use the anisotropic component to represent collagen fibres in the soft tissue extra-cellular matrix, muscle and tendon fibres for skeletal muscles. The isotropic component is assumed to be the ground substance which produces an isotropic Neo-hookean stress response to stretching. We represent the mass densities in the mathematical form as:

$$\Psi = m^{\text{iso}} \tilde{\Psi}_{\text{iso}}(a, I_1) + m^{\text{aniso}} \tilde{\Psi}_{\text{aniso}}(c_1, c_2, I_4) + m^{\text{aniso}} \tilde{\Psi}_{\text{aniso}}(e_1, e_2, I_6) \quad (5.7)$$

Therefore, specifically for remodelling of the collagen fibres in response to the degradation of the ground substance (isotropic component) and increased tissue stretch, the mass density of collagen fibres increase or decrease as a function of the stresses experienced by the collagen fibres to mitigate the tissues loss in strain energy retention due to loads experienced. Given that the collagen extra-cellular matrix fibres are regulated i.e. synthesised or digested based on enzymatic secretions of fibroblasts which themselves modify their structural characteristics and behaviour based on their mechanical environment (Chen & Frangogiannis (2013), Ma et al. (2014), MacKenna et al. (2000)), the collagen fibre stretches can be considered to be the fibroblast stretches as experienced due to changing external stimuli. Equations [5.8, 5.9] depict these functional forms of growth assumptions in our model.

$$\frac{dm^{\text{aniso}}}{dt}(I_x) = \beta m^{\text{aniso}} (f(\sigma_{\text{aniso}}(\mathbf{X}, I_x, t) - \sigma_{\text{aniso}}(\mathbf{X}, I_x, t = 0))) \quad (5.8)$$

$$\frac{dm^{\text{aniso}}(I_x)}{dt} = \beta m^{\text{aniso}} f(\lambda_F(I_x, t) - \lambda_F(I_x, t = 0)) \quad (5.9)$$

In the above equations, the  $I_x$  describes invariants of tissue stretch i.e.  $x = 4, 6$ , which describe the stretch experienced by the collagen fibres in the two specific directions as described in the material model. Therefore, depending on the relative variations in stretches in each direction, the mass density due to the stretch experienced by the fibroblasts as a consequence either synthesises or degrades in the respective fibre direction.

### 5.1.2 Remodelling Hypotheses

In response to changing stretches experienced by the anisotropic collagen fibres or muscle/tendon fibres, given the modelling scenario, the pertinent material parameters adapt to these changes so as to maintain a target homoeostatic Cauchy stress in those fibres. This is in line with the material adapting to changing external mechanical stimuli due to micro-structural constituent reconfiguration (Ambrosi et al. (2019), Watton et al. (2004)). In the HGO material model considered, the parameters  $c_1, c_2, e_1, e_2$  are the material parameters associated with the fibre strain energy functions and therefore their stress responses as seen in atria(5.1.4.1). There after, any modification in the material parameter affects the stress response of that constituent. This is captured by the equation shown below:

$$\frac{dc_2}{dt} = -\alpha c_2 (f(\sigma_{\text{aniso}}(\mathbf{X}, I_4, t) - \sigma_{\text{aniso}}(\mathbf{X}, I_4, t = 0))) \quad (5.10)$$

$$\frac{de_2}{dt} = -\alpha e_2 (f(\sigma_{\text{aniso}}(\mathbf{X}, I_6, t) - \sigma_{\text{aniso}}(\mathbf{X}, I_6, t = 0))) \quad (5.11)$$

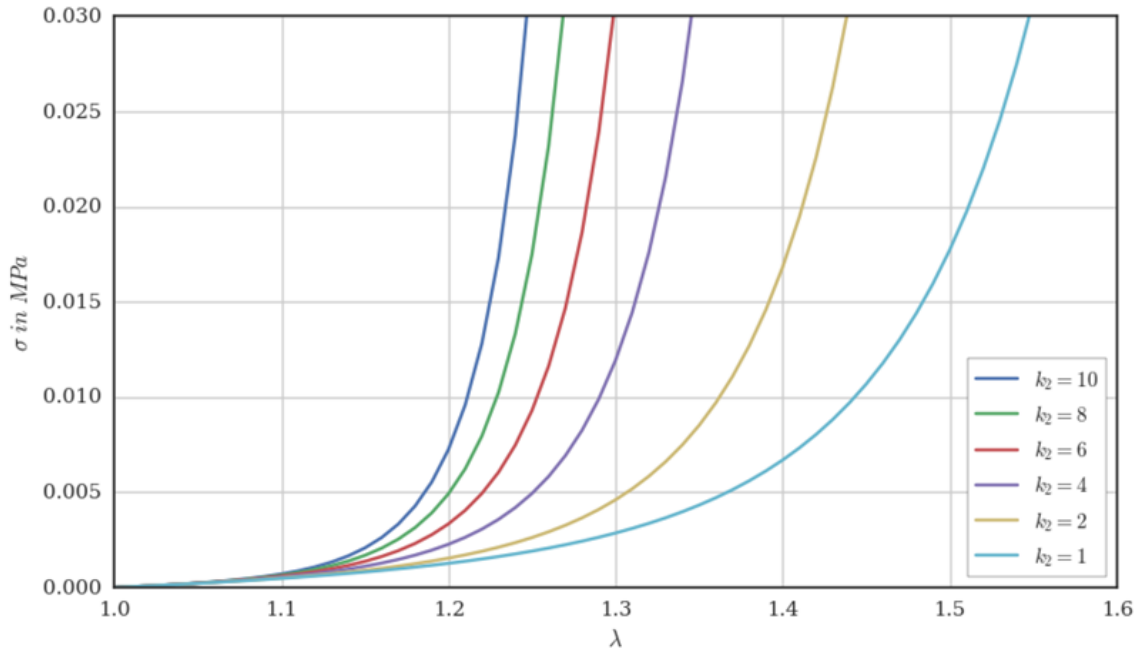


**Figure 5.6:** Remodelling of the material parameter  $c_2$  or  $e_2$  represented by  $k_2$  shows the right ward shift in the stress-strain profile of the anisotropic contribution in the strain energy density function (Equation [5.4] for decreasing values of  $k_2$  as per Equations [5.10, 5.11]). Blue line indicates the initial profile with  $k_2 = 10$  and the right-most cyan line displays the final remodelled profile.

This remodelling enables the fibres to bear more stretch before reaching the toe region after which a strain-stiffening effect is observed. This is shown in the Figure [5.6]. The rightward shift indicates the remodelling of the fibres to restore the change in Cauchy stress to homeostatic levels (in this model this homeostatic stress is at time  $t = 0$ ).

### 5.1.3 Reference Configuration

For growth and remodelling of a body in finite elements, our approach differs from the multiplicative decomposition ( $F = F^e F^g$  theory, which assumes an independent stress-free configuration for mass changes in the body multiplied with an elastic part of the deformation gradient to obtain a final deformed body with mass changes). We assume each constituent in the body is multiplied by an individual mass density variable  $m^x$ ,  $m$  representing the mass and  $x$  denoting the constituent. This is carried out by modifying the constitutive equation with scalar multipliers for each isotropic and anisotropic component as seen in Equation [5.7]. The implication being, we do not model or provide any means to modify the reference configuration of the body after each iteration in the growth and remodelling cycle. This is represented in Figure[5.7].

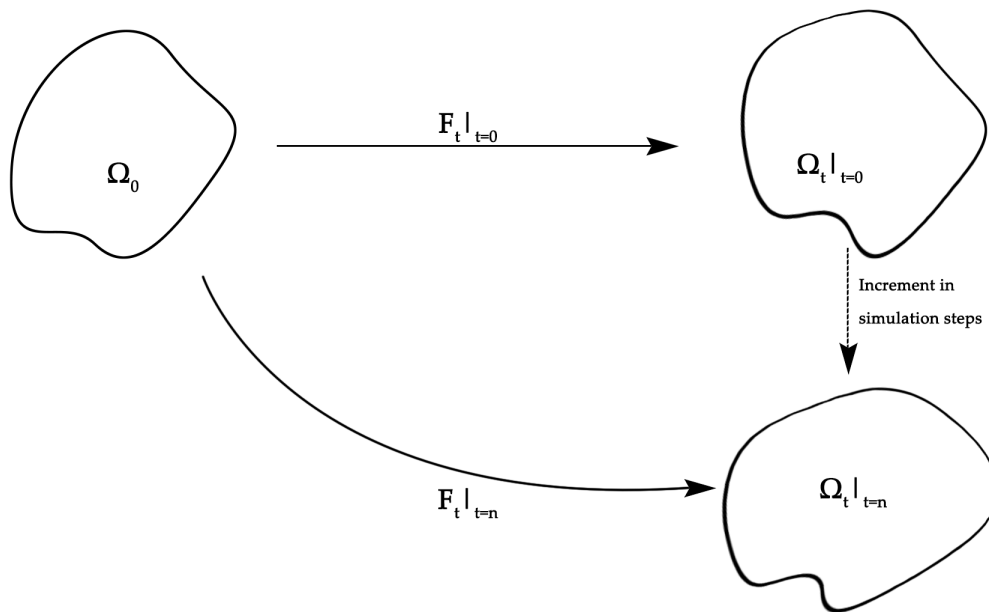


**Figure 5.7:** The initial reference configuration, remains unchanged the subsequent steps in the growth and remodelling workflow. This is because the reference configuration  $\Omega_0$  is not updated after each step and modifications are done via external scripts which affect the input material parameters for the mesh in consideration. This is reflected in the figure, where the loaded configurations  $\Omega_t$  for various steps from 0 to  $n$  are portrayed on the right having the same reference configuration  $\Omega_0$ .

### 5.1.4 Test Cases for Hypotheses

To understand the behaviour of our growth and remodelling laws, we verify the numerical solutions obtained in the finite element simulation solutions to an equivalent analytical model. This helps us ascertain the behaviour of the finite element model follows our one-dimensional model and giving us a basis to employ these laws with more complex geometries. It is an important step to verify the mathematical model implementation in the finite element software with an analytical model to be sure it is the correct choice for our simulation and therefore reduce incorrect modelling of the biomechanical problem.

#### 5.1.4.1 Sustained Over-Stretch of Cubic Element

We consider the following strain energy formulation for the cubic element, replacing the variables seen in Equation [5.4], with those as presented in (Holzapfel et al. (2000)) for consistency throughout.

$$\tilde{\Psi} = \tilde{\Psi}_{\text{iso}}(c, I_1, t) + \tilde{\Psi}_{\text{aniso}}(k_1, k_2, I_4, t) + \tilde{\Psi}_{\text{aniso}}(k_3, k_4, I_6, t) \quad (5.12)$$

We assume uniaxial extension for the cubic element and the deformation gradient is given as:

$$\mathbf{F} = \begin{bmatrix} \lambda & 0 & 0 \\ 0 & \frac{1}{\sqrt{\lambda}} & 0 \\ 0 & 0 & \frac{1}{\sqrt{\lambda}} \end{bmatrix} \quad (5.13)$$

whereas, the Cauchy Green deformation tensor is derived as follows:

$$\mathbf{C} = \mathbf{F}^T \mathbf{F} = \begin{bmatrix} \lambda^2 & 0 & 0 \\ 0 & \frac{1}{\lambda} & 0 \\ 0 & 0 & \frac{1}{\lambda} \end{bmatrix} \quad (5.14)$$

The invariants are calculated as

$$I_1 = \text{tr}(\mathbf{C}) = \lambda^2 + \frac{2}{\lambda}; \quad I_4 = I_6 = \lambda^2 \quad (5.15)$$

With these formulations, we derive the Cauchy stresses for the components of the strain energy function.

$$\sigma_{\text{iso}}(c, I_1, t) = 2c\lambda \left[ \lambda - \frac{1}{\lambda^2} \right] \quad (5.16)$$

$$\sigma_{\text{aniso}}(k_1, k_2, I_4, t) = 2k_1 I_4 (I_4 - 1) e^{k_2 (I_4 - 1)^2} \quad (5.17)$$

$$\sigma_{\text{aniso}}(k_3, k_4, I_6, t) = 2k_3 I_6 (I_6 - 1) e^{k_4 (I_6 - 1)^2} \quad (5.18)$$

The remodelling formulations follow Equation [5.10, 5.11] and are given as:

$$\frac{dk_2}{dt} = -\alpha k_2 \left[ \frac{\sigma_{\text{aniso},I_4}(k_1, k_2, I_4, t) - \sigma_{\text{aniso},I_{4H}}(k_1, k_2, I_4, t = 0)}{\sigma_{\text{aniso},I_{4H}}(k_1, k_2, I_4, t = 0)} \right] \quad (5.19)$$

$$\frac{dk_4}{dt} = -\alpha k_4 \left[ \frac{\sigma_{\text{aniso},I_6}(k_3, k_4, I_6, t) - \sigma_{\text{aniso},I_{6H}}(k_3, k_4, I_6, t = 0)}{\sigma_{\text{aniso},I_{6H}}(k_3, k_4, I_6, t = 0)} \right] \quad (5.20)$$

We subject the cube to an initial stretch  $\lambda_i = 1.1$  and a final stretch  $\lambda_f = 1.5$ , from an initial time  $t_i$  to a final time  $t_f$ . The test parameters are displayed in the table below:

Parameter	Value	Units
$c$	1.0	MPa
$k_1$	0.5	MPa
$k_2$	5.0	MPa
$k_3$	0.5	-
$k_4$	5.0	-
Time (t)	100	Days
Steps (n)	100	-
$\lambda_i$	1.1	-
$\lambda_f$	1.5	-
$t_i$	t = 5	days
$t_f$	t = 20	days
$\alpha$	0.002	-
$\beta$	0.001	-

**Table 5.1:** Parameter set up for simulating sustained over-stretch of a cubic element.

Similarly, for the finite element set up of the 1D model, we create a 1 mm x 1 mm x 1 mm cube and assign the material parameter values shown in Table [5.1] using a parameters file. The remodelling hypotheses are the same as described above, we have not included the term  $(\mathbf{X})$  to represent a material point as we deal with a unit cube at the origin. The Figure [5.4], can be referred which reflects the boundary conditions involving the pulling of one end of the cube.

## Results

The results obtained by finite element analysis are visualised using Paraview as seen in Figures [5.8, 5.9, 5.12, 5.11]. Spreadsheets were exported from Paraview to be plotted along with the 1D analytical model solutions in the graphs that follow. Dots represent FEA solutions, whereas lines represent the results obtained by the 1D analytical model.

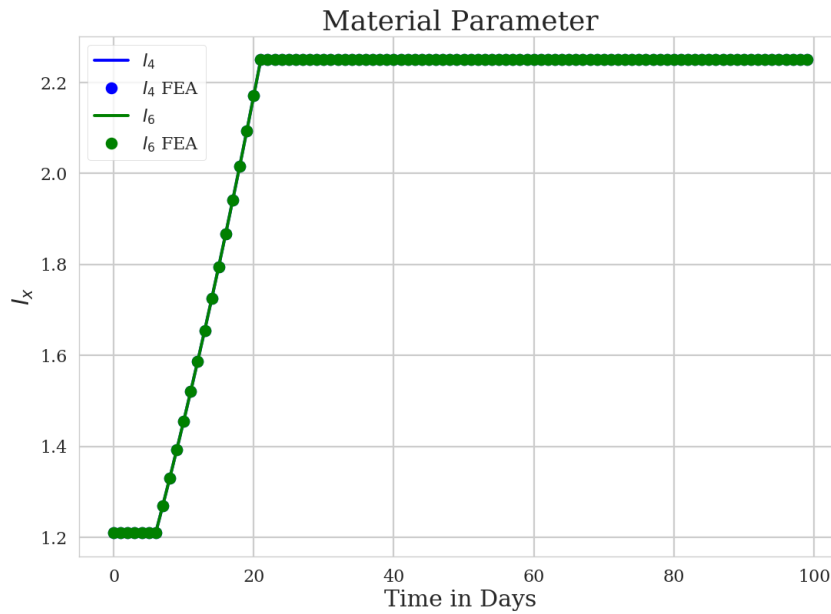


**Figure 5.8:** The stretch invariants are shown for the fibres in directions  $I_4$  and  $I_6$ . The blue line and green lines overlap as both the fibres are subjected to same levels of stretch.

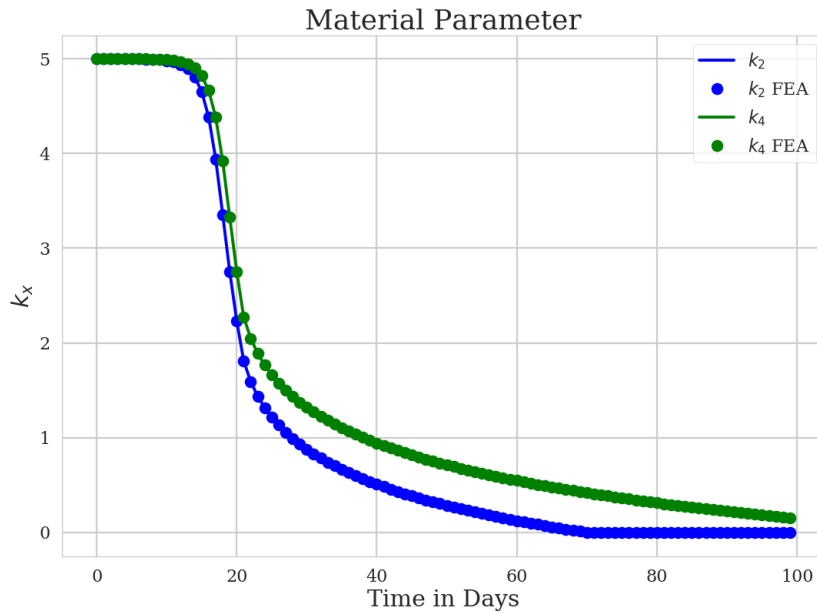


**Figure 5.9:** The material parameters  $k_2, k_4$ , associated with  $I_4, I_6$  fibre directions respectively are depicted. The  $k_2$  values remodel quicker due to having a higher rate constant  $\alpha = 0.002$  reaching stabilisation at  $t=70$  days at 0.1 % of atriails original value, as compared to  $k_4$  which remodels at a slower rate. The analytical and numerical solutions are consistent.

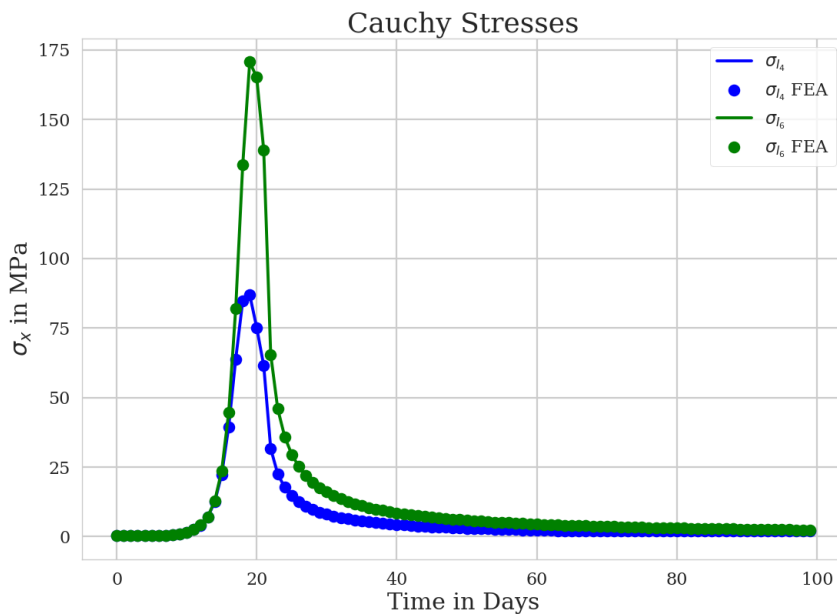


**Figure 5.10:** The Cauchy stresses experienced by the  $I_4, I_6$  fibre families are shown. It can be seen that both the fibre families remodel with a similar trend, however a quicker remodelling is observed in terms of the fibres in the  $I_4$  direction, due to a higher rate constant  $\alpha > \beta$ . The analytical and numerical solutions are consistent

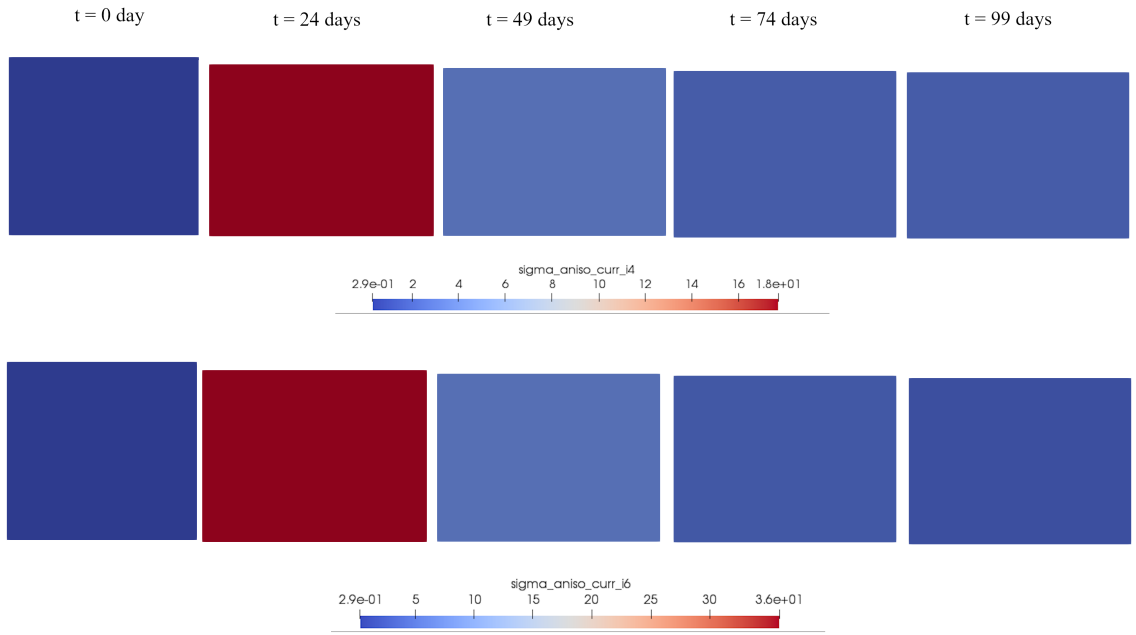


**Figure 5.11:** Snapshots of the cube experiencing sustained stretch, the Cauchy stresses  $\sigma_{\text{aniso}, I_4}$  and  $\sigma_{\text{aniso}, I_6}$  are shown.

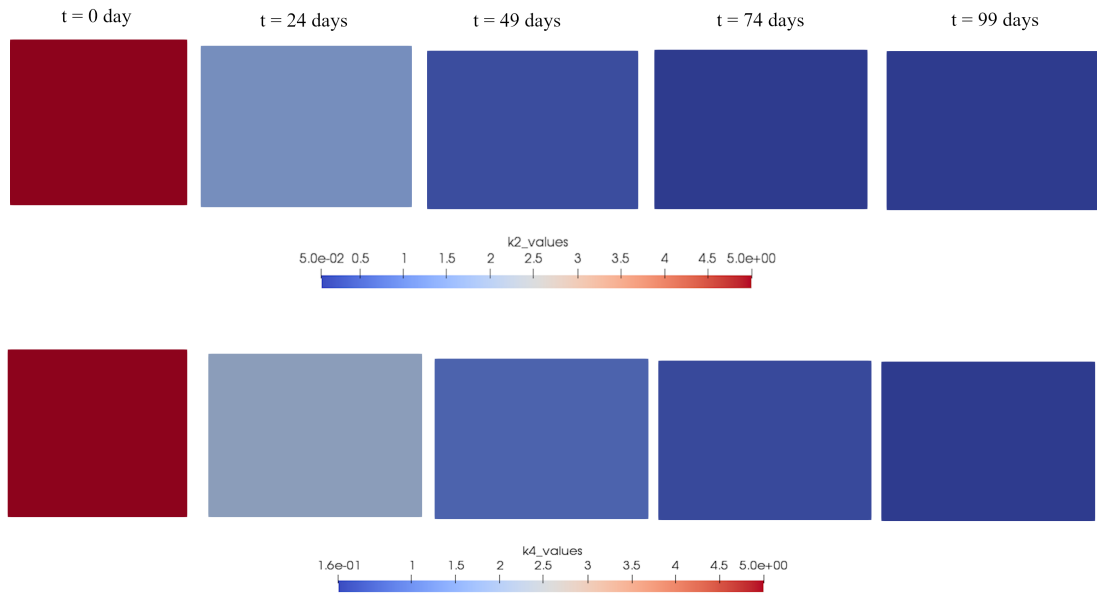


**Figure 5.12:** Snapshots of the cube experiencing sustained stretch, the remodelled material parameters  $k_2$  and  $k_4$  are shown.

## **5.2 Conclusions**

Given these verifications, we are confident of the post-processing scripts for calculating the requisite mechanical quantities to enable our growth and remodelling workflow and consider atriats applications to soft tissues.

## Chapter 6

# Applications of STGRF I: Stress Based Growth & Remodelling of the Left Ventricle Post Myocardial Infarction

---

*In this chapter the first application of the soft tissue growth and remodelling framework, in the context of an idealised left ventricle to simulate myocardial infarction is presented. The left ventricular finite element volume mesh is modelled using a modified passive, fibre-reinforced, hyperelastic, anisotropic material model. Mass density terms are associated with the isotropic and anisotropic components which represent the cardiomyocytes, ground matrix and collagen fibres having two orientations respectively. Using degradation functions, myocardial infarction is induced. Stress based formulations are employed to simulate the remodelling of the collagen fibres to maintain a preferred state of stress. A fictitious fibroblast field as a cellular component is introduced to regulate collagen mass density. Results consist of two cases, (a) Evolution of the homoeostatic collagen stress levels and (b) one without. Evolving the homoeostatic stress levels resulted in lesser dilatation and reduced collagen mass density changes but may be reflective of changing tissue properties as the original reference configuration may not be recovered due to the loss of cardiomyocytes. Patient specific geometries and better representation of collagen fibres are envisaged to provide improved results for the stress-distribution and structure, function changes of the left ventricle post-MI.*

---

## 6.1 Aims and Objectives

We develop a left ventricular model using a fibre-reinforced, hyperelastic, incompressible material model introduced in (Holzapfel et al. (2000)) which has been widely considered to model arteries, bladder and skeletal muscle fibres and available in the ANSYS® Mechanical FE software. The objective is to focus on understanding the growth and remodelling of the myocardial extra-cellular collagen matrix in response to the onset of a myocardial infarction using the STGRF code library developed (Chapter [4]). Further through this study it is aimed to understand:

1. Mass density variations in collagen within the volume of the idealised left ventricular geometry.
2. Analyse the influence of modification of the in-built material model, via external scripting.
3. Understand how a change in homeostatic Cauchy stress levels experienced by the collagen fibres impacts the growth and remodelling outcomes.
4. Utility and extension of the soft tissue growth and remodelling framework (Chapter 4), using a customised workflow script.

## 6.2 Novel Finite Element Analysis for the Growth & Remodelling of a Fibre-reinforced Passive Myocardial Tissue Post MI

By utilising the custom workflow feature of the STGRF framework (Chapter [4]), the growth and remodelling of the left ventricular myocardium using the fibre-reinforced, transversely isotropic, hyperelastic, incompressible Holzapfel-Gasser-Ogden (Holzapfel et al. (2000)) material model available in ANSYS ® Mechanical finite element software to for a transmural myocardial infarction on a region of the myocardium, is simulated.

## 6.3 Methodology

### 6.3.1 Fibre reinforced Material Model for Myocardial Tissue

The cardiomyocytes, elastin and other ground substances are represented using the passive isotropic term ( $\tilde{\Psi}_{iso}$ ) in the strain energy function [Equation 5.2]. Collagen fibres are represented by the anisotropic strain energy function term ( $\tilde{\Psi}_{aniso}$ ) and the formulation for two fibre directions, represented by their stretch invariants ( $I_4, I_6$ ), is utilised. The strain energy for the myocardial tissue is formulated as:

$$\Psi = m^{GM}\tilde{\Psi}_{GM} + m^C\tilde{\Psi}_C \quad (6.1)$$

where,  $m^X$ , indicates a normalised mass density term for a the particular constituent  $X$ , representing the ground matrix (GM) and the collagen fibres (C) The normalised mass density term depicts the concentration/amount of a constituent  $x$  at time  $t$  in the simulation cycle to the concentration present at time  $t = 0$  i.e. ( $m^x = \frac{m^x(t)}{m^x(t=0)}$ ). This allows us to collectively associate the mechanical response of not only an individual fibre, but a collective of fibres

The expanded form of the strain energy function (Equation [6.1]) as detailed in (ANSYS (2013)) including the mass density terms, is shown below:

$$\Psi = m^{GM}\frac{c}{2}[I_1 - 3] + m^{C,I_4}\frac{k_1}{2k_2}[\exp\{k_2(I_4 - 1)^2 - 1\}] + m^{C,I_6}\frac{k_3}{2k_4}[\exp\{k_4(I_6 - 1)^2 - 1\}] \quad (6.2)$$

Note the material parameter terms are represented using the notations introduced in (Holzapfel et al. (2000)) as compared to (ANSYS (2013)), to ensure notational consistency. Additionally, a modified formulation for the anisotropic components, is assumed, given as:

$$\tilde{\Psi}_{C,x} = \frac{k_{num}}{k_{den}}[\exp\{k_{den}(I_x - 1)^2\} - 1] \rightarrow \tilde{\Psi}_{C,x}^{mod} = \tilde{k}[\exp\{k_{den}(I_x - 1)^2\} - 1] \quad (6.3)$$

where,  $x = I_4, I_6$ , num = 1, 3 and den = 2, 4 as per the appropriate identifiers seen in the anisotropic component of Equation [6.2]. For details about the effect of this modification please refer to Appendix [C], done externally using custom Python scripts, without affecting the ANSYS ® material

model.

For the myocardium it is assumed that the mass density term in Equation[6.1] for the ground matrix(GM) decreases over a specified degradation time, to simulate a myocardial infarction. This indicates the necrosis of the passive cardiac muscle cells, thereafter driving the collagen fibres to take on the role of load bearing from their former protective sheathe function. The representation in done with respect to the number of steps over a given time period as:

$$m^{GM}(t) = (m^{GM, \min})^{(i/t)} \rightarrow c(t) = c(t) m^{GM} \quad c(t) > 0.01c_0 \quad (6.4)$$

The minimum value for the ground matrix material parameter ( $c$ ) has to be greater than 0 (Holzapfel et al. (2000)), and a limitation for the value it can attain using the degradation of  $m^{GM}$  multiplied to it, indicating the ground matrix degradation to a minimum value ( $m^{GM, \min}$ ), is set.

### 6.3.1.1 Difference between 1D and FE material model

A point of contention, would be the material model i.e. the strain energy function employed to represent the myocardium with a non-linear fibre-reinforced hyperelastic material model based on HGO model (Holzapfel et al. (2000)) versus the comprehensive strain energy function derived in Chapter[3], the equation [6.5] is reproduced for convenience.

$$\Psi = m^{GM} \tilde{\Psi}_{GM} + m^M \tilde{\Psi}_M + m^{C, myo} \tilde{\Psi}_{C, myo} + m^{C, epi} \tilde{\Psi}_{C, epi} \quad (6.5)$$

Compared to the passive material model for fibre-reinforced soft tissues (6.1), Equation[6.5] for the unidimensional constrained mixture model is capable of including cardiac myocytes, collagen fibre undulation distribution and active response of the muscle. Apart from mass density terms to adhere to growth and remodelling hypotheses, the passive hyperelastic model being readily available for use is one reason. The second reason for adapting HGO model(Holzapfel et al. (2000)), to our modelling hypothesis is the learning curve and difficulty in implementing user material sub routines without precise experience. This difference is intended to clarify the use of the material model over a custom user defined subroutine.

### 6.3.2 Model Configuration Assumptions

We refer back to the left ventricular pressure volume relationship (Figure [2.7]) to identify the reference configuration and loaded configuration for our finite element model. The reference configuration ( $\Omega_0$ ) is selected to be the point D at the beginning of diastole where it is assumed the cardiac muscle has undergone isovolumetric relaxation and is stress-free. The point A, which signifies the end-diastolic state for the LV is assumed to be the loaded configuration ( $\Omega_t$ ) at a pressure of about 8 mmHg or  $\approx 1.3$  kPa due to the in-flow of blood from the left atrium.

### 6.3.3 Mesh Generation

The mesh for the left ventricle is based on the dimensions for an idealised left ventricle, adapted from (Hassaballah et al. (2013)), shown in Figure [6.1].

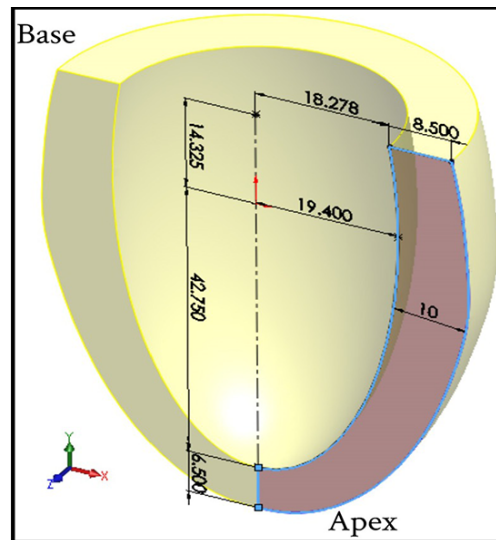


**Figure 6.1:** The dimensions of the idealised left ventricle as considered in our model, adapted from (Hassaballah et al. (2013)).

Using these dimensions as guidelines, a mesh within the ANSYS © Mechanical software itself, is created. Using SOLID185 type elements which are 8-node brick node elementsFigure[6.2]. This generation was done using lines created to define the surface as seen in Figure[6.3].

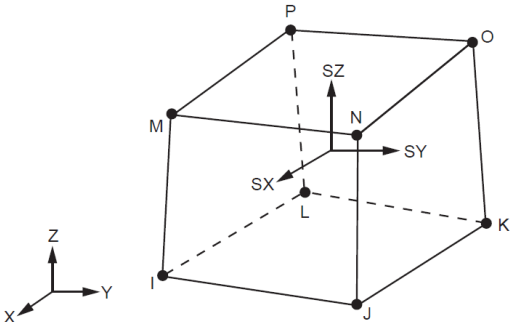


**Figure 6.2:** The element type used to create the LV mesh, identified as SOLID185 (ANSYS (2013)), is an 8-Node hexahedral brick element.

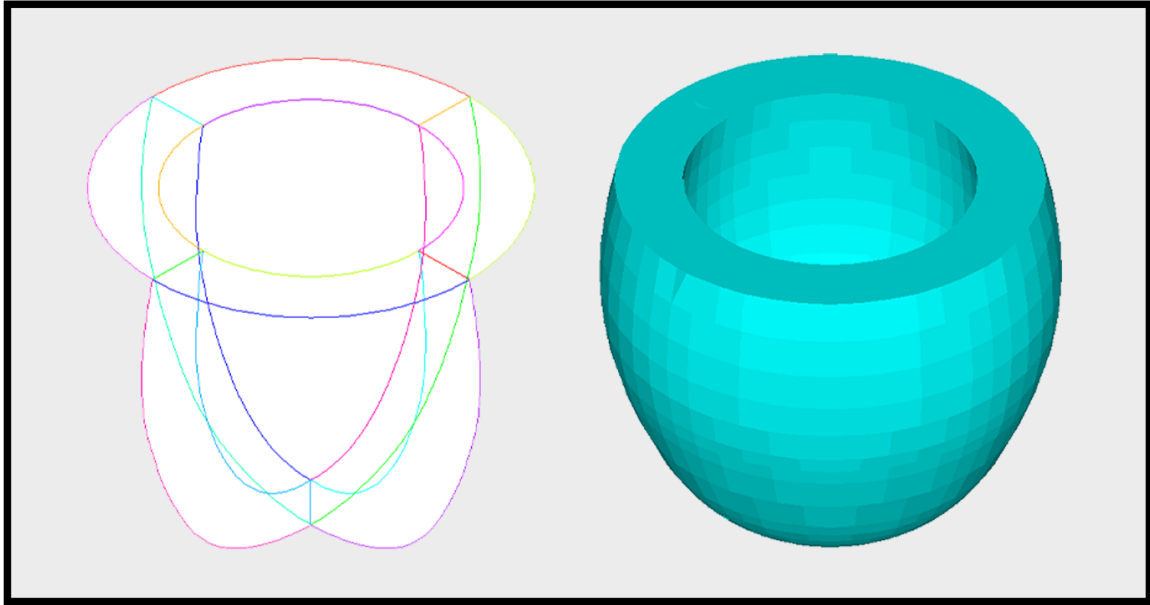


**Figure 6.3:** (Left) The lines generated in ANSYS® Mechanical, approximated dimensions of the LV from (Hassaballah et al. (2013)), Right Surfaces generated by using the lines as a guiding construct, prepared for meshing.

The Figure [6.4], shows the mesh generated as a result.

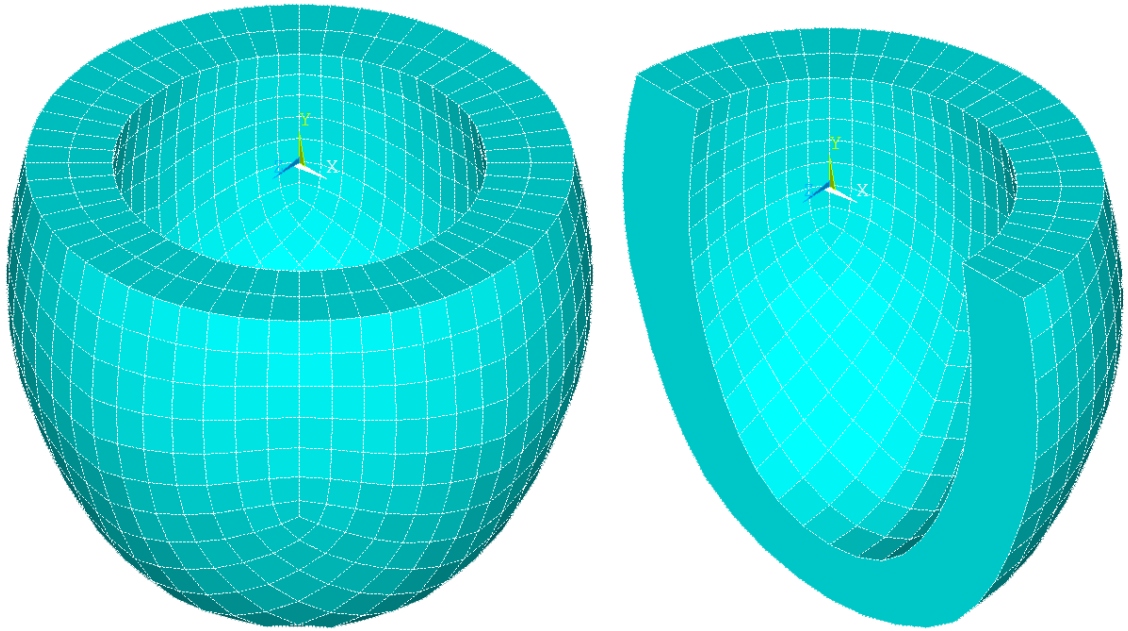


**Figure 6.4:** *The hexahedral mesh generated for the LV mesh, with an element edge size of 5 mm.*

### 6.3.4 Boundary Conditions

The boundary conditions to simulate diastolic filling of the left ventricle due to an internal blood pressure of about 1.3 kPa are provided, as has been considered in (Klepach et al. (2012)). The base of the ventricle has rolling supports for the internal nodes (Figure[6.5]), whereas the outer nodes on the bases edge are fixed, this allows the internal wall to deform on experiencing load uniformly from the base to the apex transmurally without any sharp changes in deformation between the base and the continuing myocardium towards the apex.

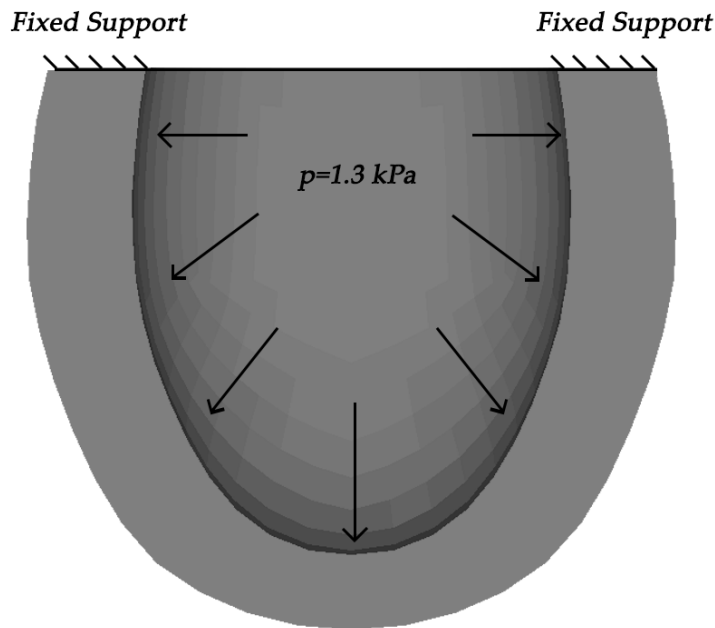


**Figure 6.5:** The left ventricle is held in place with a fixed support at the base of the ventricle, and an internal pressure of 1.3 kPa i.e. ( $\approx 10 \text{ mm Hg}$ ) is defined. These conditions are employed to simulate the passive deformation of the LV wall during its passive filling phase due to the blood entering into it via the mitral valve from the left atrium.

### 6.3.5 Collagen Fibre Directions

Collagen fibres are distributed and organised in the myocardium on different levels, from a single muscle fibre (cellular level) all the way to the tissue level fibre. Also, they are present in the interstitial space around the myocardial muscle fibres as parallel sheets. On observing previous models, it was convenient to represent the collagen fibres as running parallel to the myocardial muscle fibres, which have been defined to be organised in three major directions based on the finite element model in (Nash & Hunter (2000)). Wherein, the myocardial fibre directions are defined as fibre ( $f$ ), sheet ( $s$ ) and sheet-normal ( $n$ ) directions as shown in Figure [6.6].

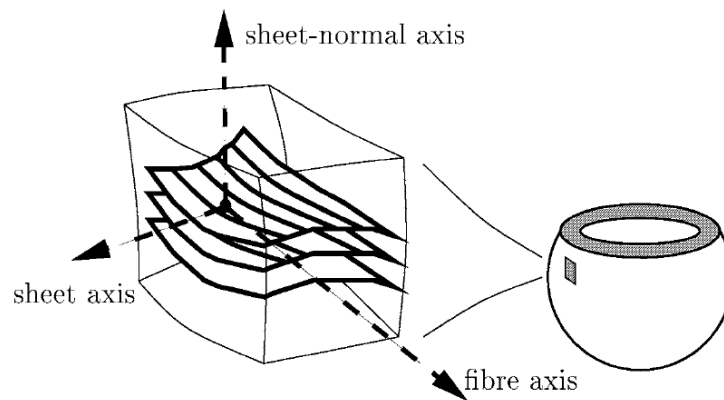


**Figure 6.6:** The three myofibre axis directions as defined by (Nash & Hunter (2000)), which are the fibre axis ( $f$ ), sheet axis ( $s$ ) and sheet-normal axis ( $n$ )

We assume the collagen fibres in our model to be aligned circumferentially along the axis running from the base to the apex (long-axis) and longitudinally aligned parallel to the long-axis (Figure [6.7]).

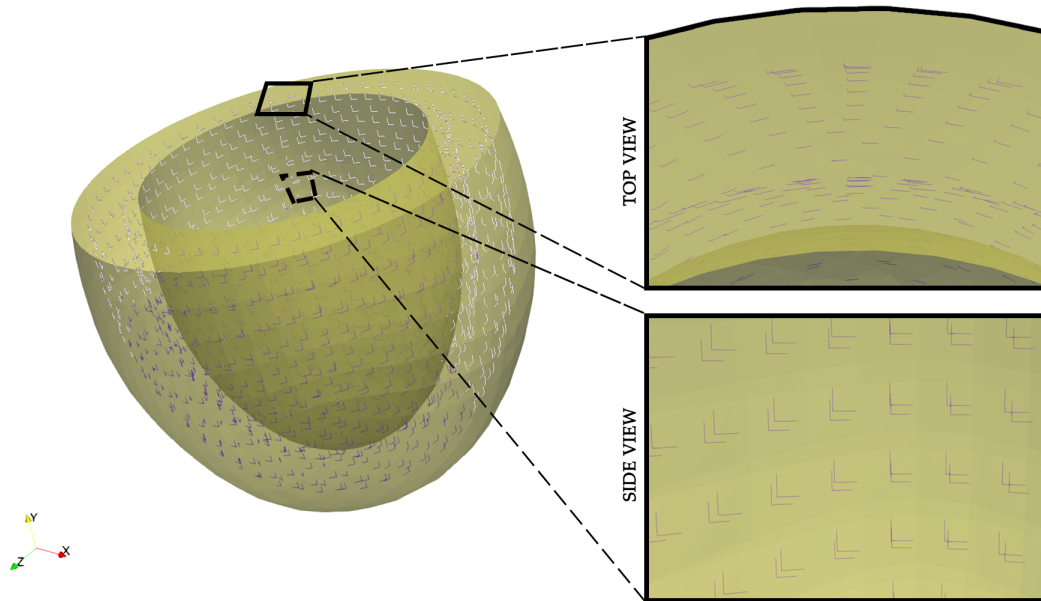


**Figure 6.7:** The fibre orientations in our model defined w.r.t the fibre and sheet-normal axis directions for the two collagen families in the  $I_4$  &  $I_6$  directions respectively. We define the  $I_4$  family of collagen fibres as circumferential and the  $I_6$  fibres as longitudinal fibres.

### 6.3.6 Growth & Remodelling

Based on the material model employed (Holzapfel et al. (2000), Equation[6.2]) growth and remodelling assumptions for the anisotropic collagen fibres in the myocardium as employed in (Chan (2019)), are defined.

#### 6.3.6.1 Collagen Remodelling Hypotheses

In (Watton et al. (2004)), the collagen remodelling is simulated by the evolution of its natural reference configuration where it is recruited to bear load, in order to remodel the fibre stretch in the loaded configuration towards a constant value, represented by the attachment stretch( $\lambda_C^{AT}$ ). Consequently, it is assumed that the strain energy stored in a collagen fibre is a function of the stretch that it experiences, implying the fibre Cauchy stress ( $\sigma_C(\lambda_C)$ ) will remodel towards a homoeostatic value i.e.  $\tilde{\sigma}_{CH} = \tilde{\sigma}_C^{AT}$  (calibrated at t=0 in our model simulation). Please note: any variable with a subscript H signifies its value at t=0

$$\frac{dk_2}{dt} = -\alpha k_2 \left[ \frac{\sigma_C(\mathbf{X}, k_1, k_2, I_4, t) - \sigma_{CH}(\mathbf{X}, k_1, k_2, I_4, t)}{\sigma_{CH}(\mathbf{X}, k_1, k_2, I_4, t)} \right] \quad (6.6)$$

$$\frac{dk_4}{dt} = -\alpha k_4 \left[ \frac{\sigma_C(\mathbf{X}, k_3, k_4, I_6, t) - \sigma_{CH}(\mathbf{X}, k_3, k_4, I_6, t)}{\sigma_{CH}(\mathbf{X}, k_3, k_4, I_6, t)} \right] \quad (6.7)$$

The Cauchy stress formulations derived with respect to invariants  $I_4, I_6$ , are shown below:

$$\begin{aligned} \sigma_C(\mathbf{X}, k_1, k_2, I_4, t) &= \tilde{\sigma}_C(\mathbf{X}, k_1, k_2, I_4, t) = 2(\mathbf{X}, t) I_4 k_1 (I_4 - 1) e^{(k_2[I_4 - 1]^2)} \\ \sigma_C(\mathbf{X}, k_3, k_4, I_6, t) &= \tilde{\sigma}_C(\mathbf{X}, k_3, k_4, I_6, t) = 2(\mathbf{X}, t) I_6 k_3 (I_6 - 1) e^{(k_4[I_6 - 1]^2)} \end{aligned} \quad (6.8)$$

The fibre Cauchy stress is post-processed from the previous step's simulation results, using the Hencky/ Logarithmic strain tensor( $\mathbf{h}$ ) for each element. This is achieved by deriving the invariants ( $I_4, I_6$ ) and substituting their values in the Equations [6.8]. The derivation of the invariants is shown below:

$$\begin{aligned} \mathbf{U} &= \mathbf{F}^T \mathbf{F} \\ \mathbf{C} &= \mathbf{U}^2 \\ \mathbf{C} &= e^{\mathbf{h}^2} \\ I_4 &= \mathbf{C} : \mathbf{A}_{01} = \mathbf{F}^T \mathbf{F} : a_{01} \otimes a_{01} \\ I_6 &= \mathbf{C} : \mathbf{A}_{02} = \mathbf{F}^T \mathbf{F} : a_{02} \otimes a_{02} \end{aligned} \quad (6.9)$$

where,

$\mathbf{h}$  - Hencky/ Logarithmic Strain Tensor

$\mathbf{U}$  - Right Biot Stretch Tensor

$\mathbf{C}$  - Cauchy Green Deformation Tensor

$\mathbf{F}$  - Deformation Tensor

The stretch invariants are calculated by multiplying  $C$ , with the directin structure tensors  $\mathbf{A}_{01}, \mathbf{A}_{02}$  based on their vector direction given by  $a_{01}, a_{02}$  (Holzapfel et al. (2000)). Additionally, a modified version of the constitutive model, (Section [C.1]), is employed.

### 6.3.6.2 Collagen Growth Hypotheses

Fibroblasts are introduced as a cellular component to the model, without partaking in the force-balance. They are a function of the tissue stretch in the  $I_4, I_6$  collagen fibre directions (calculated as shown in Equation[6.12]). They are assumed to be recruited to bear load at an independent reference configuration at a level of recruitment stretch( $\lambda_F^R$ ), attaining a certain stretch ( $\lambda_F$ ) in the loaded configuration ( $\Omega_t$ ).

The recruitment stretch for fibroblasts are calculated as follows:

$$\lambda_{F,x}^R|_{t=0} = \frac{\lambda_x}{\lambda_{FH}}|_{t=0}; \quad x = I_4, I_6 \quad \text{at } t = 0 \quad (6.10)$$

where,  $\lambda_{FH}$ , is assumed to be the homoeostatic stretch level for a fibroblast and is prescribed to be 1.05 associated with the collagen fibres in two directions i.e.  $I_4, I_6$ , respectively, at time  $t=0$ .

The fibroblast recruitment stretch evolves based on the deviations of the current fibroblast stretch at time  $t$  from the homoeostatic fibroblast stretch. This is assumed to remodel and restore the fibroblast stretch towards a homoeostatic stretch value ( $\lambda_{FH}$ ).

$$\frac{d\lambda_{F,x}^R}{dt} = \gamma \lambda_{F,x}^R \left[ \frac{|\lambda_{F,x}(\mathbf{X}, t) - \lambda_{FH,x}(\mathbf{X}, t)|}{\lambda_{FH,x}(\mathbf{X}, t)} \right]; \quad x = I_4, I_6 \quad (6.11)$$

After time ( $t=0$ ) and the remodelling of the fibroblast recruitment stretch, the stretch experienced by the fibroblast themselves is calculated by:

$$\lambda_{F,x} = \frac{\lambda_x}{\lambda_{F,x}^R}; \quad x = I_4, I_6 \quad (6.12)$$

The collagen fibre mass density( $m^{c,x}$ ) growth is driven by changes in the fibroblast stretch ( $\lambda_F$ ) at time  $t$  from the homoeostatic fibroblast stretch ( $\lambda_{FH}$ ), formulated as:

$$\frac{dm^{c,x}}{dt} = \beta m^{c,x} \left[ \frac{\lambda_{F,x}(\mathbf{X}, t) - \lambda_{FH,x}(\mathbf{X}, t)}{\lambda_{FH,x}(\mathbf{X}, t)} \right]; \quad x = I_4, I_6 \quad (6.13)$$

### 6.3.6.3 Infarct Zone Elements

The selection of infarct zone elements is carried out using a sphere of influence abstraction. An element centroid is selected as the centre of the infarct and the infarct radius is provided as an input for the sphere of influence. The sphere of influence here is defined as sphere within which each selected element in the left ventricular mesh is considered to be in the infarction zone of the myocardium, for which cardiomyocyte mass density degradation is prescribed to drive the onset of a myocardial infarction. This is illustrated in the Figure[6.8] below:

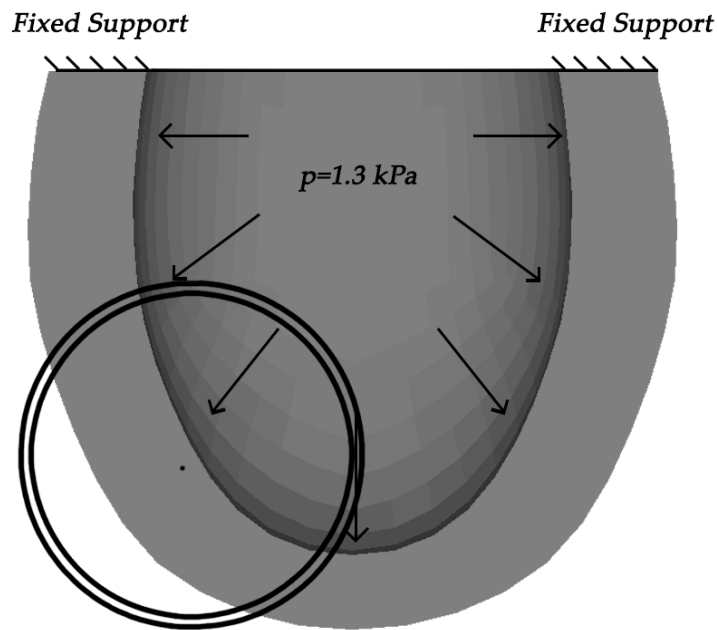


**Figure 6.8:** The infarct zone is prescribed, by selecting a spherical region with a centre ( $i_c$ ) and providing a radius. We define a radius of 20 mm i.e. a 2cm infarct and selected hexahedral elements are subjected to degradation of the ground matrix.

In a study, the correlation with infarct sizes to mortality was carried out for humans and animals, the sizes of infarcts had a median size of 12 % (Miller et al. (1995)). Assuming the idealised LV (Hassaballah et al. (2013)), to be a perfect hemisphere, we can consider the circumference of the base to be the diameter ( $\approx 168.18$  mm) of the semi-circle obtained by opening up the hemisphere into a planar surface. This allows us to calculate the surface area of the LV as a semi-circle ( $\frac{\pi r^2}{2} = \frac{\pi(84.09)^2}{2} = 11,101.67\text{mm}^2$ ) and a sphere of influence of 20 mm would project a circle of influence on the opened up surface area, the area of the infarction elements selection circle would be ( $\frac{\pi(20)^2}{2} = 1256\text{mm}^2$ ). The area of the infarction within the selection zone comes to  $\approx 11.314$  % of the LV surface area. Though a better criteria is required to identify selected elements volumes and measured against the volume of the entire LV, the surface area method was an initial attempt to provide an infarct region to model.

In the study (Hreybe & Saba (2009)), location of acute myocardial infarctions (AMI) have been

perused to understand their association with arrhythmias and conduction abnormalities linking to their in-hospital mortality impact. Given the number of patient records (n=21,807) the data suggests 41.2 % of patients had anterior infarctions and 52.9 % had inferior infarctions. Given the generated idealised LV mesh, where the other chambers of the heart are not modelled, it is difficult to discern between the anterior and posterior locations for the left ventricle. Therefore, the infarction region/ zone can be considered to be either, and until a completely realised mesh is utilised, this can be treated as an initial test case to understand the behaviour of the growth and remodelling hypotheses on the LV finite element mesh.

### **6.3.6.4 Material Parameter Values**

The table below (Table 6.1), lists a set of finite element models which have been used in research for modelling the myocardium and the values used for material parameters in their respective constitutive model strain energy functions.

No.	Article	Strain Energy Density Function	Material Property
1	<a href="#">Humphrey et al. (1990)</a>	$W(I_1, \alpha) = c_1(\alpha - 1)^2 + c_2(\alpha - 1)^3 + c_3(I_1 - 3) + c_4(I_1 - 3)(\alpha - 1) + c_5(I_1 - 3)^2$	$c_1 = 20.05, c_2 = 63.27, c_3 = 1.674$ (values in kPa)
2	<a href="#">Holzapfel &amp; Ogden (2009)</a>	$\Psi(I_1, I_{4s}, I_{4f}, I_{8fs}) = \frac{a}{2b} \exp[b(I_1 - 3)] + \sum_{i=f,s} \frac{a_i}{2b_i} \exp\{[b_i(I_4 i - 1)^2] - 1\} + \frac{a_{fs}}{b_{fs}} \{\exp[b_{fs} I_{8fs}^2] - 1\}$	$a = 0.798, b = 8.614, a_f = 13.88, b_f = 15.87, c_{a_s} = 4.661, b_s = 9.0395, a_{fs} = 0.216, b_{fs} = 11.436$ (values in kPa)
3	<a href="#">Göktepe et al. (2011)</a>	$\Psi(I_1, I_{4s}, I_{4f}, I_{8fs}) = \frac{a}{2b} \exp[b(I_1 - 3)] + \sum_{i=f,s} \frac{a_i}{2b_i} \exp\{[b_i(I_4 i - 1)^2] - 1\} + \frac{a_{fs}}{b_{fs}} \{\exp[b_{fs} I_{8fs}^2] - 1\}$	$a = 0.496, b = 7.209, a_f = 15.193, b_f = 20.417, a_s = 3.283, b_s = 11.176, a_{fs} = 0.662, b_{fs} = 9.466$ (values in kPa)
4	<a href="#">Wenk et al. (2011)</a>	$W_{passive} = \frac{c}{2} [b_f E_{11}^2 + b_t (E_{22}^2 + E_{33}^2 + E_{23}^2 + E_{32}^2) + b_{fs} (E_{12}^2 + E_{21}^2 + E_{13}^2 + E_{31}^2) - 1]$	$c_R = 0.017, c_B = 0.0017, T_{max_R} = 180, T_{max_B} = 115.4, T_{max_I} = 0$ (values in kPa)
5	<a href="#">Kerckhoffs (2012)</a>	$W = \frac{1}{2} c_{pas} (e^Q - 1) + c_{comp} (J - 1)$ $Q = b_f E_{ff}^2 + b_c (E_{cc}^2 + E_{rr}^2 + E_{cr}^2) + b_f (2E_{fc}^2 + 2E_{fr}^2)$	$c_{pas} = 1.1, b_f = 9.2, b_c = 2.0, b_{fr} = 3.7, c_{comp} = 350$ (values in kPa), $\rho = 1.053$ g/ml
6	<a href="#">Zhuan et al. (2019)</a>	$\Psi = \Psi_m + \Psi_{cf}$ $\Psi_m = \frac{a}{2b} \{\exp[b(I_1 - 3)] - 1\}$ $\Psi_{cf} = \frac{a_{cf}}{2b_{cf}} \{\exp[b_{cf} (I_4(\theta) - 1)^2] - 1\}$	$a = 2.28, b = 1.8, a_{cf} = 132.0, b_{cf} = 3.45$

**Table 6.1:** List of constitutive models developed for the myocardium.  $W$  and  $\Psi$  represent notations used to define the Strain Energy Density Function in each constitutive model. The values used for the parameters in these models are listed on the far right column, to identify parameter values for our model.

### 6.3.6.5 Model Parameter Values

A wide range of implementations for the left ventricular myocardium exists in literature, and have values assigned to the material parameters of the respective constitutive model. On perusing the Table [6.1], and the model resembling the HGO model in ANSYS ® similar to the transversely orthotropic model by (Zhuan et al. (2019)) and ascribed the following values.

Material Parameter	Value	Units
$c$	0.0228	MPa
$k_1$	0.00132	MPa
$k_2$	3.45	-
$k_3$	0.00132	MPa
$k_4$	3.45	-
$\alpha$	1.5	-
$\beta$	2.5	-
$\gamma$	0.1	-
Time (t)	56	Days

**Table 6.2:** Material parameter values identified for the left ventricular myocardium using the HGO hyperelastic material model from table [6.1].

The models listed in Table[6.1] are detailed in Chapter [2], Section [2.3]. In pertinence to the HGO model (Holzapfel et al. (2000)), employed in the soft tissue growth and remodelling Framework introduced in Chapter[4] models closely related are (Kerckhoffs (2012), Zhuan et al. (2019)) due to their volume fractions considerations and anisotropic formulations. Material parameters are chosen, based on (Zhuan et al. (2019)), due to nearly identical functional forms in the strain energy functions to describe infarcted myocardial tissue, detailed in Table[6.2]. The rate parameters  $\alpha, \beta, \gamma$  are arbitrarily chosen so as to attain appreciable deformation of the infarcted zone prescribed (Section [6.3.6.3]) to drive growth and remodelling hypotheses. The number of days set to 56, 8 weeks, was roughly based on the number of days empirical, experimental studies which range from 8 days to 8 weeks (Fishbein et al. (1978), Fletcher et al. (1981), Gupta et al. (1994), Lerman et al. (1983), Rohde et al. (1999)).

### 6.3.6.6 Result Cases

We consider two special cases to simulate our results:

1. **Case 1:** We assume the homoeostatic collagen fibre stress ( $\tilde{\sigma}_{CH,x}$ ) to have a constant value.
2. **Case 2:** We assume, the homoeostatic collagen fibre stress ( $\tilde{\sigma}_{CH,x}$ ) evolves at each time step  $t$ . This evolution is carried out using the formula:

$$\sigma_{CH,x}(\mathbf{X}, I_x, t) = \xi \left[ \frac{\sigma_{C,x}(\mathbf{X}, I_x, t-1) + \sigma_{CH,x}(\mathbf{X}, I_x, t=0)}{2} \right] \quad (6.14)$$

where  $x$  denotes the particular family of collagen fibres based on the invariant direction  $I_4, I_6$  and  $\xi = 1$  is a rate of change parameter. Also, the Cauchy stress of the collagen fibre is multiplied by its mass density  $\sigma_{CH,x}(\mathbf{X}, t) = m^{C,x} \tilde{\sigma}_{CH,x}(\mathbf{X}, t)$ . An important point to note, this evolution is performed until a maximum point is reached, thereafter, it is considered to be the new homoeostatic stress for the particular family of collagen fibres until.

The graphs seen in the subsequent sections, are plotted by averaging the values observed in the infarcted myocardial region of elements in the LV mesh (Section[6.3.6.3]).

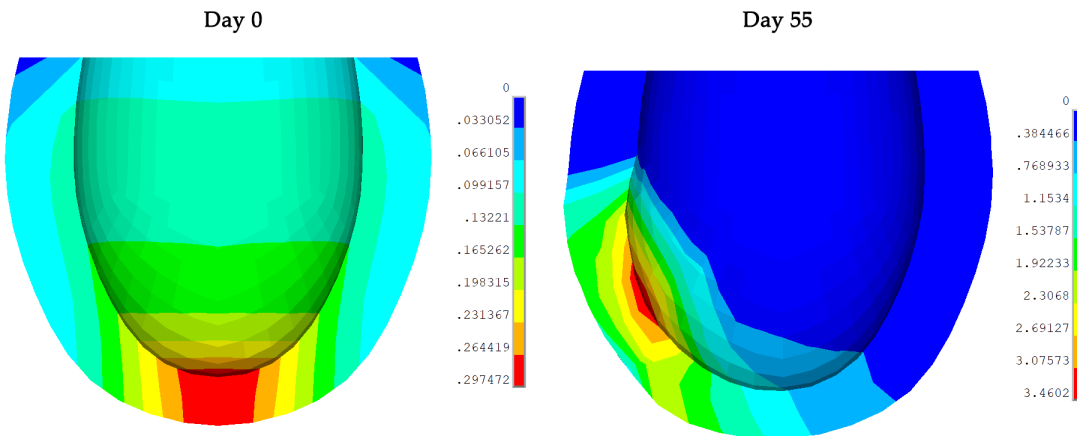
Also, cross-sectional results are displayed at 4 distinct time steps in the simulation, i.e. at  $t = 0$ ,  $t = 13$ ,  $t = 27$  and  $t = 55$  days.

Please note: 3 Dimensional images done in Paraview resulted in a shadow being cast due to a light source on the left, this is the region opposite the infarcted zone and the values are constant as the central region of the image. This is a fault while capturing the images and need to be rectified.

## 6.4 Results

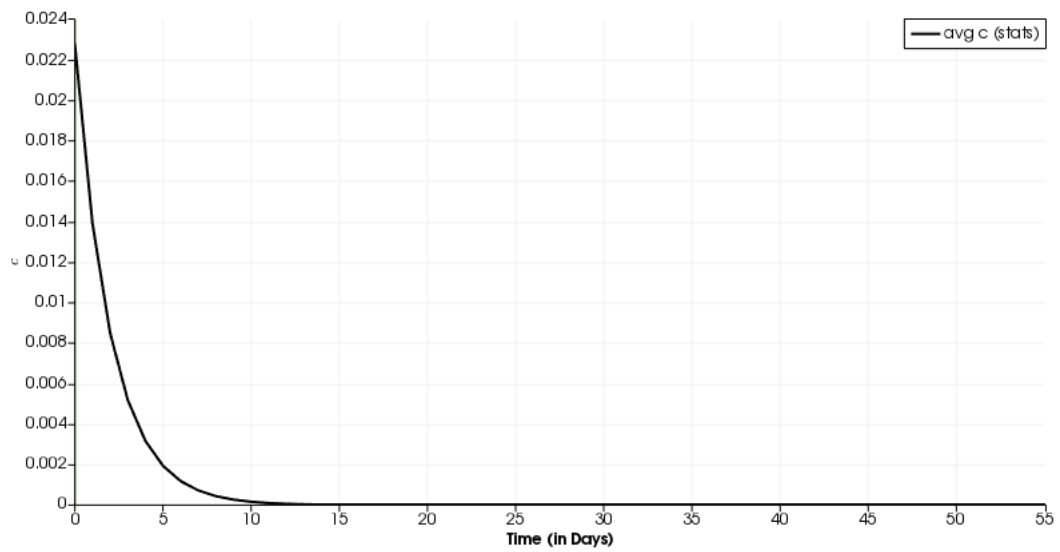
### 6.4.1 Case 1: Growth & Remodelling with out evolution of homoeostatic collagen fibre Cauchy stress

Figure [6.9], displays the nodal displacement sum, over the x,y and z directions. Snapshots of day 0 and day 55 are shown. The ground matrix degradation is represented by the reduction in



**Figure 6.9:** Nodal displacements for days 0 and 55 post-MI, for case considered with constant homoeostatic Cauchy stress for the collagen fibre families.

the material parameter  $c$  i.e. the isotropic contribution in the strain energy function Equation [6.1]. Figure[6.10], portrays this degradation over a period of 14 days, which drives the myocardial tissue to simulate the onset infarction.



**Figure 6.10:** Degradation of the ground matrix over a period of 14 days, reflecting tissue necrosis due to ischaemia, marking the onset of a myocardial infarction.

### 6.4.1.1 Collagen Fibre Cauchy Stresses

The collagen fibres stresses for the two fibre families oriented in the circumferential ( $I_4$ ) and longitudinal ( $I_6$ ) directions are shown in Figures [6.11, 6.12]. The circumferential collagen fibre Cauchy stress (Figure [6.11]), increases from  $2.6 \times 10^{-3}$  MPa at day 0 to about  $4.36 \times 10^{-3}$  MPa at day 9 and stabilises at a value of  $3.67 \times 10^{-3}$  MPa at day 55. The longitudinal collagen fibres Cauchy Stresses (Figure [6.12]), see an increase from  $0.576 \times 10^{-4}$  MPa to about  $1.5 \times 10^{-3}$  MPa at day 6, a subsequent decrease at day 13 to  $1.48 \times 10^{-3}$  MPa followed by an increase to  $\approx 4.6 \times 10^{-3}$  MPa at day 32. This is followed by a steady reduction to  $\approx 4.53 \times 10^{-3}$  MPa at day 55.

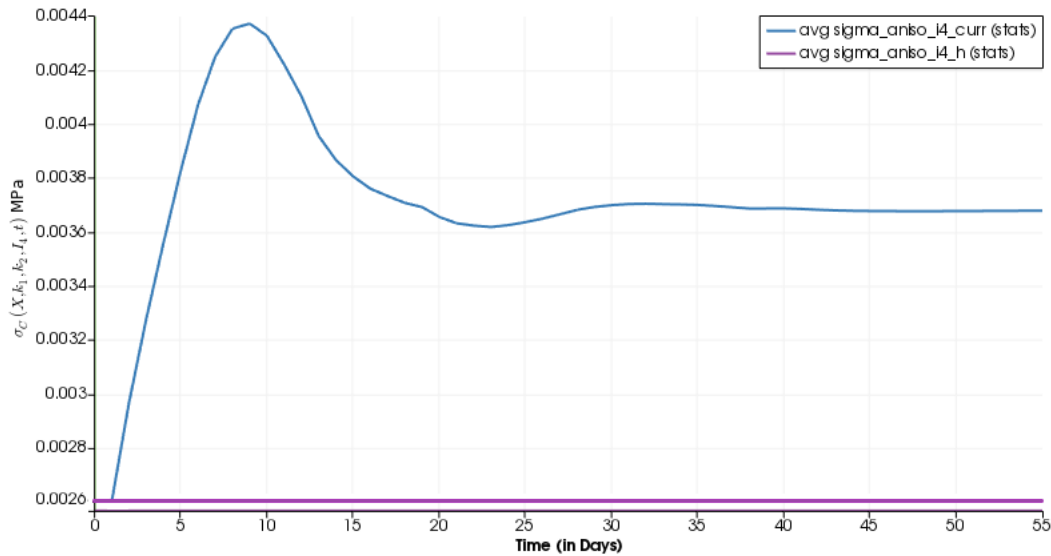


**Figure 6.11:** The averaged circumferential ( $I_4$ ) collagen fibre Cauchy Stress is shown. An initial increase from  $2.6 \times 10^{-3}$  MPa at  $t=0$  day, to a maximum of  $4.36 \times 10^{-3}$  MPa at  $t=10$  days and stabilising at a value of  $3.67 \times 10^{-3}$  MPa from  $t=45$  days to the end of the simulation.

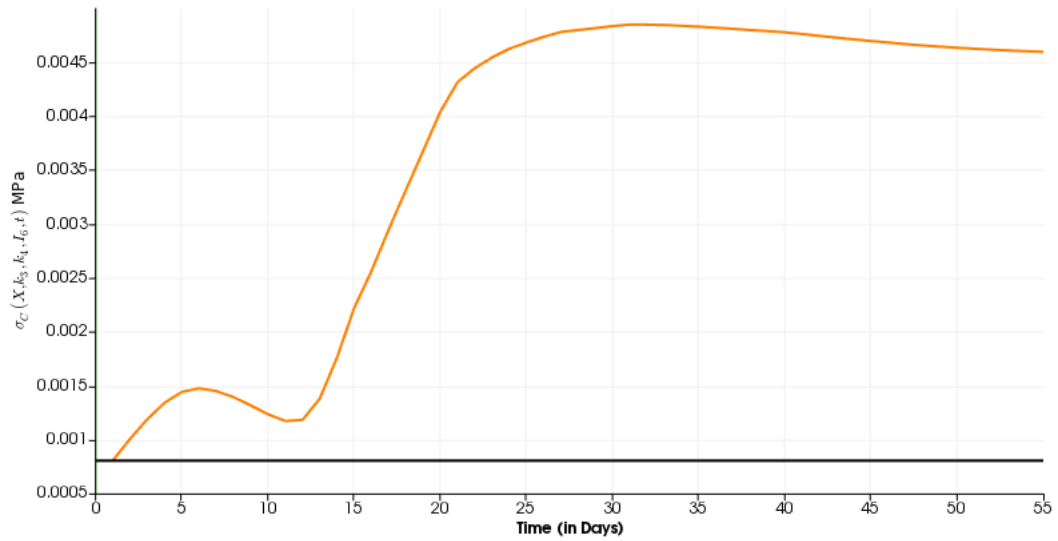


**Figure 6.12:** The averaged longitudinal collagen fibre Cauchy stress is shown. An initial increase from  $0.576 \times 10^{-4}$  MPa at  $t=0$  day is observed upto  $1.5 \times 10^{-3}$  MPa at  $t=6$  days, diving in value at  $t=13$  days to  $1.48 \times 10^{-3}$  MPa and oscillating upwards again at  $t=32$  days to  $4.6 \times 10^{-3}$  MPa reaching a terminal value of  $4.53 \times 10^{-3}$  MPa at  $t=55$  days indicating further decline after day 55.

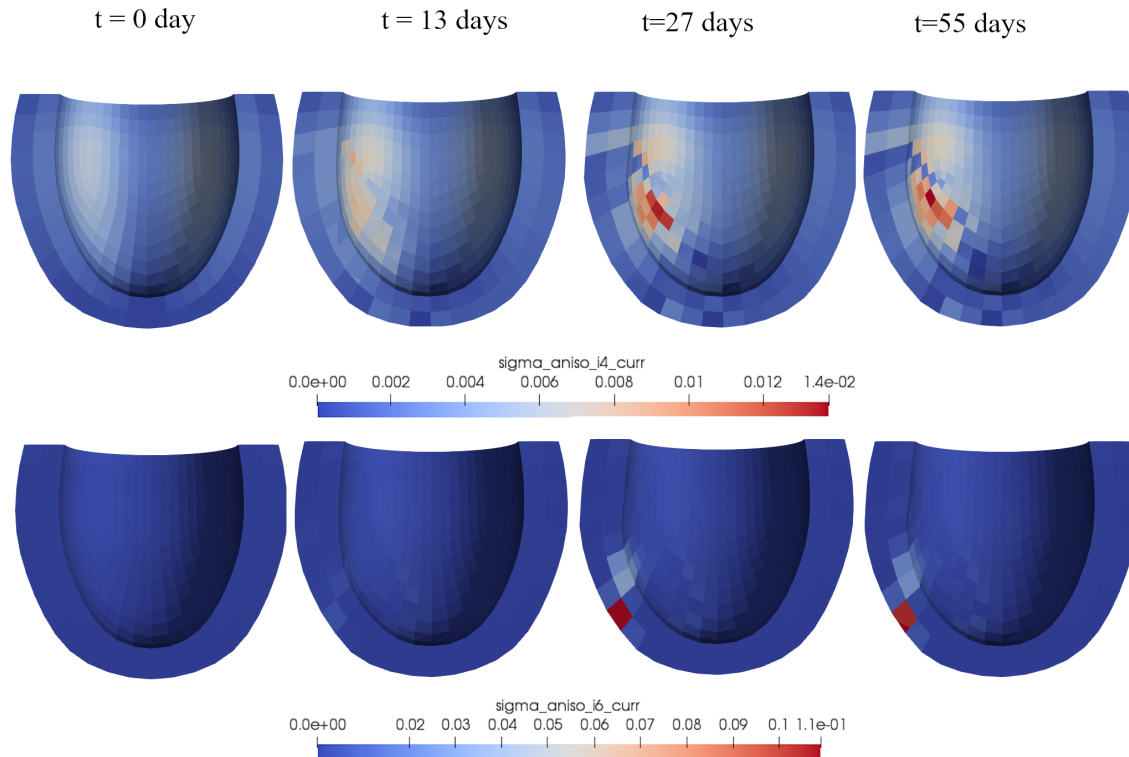


**Figure 6.13:** The Cauchy stresses experienced by the collagen fibre families are depicted. **(Top)**, Circumferential fibre Cauchy stresses are shown, at  $t=0$  day it ranges from  $\approx 0.0015$  MPa to  $\approx 0.05$  MPa, varying to  $\approx 0.03$  MPa to  $0.07$  MPa in the infarcted to at  $t=13$  days, and subsequently to  $\approx 0.01$  MPa to  $\approx 0.13$  MPa at  $t=27$  days. Terminally at  $t=55$  days, the remodelled infarcted zone observes a Cauchy stress distribution in the range of  $\approx 0.005$  MPa to  $0.05$  MPa with a few elements in the higher range of  $\approx 0.07$  to  $\approx 0.11$  MPa. **(Bottom)** The longitudinal collagen fibres Cauchy stress is shown, observing an initial distribution at  $\approx 0.0005$  MPa to  $\approx 0.001$  MPa at  $t=0$  days. The stress range varies slightly between  $\approx 0.01$  MPa to  $0.02$  MPa at  $t=13$  days. An increase upto a range of  $\approx 0.05$  MPa to  $1.1$  MPa is seen around  $t=27$  and  $t=55$  days, as seen a few elements at the bottom of the infarct experience higher stresses than other regions.

### 6.4.1.2 Material Parameter Remodelling

Figure [6.14], represents the material parameter remodelling driven by the stress deviations of the collagen fibre families in their respective directional orientations. The material parameter ( $k_2$ ), associated with the circumferentially aligned collagen fibres ( $I_4$ ), declines steadily from an initial value of 3.45 at day 0, to  $\approx 2.96$  at day 20, observing a steady rise to 0.42 at day 37 before stabilising at that value at the end of the simulation (day 55). For ( $k_4$ ), associated with the longitudinally aligned collagen fibres ( $I_6$ ), An initial decrease is observed from 3.45 at  $t=0$  days, to  $\approx 1.5$  at day 7, observing an increase to  $\approx 1.61$  at  $t=13$  days to a decrease at  $t=16$  to a value of  $\approx 1.24$ . Consequently a rise is observed at various intervals, terminally at  $t=55$  days reaches a value of 1.89 with an upward slope indicating increases in value post  $t=55$  days.

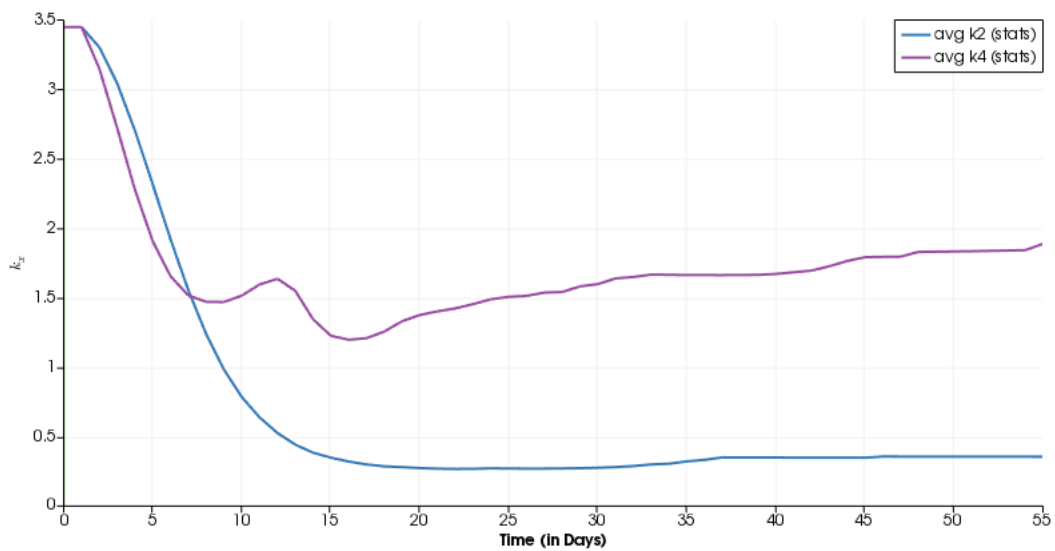


**Figure 6.14:** The remodelling of averaged material parameters  $k_2, k_4$  occurs to maintain a preferred homeostatic collagen fibre Cauchy stress (here, at  $t=0$ ). (**Blue line**) Averaged values of  $k_2$ , associated with the collagen family of fibres oriented in the  $I_4$  direction, over the infarct region show a steady decline from 3.45 at  $t=0$  to about 0.42 at  $t=55$  days, seeing a slight rise from 0.36 to 0.42 at  $t=37$  days. (**Purple line**) Averaged values of  $k_4$ , associated with the collagen family of fibres oriented in the  $I_6$  direction, over the infarct region show a steady decline from 3.45 at  $t=0$  to about 1.89 at day 55, observing a slow increase beyond day 55.

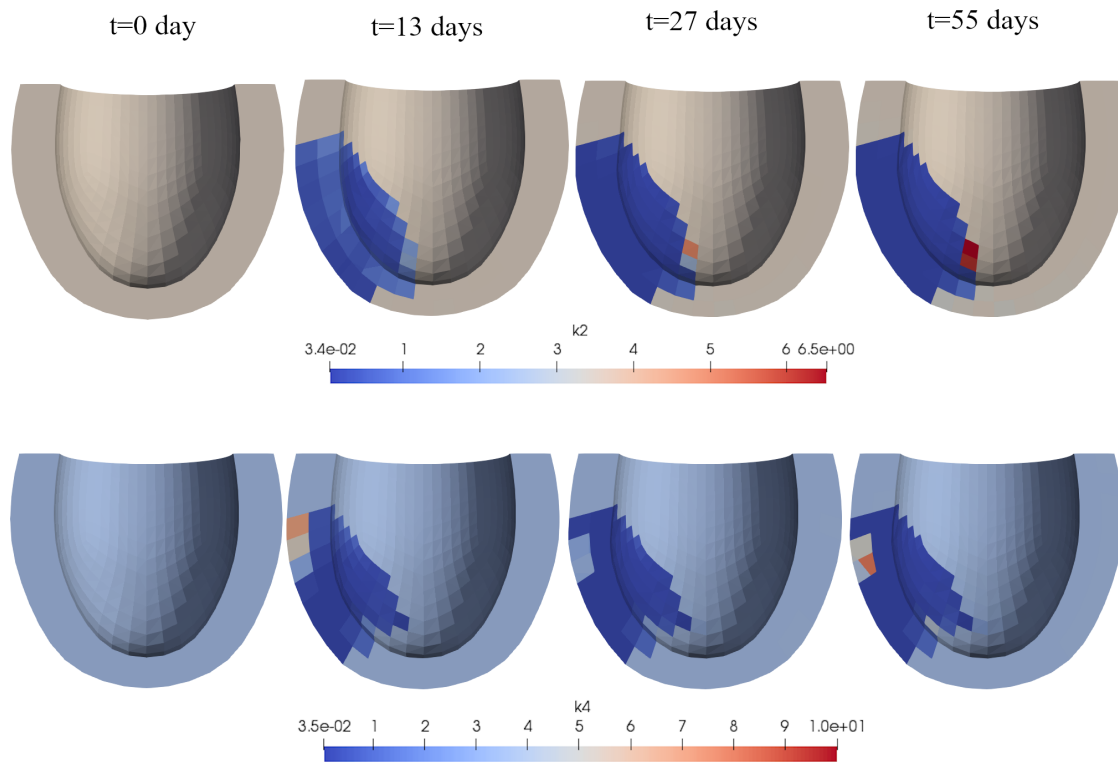


**Figure 6.15:** Material Parameter changes due to remodelling are shown in this figure. **(Top)** Circumferential collagen fibre material parameter  $k_2$  is shown, with an initial distribution of 3.45 as prescribed at  $t=0$ . Post 13 days, the value ranges from  $\approx 0.035$  in the outer boundary to  $\approx 3$  going inwards. The range is more or less similar at  $t=27$  days and  $t=55$  days, with majority elements in the range of 0.035 i.e. the lower limit for  $k_2 > 0$  with a few elements in the range of  $\approx 3$  to 5 and 10 at  $t=27$  and  $t=55$  days respectively. The increase can be associated to compression which leads to a reduction in the Cauchy stress experienced, thereby reversing the effect of remodelling formulation seen in Equation [6.6]. **Bottom** The longitudinal collagen fibre material parameter  $k_4$  are shown, with an initial prescribed value of 3.45 at  $t=0$  days. The ranges vary from 0.035 to  $\approx 7$  at  $t=13$  days, consequently the maximum reducing to  $\approx 3.7$  at  $t=27$  days and rising again to a maximum value of  $\approx 6.8$  at  $t=55$  days, which again can be attributed to the reversal of behaviour in the remodelling formulation, Equation [6.7] due to reduced Cauchy stress experienced by the volume element at  $t=55$  days.

### 6.4.1.3 Collagen Fibres Stretch Invariants

Figure [6.16], depicts the variations in the averaged collagen fibre stretch invariants. For circumferential fibres ( $I_4$ ), the value rises from an initial value of  $\approx 1.012$  at  $t=0$  day to a maximum of  $\approx 1.228$  at  $t=16$  days, before steadily declining to stabilise at a value of  $\approx 1.184$  by day 45 till the end of the simulation at  $t=55$  days. For longitudinal collagen fibres ( $I_6$ ), the invariant value rises from  $1.005$  at  $t=0$  day to  $\approx 1.136$  at  $t=15$  days before declining in a similar fashion to  $I_4$ , reaching a steady value and stabilising around  $1.12$  from  $t=45$  days to  $t=55$  days.

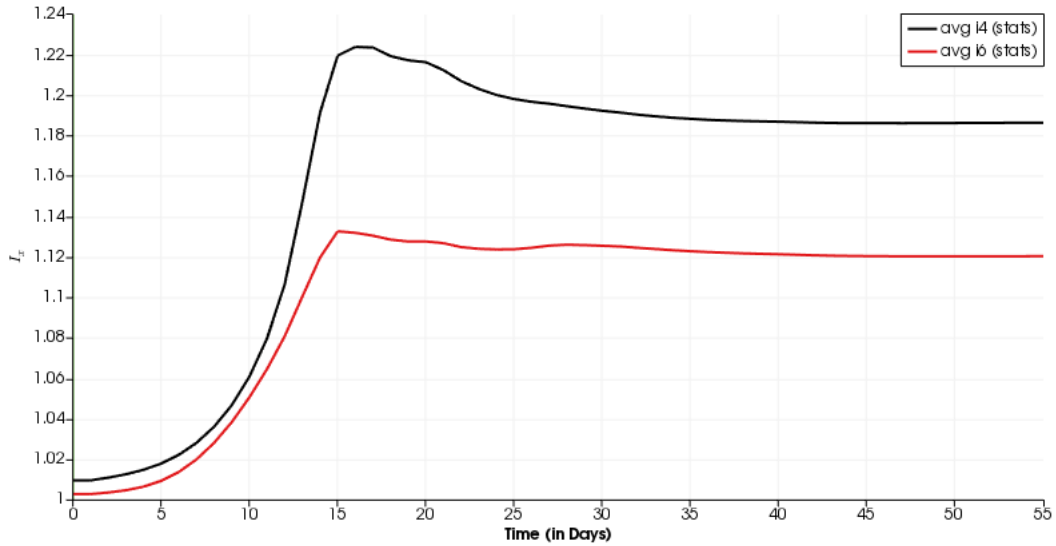


**Figure 6.16:** The averaged circumferential ( $I_4$ ) and longitudinal ( $I_6$ ) collagen fibre stretch invariants are displayed over a the simulation period of 56 days. **(Black line)** The value for  $I_4$  rises from  $\approx 1.012$  at  $t=0$  day to a maximum of  $1.228$  at  $t=16$  days, before stabilising at  $1.184$  at  $t=55$  days. **(Red line)** The  $I_6$  value rises from  $\approx 1.005$  at  $t=0$  day, to  $\approx$  value of  $1.136$  at  $t=15$  days before stabilising at a value of  $1.12$  by  $t=55$  days.

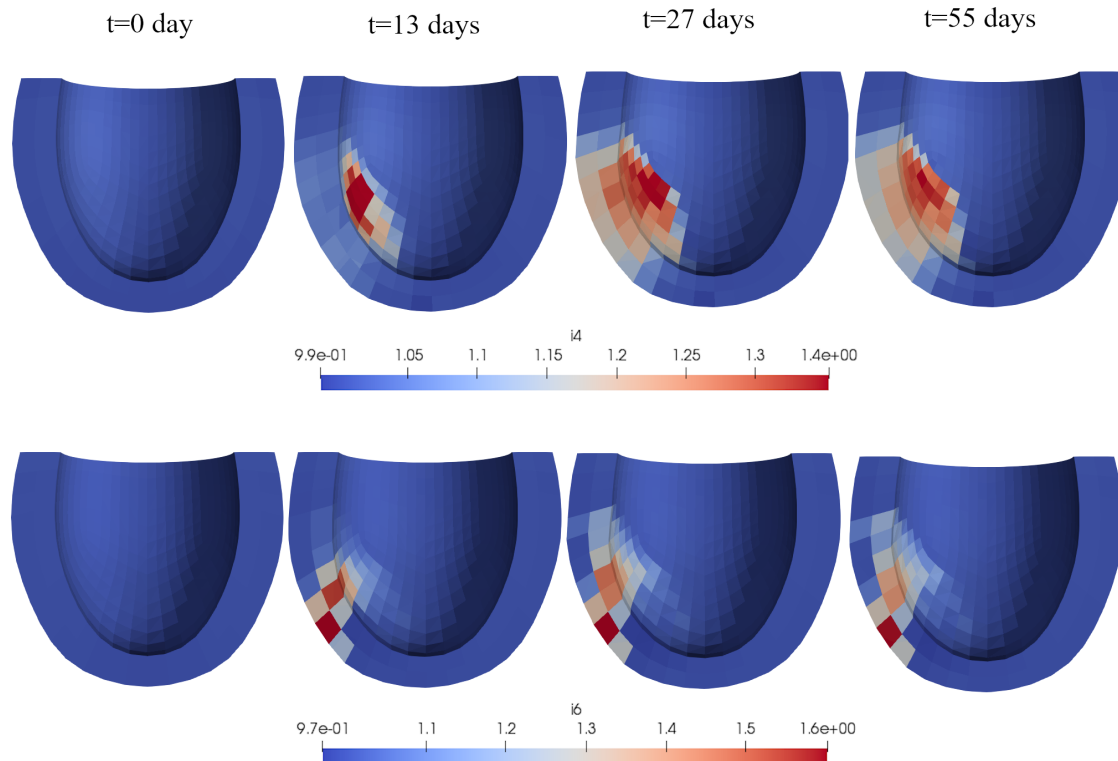


**Figure 6.17:** The stretch invariants experienced by the collagen family of fibres is shown in this figure. **(Top)** The circumferential collagen fibre stretch invariants  $I_4$  are displayed. At  $t=0$  the  $I_4$  values range from  $\approx 1$  to  $\approx 1.105$ , increasing to  $1.1$  to  $\approx 1.4$  in the infarcted region at  $t=13$  days. The values at  $t=27$  days attain a range of  $\approx 1.16$  to  $\approx 1.38$  in the infarcted region and terminally at  $t=55$  days, it varies from  $\approx 1.16$  to  $\approx 1.3$ . **(Bottom)** The longitudinal collagen fibre stretch invariants  $I_6$  are displayed. At  $t=0$  day the  $I_6$  values range from  $0.97$  to  $\approx 1.05$ , post-MI at  $t=13$  days the  $I_6$  values in the infarct range from  $\approx 1.12$  to  $\approx 1.6$  (seen in only one volume element at the bottom). At  $t=27$  days and  $t=55$  days the range remains similar however, there is a slight increase in the  $I_6$  values through the infarcted region from  $\approx 1.12$  at  $t=13$  days to  $\approx 1.26$  at  $t=55$  days.

#### 6.4.1.4 Fibroblast Stretches

The averaged fibroblast stretches experienced by the collagen fibres is shown in Figure[6.18]. The fibroblasts affected by circumferential collagen fibre stretch ( $\lambda F, I_4$ ), observe a gradual increase from a value of 1.05 at  $t=0$  day to a maximum of 1.124 at  $t=15$  days, before steadily decreasing to the original value of 1.05 at  $t=55$  days, stabilising around  $t=51$  days. Likewise, the fibroblasts associated with the longitudinal collagen fibre stretch ( $\lambda F, I_6$ ), rise in value a little slower compared to ( $\lambda F, I_4$ ), going from 1.05 at  $t=0$  day to a maximum of 1.09 at  $t=15$  days, before declining steadily to 1.05 at  $t=55$  days.

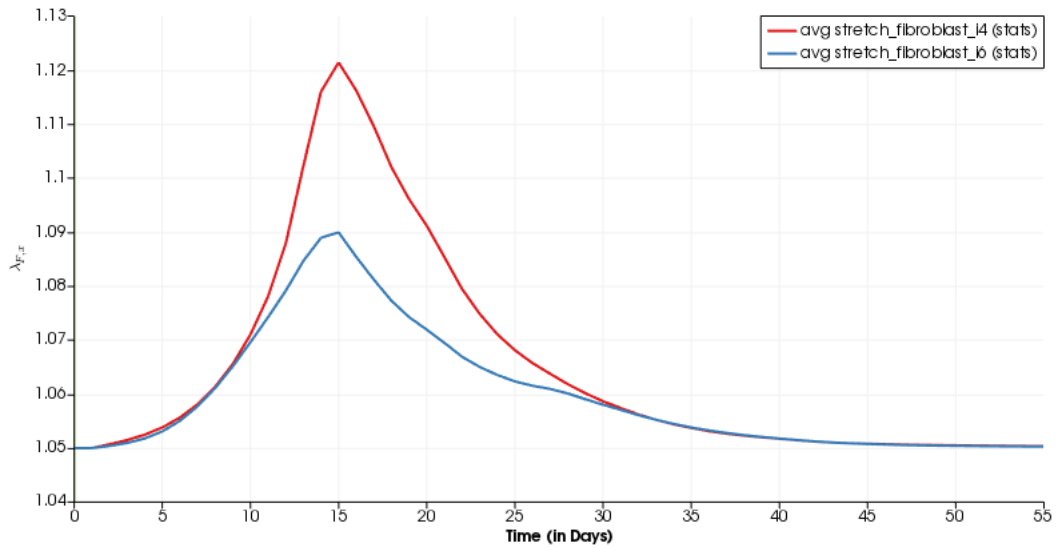


**Figure 6.18:** The averaged fibroblast stretch experienced due to the stretch invariant variations of the circumferential ( $I_4$ ) and longitudinal ( $I_6$ ) collagen fibres are shown. For circumferential fibres ( $I_4$ ), fibroblast stretch ( $\lambda_{F,I_4}$ ) increases from a value of 1.05 at  $t=0$  day to a maximum of 1.124 at  $t=15$  days, before coming back to a value of 1.05 steadily at  $t=55$  days. A similar behaviour is observed for  $\lambda_{F,I_6}$ , where in an increase from 1.05 at  $t=0$  day to a maximum of 1.09 at  $t=15$  days is reached before coming back to a value of 1.05.

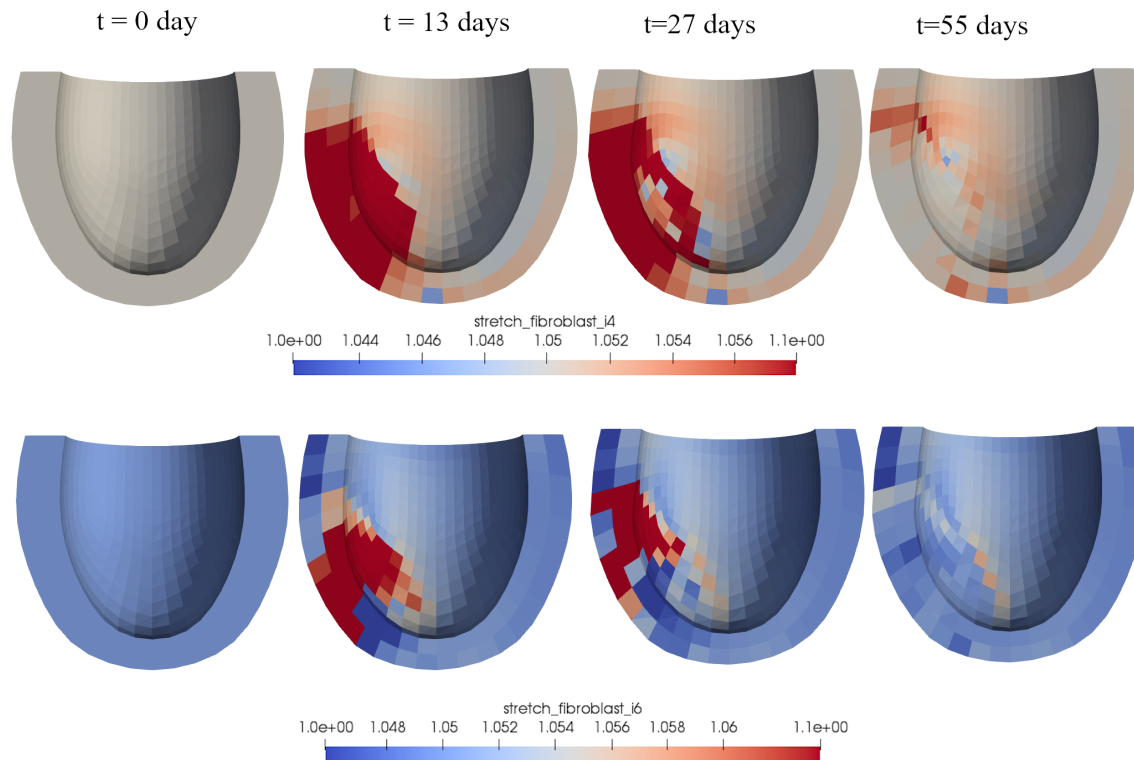


**Figure 6.19:** The fibroblast stretches experienced with respect to the two collagen family of fibres are shown. **(Top)** The fibroblasts associated with the maintenance of circumferential collagen fibres are displayed. At  $t=0$  the prescribed value of 1.05 is seen throughout the myocardium, increasing to a range of  $\approx 1.0581$  to 1.1 in the infarcted zone. At  $t=27$  days the range is similar to  $t=13$  days however, in the inner regions of the infarct the stretches reduce to a range of  $\approx 1.052$  to  $\approx 1.058$ . Terminally at  $t=55$  days the fibroblast stretches reduce to a range of  $\approx 1.051$  to  $\approx 1.052$ . **(Bottom)** The fibroblasts stretches with respect to the longitudinal collagen fibre family are shown. An initial prescribed value of 1.05 is seen at  $t=0$  day. At  $t=13$  days the fibroblast stretches are in the higher range of 1.1 near the bottom centre of the infarcted region and the centre, also a reduction upto  $\approx 1.0$  is seen. At  $t=27$  days, the range varies from  $\approx 1.04$  to  $\approx 1.1$ , with higher stretches seen at the upper region. Terminally, the fibroblast stretches reach reduced range of  $\approx 1.048$  to  $\approx 1.053$ .

### 6.4.1.5 Collagen Fibre Matrix Mass Density Changes

Figure [6.20], depicts the variations in averaged mass densities ( $m^{C,I_4}$ ,  $m^{C,I_6}$ ) of the collagen fibres oriented in the ( $I_4$ ,  $I_6$ ) directions. For circumferential collagen fibres, the mass density ( $m^{C,I_4}$ ) rises from a value of 1 and  $t=0$  day to about  $\approx 4.5$  at  $t=55$  days while continuing to rise at a slower rate at the end. A gradual increase from 1 to  $\approx 4.5$  in  $m^{C,I_4}$  value is observed between days 5 and  $t=40$  days. For longitudinal collagen fibres ( $I_6$ ), the mass density changes ( $m^{C,I_6}$ ) are comparatively lower than  $m^{C,I_4}$ , values. Increasing from 1 at  $t=0$  day gradually to 1.2 at  $t=10$  days and  $\approx 4$  at  $t=55$  days. These changes are driven by fibroblast stretches in their respective directions (seen in Figure 6.18)

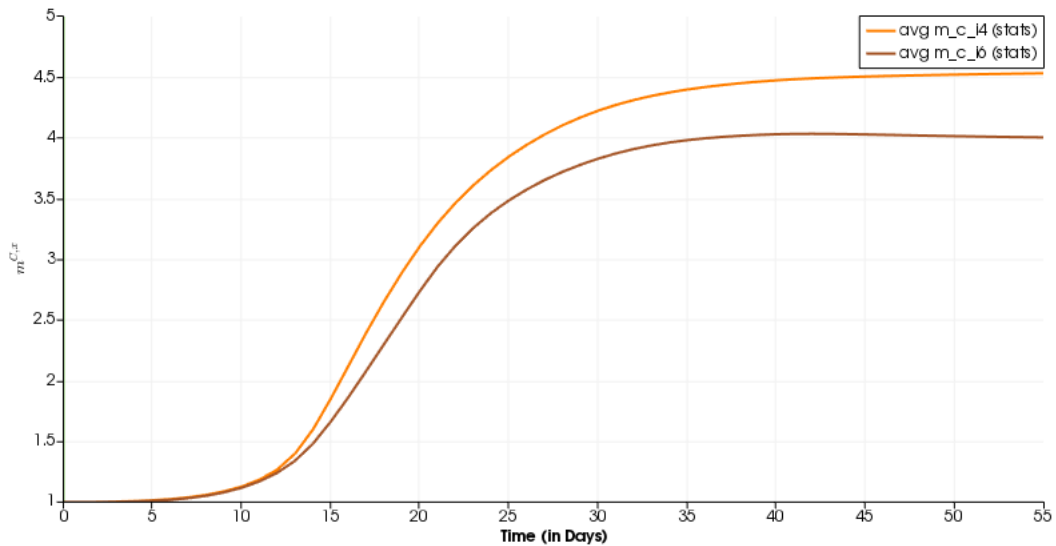


**Figure 6.20:** The averaged mass densities of circumferential and longitudinal collagen fibres are shown. (Orange Line) The circumferential fibre mass densities ( $m^{C,I_4}$ ) increase from a value of 1 at  $t=0$  day steadily to a value of  $\approx 4.5$  at  $t=55$ , seeing a continued rise thereafter. For longitudinal fibre mass density ( $m^{C,I_6}$ ), a lower rise is observed in comparison, from 1 at  $t=0$  day to a maximum of 4.03 at  $t=37$  days to a final value of  $\approx 4$  at  $t=55$  days.

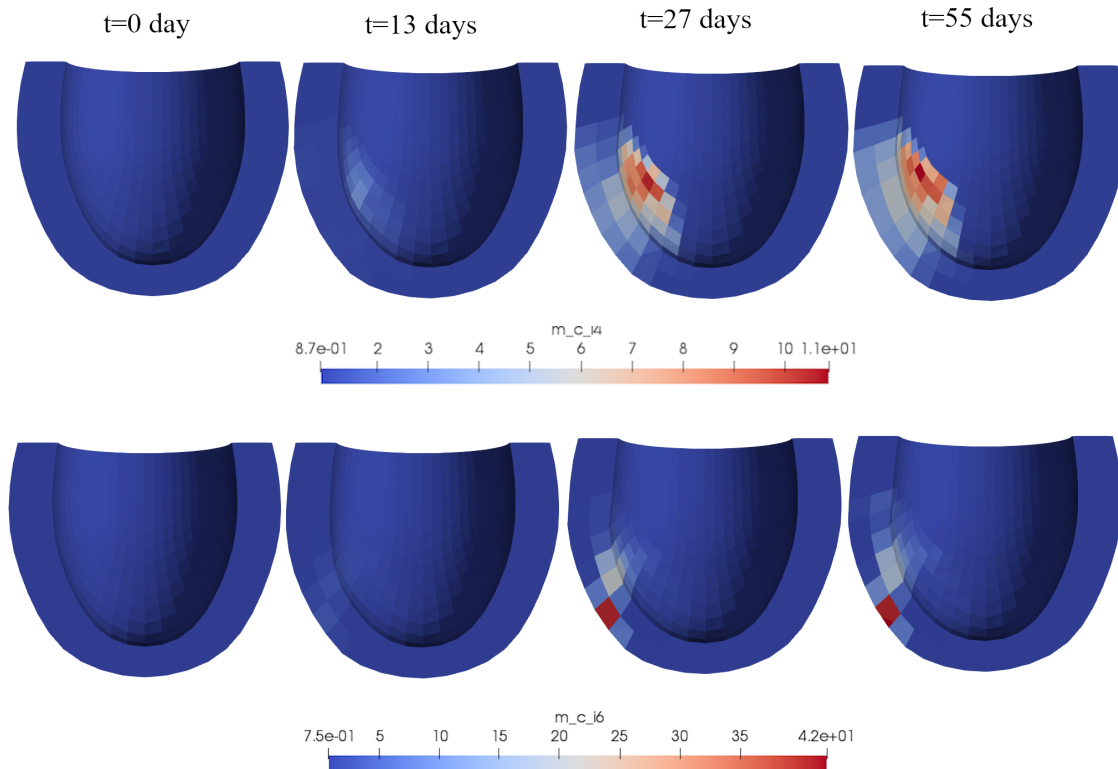


**Figure 6.21:** The mass density variations for the collagen fibre families are shown in this Figure. **(Top)** The mass densities for the circumferential collagen fibres ( $m_c^{I4}$ ) is shown. An initial value of 1 at  $t=0$  days is seen, with an increase to  $\approx 1.0$  to  $\approx 5.1$  in the infarcted region at  $t=13$  days. A further increase is seen to a range of  $\approx 3.5$  to  $\approx 9.6$  is seen with a few elements nearing 11. Terminally at  $t=55$  days a range of  $\approx 3$  to a maximum of 10.5 is seen with only a few elements in the higher range of values. **(Bottom)** The mass densities associated with longitudinal collagen fibres are shown. Initially, at  $t=0$  day the  $m_c^{I6}$  values are at unity. Subsequently, a minimum rise is observed upto a range of 1.0 to 3.5 at  $t=13$  days, and a rise to a maximum of  $\approx 20$  is seen at  $t=27$  days and  $t=55$  days, with one element exhibiting a high value of 42.

### 6.4.2 Case 2: Growth & Remodelling with evolution of homoeostatic collagen fibre Cauchy stress

Figure [6.22], displays the nodal displacement sum, over the x,y and z directions. Snapshots of day 0 and day 55 are shown.

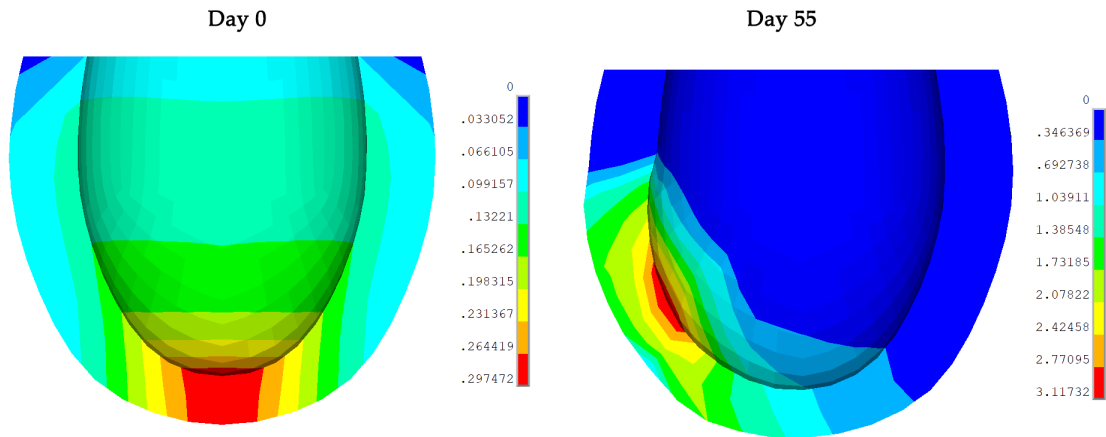


**Figure 6.22:** Nodal displacements for days 0 and 55 post-MI, for case considered with evolving homoeostatic Cauchy stress for the collagen fibre families.

### 6.4.2.1 Collagen Fibre Cauchy Stresses

The circumferential ( $I_4$ ) collagen fibre Cauchy stresses are displayed in Figure [6.23]. The collagen fibre homoeostatic Cauchy stress (calibrated at time  $t=0$  in our simulation) evolves to a maximum  $\approx 3.72 \times 10^{-3}$  MPa at time  $t=14$  days (6.14) from  $\approx 2.558 \times 10^{-3}$  MPa at time  $t=0$  day. The collagen fibre Cauchy stress increases from  $\approx 2.558 \times 10^{-3}$  MPa at  $t=0$  days to a maximum of  $\approx 4.82 \times 10^{-3}$  MPa at  $t=12$  days, owing to muscle mass density ( $m^M$ ) necrosis, it reaches homoeostatic Cauchy stress levels at  $t=24$  days but interestingly decreases below that level and continues to a minimum of  $\approx 3.32 \times 10^{-3}$  MPa at  $t=45$  days before increasing to  $\approx 3.39 \times 10^{-3}$  MPa at  $t=55$  days with an increasing slope.

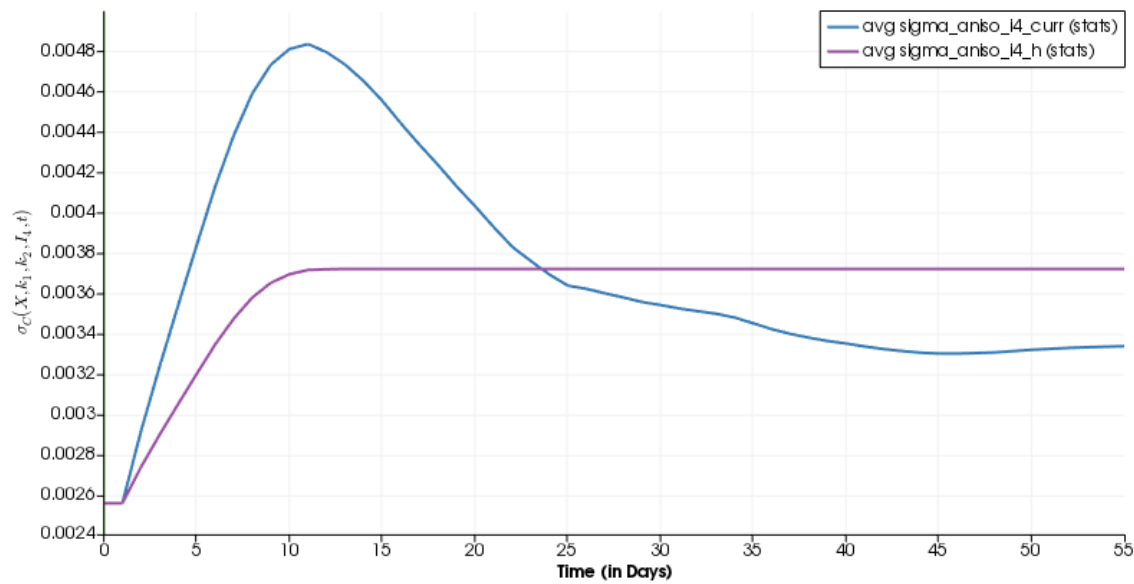


**Figure 6.23:** The circumferential collagen fibre Cauchy stress is displayed. **(Purple Line)** Homoeostatic stresses evolve as per Equation [6.14] and reach a maximum of  $\approx 3.72 \times 10^{-3}$  MPa at  $t=14$  days from an initial value of  $\approx 2.558 \times 10^{-3}$  MPa at  $t=0$  day. **(Blue Line)** The Cauchy stress experienced by the  $I_4$  collagen fibre family increases from  $\approx 2.558 \times 10^{-3}$  MPa to a maximum of  $\approx 4.82 \times 10^{-3}$  MPa at  $t=12$  days, subsequently decreasing below the homoeostatic stress levels post  $t=24$  days reaching a final value of  $\approx 3.39 \times 10^{-3}$  MPa at the end of the simulation.

Figure [6.24], shows the changes in the collagen fibre Cauchy stress in the longitudinal direction ( $I_6$ ). **(Black Line)** The homoeostatic value evolves from a value of  $\approx 0.8 \times 10^{-3}$  MPa at  $t=0$  day to a maximum of  $\approx 1.65 \times 10^{-3}$  MPa at time  $t=9$  days. **(Orange Line)** The longitudinal collagen fibre Cauchy stress increases from  $\approx 0.8 \times 10^{-3}$  MPa to a maximum of  $\approx 2.35 \times 10^{-3}$  MPa at time  $t=9$  days. A decrease below homoeostatic Cauchy stress (black line), to a minimum value of  $\approx 1.46 \times 10^{-3}$  MPa is seen at  $t=19$  days. Another peak is noticed following the previous low at  $t=38$  days with a value of  $\approx 3.25 \times 10^{-3}$  MPa before decreasing to a final value of  $\approx 2.7 \times 10^{-3}$  MPa at  $t=55$  days. The stress is observed to further decline post the simulation.

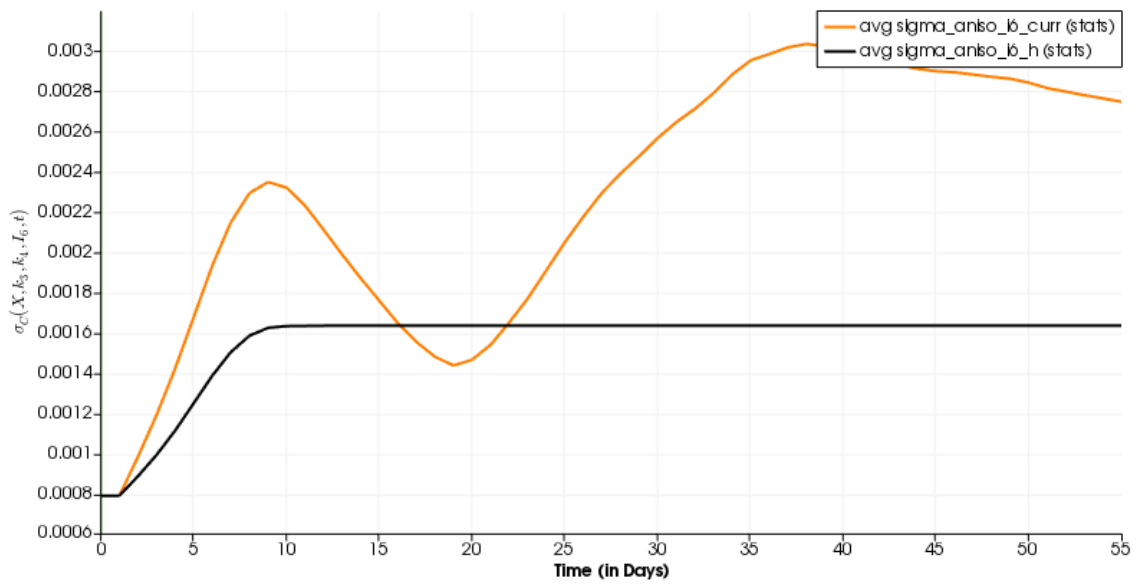


**Figure 6.24:** The longitudinal collagen fibre( $I_6$ ) stress is plotted. **(Black Line)** depicts the evolution of the homoeostatic stress ( $\sigma_{CH,I_6}(X, k_3, k_4, I_6, t)$ ) from an initial value of  $\approx 0.8 \times 10^{-3}$  MPa to  $\approx 1.65 \times 10^{-3}$  MPa at  $t=9$  days. **(Orange Line)** The longitudinal collagen fibre stress observes an increase from the homoeostatic value at  $t=0$  day to an increase of  $\approx 2.35 \times 10^{-3}$  MPa at  $t=9$  days, with a trough at  $t=19$  days, with a minimum value of  $\approx 1.46 \times 10^{-3}$  MPa at  $t=19$ . Another peak is observed at  $t=38$  days steadily declining till  $t=55$  days from  $\approx 3.25 \times 10^{-3}$  MPa to  $\approx 2.7 \times 10^{-3}$  respectively, with a downward trend after the simulation ends.

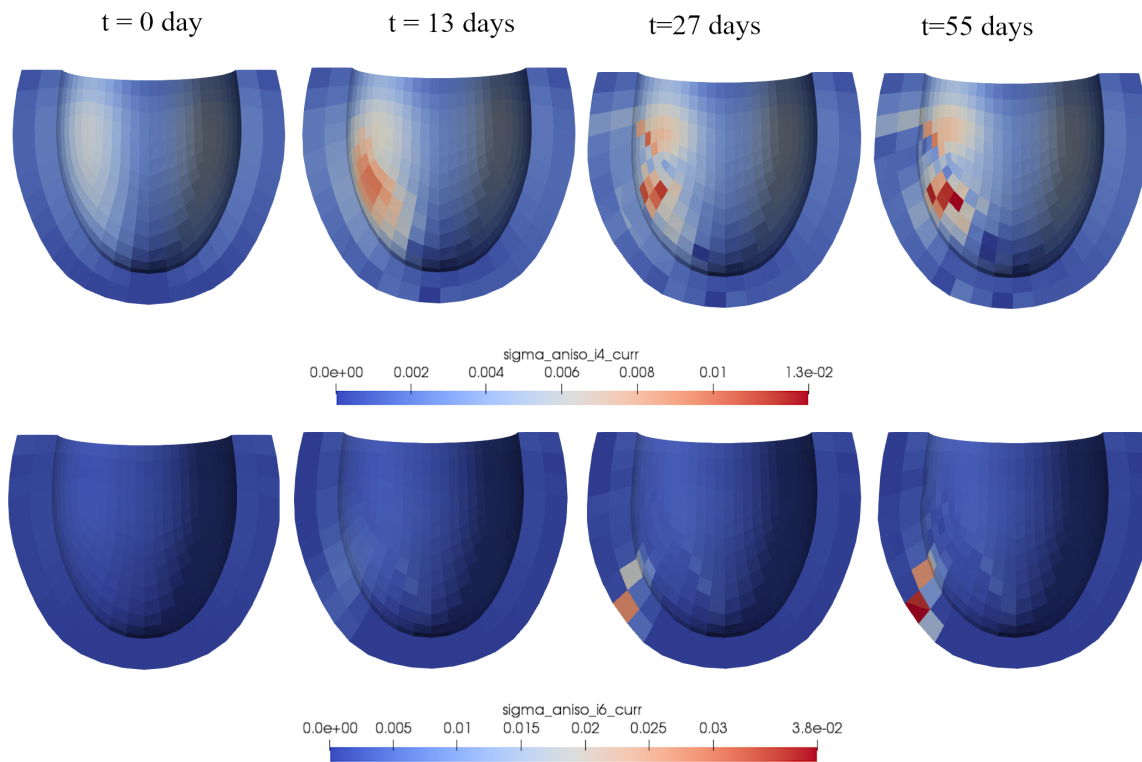


**Figure 6.25:** The Cauchy stresses for collagen family of fibres are displayed. **(Top)** The circumferential collagen fibre Cauchy stresses are displayed, with an initial distribution at time  $t=0$  day ranging from  $\approx 0.002$  MPa to  $\approx 0.02$ . At  $t=13$  days an increase is seen due to myocardial infarction to a range of  $\approx 0.005$  MPa to  $0.025$  MPa, with a further increase of the maximum value to  $\approx 0.035$  MPa, and the minimum reducing to  $\approx 0.005$  MPa at  $t=27$  days. Terminally while majority of the infarcted zone is well below  $\approx 0.01$  MPa, a few elements experience a higher maximum of  $\approx 0.013$  MPa. **(Bottom)** The Cauchy stress distribution for the longitudinal collagen fibres ( $\sigma_{C,I_6}$ ) are displayed. An initial distribution of  $\approx 0.0003$  MPa to  $0.001$  MPa is seen at  $t=0$  day. Increasing to a maximum of  $\approx 0.005$  in the infarcted zone at  $t=13$  days. At  $t=27$  days a few elements experience higher stresses around the range of  $\approx 0.02$  MPa to  $0.032$  MPa with majority of the infarcted region experiencing stresses at about  $\approx 0.007$  MPa. Terminally at  $t=55$  days the stresses range from  $0.003$  MPa to a maximum of  $0.038$  MPa (skewing the average due to a few elements in the higher range).

### 6.4.2.2 Material Parameter Remodelling

Figure [6.26], represents the material parameter remodelling driven by the stress deviations of the collagen fibre families in their respective directional orientations. The material parameter ( $k_2$ ), associated with the circumferentially aligned collagen fibres ( $I_4$ ), declines steadily from an initial value of 3.45 at day 0, to  $\approx 0.5$  at day 30, observing a minor increase to 0.52 at  $t=0$  and stabilising at 0.5 from  $t=46$  days to  $t=55$  days. For ( $k_4$ ), associated with the longitudinally aligned collagen fibres ( $I_6$ ), An initial decrease is observed from 3.45 at  $t=0$  days, to  $\approx 2.25$  at day 8, observing an increase to  $\approx 4.5$  at  $t=18$  days to a decrease at  $t=25$  to a value of  $\approx 2.9$ . Consequently a rise is observed at various intervals, terminally at  $t=55$  days reaches a value of  $\approx 5.49$  with an upward slope indicating increases in value post  $t=55$  days.

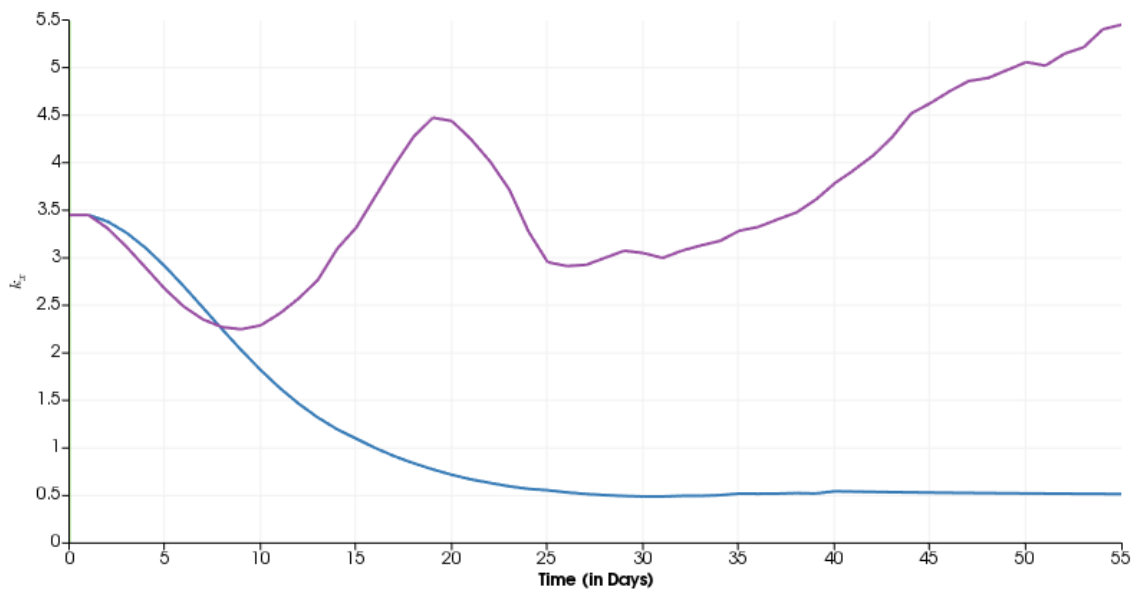


**Figure 6.26:** (Blue Line)  $k_2$  material parameter remodelling, associated with circumferential collagen family of fibres ( $I_4$ ), declines from an initial value of 3.45 at  $t=0$  day, stabilising at 0.5 by the end of the simulation at  $t=55$  days. (Purple Line The longitudinal collagen fibres' material parameter ( $k_4$ ) remodels with an initial decrease from 3.45 to 2.25 from  $t=0$  day to  $t=8$  days, peaking at  $\approx 4.5$  at  $t=18$  days and lastly reaching a maximum of 5.49 at  $t=55$  days.)

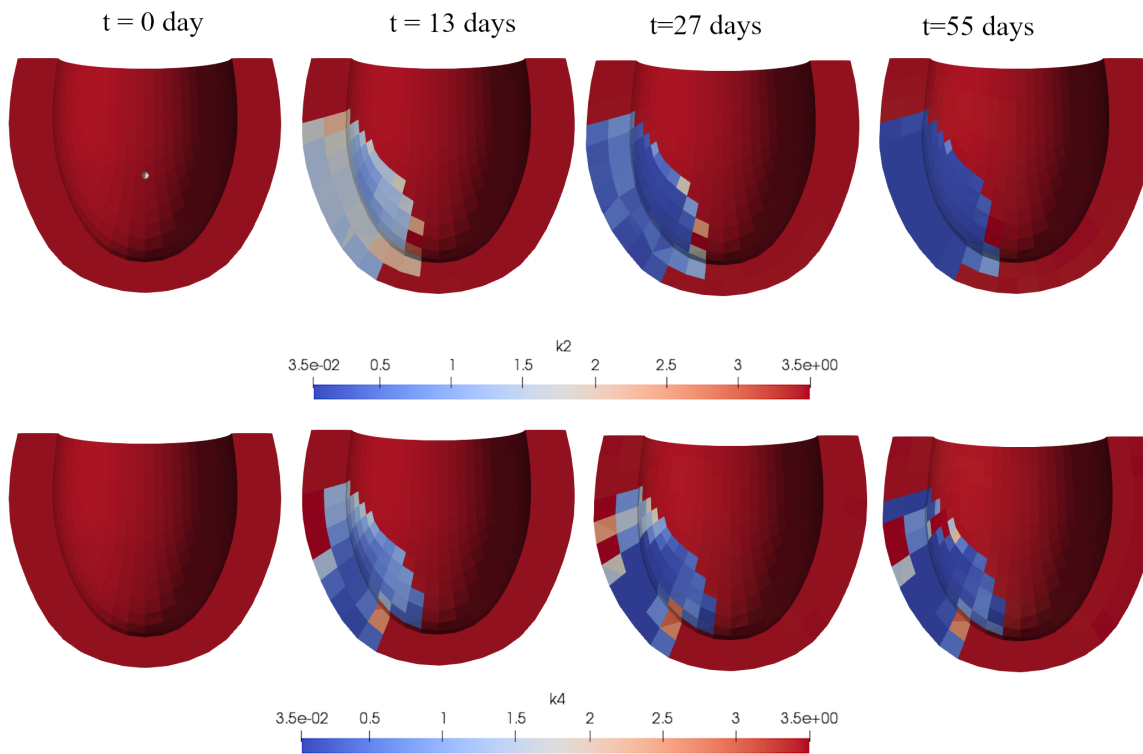


**Figure 6.27:** The material parameter remodelling over the course of the myocardial infarction in the left ventricle is shown in this figure. **(Top)** The circumferential collagen family of fibres' material parameter is displayed. An initial distribution of 3.5 is seen at  $t=0$ . Note: 3.5 has been set to be the maximum to see better distribution of the material values in the later stages. At  $t=13$  days, the  $k_2$  value ranges from  $\approx 1.2$  to  $\approx 2.5$ . Further at  $t=27$  days the values decrease further to a range of 0.035 to  $\approx 1.5$  with a few elements exhibiting higher values around 2. Terminally at  $t=55$  days, most of the infarct region  $k_2$  values have remodelled to a value of 0.035. **(Bottom)** The longitudinal collagen family of fibres material parameter  $k_4$  is shown in here. An initial distribution of values at 3.5 is seen at  $t=0$  day. At  $t=13$  days, the values range from  $\approx 0.04$  to  $\approx 1.7$  with a few elements reaching  $\approx 2.7$ . Further at  $t=27$  days, the  $k_4$  values range from 0.035 to  $\approx 1.6$  with a few elements on the outer boundary and inner region of the infarct at  $\approx 2.5$ . Terminally, at  $t=55$  days, the range of values goes from 0.035 to 3.5 and above, with the maximum seen in a few elements.

### 6.4.2.3 Collagen Fibres Stretch Invariants

Figure [6.28], depicts the variations in the averaged collagen fibre stretch invariants. **(Black Line)**, depicts the averaged circumferentially oriented collagen fibre stretch invariant ( $I_4$ ). It rises from an initial value of  $\approx 1.01$ , owing to the cardiac muscle degradation steeply increasing to a maximum of  $\approx 1.17$  at  $t=27$  days, observing a crest and a another peak at  $t=35$  days with a value of  $\approx 1.178$ . Finally reaching a value of  $\approx 1.175$  at  $t=55$  days. **(Red Line)** shows the variation in the longitudinally oriented collagen fibres stretch invariant ( $I_6$ ), observing a rise from  $1.005$  to an  $\approx$  peak value of  $1.089$  at  $t=26$  days. The trend sees a decline to about  $1.078$  at  $t=45$  days and with an increasing trend culminating with a value of  $\approx 1.081$  at  $t=55$  days.

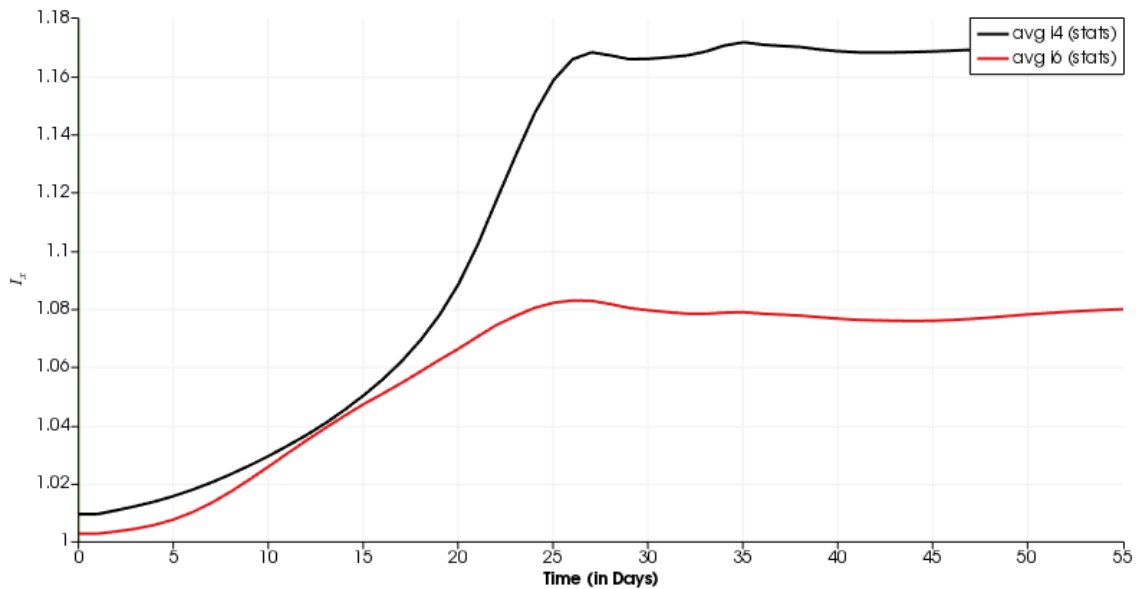


**Figure 6.28:** **(Black Line)** The circumferential collagen fibre stretch invariant ( $I_4$ ), increases gradually from an initial value of  $1.01$  at  $t=0$  days to a maximum of  $1.165$  at  $t=27$  days, with another peak at  $t=35$  days with a value of  $1.17$ , reaching a value of  $1.173$  by  $t=55$  days with an upward slope. **(Red Line)** The longitudinal collagen fibre stretch invariant ( $I_6$ ) increases from  $\approx 1.0065$  at  $t=0$  day to a maximum of  $1.085$  at  $t=25$  days decreasing to  $1.076$  at  $t=45$  days, terminally attaining a value of  $1.08$  at  $t=55$  with an upward trend.

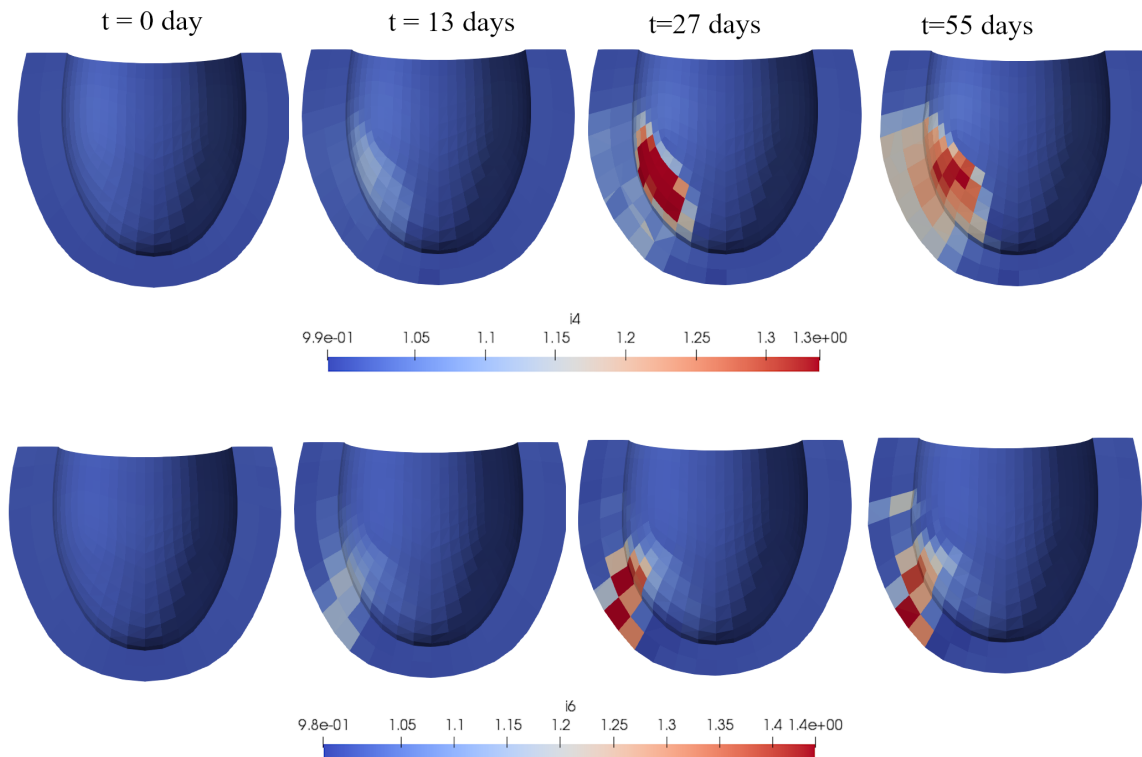


**Figure 6.29:** The stretch invariants experienced by the collagen fibres are shown in this figure. **(Top)** The invariant ( $I_4$ ) associated with the circumferential family of collagen fibres is seen. Initially, at  $t=0$  day a range of 0.99 to  $\approx 1.1$  is observed. Consequently, at  $t=13$  days the maximum increases to  $\approx 1.2$ , as the infarction progresses at  $t=27$  days,  $I_4$  values reach a higher range from 1.15 to 1.4+. Terminally at  $t=55$  days, the stretch invariants range reduces to a range between 1.2 to  $I_4$  1.35. **(Bottom)** The stretch invariant ( $I_6$ ) associated with the longitudinal collagen fibres are shown. At  $t=0$  a range of 0.98 to  $\approx 1.05$  is observed, increasing to a range of 1.01 to  $\approx 1.18$  at  $t=13$  days. At  $t=27$  days, the value range increases to a maximum of 1.4+ and terminally at  $t=55$  days, higher values are seen in a few elements whereas the majority of the infarcted region observes a range of 1.05 to  $\approx 1.25$ .

#### 6.4.2.4 Fibroblast Stretches

Figure [6.30], depicts the variation in fibroblast stretch in response to changes in the collagen fibre stretch invariants i.e. for circumferential fibres  $I_4$  and for longitudinal fibres  $I_6$  from their homoeostatic values calibrated at  $t=0$  days. The circumferential fibroblast stretch ( $I_4$ ) gradually increases from a value of 1.05 at  $t=0$  to a maximum of 1.089 at  $t=25$  days. Thereafter a decrease is noticed until the end of the simulation at  $t=55$  days with a value of 1.056, with a downward trend. The longitudinal fibroblast stretch rises quicker than the circumferential fibroblast stretch from 1.05 at  $t=0$  day to a maximum of 1.0652 at  $t=23$  days, thereafter declining to 1.0525 at  $t=43$  days, reaching a final stabilising value of 1.053 from  $t=52$  days to  $t=55$  days.

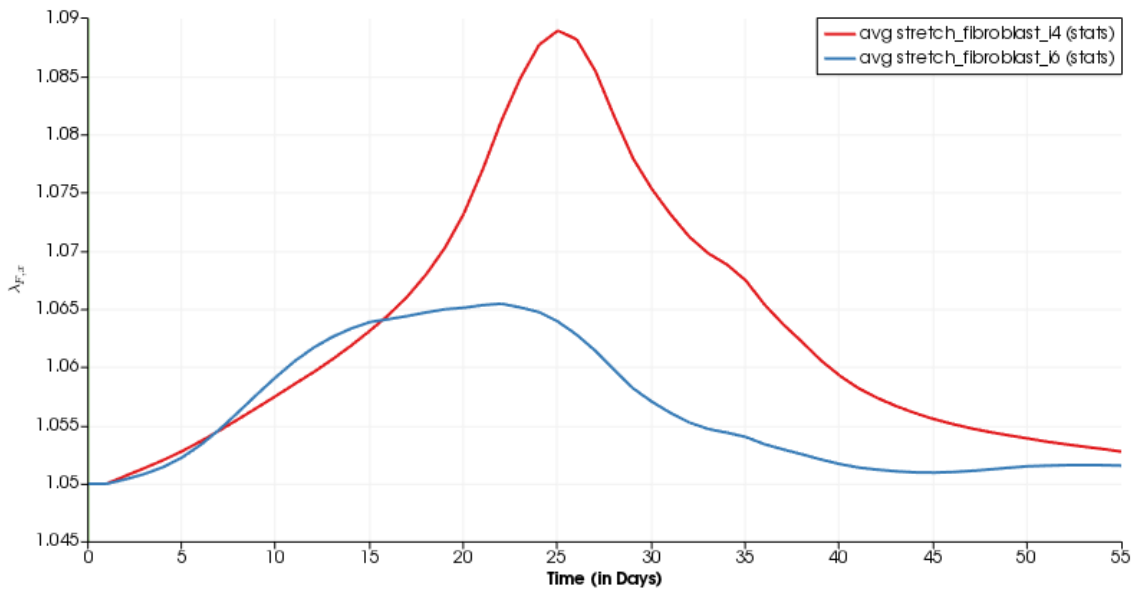


**Figure 6.30:** *(Red Line)* The circumferential fibroblast stretch ( $\lambda_{F,I_4}$ ) increases from 1.05 to a maximum of 1.089 at  $t=25$  days reaching a minimum with a downward trend at  $t=55$  days with a value of 1.056. *(Blue Line)* The longitudinal fibroblast stretch ( $\lambda_{F,I_6}$ ) increases from an initial value of 1.05 at  $t=0$  day, to a maximum value of 1.0652 at  $t=23$  days, thereafter stabilising at 1.053 at  $t=52$  days to the end of the simulation.

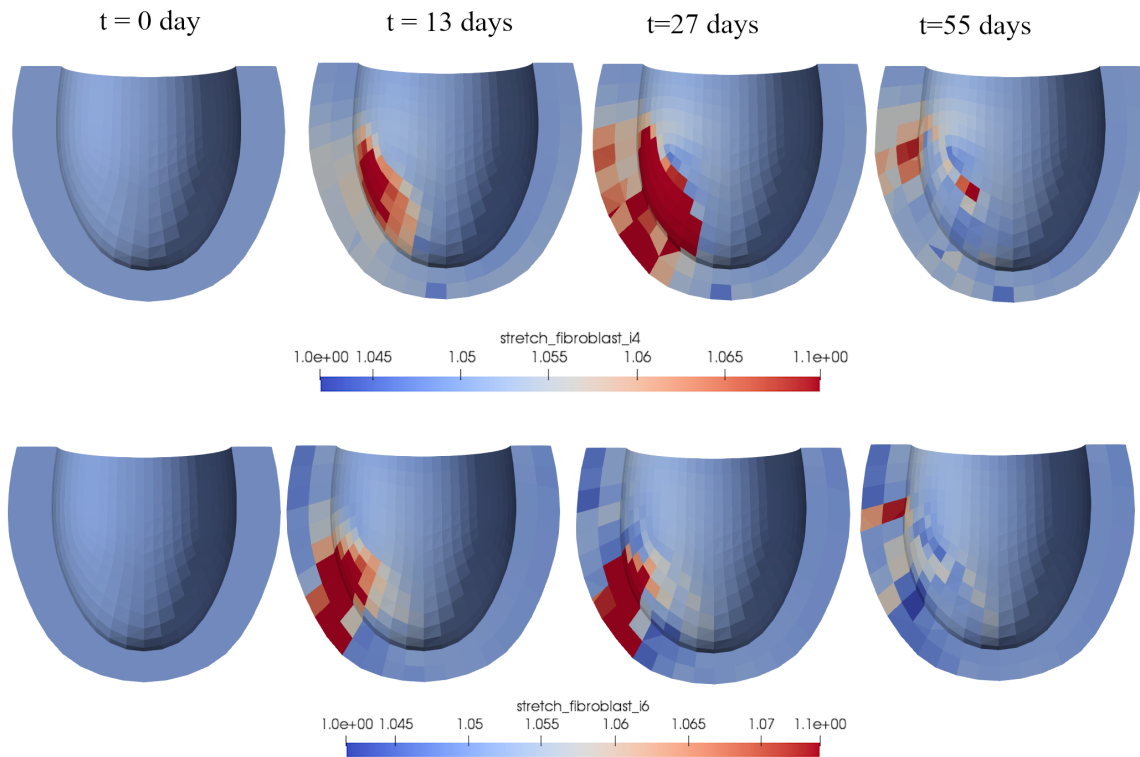


**Figure 6.31:** The stretches experienced by the fibroblast cells are displayed in this figure. **(Top)** An initial prescribed value of 1.05 is seen at  $t=0$  day. The values increase to a range of 1.058 to 1.1 at  $t=13$  days, seeing a further increase in stretch in the infarcted zone elements to 1.1, with an increase in the minimum to  $\approx 1.6$ . Terminally, at  $t=55$  days, the values for  $\lambda_{F,I_4}$  in the infarcted zone attain a range of 1.05 to  $\approx 1.057$ , with a few elements possessing higher values upto 1.1. **(Bottom)** The fibroblast cells maintaining the longitudinal collagen fibres, have their stretches displayed here. An initial prescribed distribution of 1.05 is seen at  $t=0$  days. An increase to a range of 1.05 to 1.1+ is seen at  $t=13$  days, with a reduction in the minimum seen at  $t=27$  days to values around 1.046. Terminally, at  $t=55$  days, majority of the infarcted volume elements attain a value range of 1.001 to  $\approx 1.057$  with a few elements exhibiting higher  $\lambda_{F,I_6}$  values of around  $\approx 1.09$ .

### 6.4.2.5 Collagen Fibre Matrix Mass Density Changes

Figure [6.32], depicts the variations in averaged mass densities ( $m^{C,I_4}$ ,  $m^{C,I_6}$ ) of the collagen fibres oriented in the ( $I_4$ ,  $I_6$ ) directions. **(Orange Line)** indicates the collagen mass density changes in the circumferential direction, Observing an increase at  $t=5$  days from a value of 1 with a steep incline upto  $\approx 3.5$  at  $t=35$  days and increasing albeit with a slower turnover post  $t=35$  days, reaching a maximum of  $\approx 4.3$  at  $t=55$  days. **(Brown Line)**, depicts the longitudinally oriented collagen fibres mass deposition, following a similar increase from  $t= 5$  days from 1 to a maximum of 2.78 at  $t=43$  days. It displays a stabilising trend from  $t=50$  days to  $t=55$  days i.e. the end of the simulation.

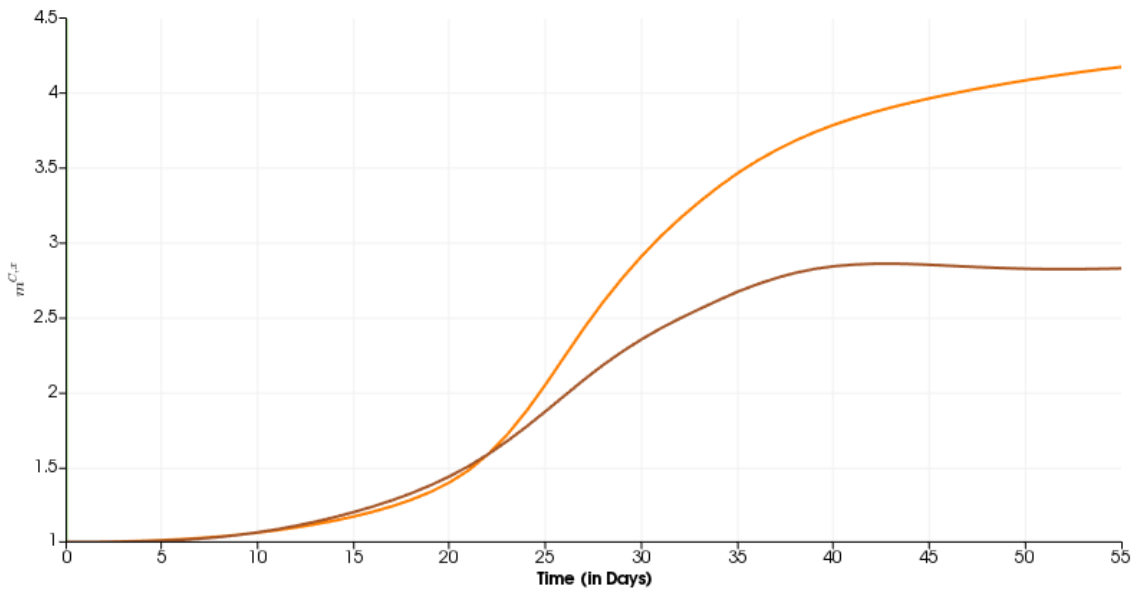


**Figure 6.32:** **(Orange Line)** The circumferential collagen fibre mass density changes are seen to rise from 1 at  $t=1$ , with an upward slope from time  $t=5$  days to a maximum of 4.25 at  $t=55$  days. **(Brown Line)**, In a similar trend but with a slightly faster increase in mass deposition the longitudinal collagen fibre mass density increases from 1 at  $t=0$  day to a maximum of 2.76 at  $t=40$  days and stabilises from  $t=50$  days to the end of the simulation with a value of 2.7.

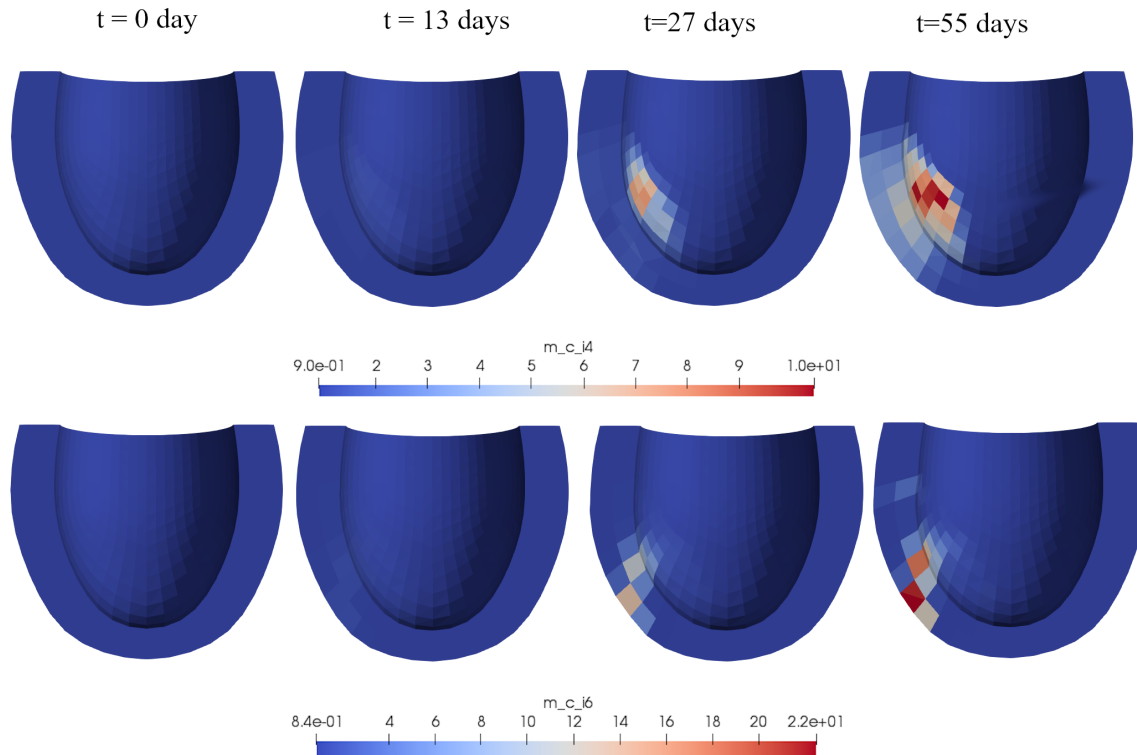


**Figure 6.33:** The collagen fibres mass densities are displayed in this figure. **(Top)** An initial mass density of 1.0 is observed at  $t=0$  day for circumferential collagen fibres ( $m^{C,I_4}$ ), a slight increase of the maximum upto  $\approx 2.1$  is observed in the infarcted region at  $t=13$  days. AT  $t=27$  days, the ( $m^{C,I_4}$ ) values rise to a range of 2 to  $\approx 8$  in the infarcted zone and terminally at  $t=55$  days an increase value range is seen from 4.3 to  $\approx 10+$ . **(Bottom)** For longitudinal collagen fibres, mass density changes are shown. An initial distribution of unity is observed at  $t=0$  day, with a minor increase to a range of 1 to 1.5 are seen at  $t=13$  days. At  $t=27$  days the range of ( $m^{C,I_6}$ ) the range rises from a minimum of 4 to upto 14, with higher values observed in a few volume elements at the bottom of the infarct. Terminally, at  $t=55$  days a range of  $\approx 4$  to  $\approx 22+$  is observed, again with maximum values restricted to a few elements.

## 6.5 Discussion

Before understanding the model behaviour and qualitative analysis of the results acquired, it is important to note a few points.

1. We model growth of the collagen fibre mass densities by using scalar mass density variables multiplied to the respective strain energy functions. This follows the mass growth approach as adopted in (Watton et al. (2009)).
2. Remodelling of the material parameter involves a stress-based approach, in contrast with the 1D Constrained mixture model (discussed in Chapter [3]). This is done via material parameter alterations using partial differential equations based on the variations in Cauchy stresses experienced by the collagen fibres in its respective direction.
3. Utilising an in-built fibre-reinforced passive hyperelastic material model(ANSYS (2013)), restricts access to the deformation gradient, thereafter proving to be a limitation in terms of (a) Accessing the deformation gradient to update natural reference configurations for individual constituents as seen in the constrained mixture model (Chapter [3]) and (b) Using the multiplicative decomposition of the deformation gradient to incorporate stress-free growth of the collagen fibre constituents as observed in (Rodriguez et al. (1994)). It would be feasible to develop a custom user material subroutine, which provides a basis for future work to be done given the background knowledge required to implement it.
4. The fibre directions assumed for a single homogeneous layer of myocardial tissue, i.e. in the circumferential direction ( $I_4$ ) and longitudinal direction ( $I_6$ ). A gross simplification of the collagen extra-cellular matrix organisation in the myocardium, it follows the concept of using the fibre direction, sheet direction and fibre normal direction for cardiac muscle (termed myofibres) introduced in (Nash & Hunter (2000)). From which myofibre directions of fibre ( $f$ ) and sheet-normal( $n$ ) for collagen fibres in the ( $I_4$ ) and ( $I_6$ ) directions respectively, are assumed.

With these points in perspective, the implications of the growth and remodelling of the collagen mass density and its material characteristics based on the two Cases, with respect to the homeostatic Cauchy stress distribution and modelling the hypotheses, are discussed. Also, the graphs represented are averaged over the infarcted area and each horizontal unit depicts the full range of values observed for each element in the infarcted tissue region, an averaged value line is depicted to provide an idea about the behaviour of the respective mechanical quantity over time.

As the mass density of the ground matrix is degraded to 1 % of its original value it causes the tissue to experience increased load due to the internal diastolic blood pressure. Leading to an increase in the tissue stretch ( $\lambda$ ), by which the stretch invariants  $I_4, I_6$  rise being a function of ( $\lambda$ ). Subsequently  $\sigma_C(\mathbf{X}, k_1, k_2, I_4, t)$  and  $\sigma_{CH}(\mathbf{X}, k_1, k_2, I_4, t = 0)$  increase, thereby triggering the remodelling equations [6.6, 6.7] due to the deviation of the Cauchy stresses from their homoeostatic values  $\sigma_{CH}(\mathbf{X}, k_1, k_2, I_4, t = 0)$  and  $\sigma_C(\mathbf{X}, k_1, k_2, I_4, t = 0)$ . The remodelling of the material values  $k_2, k_4$  aims to maintain the preferred Cauchy stress value, as seen in Figures [6.26, 6.14]. The collagen fibres in the extant matrix, or fibroblast mediated new collagen fibres are deposited with a stretch so as to maintain a preferred collagen fibre stress value in the updated tissue configuration. This ties in with the idea that the extant collagen matrix reconfigures itself with or without mass density changes in order to maintain homoeostasis in the tissue (Ambrosi et al. (2019), Watton et al. (2004)).

An important point to note that the collagen fibre remodelling is independent of restoration of the tissue stress or strain energy to homoeostatic levels, which is modelled through the mass density material parameters  $m^{C,x}$ , where  $x = I_4, I_6$ . Equation [6.13] captures the changes in mass density of collagen family of fibres for their respective directions. It is mediated by changes in the stretch experienced by fibroblasts i.e.  $\lambda_{F,x}$  from their homoeostatic stretch levels at time  $t=0$  ( $\lambda_{FH,x}$ ) (Watton et al. (2004)). The concept of a fibroblast field was introduced in order to add a layer of depth to the tissue level model with a cellular level model inclusion. Although simplistic it captures, implicitly, the process of fibroblasts changing gene expressions to produce more collagen fibres by mediation of various chemical enzymes (Ma et al. (2014)). The fibroblasts possess a recruitment stretch  $\lambda_{F,x}^R$  which remodels over time as per Equation [6.11], to maintain a preferred state of stretch  $\lambda_{FH,x}(t = 0)$ . This captures the fibroblast innate cellular capability of reconfiguring in response to changes in its mechanical environment and stretches it experiences via surface mechano receptors (integrins in particular which are its focal adhesions to the extra-cellular matrix) (Chiquet et al. (2003)). It is a gross approximation of the fibroblasts cell's behaviour from a purely mechanical standpoint and sophistications based on molecular models, cellular signalling pathways as well as chemokine interactions need to be considered to fully realise cell behaviour in LV pathophysiology.

The mass density term  $m^{C,x}(t)$  mediated by fibroblast cell stretch  $\lambda_{F,x}(t)$  aims to restore the collagen fibre stress to homoeostatic levels, this in turn attempts to restore the strain energy within the fibres to its homoeostatic levels as it is a function of the Cauchy stresses derived (see Equations [6.13]) (calibrated at time  $t=0$ ). Our model therefore, is motivated by the restoration of the micro-structural collagen Cauchy stresses identifies the compensatory mechanisms of the extra-cellular matrix, triggered by the necrosis of the ground matrix and cardiomyocytes. Therefore, the amount of collagen fibres present in the infarcted scar tissue, could shed light based on the mass density changes in the collagen fibres as seen in clinical/ experimental observations (Cleutjens et al. (1995), Jugdutt & Amy (1986), Jugdutt et al. (1996)).

On comparing the cases where **(Case 1)**: the homoeostatic collagen fibre Cauchy stress ( $\sigma_{CH}(\mathbf{X}, t)$ , shortened for convenience) is maintained at a constant value and **(Case 2)**: evolving this stress value (please refer Section [6.3.6.6]) a few observable differences are:

1. The enlargement of the infarcted zone, is smaller in Case 2 than in Case 1. This is attributed to the evolution of the homoeostatic collagen fibres Cauchy stress which leads to a smaller difference between the Cauchy stress at time  $t$ ,  $\sigma_{C,x}(\mathbf{X}, t)$  and homoeostatic stress  $\sigma_{CH}(\mathbf{X}, t = 0)$ . In turn the  $k_2, k_4$  parameters remodelling is affected and in Case 1 values are lower than Case 2, thereby limiting the stretching capability of the tissue elements (Figures [6.16, 6.28]).
2. Due to the limited stretching in Case 2, the effect is observed in fibroblast stretches  $\lambda_{F,x}(t)$  which deviate less from homoeostatic values  $\lambda_{FH,x}(t = 0)$ . In turn the collagen mass density observes reduced growth compared to Case 1.

This suggests when the homoeostatic Cauchy stress of collagen fibres leads to lesser dilatation of the LV and therefore a lower deposition of collagen fibre mass density. This could shed light on the configuration of collagen fibres, though we model stress it implicitly allows us to infer understanding about the state of stretch of the collagen fibres implicitly via the stretch invariants  $I_4, I_6$ . If a higher dilatation is observed, a higher mass density evolution is observed for collagen, due to fibroblast stretch deviations. The stresses for the collagen fibres ( $\sigma_{C,I_4}(X, t), \sigma_{C,I_6}(X, t)$ ) decrease as the disease progresses indicating the stiffening of the myocardium. This is the case for circumferential fibres (Figure[6.11, 6.23]), whereas for longitudinal fibres an initial decrease is observed with increases later, however they seem to follow a downward trend by the end of the simulation (Figure[6.12, 6.24]). Our model suggests that increases in mass density of collagen fibres  $m^{C,I_4}, m^{C,I_6}$  causes the increase in stiffness and reduction of stress as the remodelling of collagen material parameter  $k_2, k_4$  (Equations[6.6, 6.7]) based on their functional form makes the collagen fibres more compliant rather than stiffer. In the case of evolution of homoeostatic Cauchy stress for the collagen fibres, the fibre stress in the circumferential fibres goes below the original Cauchy stress at  $t=0$  (Figure [6.23]). The reduction in myocardial collagen stress correlates to a reduction in the tissue stress as the isotropic component no longer plays a role in load bearing due to degradation (Figure[6.10], Equation[6.4]). This is consistent with observations in computational models and experimental observations leading to stiffer infarcts (Omens et al. (1997), Rouillard & Holmes (2012), Zhuan et al. (2019)).

### 6.5.1 Comparison with relevant studies

Please note the model introduced in this chapter is referred to as "stgrf-model" for simplification in the following discussion. For ease in comparison of stress values, averaged Cauchy stresses in both collagen fibre directions ( $I_4$ ,  $I_6$ ) are calculated for convenience and for the reason that not every empirical data set or study would consider collagen fibre directions as has been modelled in the stgrf-model for LV. The results produce by the model are purely qualitative, with the rates parameters tuned to attain a certain deformation indicative of myocardial thinning post-MI. Even though the model is capable of providing behavioural observations for the myocardial tissue, it is necessary to compare with existing data to understand the utility and possible insights which could be obtained.

In a study (Lerman et al. (1983)), rabbit hearts were subjected to coronary ligation, to induce myocardial infarction in the left ventricle. Results were noted, for the change in collagen content by measuring hydroxyproline content (a component of collagen triple helix chains and is helpful in measuring collagen quantities in soft tissues), mechanical resistance of the left ventricle (stiffness) versus stretch and rupture. The experiment was carried over a period of 8 days, up until which a scar tissue was visible. The hearts were then excised and subjected to balloon inflation to test for tissue stiffness and resistance to rupture. The hydroxyproline content increased from a control  $2.8 \pm 0.2$  mg/g dry weight to  $5.3 \pm 0.6$  at 72 hours to an increased value at day 8 of  $14.5 \pm 1.7$  mg/g dry weight. This corresponds to an average increase of 1.89 times control hydroxyproline content at 72 hours and 5.17 times control hydroxyproline content on day 8. Compared to our two cases the collagen mass density is observed, which is comparable to hydroxyproline content, for unchanging homeostatic collagen fibre stress it is observed an increase of  $m^{C,I_4}$ ,  $m^{C,I_6}$  of about 1.1 each at 72 hours, at day 55 terminal 4.5 times increase in  $m^{C,I_4}$  and 4 times increase in  $m^{C,I_6}$  (please refer to Figures[6.20,6.32]). In the case of evolving the homoeostatic collagen fibres stresses (Section [6.4.2]), the mass densities increase only after 5 days and reach a terminal point of 4.2 ( $m^{C,I_4}$ ) and 2.5 ( $m^{C,I_6}$ ) at day 55. Though the timeline for the experiments on rabbit hearts in (Lerman et al. (1983)) is 8 days, the simulation is based on an idealised human LV for a period of 55 days.

Also, the initial increase in collagen mass density is not reflective of observations in rabbit hearts, which can be attributed to the degradation regime employed for ground matrix in the model. However, with these differences aside, the growth and remodelling results are fairly realistic in the amount of increase in the collagen mass densities and on averaging  $m^{C,I_4}$ ,  $m^{C,I_6}$  for Case 1 results provides a value of 4.25 at t=55days and for Case 2: average collagen mass density change in fibre directions is 3.35. These values are fairly within terminal observed hydroxyproline ratios in rabbit heart scar tissue at t=8 days i.e 5.17 times as seen earlier.

In pertinence to the growth and remodelling results from finite element simulations, the passive stiffness of the rabbit myocardium is of interest. It is noted in (Lerman et al. (1983)), there is an increase in the passive stiffness from a control  $61 \pm 5$  mmHg/100 $\mu$ l ( $8.13 \times 10^{-3} \pm 6.6 \times 10^{-4}$ MPa/100 $\mu$ l) of the infarcted tissue to about  $100 \pm 7$  mmHg/100 $\mu$ l ( $1.3 \times 10^{-2} \pm 9.3 \times$

$10^{-4}$ MPa/ $100\mu$ l). Also, it is stated as an inference that the stiffness is directly influenced by the amount of hydroxyproline content. These points can be compared to stress responses in both cases as well as the collagen fibre remodelling. For Case 1: An average (taken over both  $I_4, I_6$  directions) stress increase is observed to increase from  $\approx 1.588 \times 10^{-3}$  MPa at  $t=0$  days to  $\approx 4.1 \times 10^{-3}$  at  $t=55$  days; for Case 2: average collagen fibre stress increases from  $1.679 \times 10^{-3}$   $t=0$  days upto  $3.045 \times 10^{-3}$  at  $t=55$  days is observed. For both cases  $k_2, k_4$  values reduce, indicating increasing compliance and reducing stiffness of individual collagen fibres there is an increase in the mass densities. Therefore, it can be inferred from the stgrf-model as well that the stiffness of the infarcted tissue can be attributed to the collagen mass density in contrast to the mechanical strength of individual collagen fibres.

Another study (Rohde et al. (1999)), observes regional changes in the wall stress experienced in the left ventricular wall post-MI for a period of 21 days, and its association with extra-cellular matrix changes. This ties in with our growth and remodelling of extra-cellular collagen matrix and stress-based growth and remodelling formulations. Though the STGRF-model calculates collagen fibre stresses, tissue stress observed in (Rohde et al. (1999)) can be indicative of collagen fibre stresses, as the infarcted tissue is heavily proliferated with collagen fibres post-MI. A key difference is the data from the study details stresses experienced at end-systolic configuration and the model loaded configuration is taken to be at end-diastolic state. This needs to be considered while validating the model in the future with experimental/ clinical or empirical studies. It was noted the increase in infarcted region regional stress ranged from  $25.1 \pm 5.9$  kdyn/cm<sup>2</sup> ( $2.51 \times 10^{-6} \pm 5 \times 10^{-7}$  MPa) at day 1 to  $69.9 \pm 4.4$  kdyn/cm<sup>2</sup> ( $6.99 \times 10^{-6} \pm 4.4 \times 10^{-7}$  MPa), at day 21.

The average regional stress at  $t=21$  days to that of  $t=1$  day has a ratio of 2.78, for Case 1 in stgrf-model, the ratio between the stresses at  $t=55$  days to  $t=1$  days is 2.58 and for Case 2 the ratio possesses a value of 1.217. The average stress values for the results in the stgrf-model and (Rohde et al. (1999)) differ by an order of magnitude of  $10^{-3}$  MPa. This indicates that the model can be better calibrated to experimental data by tuning input parameters i.e. material parameter values. Also, in comparison to the two studies above shows Case 1 has better agreement in terms of collagen mass density changes and average stress change ratios over the period of growth and remodelling post-MI. This indicates further studies to be undertaken to confirm the validity of evolving the homoeostatic collagen fibre Cauchy stresses, to understand necessity as it has been seen in the Constrained Mixture Model (Chapter [3]).

### 6.5.2 Model Limitations in the representation of the LV Tissue

A few limitations in the modelling of the myocardium using the HGO material model available in ANSYS ® APDL software are apparent when compared to literature for representing the cardiomyocytes. A few more points are discussed.

1. *Left Ventricular Geometry & Fibre Directions:*

We considered an idealised left ventricular geometry ([Hassaballah et al. \(2013\)](#)) in our model with fibre directions along circumferential and longitudinally configured. However, these are simplifications of the actual micro-structure and results though qualitatively reflective are not sufficient to be compared with realistic changes in the complex extra-cellular arrangement in the myocardium. Therefore, it is essential to model fibre directions along the muscle architecture ranging from  $-60^\circ$  to  $+60^\circ$  from the endocardium to the epicardial layer ([Scollan et al. \(1998\)](#)) alongwith consideration for patient specific geometries.

2. *Monolayered Myocardium:*

Our model assumes a homogeneous layer of the left ventricle in a single layer with the same material properties at time  $t=0$ . However, the heart is a complex multi-layered organ with different compositions in terms of cells, extra-cellular matrix and ground substances. To consider, this in the HGO model, the left ventricular layers would need to be represented as three layers, endo-cardium, myocardium and epicardium with material properties based on their mechanical properties ([Holzapfel & Ogden \(2009\)](#)). This would allow us to obtain stress distributions more in tune with clinical/ experimental observations. Given the generation of the mesh was done using automated methods present within ANSYS © Mechanical APDL, control over the locations of the elements was limited due to a lack of understanding of the software. This could be rectified by understanding either the generation technique within FE software or by creation of a mesh manually with defined layers to assign multiple material properties pertinent with the layers of the left ventricular myocardium.

3. *Chemical Signalling Pathways:*

Though there is a representation of a fictitious fibroblast field regulating collagen mass density in the myocardial tissue, it can be further sophisticated to consider enzymatic action and balance of Matrix-metallo-proteinases and Tissue Inhibitors of Metalloproteinases, and in turn the production of collagen based on available models ([Aparício et al. \(2016\)](#)).

4. *Passive Material Model:*

The hyperelastic material model available in ANSYS ® Mechanical APDL ([Holzapfel et al. \(2000\)](#)) is an established representation for fibre-reinforced soft tissue. Though suitable to understand passive material deformations and mechanical quantities in simulations, the myocardium consists of cardiomyocytes which have an active nature due to the presence of sarcomeres. This contractile behaviour would be beneficial in our studies, where in growth and remodelling for the entire cardiac cycle could be obtained instead of a fixed configura-

tion . Though this would be computationally more intensive, it is useful in understanding how the contractile properties affect the growth and remodelling of the myocardium and their contribution to LV thinning and dilatation, further providing insights to stratify risk, prognosis and developing novel therapeutic strategies.

With additional sophistications to the model with testing on patient specific geometries, an active component to cardiomyocytes, multi-layered model and incorporation of a chemo-mechano-biological model as in (Aparício et al. (2016)) a complete model can be achieved which would enable the modelling of long-term growth and remodelling of the LV myocardium including complete cardiac cycle observations to understand LV structure and function at each time point.

## 6.6 Conclusions

The initial application of the STGRF framework to the left ventricular myocardium post-MI, was to investigate the effect of remodelling of collagen fibres based on the collagen fibre stresses in the respective direction, contrasting with the utilisation of tissue first principal stress obtained from ANSYS ® Mechanical APDL outputs. Growth and remodelling of the myocardial extra-cellular matrix is carried out based on mass density changes and collagen material parameter remodelling respectively. Additionally, the effect of a fictitious fibroblast recruitment field on the mass density variations of the collagen fibres as a consequence of fibroblast stretching. It can be deduced from the model that **(a)** collagen fibres remodel to maintain a preferred state of homoeostasis, **(b)** collagen mass density depends on its regulation by fibroblasts which are sensitive to changes in the mechanical stretch they sense for a family of collagen fibres, **(c)** Evolving the homoeostatic stress for the collagen fibres impacts the dilatation of the LV myocardium that can be modelled which is enhanced by the modification of the HGO model, in turn fibroblast stretches are lower as compared to a case with constant homoeostatic collagen fibre stress levels and thirdly a reduced mass density deposition. Terminally, it is an adaptation of (Watton et al. (2004)) into a commercial finite element software (ANSYS ®Mechanical).

This page has been intentionally left blank.

## Chapter 7

# Applications of STGRF II: Gastrocnemius Skeletal Muscle Remodelling in Response to Sustained Stretch

---

*This chapter introduces another application of the soft tissue growth and remodelling framework, in terms of remodelling of the gastrocnemius skeletal muscle subject to over-stretch. The gastrocnemius finite element volume domain is partitioned into regions namely muscle, tendon and aponeurosis regions by means of a volume fraction variable. This allows us to understand the changes occurring not only solely in the muscle but also the dense tendinous and tendinous aponeurosis region. Remodelling hypothesis have been introduced for the muscle and tendon along with separate rate parameters. A ramp function is defined to simulate over-stretch. Remodelling is triggered due to this increase as the stress increases from a homoeostatic level to a higher value, and the remodelling hypotheses always aim at maintaining a preferred state of homoeostatic stress. This preliminary study considers a few cases which utilise a combination of values for the rate parameters to understand the effect of only remodelling the muscle region, tendon region or both. This allows us to understand the model behaviour and adapt it to reflect cases such as toe-walking and serial casting. It is hoped that sophistications including anatomical muscle fibre definitions, boundary conditions associated with different muscle biomechanical problems can provide a more complete realisation of the model.*

---

## 7.1 Introduction

Skeletal muscles are a part of the muscular system in the human body and is named so due to its connection to the bones via tendons. Tendons are dense connective tissues which are present between muscles and bones acting as a connection for transfer of forces due to contraction of the muscles involved in various physical activities. Muscles are organised into fascicles, which include three layers i.e. a muscle fibre is surrounded by connective extra-cellular tissue (consisting of collagen and elastin) known as the endomysium and the entire muscle consisting of multiple muscle cells is covered by the epimysium, terminally bundled whole muscle fibres together are surrounded by the perimysial connective tissue and together form a fascicle (Betts et al. (2018)). Multiple fascicles together form a complete skeletal muscle, this is shown in Figure[7.1]. The

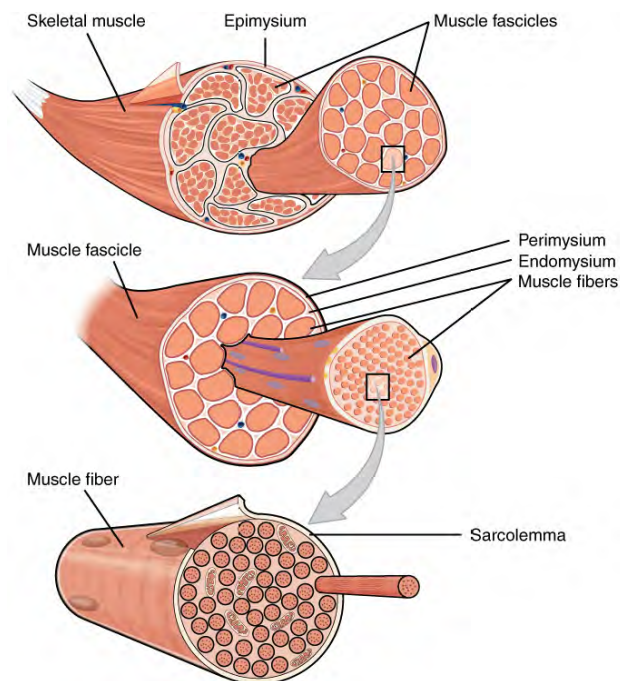


**Figure 7.1:** *Skeletal Muscle Taxonomy (Betts et al. (2018))*

skeletal muscle fibres (cells) are made up of contiguous contractile units, known as sarcomeres. These contractile units consist of an assembly of thick and thin filament proteins called myosin and actin respectively which slide across each other when activated to produce contraction within a fibre, and on activation of the cells in a particular skeletal muscle as a whole brings about a contraction of the entire muscle. These contractile units are shown in Figure[7.2]. Remodelling of muscle fibres occurs due to the addition or removal of sarcomeres depending on the mechanical stimuli and environment they are subjected to. (Wisdom et al. (2015)) succinctly defines these changes as with respect to resting length ( $l_r$ )

1. *Overstretch*: The extension of the muscle beyond  $l_r$ .
2. *Understretch*: The shortening of the muscle below  $l_r$ .

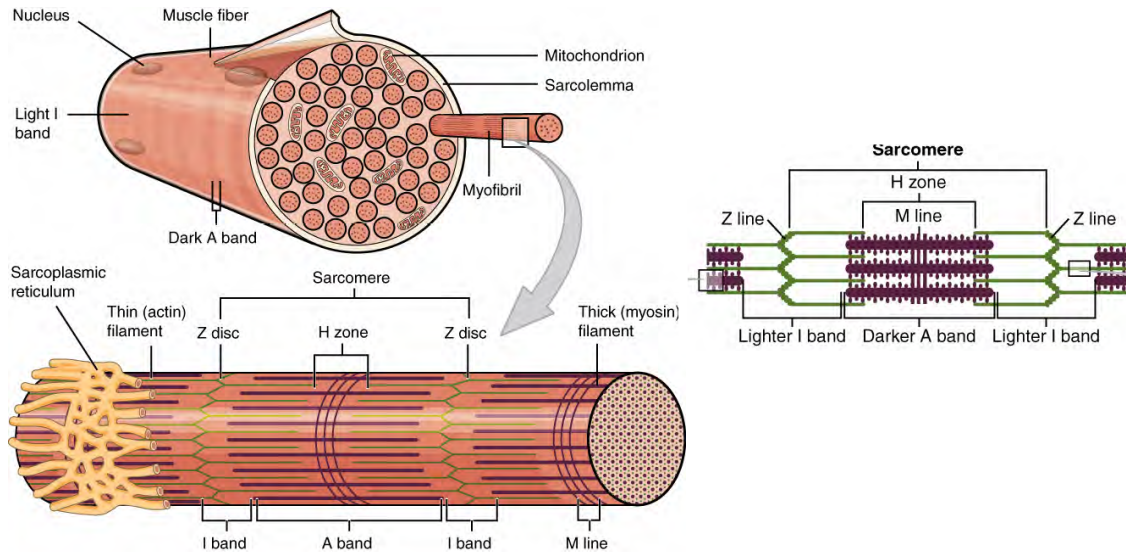


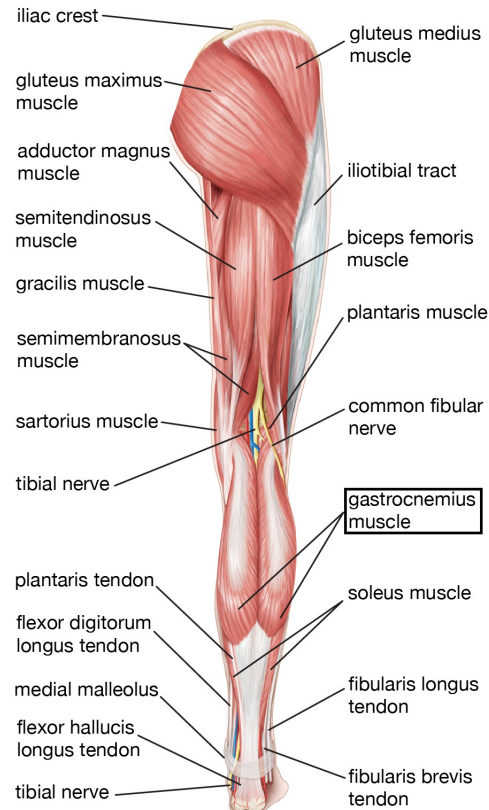
**Figure 7.2:** *Sarcomere Macroscopic Structure (Betts et al. (2018))*

3. *Overload:* Force generation beyond physiological need to maintain the muscle.
4. *Underload:* Force generation below physiological need to maintain the muscle.

The overstretch and understretch are both done passively, while the overload and underload force generation is actively produced. For the current research focus, with muscle over-stretch and the remodelling pattern the sarcomeres attain in response to it are considered. *Eccentric Remodelling:* Chronic overstretching of a muscle causes it to extend i.e. lengthen in response to it by adding sarcomeres in series to existing sarcomere chain. This is attributed to eccentric exercise, limb lengthening and other stretch regimens (Boakes et al. (2007), Goldspink (1999), Lindsey et al. (2002), Nakamura et al. (2012), Seynnes et al. (2007)), an extensive literature survey can be found in (Wisdom et al. (2015)).

### 7.1.1 Gastrocnemius Muscle

The gastrocnemius muscle exists between the knee-cap and the Achilles tendon which connects it to the dorsal side of the foot i.e. the heel bone. The lower limb, hip movement and lumbar area are all affected by the gastrocnemius muscle which is called to action during various activities like sports as well as maintain orthostatism (Bordoni & Varacallo (2018)). Muscles are fibres containing fascicles of muscle sheets and fibres which are composed of contractile sarcomeric units, responsible for the contraction of the muscles in response to various physical activities and mechanical stimuli. The skeletal muscles are connected to the bone by tendons which are dense connective tissues capable of withstanding large amounts of tension and are similar to ligaments (which connect bone-to-bone). A region known as aponeurosis exists between a tendon and muscle, serving as a transition region between muscles and tendons. It is a tendinous complex having a unique structure and in biomechanical models are either over or under represented,



© 2015 Encyclopædia Britannica, Inc.

**Figure 7.3:** *Gastrocnemius muscle anatomy (Britannica (2015)). It is located in the upper region of the calf region (boxed in image).*

leading to complications in representing the actual structure. But in order to better understand musculoskeletal disorders, adaptation to mechanical stimuli and other factors it important to be able to represent the complex aponeurosis structure. Not only does it provide a better representation of the mechanical quantities over the muscle-tendon complex but would be useful in better designing exercise regimes, rehabilitation programmes and long-term recovery procedures.

### 7.1.2 Motivation

Our model observes an implementation around a material model (HGO model [Holzapfel et al. \(2000\)](#)) available in a commercial software (refer to Chapter 4). We model the tissue level of the muscle-tendon complex and understand the variations in stress, strains induced as a consequence of overstretch of the muscle, a general underlying principle observed in various therapies and scenarios ([Lambert et al. \(2004\)](#)). This allows insight into the gross behaviour of the mt complex and can guide further research by the inclusion of chemical, electrical and other biophysical principle.

1. Test the utility of HGO model specific framework (STGRF) in understanding the remodelling of fibre-reinforced skeletal muscle model with aponeurosis definition.
2. Understand the remodelling of gastrocnemius skeletal muscle to over-stretch using a fibre-reinforced material model ([Holzapfel et al. \(2000\)](#)) .

### 7.1.3 WorkContribution

Before proceeding with the methods and results, the contribution to this body of work for skeletal muscle has been made by others and are duly listed below:

1. The surface mesh to volumetric generation is a concerted effort by the supervisor and author (Section[[7.2.1](#)]).
2. Regional Volume Fraction Definition and Volume Fraction assignment algorithm are jointly contributed by ([Civisilli \(2019\)](#), [Gondwe \(2019\)](#), [Harms \(2020\)](#)).
3. The model set up, automation of work flows, framework external scripting and results are undertaken by the author.

## 7.2 Methods

The approach used for understanding the remodelling of gastrocnemius muscle-tendon complex fibres, is based on the finite element analysis approach. The framework (STGRF) introduced in Chapter [4], is utilised to set up a customised workflow for skeletal muscle simulations in particular. It therefore show cases the flexibility of the STGRF in terms of the HGO material model for modelling soft tissues and secondly, the particular application to remodelling of the gastrocnemius muscle subject to over-stretch sustained over a period of time.

### 7.2.1 Mesh Generation

The mesh for the gastrocnemius muscle was generated using an .stl (stereo-lithography (Roscoe et al. (1988))) surface geometry file, which uses triangular between surface points to create a surface. Algorithm for obtaining a volume mesh and a secondary .vtk (File Formats for VTK Version 4.2 (2002)) file is shown in Figure [7.4]. The dimensions of the obtained surface geometry is as follows:

- Length: 145 mm / 14.5 cm
- Maximum Radius:  $\approx$  13.62 mm / 1.362 cm

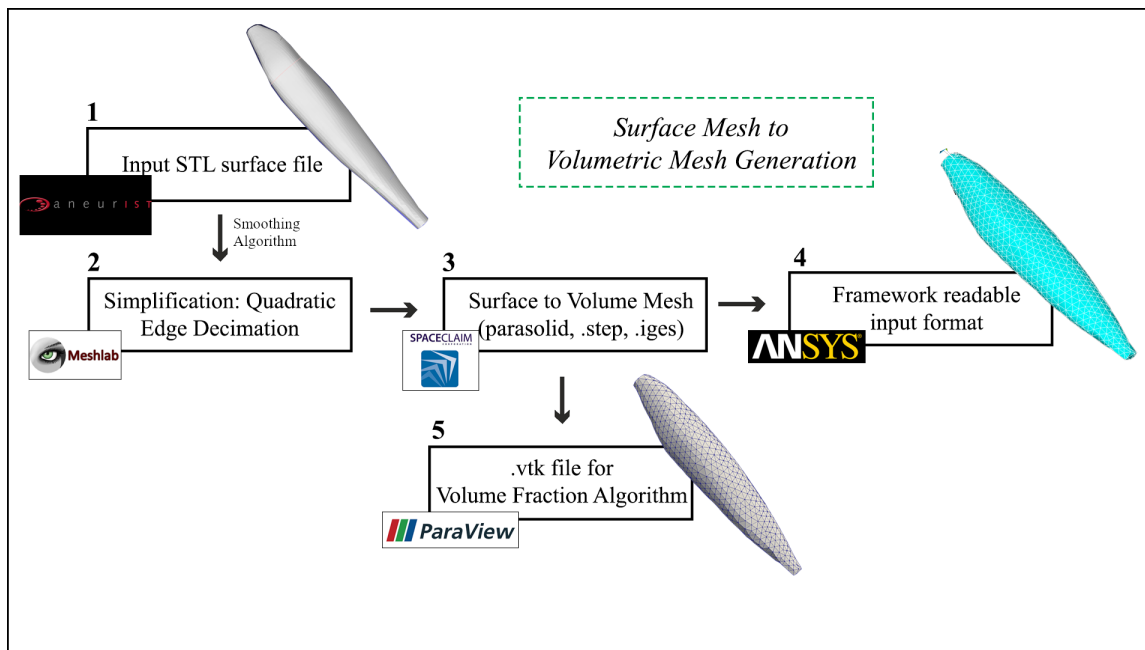


**Figure 7.4:** The diagram depicts the steps taken for the generation a volume mesh for finite element simulations, and a separate .vtk file to compute muscle-tendon volume fractions to incorporate with the volume mesh to define material parameters.

The steps shown in the Figure[7.4], are detailed below:

1. A smoothing algorithm in (@neufuse by @neurist) was applied to an stl file and used as an

input.

2. This .stl file has a fine triangulated surface mesh which would result in a very fine mesh with a high number of cells or elements. This is simplified using MeshLab with a technique known as Quadric Edge Collapse Decimation by means of which coarser meshes can be obtained and tested.
3. The simplified .stl file is then imported into SpaceClaim software available in ANSYS ® Workbench, and a volumetric mesh is generated which is then saved in various formats.
4. The Previous step helps in importing the a compatible format using the ANSYS ® Mechanical APDL software to produce mesh information which is readable by our framework.
5. An additional file i.e. .vtk format file is generated to obtain a volume fraction defined mesh for the muscle, tendon aponeurosis regions definition using a Volume Fraction Assignment Algorithm.

## 7.2.2 Regional Volume Fraction Definition

The .vtk file output for Volume Fraction Assignment Algorithm displayed in Figure[7.4, Section [7.2.1]] is utilised in tandem with an algorithm developed in (Civisilli (2019)), to demarcate regions on the extracted gastrocnemius geometry with respect to a muscle region (MR), tendon region (TR) and aponeurosis region (AR). This is employed in order to better capture gastrocnemius muscle details for defining the material properties in the finite element simulation.

We first describe the workflow developed with MSc students (Civisilli (2019)) and in the further section how the particular algorithm for defining the muscle, tendon and aponeurosis regions

### 7.2.2.1 Workflow Description

A workflow is in place for the volume fraction assignment to demarcate muscle, tendon and aponeurosis regions, i.e. MR, TR and AR respectively. A flowchart shown in Figure[7.5], encapsulates the idea and is described below:

1. *muscle.pl*:

This perl script initiates and manages the procedures between various MATLAB scripts, directory information, providing inputs to scripts and point output directories. It can be said to be the heart of the workflow.

2. *ranges.txt*:

A file which includes information to be set, which includes the position and size of the various regions (MR, TR and AR). Also, a parameter to control the type of aponeurosis region from a simple linear interpolation to a radial interpolation method.

3. *muscle\_surface.vtk*:

An initial surface file of the gastrocnemius muscle with triangular cell/ element faces as the input mesh.

4. *model\_analysis.m*:

A MATLAB script, which runs the partitioning algorithm for projecting the surface mesh inwards into regions to define the MR, TR and AR in 3-dimensions. It also, associates each resulting surface i.e. inner projection of the outer muscle surface with a number.

5. *Combination of centroids from a volume mesh*:

*analyzed\_model.dat* is the output obtained from *model\_analysis.m* which is used in tandem with a centroids file as an input to TECPLOT, which manages carries out the ascription of muscle or tendon region based on the volume fraction assignment algorithm defined below.

6. *new\_centroids\_file\_C.dat*:

after the interpolation of the volume fractions for MR, TR and AR, this is the output file obtained which contains all points in the 3D geometry with a value associated in the range [0, 1].

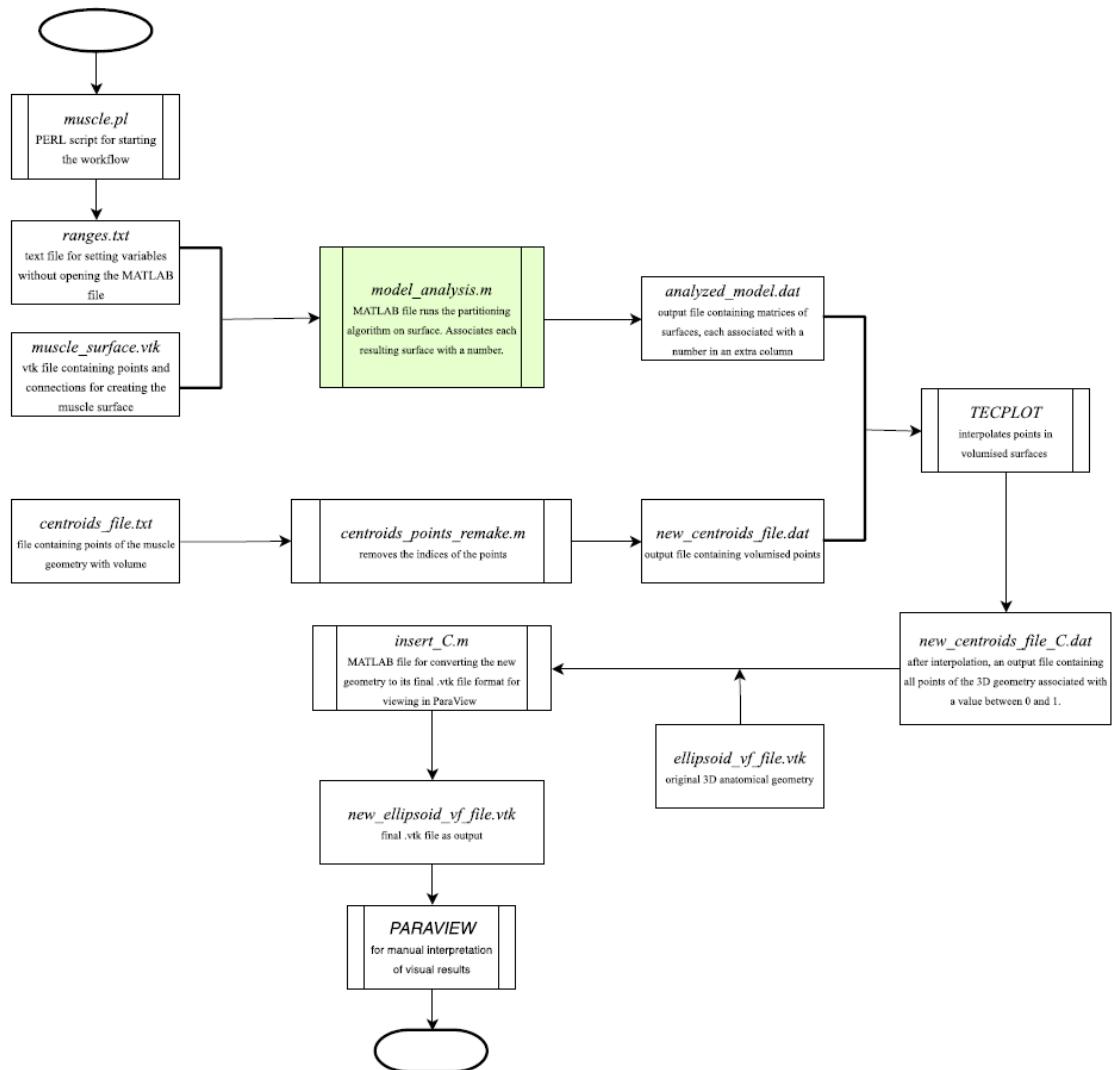


**Figure 7.5:** A flowchart, describing the methods employed for generating volume fraction demarcation, for the gastrocnemius muscle.

### 7. Combining with 3D anatomical geometry mesh:

Here in the *new\_centroids\_file\_C.dat*, is combined with the original volume mesh of the gastrocnemius muscle and provided as an input to the *insert\_C.m*, a MATLAB script, which takes in the volume fractions output from *new\_centroids\_file\_C.dat* and interpolates it into the gastrocnemius mesh (*ellipsoid\_vf\_file.vtk*) to produce the final vtk file which is ready to be used for defining material properties in our finite element simulations, with the muscle, tendon and aponeurosis region defined.

### 8. PARAVIEW:

Paraview is utilised to visualise the output of the workflow and take corrective action if any discrepancy is encountered.

### 7.3 Volume Fractions Assignment Algorithm

The volume fractions are defined with parameters  $f_M$  &  $f_T$  which relate to the muscle region volume fraction and tendon region volume fraction respectively. It is assumed that  $f_T(x) + f_M(x) = 1$ . Therefore, this implies,

$$f_M(x) = 1 - f_T(x) \quad 0 \leq f_T(x) \leq 1 \quad (7.1)$$

Using this relation, the volume fractions throughout the skeletal muscle can be defined with respect to one variable i.e. ( $f_T$ ). The Figure[7.6], shows the end-result on our volumetric mesh

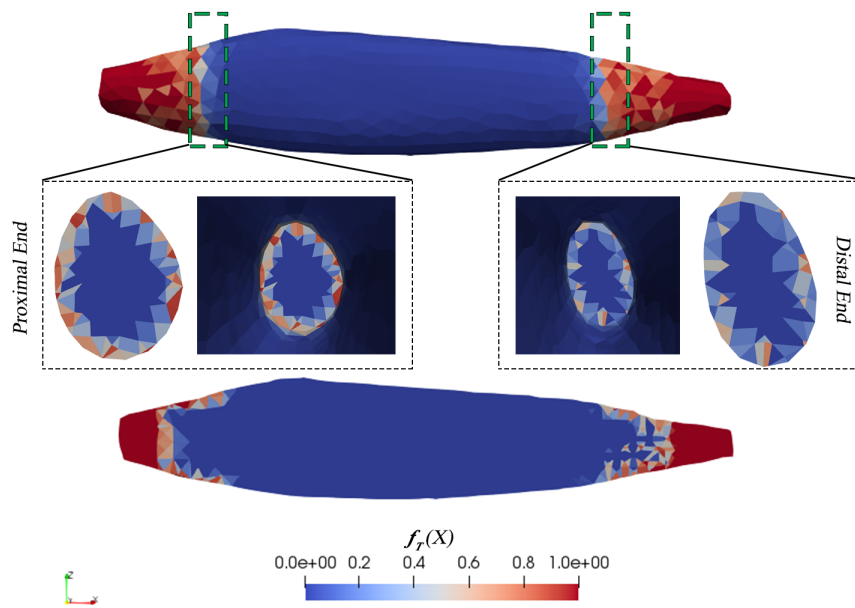


**Figure 7.6:** The assignment of  $f_T(X)$  based on the Volume Fraction Assignment Algorithm (Civisilli (2019)), where  $f_T(X)=1.0$  indicates tendon region (TR),  $f_T(X) = 0$  indicates muscle region (MR) and  $f_T(X)$  values between 0-1 are interpolated to indicate the tendinous aponeurosis region (AR). (**Top**): shows the X-Z view of the gastrocnemius muscle mesh and (**Bottom**): displays the sliced X-Z view clearly displaying the different regions. (**Centre**): The slices show a cross-sectional view in the Y-Z plane showing the sliced-through variation in the  $f_T(X)$  parameter indicating depth-wise assignment.

indicating the  $f_T$  values assigned to demarcate tendinous regions to muscle regions. This is achieved by ascribing values from 0 to 1 for the definition of a muscle region - 0, aponeurosis region - [0-1] and tendon region - 1.

The algorithm for defining the volume fractions in the MR, TR and AR is described below (The code can be found in Appendix B).

1. The inputs for the script *model\_analysis.m* include point information i.e. spatial positions for each point with the x, y, z co-ordinates, and connectivity matrix describing the points associated with each surface cell (i.e. each triangle in the .stl surface mesh). The connectivity matrix is formatted as:

$$e_{no} \quad | \quad n_1 \quad | \quad n_2 \quad | \quad n_3$$

where,

$e_{no}$  - is the cell number

$n_x$ ;  $x = 1, 2, 3$  is the point number.

2. Points co-ordinate list containing co-ordinate information of each vertex on the surface geometry is formatted as:

$$x_i, \quad y_i, \quad z_i \quad i = 1, 2, \dots, n$$

3. The normal for each cell is calculated by taking the cross-product of any two sides as vectors.
4. Each point has a normal associated based on the average of the normals of each cell it is connected with.
5. After the calculation of weighted normals for each point, they are projected inwards in the direction of their normals. This is formulated as follows:

$$\begin{aligned} x'_i &= x_i + h_{apo} \quad x_n \\ y'_i &= y_i + h_{apo} \quad y_n \\ z'_i &= z_i + h_{apo} \quad z_n \end{aligned} \tag{7.2}$$

$$\begin{aligned} x''_i &= x'_i + h_{trans} \quad x_n \\ y''_i &= y'_i + h_{trans} \quad y_n \\ z''_i &= z'_i + h_{trans} \quad z_n \end{aligned} \tag{7.3}$$

where,  $(x'_i, y'_i, z'_i)$  is the point projected inwards from the initial point on the surface mesh  $(x, y, z)$ , say surface  $a$  and  $(x''_i, y''_i, z''_i)$  is the point on the second projection from surface  $a$  to surface  $b$ . The variables  $h_{apo}$ ,  $h_{trans}$ , are the thickness between the outer surface and surface a, and, surface a and b respectively. The averaged normal associated with the point  $(x, y, z)$  is denoted as  $(x_n, y_n, z_n)$ .

6. Repeating two steps above (Steps 4 and 5), till all points are projected inwards to obtain a new surface. Patch command in matlab utilised for visualisation of new surfaces. Figure [7.7] depicts these surfaces.

7. An output file named `analyzed_model.dat` is produced, which contains matrices of the surface data i.e. points and cells. An additional column is associated with each cell, with a value defining the surface it belongs to.

The co-ordinates associated with centroids for all three layers (outer, middle and inner) surface mesh faces, are stored in the `new_file_centroids.dat` file. The regions for muscle tendon and aponeurosis are defined w.r.t demarcations on the long-axis of the muscle and a linear interpolation scheme ascribes volume fractions values between the muscle and tendon region from 0 - 1, muscle regions as 0 and tendon regions as (by means of Equation[7.1])1. These are finally assigned to centroids in the finite element mesh, using the `insert_C.m` MATLAB script. An in depth explanation about the ascription and different schemes for interpolation to define regions of linear and nonlinear shapes can be found in the MSc theses (Civisilli (2019), Harms (2020)). Further this surface partitioning algorithm is provided along with a centroids data file from the volumetric mesh of the gastrocnemius to a Tecplot macro (Appendix B) which produces the final output file for definition of the various regions with respective volume fraction values (see Figure [7.6]).



**Figure 7.7:** Figure depicting the surfaces obtained after partitioning algorithm. The outer surface is shown in lightest shade of red, surface a i.e. the middle layer is shown with light red and finally the inner surface b is shown with a solid color red.

### 7.3.1 Strain Energy Function

The material model available in ANSYS® Mechanical APDL material library i.e. an exponential hyperelastic fibre-reinforced material model (see Section[5.0.1]), is employed to model the gastrocnemius skeletal muscle. The general form of the strain energy function adapted for skeletal muscle representation is shown below,

$$\Psi_{\text{gastro}} = \mathbf{f}_T(x)\tilde{\Psi}_T + \mathbf{f}_M(x)\tilde{\Psi}_M \quad (7.4)$$

The parameters  $\mathbf{f}_T(x)$  and  $\mathbf{f}_M(x)$ , are introduced to represent the volume fractions of the tendinous region (TR) and for the muscular region respectively (MR) (see Section[7.2.2]). The strain energy function therefore in its expanded form utilising the  $\mathbf{f}_T(x)$  volume fraction parameter is,

$$\begin{aligned} \Psi_{\text{gastro}} = \mathbf{f}_T(x) & \left[ \frac{c^T}{2}(I_1 - 3) + \frac{k_1^T}{2k_2^T} \{ \exp[k_2^T(I_6 - 1)^2] - 1 \} \right] \\ & + (1 - \mathbf{f}_T(x)) \left[ \frac{c^M}{2}(I_1 - 3) + \frac{k_1^M}{2k_2^M} \{ \exp[k_2^M(I_4 - 1)^2] - 1 \} \right] \end{aligned} \quad (7.5)$$

As seen in Chapter [6], the strain energy formulation for the anisotropic components are modified as follows, with details provided in Appendix [C]:

$$\tilde{\Psi}_{C,x} = \frac{k_1^j}{2k_2^j} [ \exp \{ k_2^j (I_x - 1)^2 \} - 1 ] \rightarrow \tilde{\Psi}_{C,x}^{\text{mod}} = \tilde{k} [ \exp \{ k_2^j (I_x - 1)^2 \} - 1 ] \quad (7.6)$$

where,  $x = I_4, I_6$ ,  $j = T, M$  as per the appropriate identifiers seen in the anisotropic component of Equation [7.5].

### 7.3.2 Fibre Orientation

The fibre directions of the muscle fibres and tendon fibres are assumed to be directed along the major axis of the muscle (Figure[7.8]). Though anatomical fibre directions are not simply a directed along one axis, it is assumed to be in the axial direction to simplify our assumptions and understand the effects in the remodelling simulation. It provides a first step to understanding the changes due to over-stretch and could thereafter be defined w.r.t anatomical origins to better approximate the results.

### 7.3.3 Remodelling Assumption

The Cauchy stress experienced by the muscle and tendon fibres, derived from differentiating Equation [7.5] w.r.t  $I_4, I_6$  for muscle and tendon respectively is given as:

$$\begin{aligned} \sigma_M(\mathbf{X}, k_1^M, k_2^M, I_4, t) &= 2 I_4 k_1^M (I_4 - 1) e^{(k_2^M [I_4 - 1]^2)} \\ \sigma_T(\mathbf{X}, k_1^T, k_2^T, I_6, t) &= 2 I_6 k_1^T (I_6 - 1) e^{(k_2^T [I_6 - 1]^2)} \end{aligned} \quad (7.7)$$

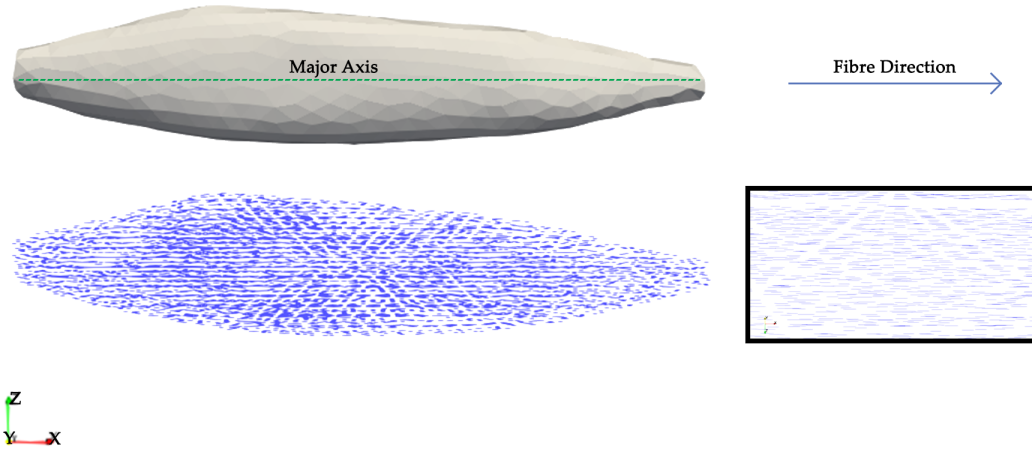


**Figure 7.8:** The prescribed fibre directions for both the muscle and tendon fibres, i.e. in the direction of the major axis of the gastrocnemius muscle.

On experiencing an extension due to the prescribed displacement boundary conditions, the muscle and tendon fibres experience an increase in the experienced Cauchy Stress. Equations [7.8, 7.9], are employed in order to remodel the fibres. On observing the equations, it can be seen the material parameters ( $k_2^M, k_2^T$ ) vary negatively based on the differences between the current Cauchy stress ( $\sigma_M(\mathbf{X}, t), \sigma_T(\mathbf{X}, t)$ , abbreviated) in the muscle and tendon at time  $t$  and the homoeostatic Cauchy Stress ( $\sigma_{MH}(\mathbf{X}, t), \sigma_{TH}(\mathbf{X}, t)$ ). Therefore, the material parameters ( $k_2^M, k_2^T$ ) remodel in an attempt to restore the change in the Cauchy stresses experienced by the muscle, tendon fibres to a preferred homoeostatic Cauchy stress values ( $\sigma_{TH}, \sigma_{MH}$ , in our model calibrated at  $t=0$ ).

$$\frac{dk_2^M}{dt} = -\beta_M k_2^M \left[ \frac{\sigma_M(\mathbf{X}, k_1^M, k_2^M, I_4, t) - \sigma_{MH}(\mathbf{X}, k_1^M, k_2^M, I_4, t)}{\sigma_{MH}(\mathbf{X}, k_1^M, k_2^M, I_4, t)} \right] \quad (7.8)$$

$$\frac{dk_2^T}{dt} = -\beta_T k_2^T \left[ \frac{\sigma_T(\mathbf{X}, k_1^T, k_2^T, I_6, t) - \sigma_{TH}(\mathbf{X}, k_1^T, k_2^T, I_6, t)}{\sigma_{TH}(\mathbf{X}, k_1^T, k_2^T, I_6, t)} \right] \quad (7.9)$$

### 7.3.4 Boundary Conditions

The gastrocnemius proximal end (closer to the knee-cap) is fixed in all directions, and has no movement in any degree of freedom. The distal end (closer to the Achilles Tendon), is pulled in the positive x-direction (Figure[7.9]) from an initial extension of 7.25 mm i.e. an initial stretch of  $\lambda_i = \frac{145+7.25}{145} = 1.05$  to a maximum stretch of  $\lambda_f = \frac{145+14.5}{145} = 1.1$  over a small period of time given with an initial time  $t_i$  and a final time  $t_f$ , at which  $\lambda_f$  is reached and sustained till the end of the simulation.

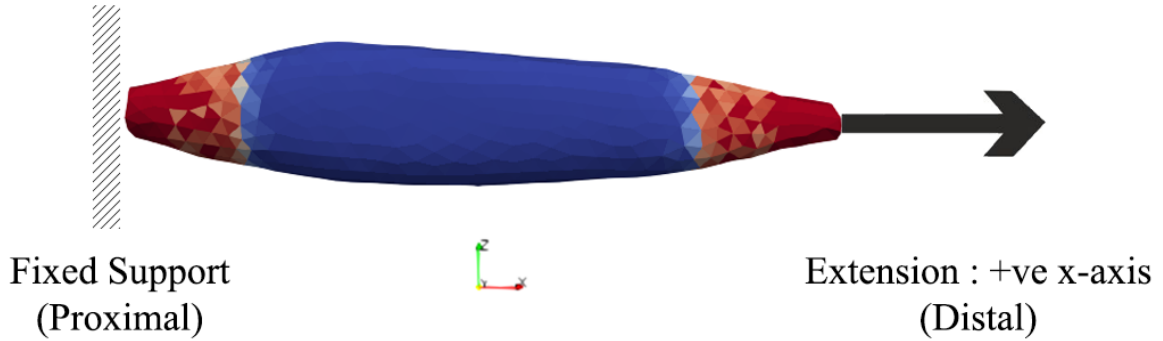


**Figure 7.9:** The prescribed boundary conditions for extension of the gastrocnemius muscle, the proximal end is fixed in all directions while the distal end is allowed to be free in all degrees of freedom and an extension is applied in the positive x-direction over time with a ramp function (from a  $\lambda_i = 1.05$  to  $\lambda_f = 1.1$ ).

#### 7.3.4.1 Single-Step Displacement Function

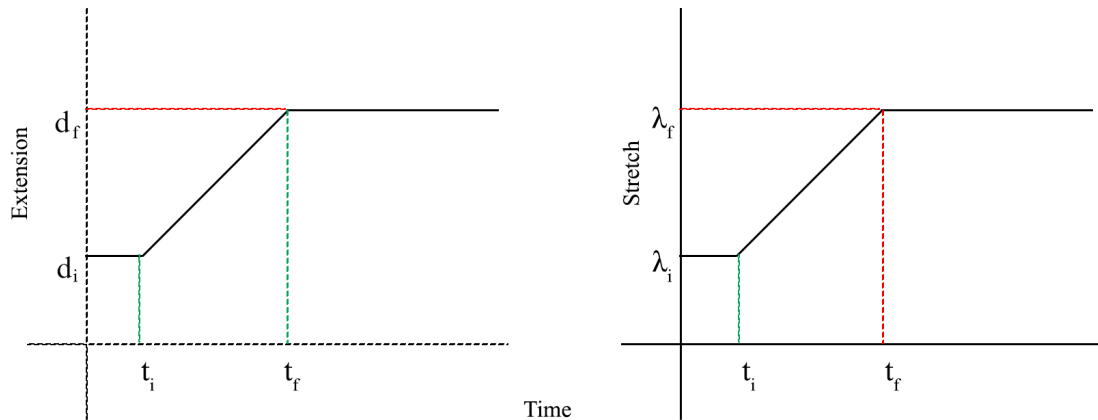


**Figure 7.10:** The extension boundary condition, for stretching the muscle beyond the initial value ( $\lambda_i$ ) to a maximum stretch ( $\lambda_f$ ) from an initial time  $t_i$  to a final time point  $t_f$  is based on a linear ramp function shown.

The increase in the extension i.e. displacement of the distal end is carried out using a ramp function. Consider an initial time  $t_i$  at which the original extension/ displacement ( $d_i$ ) or stretch ( $\lambda_i$ ) is increased over a period of time to a maximum value ( $d_f, \lambda_f$ ) at a final time ( $t_f$ ).

1. The slope of the ramp function, depicted as an extension vs time graph (please note stretch follows the same graph of extension, with only difference is by definition, as the addition of the muscle length to the extension divided by original muscle length) is given as.

$$m = \frac{d_f - d_i}{t_f - t_i} \quad (7.10)$$

2. The displacement ( $d_t$ ) or stretch ( $\lambda_t$ ) at a given time  $t$  is given as:

$$d(t) = m(t_f - t_i) + d_i; \quad \text{or} \quad \lambda(t) = m(\lambda_f - \lambda_i) + d_i \quad (7.11)$$

In this simulation the units of time are taken to be steps i.e. each simulation cycle. Therefore, it is converted into days for interpretation of the results and is obtained as: current step ( $n_c \times dt$ ), where  $n_c$  is the current step and  $dt$  is the ratio of time and the number of steps ( $t/n$ ).

## 7.4 Parameter Set up

The Table [7.1], lists the material parameters used for the muscle and tendon as per Equation[7.5] in the upper half of the table. The lower half of the table details the time scheme used for the simulation i.e. the number of days considered, number of simulation steps and calculation of  $dt$ , and terminally the displacement boundary conditions at the distal end to simulate extension over a period of time from an initial stretch  $\lambda_i$  at an initial time  $t_i$  to a maximum final stretch  $\lambda_f$  at a terminal time  $t_f$ .

Parameter	Value	Units
$c^M$	0.01	MPa
$c^T$	1	MPa
$k_1^M$	0.001	MPa
$k_1^T$	1	MPa
$k_2^M$	0.5	-
$k_2^T$	5	-
Time (t)	10	Days
Steps (n)	20	-
dt (t/n)	0.5	-
$\lambda_i$	1.05	-
$\lambda_f$	1.1	-
$d_i$	7.25	mm
$d_t$	14.5	mm
$t_i$	t = 2	days
$t_f$	t = 3	days

**Table 7.1:** Material parameter values assigned for the muscle (superscript  $M$ ) and tendon (superscript  $T$ ) for representing a fibre reinforced hyperelastic material, based on the aponeurosis algorithm (Civisilli (2019)) for the volume fractions.

The material parameters ascribed to the muscle ( $c^M, k_1^M, k_2^M$ ), and tendon ( $c^T, k_1^T, k_2^T$ ) are assigned on the basis of tendon stiffness being greater than muscle stiffness. For a comprehensive list of pertinent material parameter values based on available models. Given that these parameters are not directly measurable physically due to its general fibre-reinforced formulation (Equation[7.5]), the values selected can be used to understand qualitative changes in the tissue properties as a consequence of remodelling.

### 7.4.1 Rationale for Parameter Values

Though as stated above qualitative changes are the focus, the values chosen for the stiffness are purely for testing the remodelling hypotheses outcome, given the stiffness of the tendon is greater than the muscle. The combination of values for  $c^M$ ,  $c^T$ ,  $k_1^{TM}$ ,  $k_1^T$ ,  $k_2^M$  and  $k_2^T$  are chosen based on a few simulation runs and obtaining results which can be clearly understood for the muscle and tendon remodelling. The rates have been adjusted to achieve remodelling to homoeostatic stresses in tendons and muscles over a small period of time to test the remodelling scheme i.e 10 days. In essence, the remodelling of skeletal muscle, tendon and aponeurosis regions in the gastrocnemius muscle is simulated to understand the consequences of stretching. Test values utilised for material parameters and rate constants are reflective of the consideration to test the soft tissue growth and remodelling framework extension for skeletal muscles. Validation techniques and material tuning are important for application to real world scenarios and are discussed in Section [7.7].

## 7.5 Results

To understand the model behaviour for remodelling of skeletal muscle to increasing stretch i.e. stretching the muscle from  $\lambda_0 = 1.05$  to  $\lambda_F = 1.1$  from  $t=1$  days to  $t=3$  days and maintain the stretch value till the end of the simulation i.e.  $t=10$  days.

In terms of analysing the distribution of resultant quantities, three regions as described in Section [7.3] are considered. These regions are marked in the Figure [7.11], shown as the Tendon Region (TR), Aponeurosis Region (AR) and Muscle Region (MR).

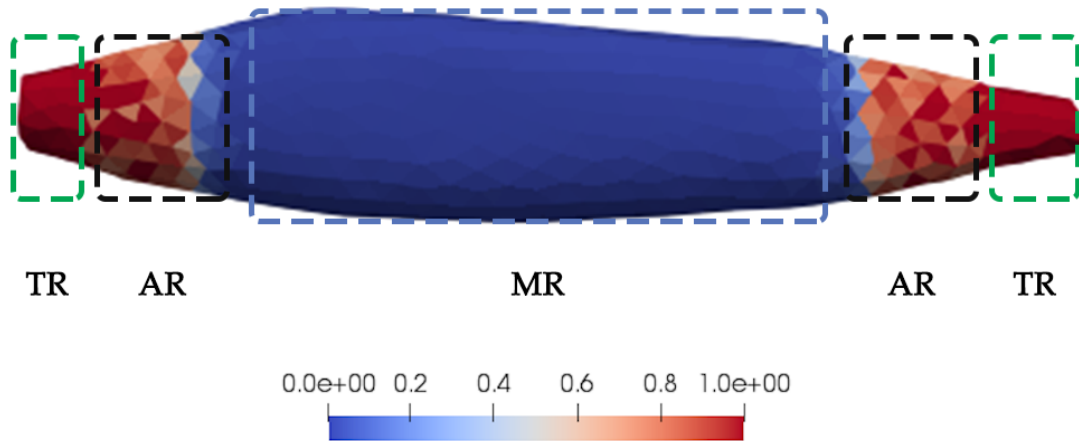


**Figure 7.11:** The regions demarcated based on the  $f_T$  volume fraction variable and the volume fraction assignment algorithm (Appendix B). The regions are abbreviated as: (a) Tendon Region (TR), (b) Aponeurosis Region and (c) Muscle Region (MR).

A test case scenario and another scenario with four different cases are considered. They are depicted in the following sections.

## 7.6 Test Case

Initially a test case is considered, where the tendon and muscle remodel with the same rate constant i.e.  $\beta_M = \beta_T = 1.0$ .

### 7.6.1 Cross-sectional Views of Gastrocnemius Muscle

The cross-sectional results are displayed via a slice through the X-Z plane, i.e. a Y-normal to show the variations in mechanical quantities as well as material parameters for the gastrocnemius skeletal muscle. These are followed by a plot showing the averaged values for the respective quantities. Additionally, any difference in the averaged graph and the cross-sectional view, is because the average is taken across all the elements and therefore includes the peak and valley values throughout the geometry. However, the averaged values provide an understanding about the quantity variations throughout the simulation succinctly and help understand model behaviour. In short, the cross-sectional results provide spatial information and the averaged results with an overall change in the requisite quantity throughout the gastrocnemius muscle.

The time periods of  $t = 1$  days,  $t = 3$  days and  $t = 10$  days are considered, as the initial homeostatic values are calibrated at  $t = 0$  days with an initial displacement at the free end of 7.25 mm i.e. a stretch of  $\lambda = 1.05$  for the gastrocnemius muscle with length 145 mm, the muscle is stretched with a maximum displacement of 14.25 at  $t = 3$  days to  $\lambda = 1.1$  and held to observe remodelling of the muscle, tendon fibres by the terminal time point of  $t = 10$  days. An important point to note, is it is assumed that the homeostatic configuration for Cauchy stress values and material parameters to be at  $t=0$  days, which can be treated as a control case pre-stretching of the gastrocnemius. The values are same at  $t=1$  days as the muscle is stretched post  $t=1$  days and remodelled results are obtained.

### 7.6.1.1 Fibre Stretch Invariants values

The fibre stretch invariant for  $I_4$  is shown in Figure [7.12], which relates to the stretch experienced in the Muscle Region, however since extension based boundary conditions are applied, it is reflective of changes in tendon region as well.

**Muscle Region** At  $t=1$  day, the stretches in the MR range from  $\approx 1.1$  to  $\approx 1.35$  and on  $t=3$  days an due to increase in stretch from  $\lambda_0 = 1.05$  to  $\lambda_f = 1.1$  for the entire gastrocnemius muscle, an  $I_4$  value of  $\approx 1.16$  to  $\approx 1.3$  is observed in the MR, with an increased variation upto  $\approx 1.7$  on the distal end.

**Tendon Region** In the TR, a stretch invariant value of  $\approx 1.0$  to  $1.115$  is observed throughout the simulation from  $t=1$  day to  $t=10$  days.

**Aponeurosis Region** In the AR, the  $I_4$  values range from  $\approx 1.0$  to  $\approx 1.17$  at  $t=1$  day. These values increase to a range of  $\approx 1.03$  to  $1.24$  at  $t=3$  days and remain constant till the end of the simulation i.e. at  $t=10$  days.

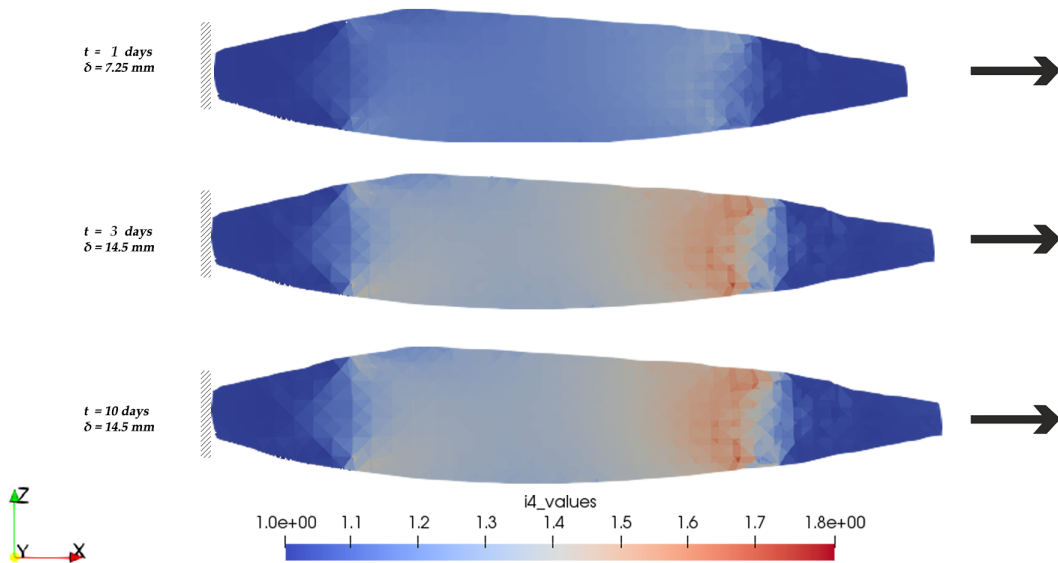


**Figure 7.12:** The stretch invariant  $I_4$  is shown, where it ranges from 1.0 to  $\approx 1.35$  at  $t=1$  day to a range of  $\approx 1.0$  to  $1.7$  at  $t=3$  days, owing to the prescribed stretching of the gastrocnemius muscle. The values thereon remain constant till  $t=10$  days indicating a sustained stretch of the gastrocnemius muscle.

### Averaged $I_4$ Values

The averaged  $I_4$  values i.e. muscle stretch invariant are shown in Figure[7.13]. Given that the gastrocnemius muscle is stretched using a prescribed value the values for  $I_6$  follow the same trend as  $I_4$ . An average  $I_4$  of 1.137 is observed till  $t=1$  day and rises upto 1.286 at  $t=3$ days after which a slight decrease is observed upto a value of  $\approx 1.284$  from  $t=4$  days to  $t=10$  days.

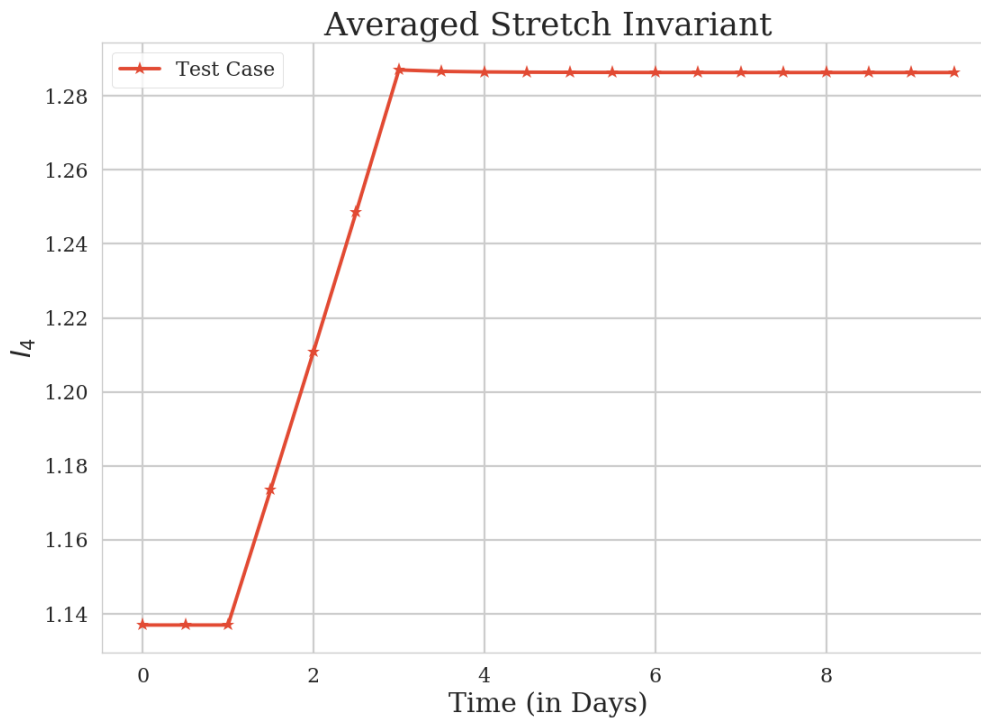


**Figure 7.13:** The prescribed stretch to the gastrocnemius muscle from  $t=2$  days to  $t=3$  days from 1.05 to 1.1 is reflected in the fibre stretch invariant  $I_4$ , from  $\approx 1.116$  to  $\approx 1.246$  between the same time steps and remains constant till the end of the simulation.

### 7.6.1.2 $k_2^M$ values

The  $k_2^M$  values across the muscle cross-section are displayed in the Figure [7.14].

#### **Muscle Region**

Starting with a uniform distribution of 0.5 at  $t=2$  days i.e. value prior stretching of the muscle i.e.  $\lambda_0 = 1.05$ . At  $t=3$  days during maximal stretch  $\lambda_f = 1.1$  the remodelled  $k_2^M$  values observe a reduction to a range of  $\approx 0.26$  to  $0.325$  for the muscle following the remodelling Equation[7.8]. At  $t=10$  days, the values further decrease to a range of  $\approx 0.018$  to  $0.25$  in the muscle region.

#### **Aponeurosis Region**

The aponeurosis region observes a decrease in  $k_2^M$  from 0.5 at  $t=2$  days, to a range of 0.21 to 0.36 at  $t=3$  days to a final range of  $\approx 0.18$  to  $0.3$  at  $t=10$  days.

#### **Tendon Region**

Since the  $k_2^M$  parameter is associated with the muscle and the  $k_2^T$  value is 5, there is no change in the tendinous region.

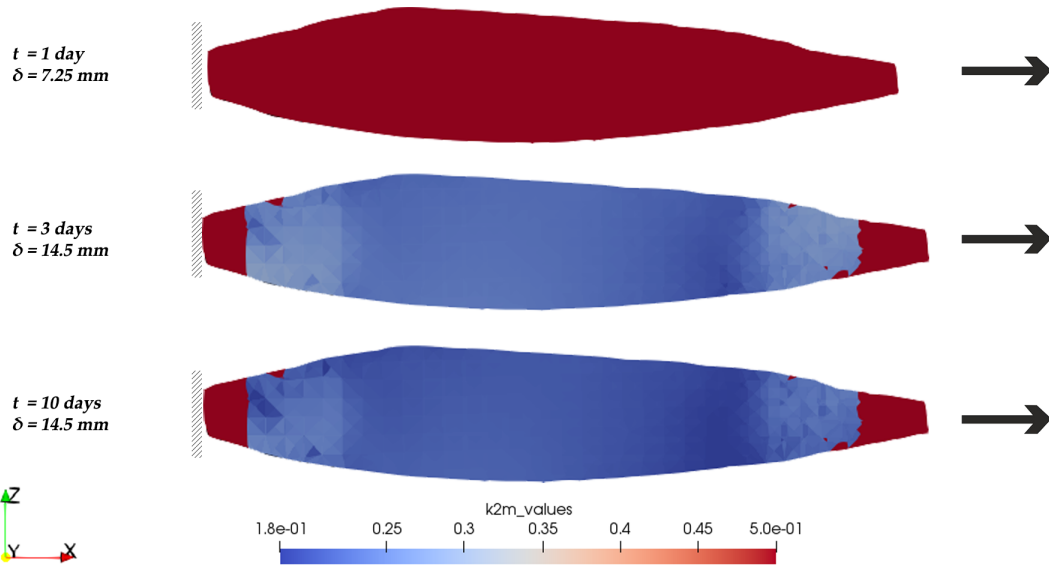


**Figure 7.14:** The  $k_2^M$  values are displayed, having a value of 0.5  $t=2$  days with  $\lambda = 1.05$ . At  $t=3$  days, the  $k_2^M$  values reduce to a range of 0.26 to 0.325 for an increased stretch  $\lambda = 1.1$ . Terminally at  $t=10$  days,  $k_2^M$  values remodel and settle between a range value of  $\approx 0.18$  to 0.25.

**Averaged  $k_2^M$  Value**

Figure [7.15], shows the averaged value of  $k_2^M$ , ranging from a value of 0.5 at  $t=0$  days, maintained till  $t=1$  day and decreases upto a value of 0.234 at  $t=6$  days after which it stabilises around  $\approx 0.234$  till the end of the simulation at  $t=10$  days. The decline is in response to the Cauchy stress differences in the muscle as per Equation [7.8].  $k_2^M$  attains stability as seen in Figure[7.18].

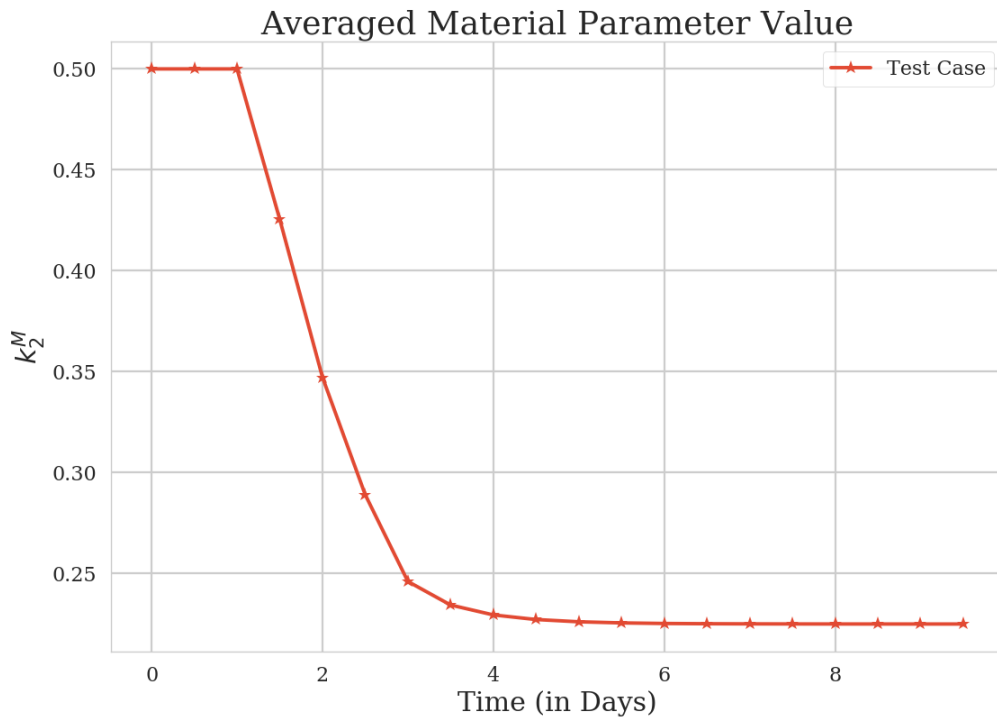


**Figure 7.15:** The averaged  $k_2^M$  value decreases from 0.5 at  $t=1$  day to about  $\approx 0.234$  at  $t=6$  days and stabilises till the end of the simulation at  $t=10$  days.

### 7.6.1.3 $k_2^T$ values

#### **Muscle Region**

Since the  $k_2^T$  parameter is associated with the tendon the value in the muscle region is neglected and does not undergo any changes.

#### **Tendon Region**

The  $k_2^T$  values are displayed in this Figure[7.16], starting with a uniform distribution of 5.0 at t=1 day i.e. value prior to stretching. At t=3 days during maximal stretch  $\lambda = 1.1$  the remodelled  $k_2^T$  values observe a reduction to a range of  $\approx 2.5$  to 3.4 for the tendon following the remodelling Equation[7.9]. At t=10 days, the values further decrease to a range of  $\approx 2.0$  to 2.4 in the tendon region.

#### **Aponeurosis Region**

The aponeurosis region observes a decrease in  $k_2^T$  from 5 at t=0 days, to a range of  $\approx 2.6$  to 3.15 at t=3 days to a final range of  $\approx 1.7$  to  $\approx 2.43$  at t=10 days.

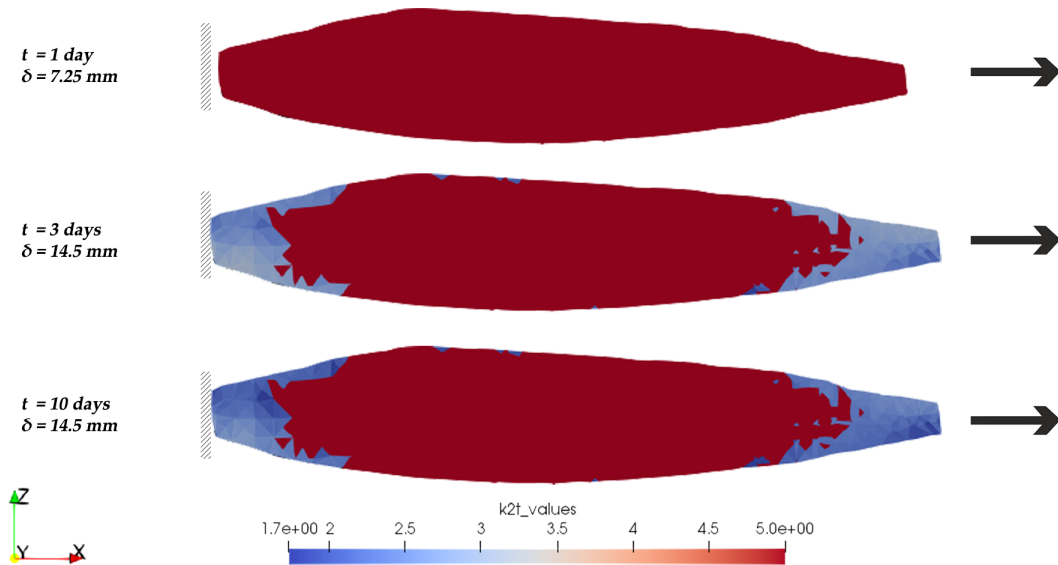


**Figure 7.16:** The  $k_2^T$  values are shown, having a uniform value of 1 at t=1 day with  $\lambda = 1.05$ . At t=3 days when the gastrocnemius is stretch to  $\lambda = 1.1$  the  $k_2^T$  values remodel to a range of  $\approx 2.5$  to 3.4 and terminally at t=10 days to a range of  $\approx 2.0$  to  $\approx 2.4$ .

**Averaged  $k_2^T$  Value**

Figure [7.17], shows the averaged value of  $k_2^T$ , (based on Equation[6.7]) where in a decrease is seen from  $t=1$  day, from a value of 5 with a declining trend upto a value of  $\approx 4.54$  at  $t=10$  days.

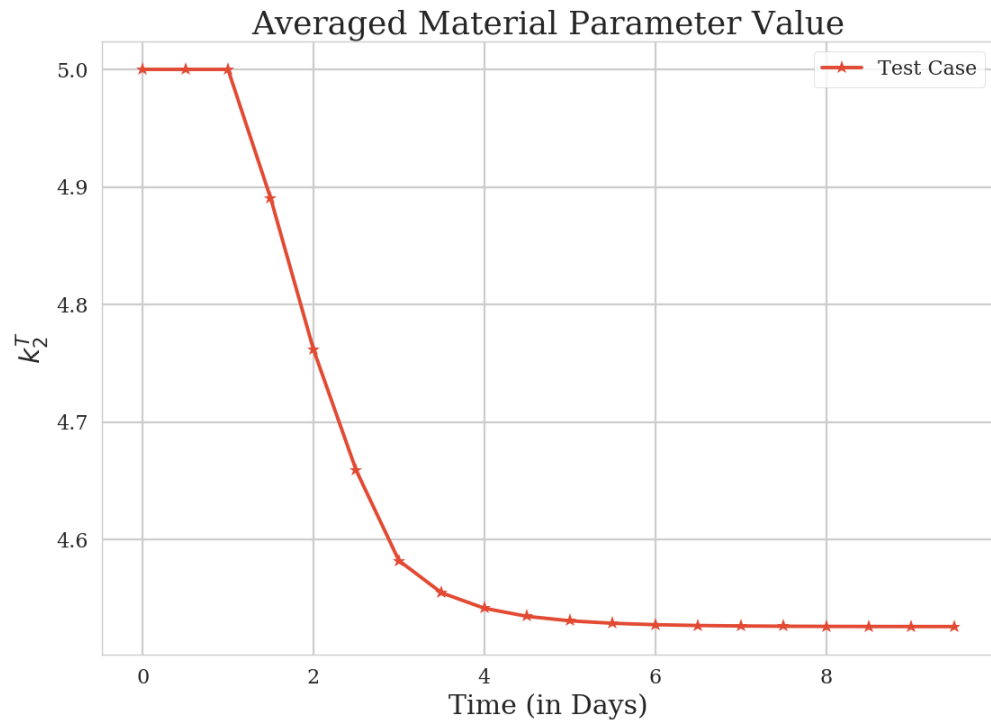


**Figure 7.17:** The averaged  $k_2^T$  value is shown. After an initial value of 5 at  $t=1$  days, it declines slowly compared to  $k_2^M$  (7.15), from 5 to a value of around  $\approx 4.54$  by the end of the simulation.

#### 7.6.1.4 $\sigma_M^{diff}$ values

##### ***Muscle Region***

The difference between the Cauchy stress levels from the initial homeostatic Cauchy stress (calibrated at  $t=0$  in our model) for muscle region is displayed in this Figure[7.18], facilitating the remodelling laws, as seen in Equation[7.8]. At  $t=1$  day, there is a difference of 0, given it is in the pre-stretch phase. There is a vast difference observed at maximum stretch of the gastrocnemius muscle i.e.  $\lambda = 1.1$  at  $t=3$  days, with a value of ranging from  $\approx 0.25$  to  $0.43$ , accounting for the proximal and the distal end of the gastrocnemius muscle. Post remodelling at a sustained stretch of  $\lambda = 1.1$  until  $t=10$  days the difference in the muscle region Cauchy stress values reduce to 0, indicating the return of the muscle Cauchy stress to homeostasis.

##### ***Aponeurosis Region***

The aponeurosis region observes a similar trend upto  $t=3$  days the difference is between  $\approx 0.25$  to  $0.38$ . At  $t=10$  days, the stress difference being 0 indicates homeostatic levels of muscle Cauchy stress are region.

##### ***Tendon Region***

The Cauchy stress difference in the tendinous region are 0 as muscle Cauchy stress differences are shown.

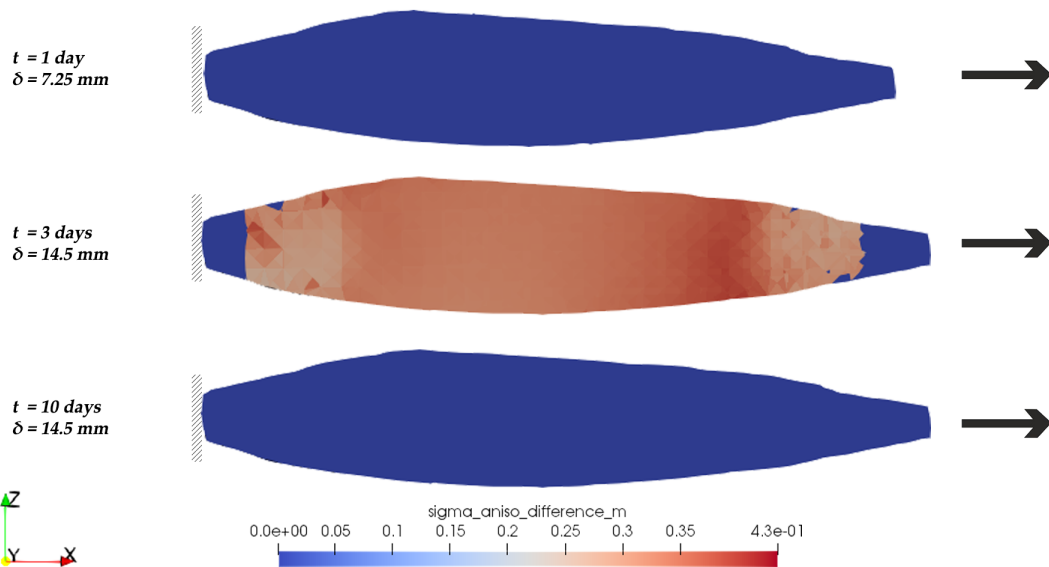


**Figure 7.18:** The difference between the muscle region Cauchy stress at a given time  $t$  and the Cauchy stress at  $t=1$  day i.e. before stretching the muscle, is shown. Initially at  $t=1$  days  $\lambda = 1.05$  and therefore there is no difference between the stress levels from  $t=0$  days. However, a maximum difference of  $\approx 0.25$  to  $0.43$  is seen at  $t=3$  post stretching to  $\lambda = 1.1$ . Terminally the difference is 0 at  $t=10$  days throughout the gastrocnemius muscle.

**Averaged  $\sigma_M^{diff}$  Values**

The averaged difference in the muscle Cauchy stress from the current time  $t$  in (days) to the time step  $t=0$  days is plotted in Figure[7.19]. It is observed the difference increases from  $t=1$  days from 0.0 to 0.356 at  $t=2$  days, finally going back to 0.0 after  $t = 6$  days i.e. the stress levels in the muscle fibres stabilise. Remodelling of material parameter  $k_2^M$  aims to maintain a preferred state of muscle fibre stress and it successful in this model as the stress stabilises after  $t=6.5$ days till the end of the simulation i.e.  $t=10$  days.

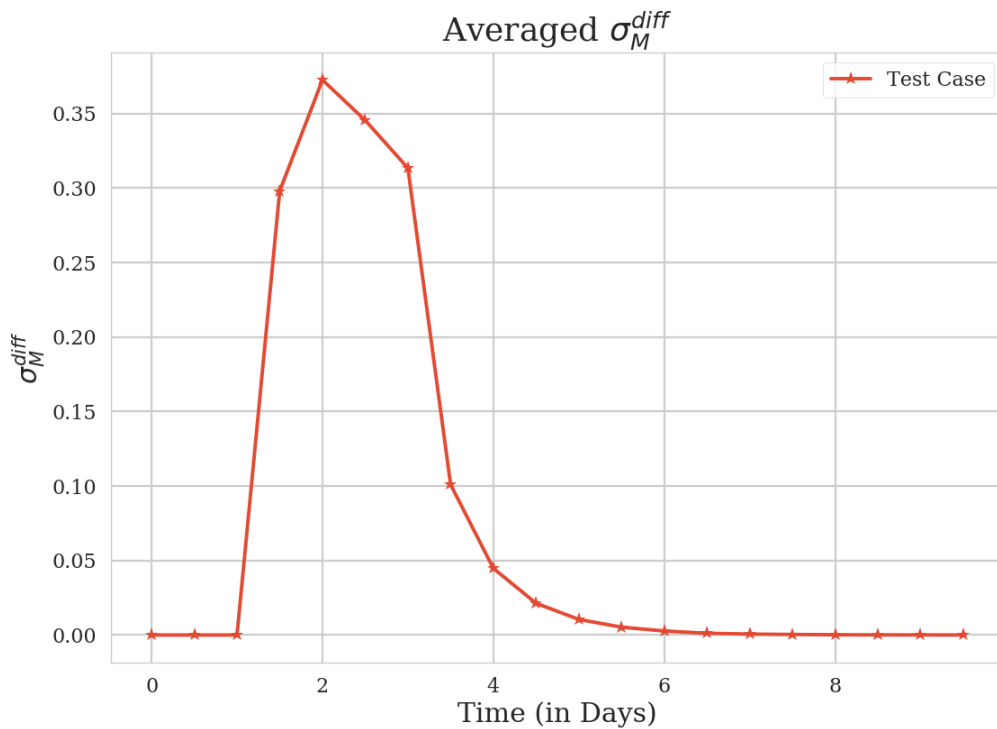


**Figure 7.19:** The muscle Cauchy stress difference is shown between stress values at time  $t$  days to time  $t=0$  days, initial difference increases at  $t= 1.0$  days, peaking at 0.356 at  $t = 2$  days and thereafter a downward trend is seen until  $t=6$  days after which the difference remains at 0.0 till the end of the simulation.

### 7.6.1.5 $\sigma_T^{diff}$ values

#### **Muscle Region**

Since the tendon Cauchy Stress difference are described, the Cauchy stress difference experienced by the muscle is not displayed.

#### **Tendon Region**

The difference between the tendon Cauchy stress values from an initial homeostatic value (calibrated at  $t=0$ ) to a current time  $t$  is shown in Figure[7.20]. The difference is 0 at  $t=1$  days, as the tendon is not yet experiencing a change in stretch. At  $t=3$  days when the gastrocnemius is stretched to a maximum of  $\lambda = 1.1$  from  $\lambda_0 = 1.05$ , the difference in the tendinous region is seen to reach values from  $\approx 0.23$  to  $\approx 0.341$ . At  $t=10$  days after remodelling under a sustained stretch, the stress difference return to 0 indicating the Tendon has remodelled and achieved the homeostatic level of Cauchy stress.

#### **Aponeurosis Region**

The aponeurosis region sees a difference change from 0 at  $t=0$  days to a range of  $\approx 0.3$  to  $0.44$  and at the termination of the simulation at  $t=10$  days the difference reaches a 0, as it returns to homeostatic Cauchy stress levels.

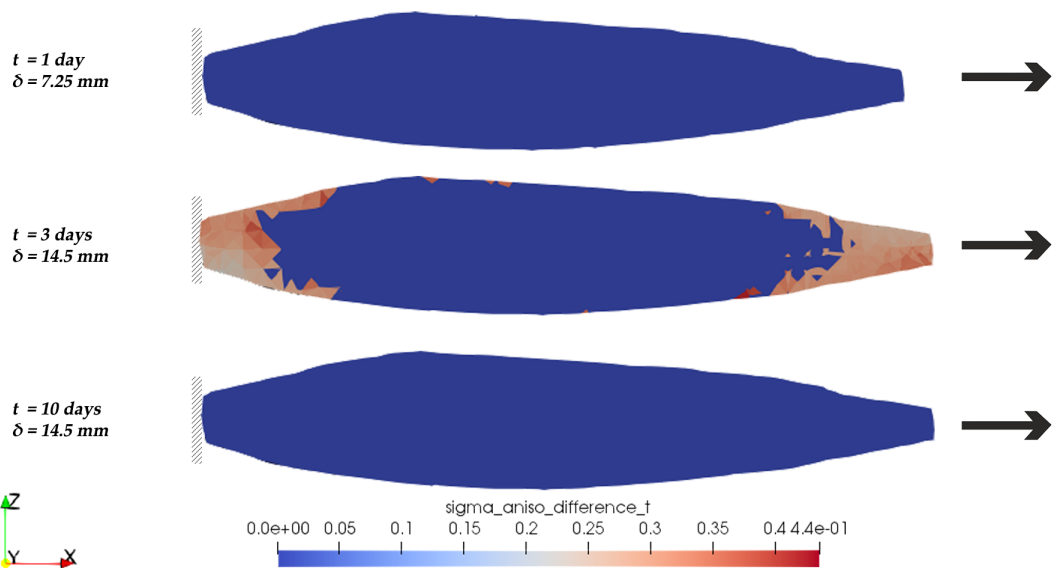


**Figure 7.20:** The Cauchy stress value differences for the tendon region are displayed here i.e. the values at time  $t=0$  days to  $t=0$  days. No difference is observed at  $t=1$  days due to the muscle not being stretched beyond  $\lambda_0$ . At  $t=3$  days the differences observed range from  $\approx 0.23$  to  $\approx 0.341$ . Terminally at  $t=10$  days, the stress differences are 0 across the gastrocnemius muscle.

**Averaged  $\sigma_T^{diff}$  Values**

The averaged difference in the tendon Cauchy stress from the current time  $t$  (in days) to the time step  $t=0$  days is plotted in Figure[7.21]. It is observed that the difference increases from  $t=1$  day from 0.0 to 0.591 at  $t=2$  steps, decreasing to 0 by the end of the simulation. The remodelling of the material parameter  $k_2^T$  aims to maintain a preferred state of tendon stress and stability is reached after  $t=6$  days.

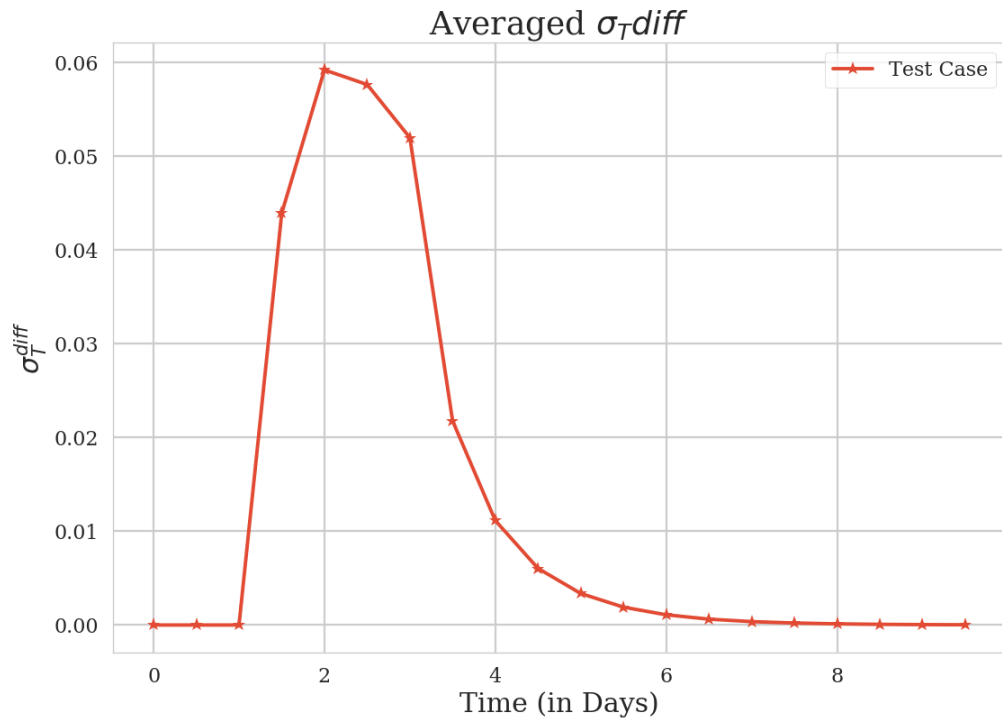


**Figure 7.21:** The averaged difference in tendon Cauchy stress levels from a time  $t$  days to  $t=0$  days. An increase from 0.0 to 0.591 is seen till  $t=2$  days and reaches an averaged value of 0 by  $t=10$  days.

### 7.6.2 Four Distinct Cases

Thereafter, after observing the variations in the remodelling of tendon and muscle independently, 3 cases are considered, with a combination of remodelling rate constants of unity as follows:

	$\beta_M$	$\beta_T$
Control Case	0.0	0.0
Case 1	1.0	0.0
Case 2	0.0	1.0
Case 3	1.0	1.0

Though Case 3 is similar to our test case in terms of equality in the rate constant parameters, we will decipher the differences it brings about in the remodelling of the tendon and muscle shedding light on the model's capabilities. An additional Control Case where no remodelling occurs either for tendon or muscle is considered for comparison. To understand the effect of the combination of rate constants  $\beta_M, \beta_T$ , we observe the averaged values to analyse the results.

#### 7.6.2.1 Averaged $I_4$

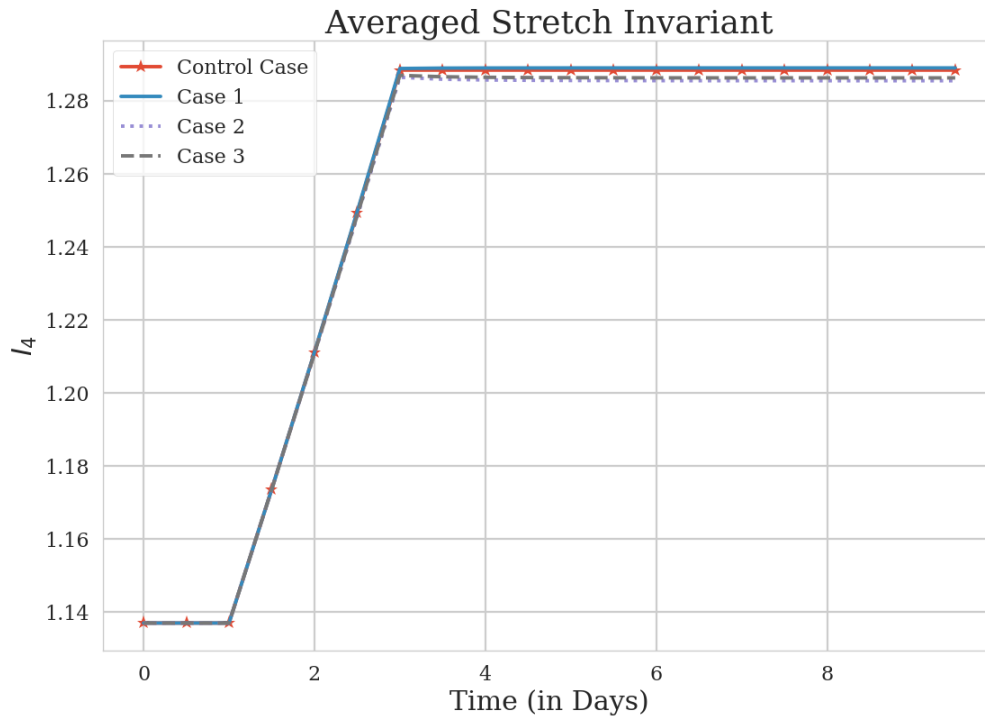


**Figure 7.22:** The averaged  $I_4, I_6$  values increase from  $\approx 1.137$  at  $t=1$  day to a maximum of 1.286 for the Control Case and Case 1, while a maximum of 1.284 is reached in Case 3 by  $t=3$  days. While consistent for other cases the value drops to 1.2832 and 1.2827 for Cases 2 and 3 till  $t=10$  days respectively.

The invariants of stretch  $I_4, I_6$  follow the same pattern as there is a fixed increase in  $\lambda$  from

$\lambda_0 = 1.05$  to  $\lambda_f = 1.1$  for the gastrocnemius muscle. The values increase from an initial 1.137 at  $t=1$  day to a maximum of 1.286 for the Control Case and Case 1 at  $t=3$  days. A maximum of 1.284 is reached in Cases 2 and 3 with a reduction to  $\approx 1.2832$  and 1.2827 respectively until the end of the simulation at  $t=10$  days.

### 7.6.2.2 Averaged $\sigma_M^{diff}$

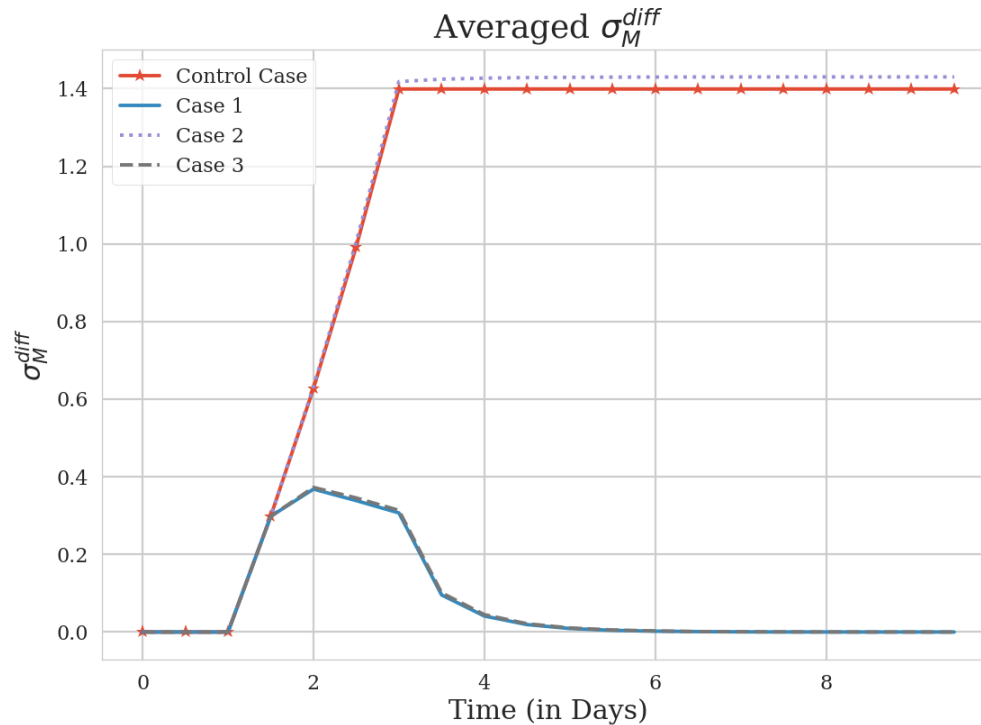


**Figure 7.23:** The averaged muscle Cauchy stress difference  $\sigma_M^{diff}$  are displayed. The control case rises from 0.0 to 1.4 from  $t=1$  day to  $t=3$  days, whereas over the same period Case 2 increases upto 1.41 and slightly increases to 1.42 after  $t=4$  days. Case 1 and Case 3 observe a similar rising pattern between  $t=1$  day to  $t=2$  days and a descent until  $t=6$  days and stabilises, with Case 3 stabilising at a slightly lesser rate.

The averaged difference in muscle Cauchy stress ( $\sigma_M^{diff}$ ) is plotted in Figure [7.23].

**Control Case:** The values are 0 until  $t=1$  day and rises to 1.4 at  $t=3$  days and remains constant till  $t=10$  days as no remodelling occurs ( $\beta_M = \beta_T = 1.0$ ).

**Case 1:** The averaged ( $\sigma_M^{diff}$ ) rises from 0.0 at  $t=1$  day to a maximum of  $\approx 0.37$  at  $t=2$  days before returning back to 0.0 at  $t=6$  days.

**Case 2:** The averaged ( $\sigma_M^{diff}$ ) increases from 0.0 at  $t=1$  day to a maximum of 1.41 at  $t=3$  days, slightly increasing till  $t=5$  days to a value of 1.42 and remains constant until  $t=10$  days. Here  $\beta_M = 0.0$

**Case 3:** The averaged ( $\sigma_M^{diff}$ ) rises from 0.0 at  $t=1$  day to a maximum of  $\approx 0.376$  at  $t=2$  days before

returning back to 0.0 at t=6 days, however the return is at a slightly slower rate than Case 1.

### 7.6.2.3 Averaged $\sigma_T^{diff}$

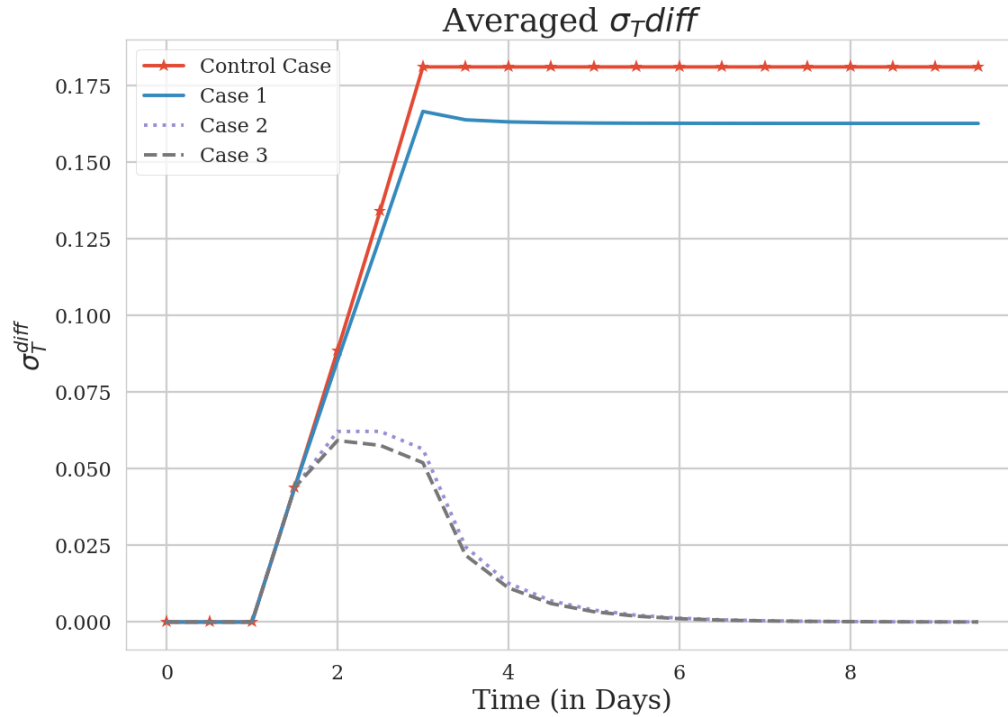


**Figure 7.24:** The averaged tendon Cauchy stress difference is shown, with the Control Case increasing from 0.0 to 0.182 at t=3 days. Case 1 rises in the same time period upto 0.167 and decreases slightly to 0.163 after t=4 days. Cases 2 and 3 observe a similar rise till t=2 days at  $\approx 0.0627$  and  $0.0624$  respectively, thereafter declining to stabilisation post t=6 days.

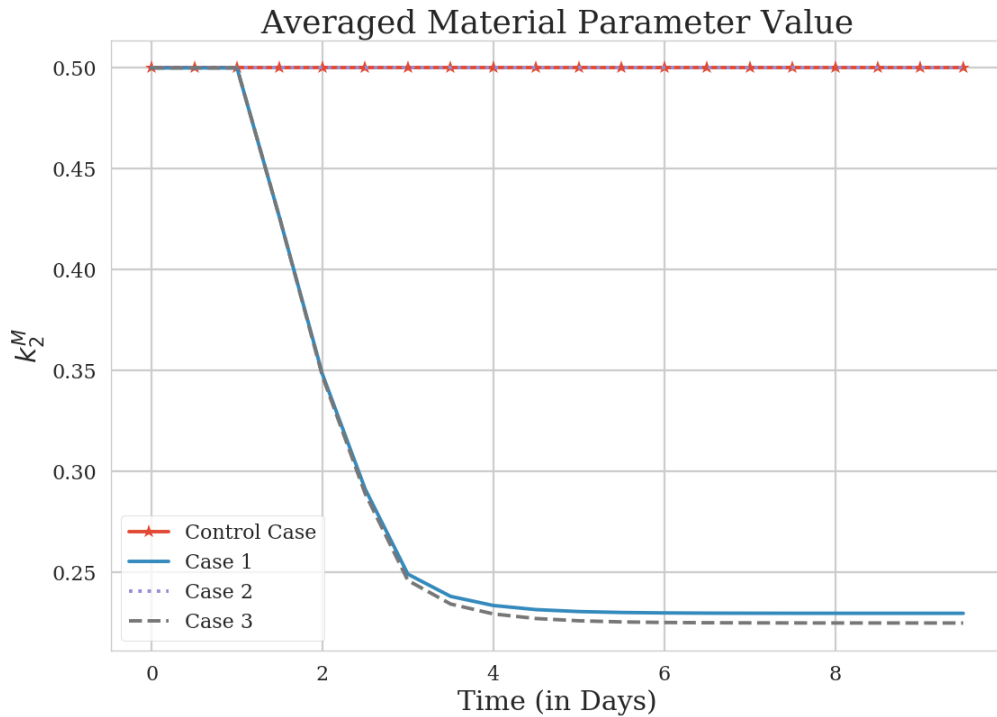
The averaged  $\sigma_T^{diff}$  is shown in Figure [7.24].

**Control Case:** The values range from 0.0 at t=1 days to a maximum of 0.182 at t= 3 days and remains constant until t=10 days as  $\beta_M = \beta_T = 0.0$

**Case 1:** The averaged ( $\sigma_T^{diff}$ ), rises from 0.0 to 0.167 i.e. it peaks at t= 3 days and reduces slightly to 0.163 at t=4 days and remains constant till t=10 days.

**Case 2:** Given the tendon region remodels, the averaged ( $\sigma_T^{diff}$ ) value increases from 0.0 to a maximum of  $\approx 0.0627$  at t=2 days and observes a decline from from a value of 0.0624 at t=2.5 days to a steady 0.0 after t=6 days.

**Case 3:** The averaged ( $\sigma_T^{diff}$ ), sees an increase from 0.0 to a maximum of  $\approx 0.059$  and decling to 0.052 at t= 2.5 days, thereafter stabilising back at 0 after t=6 days.

7.6.2.4 Averaged  $k_2^M$ 

**Figure 7.25:** The averaged  $k_2^M$  material parameter values are depicted. No remodelling occurs in the Control Case and Case 2. Case 1 the value decreases sharply from 0.5 to  $\approx 0.25$  and stabilises at  $\approx 0.23$  at  $t=3$  days and  $t=6$  days respectively.

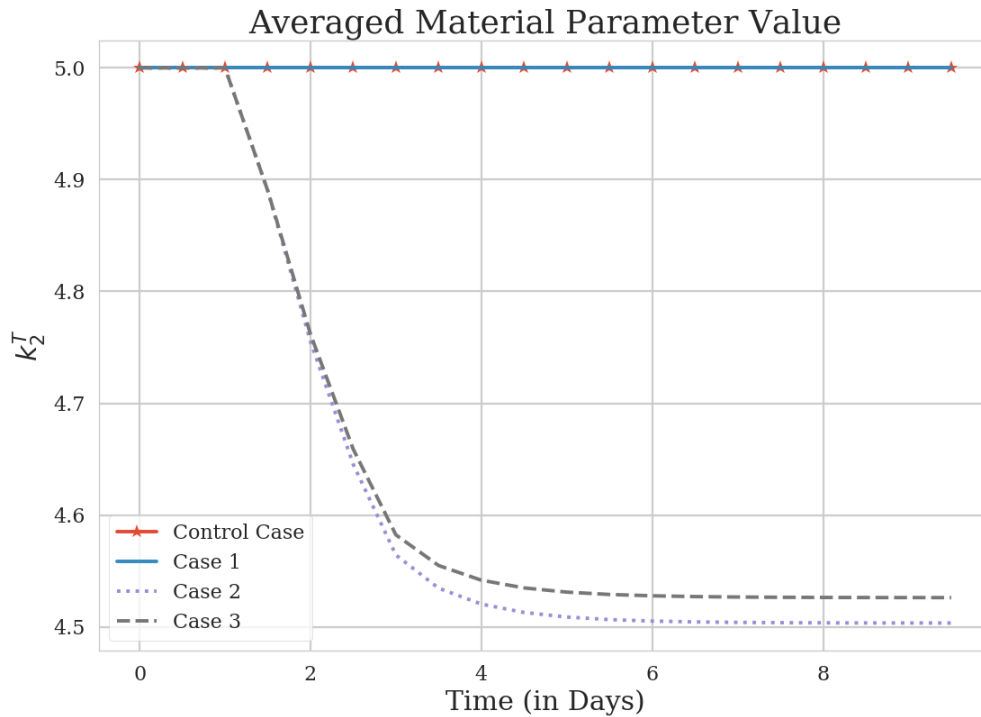
The averaged  $k_2^M$  material parameter values are displayed in Figure [7.25].

**Control Case:** The control case observes no remodelling in the muscle or tendon as  $\beta_M = \beta_T = 0.0$

**Case 1:** The averaged  $k_2^M$  value decreases from time  $t=1$  day sharply to 0.25 and declines slowly thereafter, reaching a constant value of  $\approx 0.23$  after  $t=6$  days.

**Case 2:** The rate constant  $\beta_M = 0.0$  and therefore, the values remain at 0.5 throughout the simulation.

**Case 3:** Similar to Case 2, The averaged  $k_2^M$  value decreases from time  $t=1$  day sharply to  $\approx 0.246$  and declines slowly thereafter, reaching a constant value of  $\approx 0.225$  after  $t=6$  days.

7.6.2.5 Averaged  $k_2^T$ 

**Figure 7.26:** The averaged  $k_2^T$  values are shown here, with no changes observed in the Control case and Case 1. Case 2 observes a sharp decrease to  $\approx 4.56$  and stabilises around 4.503 at  $t=3$  days and  $t=6$  days respectively. Likewise, for Case 3 the value declines to  $\approx 4.58$  and  $\approx 4.527$  at  $t=3$  days and  $t=6$  days respectively.

**Control Case:** The control case observes no remodelling in the muscle or tendon as  $\beta_M = \beta_T = 0.0$

**Case 1:** The rate constant  $\beta_T = 0.0$  and therefore, the averaged  $k_2^T$  values remain at 5 throughout the simulation.

**Case 2:** The average  $k_2^T$  value decreases with a sharp slope from 5.0 at  $t=1$  day to  $\approx 4.56$  at  $t=3$  days and the slope becomes less sharp, with  $k_2^T$  value declining upto  $\approx 4.503$  after  $t=6$  days and remains constant till  $t=10$  days.

**Case 3:** The average value for  $k_2^T$  declines with a steep slope from  $t=1$  day from a value of 5.0 to  $\approx 4.58$  at  $t=3$  days and  $k_2^T$  value declines slowly thereafter upto  $\approx 4.527$  after  $t=6$  days and remains constant till  $t=10$  days.

## 7.7 Discussions

The gastrocnemius skeletal muscle has been modelled using a hyper-elastic, incompressible, fibre-reinforced material model (Holzapfel et al. (2000)) available in ANSYS ® Mechanical APDL. It sees another application of the Soft Tissue Growth & Remodelling framework (Chapter [4]) using a customised workflow (Section [4.3.5]). The simulation consists of stretching the gastrocnemius muscle from an initial stretch  $\lambda_0 = 1.05$ , which can be considered to be the homoeostatic stretch upto a stretch of  $\lambda_f = 1.1$  after which the muscle is fixed and allowed to remodel. This provides us with the remodelling of the skeletal muscle subjected to sustained over-stretch and finds possible applications in toe-walking, casting and orthostatism(Wisdom et al. (2015)).

The fibre stretch invariants for the muscle  $I_4$  and the tendon  $I_6$  are a function of the tissue stretch  $\lambda$ , for each volume element in the finite element mesh. Given that the stresses experienced by the muscle ( $\sigma_M(X, k_1^M, k_2^M, I_4, t)$ ) and the tendon ( $\sigma_T(X, k_1^T, k_2^T, I_6, t)$ ) are functions of the invariants  $I_4$  and  $I_6$  respectively, increased stress is experienced when the tissue is stretched from  $\lambda_0 = 1.05$  to  $\lambda_f = 1.1$ . The increase in the fibre stresses drives the remodelling of the tissue i.e. of the material values  $k_2^M, k_2^T$  (Equations [7.8, 7.9]), as it creates a difference between the homoeostatic stresses, which are calibrated at time  $t=0$ . The negative symbol present in the remodelling equations, indicates a behaviour which enables the fibres to maintain the same state of stretch but at a reduced stress, (this is explained in Section[5.1.2]). The implication being the remodelling occurs such that at an increased state of stretch due to material parameter remodelling, the stress is restored to homoeostasis (Figures[7.19,7.21] in order to enable the fibres to regain their physiological function.

On observing the different cases (Section [7.6.2]), it can be seen that for the control case (Figures[7.23, 7.24]) since no remodelling occurs  $\beta_M = \beta_T = 0.0$ , the stresses rise proportionally with respect to the stretch in the tissue. Please note in the following discussion stresses refer to average stresses.

With respect to the muscle, it can be seen from the stress differences, variation in Case 1  $\sigma_M^{diff}$  peaks at a slightly lower value than Case 3, indicating that for muscle only remodelling the muscle experiences reduced stress as the tendon stress does not remodel. Whereas, in Case 3 with both the muscle and tendon remodelling a higher stress is observed in the muscle. This is reflected in the material parameter values averaged over the muscle, where the  $k_2^M$  parameter asymptotes at a higher value than Case 3 and therefore since  $\sigma_M(\mathbf{X}, t) = \mathbf{f}(k_2^M, t)$  the stresses in Case 1 are slightly lower which contradicts the stress values observed. However, on observing the stretch invariant graphs, it is observed that  $I_4$  reaches a lower value past  $t=3$  days (Figure[7.22]), which could be attributed to the tendinous region remodelling and its stretch compresses the muscle region leading to a higher stress in Case 3. Mathematically this is due to the fact that the Cauchy stress is also a function of the stretch invariant ( $\sigma_M(\mathbf{X}, t) = \mathbf{f}(k_1^M, k_2^M, I_4, t)$ ).

A reverse effect is observed in the case of the tendons, where tendon Cauchy stress difference

(Figure [7.24], is higher in Case 2 as compared to Case 3, indicating tendon only remodelling leads to higher stresses as the muscle stretch remains the same leading to a slight compression in the tendinous region. The material parameter  $k_2^T$  (Figure[7.26], observes a higher value for Case 3 as it asymptotes than Case 2 which does not correlate well with the stress differences observed, however, on perusing the stretch invariant graph Case 2 has a lower value than Case 3 which leads to higher stress differences and therefore lower material parameter value according to the remodelling assumption (Equation[7.9]).

The rate constants  $\beta_M, \beta_T$  are not calibrated according to experimental or observed datasets and are therefore instructive about the effects they have on muscle remodelling phenomenologically. They could be tuned in order to reflect a particular problem set.

The different cases for understanding the mathematical behaviour of our remodelling assumptions helps understand the scenarios where only the muscle region remodels, or the tendon region remodels or both. An additional case to inspect would be remodelling of only the aponeurosis region. These cases can help us gain an understanding of injuries related only to the muscle, tendon or aponeurosis region.

### 7.7.1 Relevance in Muscle Remodelling

In (Zöllner et al. (2012)), a novel mechanistic model is introduced to model chronic longitudinal skeletal muscle growth in response to passive mechanical stretch. Their approach focusses on the growth of skeletal muscle, via serial addition of sarcomeres as an adaptation mechanism observed in vivo for animal models for limb lengthening, immobilisation as well as tendon transfer. This suggests an inclusion of sarcomeres in the remodelling model introduced in this chapter. However, Cauchy stress remodelling provides another approach to understand the problem of muscle adaptation. Further, in the review (Wisdom et al. (2015)), the (Holzapfel et al. (2000)) model is projected onto the passive extra-cellular matrix of the skeletal muscle to understand stiffness based on varying stiffness using a uni-dimensional model. This ties in with our remodelling Equations[7.8,7.9], observing similar shift towards the right in the stress-stretch curve (Figure [5.6]), for muscle fibres.

(Nordez et al. (2009)), studies the mechanical behaviour of the musculo-articular complex (MAC) through their implementation of a rheological model. Their secondary objective involved adaptation of the model to changes in the MACs passive stiffness induced by passive stretching. The focus however, was on the torque-angle relationships, which is not tracked in this study and provides yet another venue to explore for the stgrf-model for skeletal muscle. Another study (Makarov et al. (2009), focusses on muscle stiffness and joint contractures in goat limbs, to understand muscle architecture changes involved in the tibia. Again, the focus is on the sarcomere content variations in the muscle to stretching and therefore a direct comparison is currently not possible with the stress-driven remodelling scheme.

Though studies are limited on visualising the differences in muscle, tendon and aponeurosis regions in the gastrocnemius muscle, it is not a negative aspect and provides a fresh basis to incorporate hypotheses based on observations as detailed in above studies. If direct comparison is not possible, sophistication of the model with features introduced in empirical studies with feasible hypotheses provides a direction for research, leading to quantifiable observations even if qualitative and better modelling approaches can be considered. Therefore, the effect of modelling material parameters and rate constants introduced based on stress-driven hypotheses provides an idea on the remodelling in tendon and muscle using the ([Holzapfel et al. \(2000\)](#)) model.

### 7.7.2 Limitations

1. *Fibre orientation definition* - ideal vs anatomical.

The fibres prescribed in the model are aligned along the major axis of the gastrocnemius geometry, which is a simplification of the anatomical fibres present as seen in in vivo observations (Deux et al. (2008)). The model would benefit from defining fibres with respect to anatomical geometry in order to obtain stress profiles reflective of in vivo data.

2. *Passive Material*:

The material model available (Holzapfel et al. (2000)) in the finite element package is for passive fibre-reinforced materials, while useful for understanding passive tissue behaviour under over-stretch an active contraction model would allow us to understand further implications with realistic results.

3. *User Material Subroutine*:

As is the case with the left ventricular finite element model (Chapter 6), definition of a user material subroutine requires a high level of expertise. This is a common issue for models developed using the soft tissue growth and remodelling framework (Chapter 4).

## 7.8 Conclusions

A novel finite element model for remodelling of the gastrocnemius skeletal muscle is defined in this Chapter. It sees an extension of the soft tissue growth and remodelling framework developed with a customised workflow, providing an idea about the capability of the framework. Cases for remodelling only the muscle region or tendon region are useful to determine in real life scenarios based on applicability. Terminally, it lays the foundation for future models to extend and enhance the models capabilities with sophisticated model's which could feed into the simulations through framework extensions or modifications.

This page has been intentionally left blank.

## Chapter 8

# Discussions & Conclusions

### 8.1 Summaries of the Study

The major targets of this research involved establishing a novel constrained mixture model using a uni-dimensional approach for the left ventricle post myocardial infarction, develop a framework around ANSYS® Mechanical APDL for finite element soft tissue growth and remodelling simulations. The basis being mechanical adaptation of the extra-cellular matrix collagenous constituents in the myocardium and an extension to muscle tendon fibres for skeletal muscles, from a deviated state to a preferred homoeostatic value which are strain based for the constrained mixture model and stress based for the simulations done using the framework.

1. In Chapter 3, based on the constrained mixture theory approach ([Humphrey & Rajagopal \(2002\)](#)), we adapt the idea for formulating a 1-D model of the left ventricle as a non-linear, incompressible spherical membrane approximation with representations for underlying micro-structural constituents. An infarction is simulated by a decay function associated with cardiomyocyte mass density, driving changes in tissue stretch which conversely drives the remodelling of the collagen matrix. Identifying model behaviour based on evolution of the homoeostatic stretch distribution the collagen fibre network acquire helped guide the most plausible set of hypotheses for simulating infarctions with respect to mass densities and remodelled thickness. Therefore, the adaptation of the myocardial collagen extra-cellular matrix due to progression of an infarction as a phenomenological model is presented.
2. Chapter 4, details the framework developed around an available material model. Given the implementation of user material subroutines is quite difficult to define customised material model implementations for the myocardial tissue, we use the available tissue model for passive fibre-reinforced hyperelastic materials (HGO model, [Holzapfel et al. \(2000\)](#)) enabling modelling of not only the myocardium but other fibre reinforced soft tissues. The need for such a framework rose from the fact that a collection of tasks which involved pre-processing and post-processing were identified as candidates for automation

using a workflow. Therefore, a code library in Python was developed, using PERL as the workflow execution language and ANSYS ® Mechanical APDL solver for structural analysis. Apart from the lack of a Graphical User Interface, the process of performing growth and remodelling of soft tissue biomechanics simulations pertinent with the available set of tools is completely automated and requires no user intervention for the entire run. It is hoped to bridge the gap of knowledge transfer between research and non-expert users, users interested in learning about the topic as well as can be developed into a tool to ease future researchers involved in projects implementing this methodology.

3. An application of the soft tissue growth and remodelling framework (STGRF), is presented in Chapter 6. Here the strain energy function associated with the material model ([Holzapfel et al. \(2000\)](#)) is modified to enable simulations involving large deformation of the myocardium as well as inclusion of mass density terms to drive the progression of the disease via the degradation of the ground matrix and cardiomyocytes associated with the isotropic component of the material. A custom workflow is scripted to provide the algorithm for growth and remodelling of the myocardium using an idealised LV geometry ([Hassaballah et al. \(2013\)](#)). An improvement over past implementation ([Chan \(2019\)](#)) is the calculation of the stretch invariants of the collagen fibres via post-processing the strain results from the ANSYS ® Mechanical APDL solver and employing them in our stress-driven remodelling equations. A fictitious fibroblast recruitment field is introduced which is driven by the strain experienced by the cells themselves regulating the mass density based on stretch variations. Therefore, a cellular component is introduced which could be further sophisticated to include chemical signalling pathways involved in the regulation of collagen fibre mass density. Results include the changes observed in the stresses experienced by the collagen fibres, mass densities of the constituents, based on evolution and non-evolution of their homeostatic stress distributions. They shed light on the spatial distribution of stresses, mass densities and fibroblast stretches in an attempt to maintain a preferred homeostatic stress in the collagen fibres on deviation to higher stresses. This could provide insights into the mechanical behaviour of the collagen extra-cellular matrix and suggest how their configuration affects the outcome of a MI based on its size and location. Further improvements are needed and the model would benefit from inclusion of chemical signalling models and oxygen transport model as seen in ([Chan \(2019\)](#)).
4. The second application of the STGRF is seen with respect to the gastrocnemius skeletal muscle. It is a illustrative model which provides an idea about how muscle, tendon regions remodel using a modified fibre-reinforced material model ([Holzapfel et al. \(2000\)](#)), in the case of over-stretch leading to eccentric remodelling of the muscle. A key aspect of the model is the inclusion of the aponeurosis region which is a transitional dense connective tissue region between the tendon and muscle providing a transition region for stress distribution experienced during physical activity. A volume fraction assignment algorithm

was developed to define the different regions i.e. muscle region (MR), aponeurosis region (AR) and tendinous region (TR). The stretch boundary condition at the distal end of the gastrocnemius is slowly ramped to a higher value over a period of time using a displacement function and the remodelling laws are triggered due to the differences in Cauchy stresses developed. Three cases were considered to explore model behaviour and interestingly opposite behaviour was observed for muscle and tendon remodelling in cases where one of them was allowed to remodel as compared to a case where both were allowed to remodel. This provides an idea on modelling muscle only or tendon only injuries, adaptations or pertinent simulations. Also, spatial stress distribution profiles in 3D provide information about the variations in the aponeurosis region. Therefore, it provides a basis for further sophistications to be made to better understand skeletal muscle remodelling and its applications to rehabilitation schemes, exercise regimes, treatment of injuries and therapies.

## 8.2 Limitations of the Study

Considering the limitations defined in the chapters of the thesis, we provide a succinct list below:

- ***Passive Material Model:***

Pervading through the two applications of the soft tissue growth and remodelling framework (Chapter 4) is the presence of the material model for modelling fibre-reinforced hyper-elastic tissues. Though appropriate for modelling passive behaviour, it is important to consider active contractility of the myocardium in order to simulate the entire cardiac cycle as well as introduce intracellular  $Ca^{2+}$  signalling pathways through coupled numerical models by utilising external inputs to the framework customisable scripts. It is also important in skeletal muscles to understand lengthening contraction within the muscle fibres, (sarcomere models).

- ***Residual Stresses:***

An important aspect of soft connective tissues in vivo, is that they are in a state of tension even when there is no internal blood pressure. This is seen in the case of arteries and the left ventricle, where upon an incision through a transmural section causes them to open up and reduce in size, indicating existing stresses due to the arrangement of the extra-cellular matrix and cellular components present. It would be an important consideration to better realise the stress distributions within soft tissues in growth and remodelling using the framework.

- ***Validation of G & R hypothesis:***

With respect to the constrained mixture model (Chapter 3), the left ventricular finite element model (Chapter 6), they are both phenomenological models. In this vein, they provide qualitative understanding of the changes in the extra-cellular collagen matrix while providing consistent observations in their behaviour, the parameters are either obtained from other conceptual models and observations. Therefore, functional forms for growth and remodelling assumptions and fibre orientations are difficult to formulate. However, there is room for updating the current framework and mathematical models with updated assumptions and methodologies to gain better understanding of the mechanisms that drive left ventricular infarction pathologies. It applies to the skeletal muscle remodelling as well due to the common thread of customised workflow development in the framework.

- ***Mesh Convergence Studies:***

In finite element modelling, mesh convergence deals with using an estimated mesh size with respect to a maximum mechanical quantity relevant for the study in the region of interest. This includes the infarcted region in the LV model and the aponeurosis region in the skeletal muscle model, with collagen fibres stresses and muscle, tendon fibre stresses being the point of consideration respectively. Based on reducing the mesh size, the results would asymptote to a particular value which would provide an idea to select an appropriate

mesh size, without compromising the computational efficiency. In terms of our models, though the driving factor is the difference in Cauchy stresses, essentially independent of mesh size. However, the accuracy required for instance in the infarcted region would benefit from a finer mesh in the region of interest and particularly useful for validation when compared against realistic cases in patient specific geometries. Additionally, finer meshes would provide a better representation of the stress distribution with smoother contours for various regions as compared with lower resolution meshes.

- ***Fibre Orientations:***

In Chapter 6, we modelled the myocardial collagen fibres longitudinally and circumferentially along the major axis going from the base to the apex. However, this is a simplification in terms of the multiple orientations and structural organisation of the collagen fibre matrix present in the myocardium (Holzapfel & Ogden (2009)). Inclusion of an accurate representation of fibre orientations would improve the stress distribution results and provide a better reflection of the changes that take place in the extra-cellular matrix

Similarly, in Chapter 7 for the gastrocnemius skeletal muscle, instead of prescribing axial fibre orientations it would be beneficial to provide anatomically accurate fibre organisation for better realisation of results (Pang et al. (2017)).

- ***Reference Configurations:***

A limitation in the finite element models developed using the soft tissue growth and remodelling framework, is the evolution of the reference configuration for the micro-structural collagen fibres. Inclusion of evolving reference configurations has been considered in both finite growth and constrained mixture model, following the change in the geometric structure and mass variations over the course of the disease. Our models depend on the initial undeformed geometry and limits the deformation the model can achieve in order to reflect large changes in structure and therefore impairs a comprehensive study to be carried out based on tissue evolution and its impact on function. Therefore, it is necessary to either incorporate a user material subroutine for a custom material model or devise new methods to consider the evolution of reference configurations for the micro-structural components.

### 8.3 Future Considerations

As in the previous Section [8.2], we provide a list of future work per chapter below:

1. **Chemo-Mechano-Biological Model:**

Based on the arterial wall implementation of an integrated model which incorporates biological, mechanical and chemical states (Aparício et al. (2016)), the 1D constrained mixture model sees a natural extension (Chapter 3). This allows for understanding the effects of drug delivery affecting the collagen extra-cellular matrix in the case of enlarging or stabilising infarctions in the left ventricle. Targeting personalised treatment, pharmacological therapies and understanding their contribution to infarct progression could open up novel pathways for disease risk stratification.

2. **Framework Graphical User Interface Implementation:**

In the current state of the Soft Tissue Growth & Remodelling Framework, its functioning and execution are done based on the command line interface with a few simple arguments as input to run a growth and remodelling simulation work cycle. Development of a GUI would provide a more accessible tool kit for non-experts, non-modellers, expert users to operate the software. This enables them to further experiment with the code having an extended tool set capability with buttons, graphical windows and results viewer which would enhance productivity, time cost and efficiency.

3. **Patient Specific Geometries:**

Utilisation of patient specific geometries instead of idealised Left Ventricular geometries, will enhance the results obtained and used in tandem with anatomical fibres could lead to personalisation of models, thereby providing a foundation for translation into clinical use. Though in its nascent stages, images provided by the (Luo (2019)) research group (Figure [8.1] prove to be the next step in understanding patient specific growth and remodelling using the modified HGO model formulation.

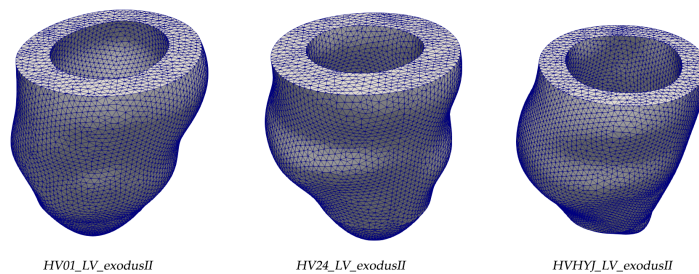


**Figure 8.1:** Geometries from patient MRI-data, provided by (Luo (2019)).

#### 4. Validation Approaches:

The validation of models introduced in this research has not received much attention, given the focus of the research was to understand the implementation of a constrained mixture model and the development of a finite element framework based on the HGO model (Holzapfel et al. (2000)) available in ANSYS to catalyse soft tissue growth and remodelling simulations. Given their applications in the left ventricular myocardium and skeletal muscles, it is important to validate the models developed therein. We detail the procedures which can be undertaken further to validate models using the STGRF and 1D constrained mixture model.

(a) *Constrained Mixture Model:*

The model has seen an initial validation on experimental data provided in (Fishbein et al. (1978)). It has proven useful in inferring insights on quantities like mass density of collagen fibres and tissue stretches by simulating thickness changes to compare with the data. However, given the approximations of LV as a spherical membrane additional studies need to be done, this can be in the form of experiments particularly suited to parametrise the model or obtain results to tune the model based on observations. Either method will help clarify the utility of the model further and allow for better understanding of the underlying extra-cellular matrix configurations in the infarcted scar tissue.

(b) *STGRF - Left Ventricle Post-MI:*

Results obtained in the left ventricular finite element model has been compared with experimental studies with rabbits (Lerman et al. (1983)) and regional wall stress variations seen in human hearts post-MI (Rohde et al. (1999)). Though the results agree well between the initial and final observed values as ratios for mass density changes and wall stress, it is not a direct correlation with the simulation results and information is inferred. Therefore, for validation of the finite element model, experimental set up mimicking the boundary conditions presumed can be realised in isolated hearts (Nash & Hunter (2000)), or MRI scanning could help parametrise input material parameters and observed ventricular dilatation, wall stresses can be utilised to infer rate constants. Thereafter, any insights obtained in terms of change in homeostatic stress, wall deformation, collagen mass density changes and even fibroblast cell mechanics can be verified. This allows for the model to be further sophisticated with other methodologies, for example FSI(Fluid Solid Interaction, Domenichini et al. (2005), Gao et al. (2017)), electro-physiology(Kojic et al. (2019), Sugiura et al. (2012)) and chemical signalling models(Aparício et al. (2016), Karamanos et al. (2019)).

(c) *STGRF - Gastrocnemius Muscle:*

Validation for the gastrocnemius muscle follows more on the lines of the finite ele-

ment model for the left ventricle, wherein imaging results would help calibrate tissue material properties like elastic modulus, bulk modulus and fibre orientations. Further customised experiments would be ideal to fit input modelling parameters to the particular form of the HGO ([Holzapfel et al. \(2000\)](#)) material model. Though not the central focus of the work and more of an extension to the Soft Tissue Growth and remodelling framework, validation with empirical data would prove useful in furthering modelling capabilities and sophistications. These sophistications could include intracellular  $Ca^{2+}$  models, stimulation by neural transmission and incorporating the skeletal muscle extra-cellular matrix into the model.

Another important point common to the finite element framework is the representation of fibre orientations, representation of accurate fibres of the extra-cellular matrix and muscle fibres would enable us to validate results with empirical data from experiments, clinical studies or established models to gain confidence in the models capability of providing reliable predictions to growth and remodelling observations based on applied hypotheses. An ongoing MSc student has implemented describing fibre directions in skeletal muscle fibres, along with custom scripts to replace TECPLOT macros for defining volume fractions for the gastrocnemius skeletal muscle ([Harms \(2020\)](#)), and provides a next step towards simulating gastrocnemius remodelling with various fibre orientations.

## 8.4 Concluding Remarks

A novel constrained mixture model of the left ventricle has been introduced in this research, representing the extra-cellular collagen matrix using distribution functions for fibre stretches defined for arteries in previous research, also including the ground matrix and cardiomyocyte constituents and further observing changes in collagen fibre stretch configurations and mass density changes post-MI. A novel growth and remodelling framework centred around a fibre-reinforced material model available in commercially established finite element software ANSYS® Mechanical APDL has been developed as a Python package, (yet to be packaged into a standard library) allowing setting up of growth and remodelling simulations for soft tissues. In extension to this, applications of frameworks are observed in the left ventricular myocardium post-MI and over-stretch of the gastrocnemius skeletal muscle. Realisation of these models require additional works to be done in terms of experimental/ clinical data acquisition, sophistication with inclusion of electro-physiology, biochemistry and blood fluid dynamics. The research introduced in this thesis is therefore, aimed at providing tools for developing workflows using ANSYS® in pertinence for simulating fibre-reinforced soft tissue growth and remodelling.

This page has been intentionally left blank.

# References

- Ambrosi, D., Ateshian, G. A., Arruda, E. M., Cowin, S., Dumais, J., Goriely, A., Holzapfel, G. A., Humphrey, J. D., Kemkemer, R., Kuhl, E. et al. (2011), 'Perspectives on biological growth and remodeling', *Journal of the Mechanics and Physics of Solids* **59**(4), 863–883.
- Ambrosi, D., Ben Amar, M., Cyron, C. J., DeSimone, A., Goriely, A., Humphrey, J. D. & Kuhl, E. (2019), 'Growth and remodelling of living tissues: perspectives, challenges and opportunities', *Journal of the Royal Society Interface* **16**(157), 20190233.
- Ambrosi, D. & Guana, F. (2007), 'Stress-modulated growth', *Mathematics and mechanics of solids* **12**(3), 319–342.
- Anderson, R. H., Ho, S. Y., Redmann, K., Sanchez-Quintana, D. & Lunkenheimer, P. P. (2005), 'The anatomical arrangement of the myocardial cells making up the ventricular mass', *European journal of cardio-thoracic surgery* **28**(4), 517–525.
- ANSYS, I. (2013), *ANSYS Mechanical APDL Material Reference*.
- Aparício, P., Thompson, M. S. & Watton, P. N. (2016), 'A novel chemo-mechano-biological model of arterial tissue growth and remodelling', *Journal of biomechanics* **49**(12), 2321–2330.
- Awada, H. K., Hwang, M. P. & Wang, Y. (2016), 'Towards comprehensive cardiac repair and regeneration after myocardial infarction: aspects to consider and proteins to deliver', *Biomaterials* **82**, 94–112.
- Ayachit, U. (2015), *The paraview guide: a parallel visualization application*, Kitware, Inc.
- Banerjee, I., Fuseler, J. W., Price, R. L., Borg, T. K. & Baudino, T. A. (2007), 'Determination of cell types and numbers during cardiac development in the neonatal and adult rat and mouse', *American Journal of Physiology-Heart and Circulatory Physiology* **293**(3), H1883–H1891.
- Belytschko, T., Kulak, R., Schultz, A. & Galante, J. (1974), 'Finite element stress analysis of an intervertebral disc', *Journal of biomechanics* **7**(3), 277–285.
- Betts, J., Desaix, P., Johnson, E., Johnson, J., Korol, O., Kruse, D. & Young, K. (2018), 'Anatomy and physiology. openstax'.
- Bhugal, P., Pederzani, G., Grytsan, A., Loh, Y., Brouwer, P. A., Andersson, T., Gundiah, N., Robertson,

- A. M., Watton, P. N. & Söderman, M. (2019), 'The unexplained success of stentplasty vasospasm treatment', *Clinical Neuroradiology*.
- URL:** <https://doi.org/10.1007/s00062-019-00776-2>
- Boakes, J. L., Foran, J., Ward, S. R. & Lieber, R. L. (2007), 'Case report: Muscle adaptation by serial sarcomere addition 1 year after femoral lengthening.', *Clinical Orthopaedics and Related Research (1976-2007)* **456**, 250–253.
- Bogen, D. K., Rabinowitz, S. A., Needleman, A., McMahon, T. A. & Abelmann, W. H. (1980), 'An analysis of the mechanical disadvantage of myocardial infarction in the canine left ventricle.', *Circulation research* **47**(5), 728–741.
- Bonet, J. & Wood, R. D. (1997), *Nonlinear continuum mechanics for finite element analysis*, Cambridge university press.
- Bordoni, B. & Varacallo, M. (2018), Anatomy, head and neck, sternocleidomastoid muscle, in 'StatPearls [Internet]', StatPearls Publishing.
- Boron, W. F. & Boulpaep, E. L. (2012), *Medical Physiology, 2e Updated Edition E-Book: with STUDENT CONSULT Online Access*, Elsevier Health Sciences.
- Boron, W. F. & Boulpaep, E. L. (2016), *Medical Physiology E-Book*, Elsevier Health Sciences.
- Bovendeerd, P. H. (2012), 'Modeling of cardiac growth and remodeling of myofiber orientation', *Journal of biomechanics* **45**(5), 872–881.
- Bray, M.-A., Sheehy, S. P. & Parker, K. K. (2008), 'Sarcomere alignment is regulated by myocyte shape', *Cell motility and the cytoskeleton* **65**(8), 641–651.
- Britannica, E. (2015), 'Britannica academic', *Encyclopædia Britannica Inc*.
- Brodland, G. W. (2015), How computational models can help unlock biological systems, in 'Seminars in cell & developmental biology', Vol. 47, Elsevier, pp. 62–73.
- Burton, R. (1972), 'Heart growth and size in homeotherms', *Regulation of organ and tissue growth* pp. 101–125.
- Campbell, P. H., Hunt, D. L., Jones, Y., Harwood, F., Amiel, D., Omens, J. H. & McCulloch, A. D. (2008), 'Effects of biglycan deficiency on myocardial infarct structure and mechanics', *Molecular & cellular biomechanics: MCB* **5**(1), 27.
- Chabiniok, R., Wang, V. Y., Hadjicharalambous, M., Asner, L., Lee, J., Sermesant, M., Kuhl, E., Young, A. A., Moireau, P., Nash, M. P. et al. (2016), 'Multiphysics and multiscale modelling, data-model fusion and integration of organ physiology in the clinic: ventricular cardiac mechanics', *Interface focus* **6**(2), 20150083.

- Chan, I.-T. (2019), 'A novel fluid-solid-growth-transport framework for modelling the evolution of arterial disease: Application to aneurysms'.
- Chen, H. (2014), Intracranial aneurysm disease: novel modelling of inception and the microstructural adaption of collagen fabric, PhD thesis, University of Oxford.
- Chen, W. & Frangogiannis, N. G. (2013), 'Fibroblasts in post-infarction inflammation and cardiac repair', *Biochimica et Biophysica Acta (BBA)-Molecular Cell Research* **1833**(4), 945–953.
- Chiquet, M., Renedo, A. S., Huber, F. & Flück, M. (2003), 'How do fibroblasts translate mechanical signals into changes in extracellular matrix production?', *Matrix biology* **22**(1), 73–80.
- Civisilli, C. F. (2019), A computational model of the gastrocnemius aponeurosis, Master's thesis, The University of Sheffield.
- Cleutjens, J., Verluyten, M., Smiths, J. & Daemen, M. (1995), 'Collagen remodeling after myocardial infarction in the rat heart.', *The American journal of pathology* **147**(2), 325.
- Cowin, S. C. (1996), 'Strain or deformation rate dependent finite growth in soft tissues', *Journal of biomechanics* **29**(5), 647–649.
- Cyron, C. & Humphrey, J. (2017), 'Growth and remodeling of load-bearing biological soft tissues', *Meccanica* **52**(3), 645–664.
- Czubryt, M. P. (2012), 'Common threads in cardiac fibrosis, infarct scar formation, and wound healing', *Fibrogenesis & tissue repair* **5**(1), 19.
- Dandapani, S., Gundiah, N., Luo, X. & Watton, P. (2017), A constrained mixture model of the left ventricle and its application to simulating myocardial infarction, in 'Proceedings of the 5th International Conference on Computational & Mathematical Biomedical Engineering', CMBE, pp. 1273–1276.
- Delp, S. L. & Loan, J. P. (2000), 'A computational framework for simulating and analyzing human and animal movement', *Computing in Science & Engineering* **2**(5), 46–55.
- Detwiler, P. W., Nicolosi, A. C., Weng, Z.-C. & Spotnitz, H. M. (1994), 'Effects of perfusion-induced edema on diastolic stress-strain relations in intact swine papillary muscle.', *The Journal of thoracic and cardiovascular surgery* **108**(3), 467–476.
- Deux, J., Malzy, P., Paragios, N., Bassez, G., Luciani, A., Zerbib, P., Roudot-Thoraval, E., Vignaud, A., Kobeiter, H. & Rahmouni, A. (2008), 'Assessment of calf muscle contraction by diffusion tensor imaging', *European radiology* **18**(10), 2303–2310.
- Domenichini, F., Pedrizzetti, G. & Baccani, B. (2005), 'Three-dimensional filling flow into a model left ventricle', *Journal of Fluid Mechanics* **539**, 179–198.

- Engler, A., Bacakova, L., Newman, C., Hategan, A., Griffin, M. & Discher, D. (2004), 'Substrate compliance versus ligand density in cell on gel responses', *Biophysical journal* **86**(1), 617–628.
- File Formats for VTK Version 4.2* (2002), <https://vtk.org/wp-content/uploads/2015/04/file-formats.pdf>. Accessed: 2019-08-28.
- Finegold, J. A., Asaria, P. & Francis, D. P. (2013), 'Mortality from ischaemic heart disease by country, region, and age: statistics from world health organisation and united nations', *International journal of cardiology* **168**(2), 934–945.
- Fishbein, M., Maclean, D. & Maroko, P. (1978), 'Experimental myocardial infarction in the rat: qualitative and quantitative changes during pathologic evolution.', *The American journal of pathology* **90**(1), 57.
- Fletcher, D. A. & Mullins, R. D. (2010), 'Cell mechanics and the cytoskeleton', *Nature* **463**(7280), 485.
- Fletcher, P. J., Pfeffer, J. M., Pfeffer, M. A. & Braunwald, E. (1981), 'Left ventricular diastolic pressure-volume relations in rats with healed myocardial infarction. effects on systolic function.', *Circulation research* **49**(3), 618–626.
- Flitney, F. & Hirst, D. (1978), 'Cross-bridge detachment and sarcomere 'give' during stretch of active frog's muscle.', *The Journal of Physiology* **276**(1), 449–465.
- Flynn, C., Rubin, M. & Nielsen, P. (2011), 'A model for the anisotropic response of fibrous soft tissues using six discrete fibre bundles', *International Journal for Numerical Methods in Biomedical Engineering* **27**(11), 1793–1811.
- Fomovsky, G. M. & Holmes, J. W. (2009), 'Evolution of scar structure, mechanics, and ventricular function after myocardial infarction in the rat', *American Journal of Physiology-Heart and Circulatory Physiology* **298**(1), H221–H228.
- Fomovsky, G. M., Thomopoulos, S. & Holmes, J. W. (2010), 'Contribution of extracellular matrix to the mechanical properties of the heart', *Journal of molecular and cellular cardiology* **48**(3), 490–496.
- Fraccarollo, D., Galuppo, P. & Bauersachs, J. (2012), 'Novel therapeutic approaches to post-infarction remodelling', *Cardiovascular research* **94**(2), 293–303.
- Freytes, D. O., Stoner, R. M. & Badylak, S. F. (2008), 'Uniaxial and biaxial properties of terminally sterilized porcine urinary bladder matrix scaffolds', *Journal of Biomedical Materials Research Part B: Applied Biomaterials: An Official Journal of The Society for Biomaterials, The Japanese Society for Biomaterials, and The Australian Society for Biomaterials and the Korean Society for Biomaterials* **84**(2), 408–414.
- Fung, Y.-C. et al. (1993), *Mechanical properties of living tissues*, Vol. 547, Springer.

- Gamma, E., Helm, R., Johnson, R., Vlissides, J. & Patterns, D. (1995), 'Elements of reusable object-oriented software', *Design Patterns. massachusetts: Addison-Wesley Publishing Company* .
- Gao, H., Feng, L., Qi, N., Berry, C., Griffith, B. E. & Luo, X. (2017), 'A coupled mitral valve—left ventricle model with fluid–structure interaction', *Medical engineering & physics* **47**, 128–136.
- Garikipati, K. (2009), 'The kinematics of biological growth', *Applied Mechanics Reviews* **62**(3), 030801.
- Geisse, N. A., Sheehy, S. P. & Parker, K. K. (2009), 'Control of myocyte remodeling in vitro with engineered substrates', *In Vitro Cellular & Developmental Biology-Animal* **45**(7), 343–350.
- Gleason Jr, R. L. & Humphrey, J. D. (2005), 'A 2d constrained mixture model for arterial adaptations to large changes in flow, pressure and axial stretch', *Mathematical medicine and biology* **22**(4), 347–369.
- Göktepe, S., Abilez, O. J. & Kuhl, E. (2010), 'A generic approach towards finite growth with examples of athlete's heart, cardiac dilation, and cardiac wall thickening', *Journal of the Mechanics and Physics of Solids* **58**(10), 1661–1680.
- Göktepe, S., Abilez, O. J., Parker, K. K. & Kuhl, E. (2010), 'A multiscale model for eccentric and concentric cardiac growth through sarcomerogenesis', *Journal of theoretical biology* **265**(3), 433–442.
- Göktepe, S., Acharya, S., Wong, J. & Kuhl, E. (2011), 'Computational modeling of passive myocardium', *International Journal for Numerical Methods in Biomedical Engineering* **27**(1), 1–12.
- Goldspink, G. (1999), 'Changes in muscle mass and phenotype and the expression of autocrine and systemic growth factors by muscle in response to stretch and overload', *The Journal of Anatomy* **194**(3), 323–334.
- Gondwe, C. T. (2019), 'A novel framework to model the short and medium term mechanical response of the medial gastrocnemius'.
- Gong, X.-Y. & Riyad, M. (2002), On stress analysis for a hyperelastic material, *in* 'ANSYS Conference'.
- Green, E. M., Mansfield, J. C., Bell, J. S. & Winlove, C. P. (2014), 'The structure and micromechanics of elastic tissue', *Interface focus* **4**(2), 20130058.
- Grinnell, F. & Petroll, W. M. (2010), 'Cell motility and mechanics in three-dimensional collagen matrices', *Annual review of cell and developmental biology* **26**, 335–361.
- Grossman, W. (1980), 'Cardiac hypertrophy: useful adaptation or pathologic process?', *The American journal of medicine* **69**(4), 576–584.
- Guccione, J., Waldman, L. & McCulloch, A. (1993), 'Mechanics of active contraction in cardiac

- muscle: Part ii—cylindrical models of the systolic left ventricle', *Journal of biomechanical engineering* **115**(1), 82–90.
- Gundiah, N., Ratcliffe, M. B. & Pruitt, L. A. (2007), 'Determination of strain energy function for arterial elastin: experiments using histology and mechanical tests', *Journal of biomechanics* **40**(3), 586–594.
- Gupta, K. B., Ratcliffe, M. B., Fallert, M. A., Edmunds Jr, L. H. & Bogen, D. K. (1994), 'Changes in passive mechanical stiffness of myocardial tissue with aneurysm formation.', *Circulation* **89**(5), 2315–2326.
- Guyton, A. C. & Hall, J. E. (2006), 'Textbook of medical physiology 11th ed', *Elsevier Saunders* pp. 788–817.
- Haddad, S. M. & Samani, A. (2017), 'A computational model of the left ventricle biomechanics using a composite material approach', *International Journal of Engineering Science* **111**, 61–73.
- Harms, T. E. (2020), Computational modelling of skeletal muscle mechanics in health and disease—improving the work ow surrounding an existing soft tissue growth and remodelling framework [draft], Master's thesis, The University of Sheffield.
- Hassaballah, A. I., Hassan, M. A., Mardi, A. N. & Hamdi, M. (2013), 'An inverse finite element method for determining the tissue compressibility of human left ventricular wall during the cardiac cycle', *PloS one* **8**(12), e82703.
- Hein, S., Gaasch, W. H. & Schaper, J. (2002), 'Giant molecule titin and myocardial stiffness', *Circulation* **106**(11), 1302–1304.
- Hill, M. R., Duan, X., Gibson, G. A., Watkins, S. & Robertson, A. M. (2012), 'A theoretical and non-destructive experimental approach for direct inclusion of measured collagen orientation and recruitment into mechanical models of the artery wall', *Journal of biomechanics* **45**(5), 762–771.
- Hochman, J. S. & Bulkley, B. H. (1982), 'Expansion of acute myocardial infarction: an experimental study.', *Circulation* **65**(7), 1446–1450.
- Holzapfel, G. A. (2006), 'Determination of material models for arterial walls from uniaxial extension tests and histological structure', *Journal of theoretical biology* **238**(2), 290–302.
- Holzapfel, G. A., Gasser, T. C. & Ogden, R. W. (2000), 'A new constitutive framework for arterial wall mechanics and a comparative study of material models', *Journal of elasticity and the physical science of solids* **61**(1-3), 1–48.
- Holzapfel, G. A. & Ogden, R. W. (2009), 'Constitutive modelling of passive myocardium: a structurally based framework for material characterization', *Philosophical Transactions of the Royal Society A: Mathematical, Physical and Engineering Sciences* **367**(1902), 3445–3475.

- Holzapfel, G. A. & Ogden, R. W. (2010), 'Constitutive modelling of arteries', *Proceedings of the Royal Society A: Mathematical, Physical and Engineering Sciences* **466**(2118), 1551–1597.
- Hreybe, H. & Saba, S. (2009), 'Location of acute myocardial infarction and associated arrhythmias and outcome', *Clinical Cardiology: An International Indexed and Peer-Reviewed Journal for Advances in the Treatment of Cardiovascular Disease* **32**(5), 274–277.
- Humphrey, J. D. (2003), Continuum biomechanics of soft biological tissues, in 'Proceedings of the Royal Society of London A: Mathematical, Physical and Engineering Sciences', Vol. 459, The Royal Society, pp. 3–46.
- Humphrey, J. & Rajagopal, K. (2002), 'A constrained mixture model for growth and remodeling of soft tissues', *Mathematical models and methods in applied sciences* **12**(03), 407–430.
- Humphrey, J., Strumpf, R. & Yin, F. (1990), 'Determination of a constitutive relation for passive myocardium: I. a new functional form', *Journal of biomechanical engineering* **112**(3), 333–339.
- Janz, R. F. & Grimm, A. F. (1972), 'Finite-element model for the mechanical behavior of the left ventricle: prediction of deformation in the potassium-arrested rat heart', *Circulation research* **30**(2), 244–252.
- Jugdutt, B. I. (2003), 'Ventricular remodeling after infarction and the extracellular collagen matrix: when is enough enough?', *Circulation* **108**(11), 1395–1403.
- Jugdutt, B. I. (2005), Extracellular matrix and cardiac remodeling, in 'Interstitial fibrosis in heart failure', Springer, pp. 23–55.
- Jugdutt, B. I. & Amy, R. W. (1986), 'Healing after myocardial infarction in the dog: changes in infarct hydroxyproline and topography', *Journal of the American College of Cardiology* **7**(1), 91–102.
- Jugdutt, B. I., Joljart, M. J. & Khan, M. I. (1996), 'Rate of collagen deposition during healing and ventricular remodeling after myocardial infarction in rat and dog models', *Circulation* **94**(1), 94–101.
- Karamanos, N. K., Theocharis, A. D., Neill, T. & Iozzo, R. V. (2019), 'Matrix modeling and remodeling: a biological interplay regulating tissue homeostasis and diseases', *Matrix Biology* **75**, 1–11.
- Kass, D. A., Maughan, W. L., Ciuffo, A., Graves, W., Healy, B. & Weisfeldt, M. L. (1988), 'Disproportionate epicardial dilation after transmural infarction of the canine left ventricle: acute and chronic differences', *Journal of the American College of Cardiology* **11**(1), 177–185.
- Kerckhoffs, R. C. (2012), 'Computational modeling of cardiac growth in the post-natal rat with a strain-based growth law', *Journal of biomechanics* **45**(5), 865–871.
- Klepach, D., Lee, L. C., Wenk, J. F., Ratcliffe, M. B., Zohdi, T. I., Navia, J. L., Kassab, G. S., Kuhl, E. & Guccione, J. M. (2012), 'Growth and remodeling of the left ventricle: a case study of

- myocardial infarction and surgical ventricular restoration', *Mechanics research communications* **42**, 134–141.
- Kojic, M., Milosevic, M., Simic, V., Milicevic, B., Geroski, V., Nizzero, S., Ziemys, A., Filipovic, N. & Ferrari, M. (2019), 'Smearred multiscale finite element models for mass transport and electrophysiology coupled to muscle mechanics', *Frontiers in Bioengineering and Biotechnology* **7**.
- Kou, S., Caballero, L., Dulgheru, R., Voilliot, D., De Sousa, C., Kacharava, G., Athanassopoulos, G. D., Barone, D., Baroni, M., Cardim, N. et al. (2014), 'Echocardiographic reference ranges for normal cardiac chamber size: results from the norre study', *European Heart Journal–Cardiovascular Imaging* **15**(6), 680–690.
- Krueger, J. & Pollack, G. (1975), 'Myocardial sarcomere dynamics during isometric contraction.', *The Journal of physiology* **251**(3), 627–643.
- Krumholz, H. M., Wang, Y., Chen, J., Drye, E. E., Spertus, J. A., Ross, J. S., Curtis, J. P., Nallamothu, B. K., Lichtman, J. H., Havranek, E. P. et al. (2009), 'Reduction in acute myocardial infarction mortality in the united states: risk-standardized mortality rates from 1995-2006', *Jama* **302**(7), 767–773.
- Laine, G. & Allen, S. (1991), 'Left ventricular myocardial edema. lymph flow, interstitial fibrosis, and cardiac function.', *Circulation research* **68**(6), 1713–1721.
- Lambert, M. I., Grobler, L. & Collins, M. (2004), 'Remodelling of skeletal muscle following exercise-induced muscle damage', *International SportMed Journal* **5**(2), 67–83.
- Langille, B. L. (1993), 'Remodeling of developing and mature arteries: endothelium, smooth muscle, and matrix.', *Journal of cardiovascular pharmacology* **21**, S11–7.
- Lerman, R. H., Apstein, C. S., Kagan, H. M., Osmers, E. L., Chichester, C. O., Vogel, W. M., Connelly, C. M. & Steffee, W. P. (1983), 'Myocardial healing and repair after experimental infarction in the rabbit.', *Circulation research* **53**(3), 378–388.
- Lieberman, A. N., Weiss, J. L., Jugdutt, B., Becker, L., Bulkley, B., Garrison, J., Hutchins, G., Kallman, C. & Weisfeldt, M. (1981), 'Two-dimensional echocardiography and infarct size: relationship of regional wall motion and thickening to the extent of myocardial infarction in the dog.', *Circulation* **63**(4), 739–746.
- Lin, I.-E. & Taber, L. (1995), 'A model for stress-induced growth in the developing heart'.
- Lindsey, C. A., Makarov, M. R., Shoemaker, S., Birch, J. G., Buschang, P. H., Cherkashin, A. M., Welch, R. D. & Samchukov, M. L. (2002), 'The effect of the amount of limb lengthening on skeletal muscle', *Clinical Orthopaedics and Related Research*® **402**, 278–287.

- Linke, W. A., Popov, V. I. & Pollack, G. H. (1994), 'Passive and active tension in single cardiac myofibrils', *Biophysical journal* **67**(2), 782–792.
- Liu, S. & Fung, Y. (1988), 'Zero-stress states of arteries', *Journal of biomechanical engineering* **110**(1), 82–84.
- Lloyd, C. M., Lawson, J. R., Hunter, P. J. & Nielsen, P. F. (2008), 'The cellml model repository', *Bioinformatics* **24**(18), 2122–2123.
- Lodish, H., Berk, A., Zipursky, S. L., Matsudaira, P., Baltimore, D. & Darnell, J. (2000), 'Molecular cell biology 4th edition', *National Center for Biotechnology Information, Bookshelf*.
- Luo, X. (2019), 'School of mathematics and statistics research group', <https://www.maths.gla.ac.uk/~xl/team.html>.
- Ma, Y., de Castro Brás, L. E., Toba, H., Iyer, R. P., Hall, M. E., Winniford, M. D., Lange, R. A., Tyagi, S. C. & Lindsey, M. L. (2014), 'Myofibroblasts and the extracellular matrix network in post-myocardial infarction cardiac remodeling', *Pflügers Archiv-European Journal of Physiology* **466**(6), 1113–1127.
- Maas, S. A., Ellis, B. J., Ateshian, G. A. & Weiss, J. A. (2012), 'Febio: finite elements for biomechanics', *Journal of biomechanical engineering* **134**(1), 011005.
- MacKenna, D., Summerour, S. R. & Villarreal, F. J. (2000), 'Role of mechanical factors in modulating cardiac fibroblast function and extracellular matrix synthesis', *Cardiovascular research* **46**(2), 257–263.
- Makarov, M., Birch, J. & Samchukov, M. (2009), 'The role of variable muscle adaptation to limb lengthening in the development of joint contractures: an experimental study in the goat', *Journal of Pediatric Orthopaedics* **29**(2), 175–181.
- Martínez, G., Rigotti, A., Acevedo, M., Navarrete, C., Rosales, J., Giugliano, R. P. & Corbalán, R. (2013), 'Cholesterol levels and the association of statins with in-hospital mortality of myocardial infarction patients insights from a chilean registry of myocardial infarction', *Clinical cardiology* **36**(6), 305–311.
- Martini, F. et al. (2006), *Anatomy and Physiology'2007 Ed*, Rex Bookstore, Inc.
- Martufi, G. & Gasser, T. C. (2012), 'Turnover of fibrillar collagen in soft biological tissue with application to the expansion of abdominal aortic aneurysms', *Journal of the Royal Society Interface* **9**(77), 3366–3377.
- Martyn, C. & Greenwald, S. (1997), 'Impaired synthesis of elastin in walls of aorta and large conduit arteries during early development as an initiating event in pathogenesis of systemic hypertension', *The Lancet* **350**(9082), 953–955.

- Miller, K., Joldes, G., Lance, D. & Wittek, A. (2007), 'Total lagrangian explicit dynamics finite element algorithm for computing soft tissue deformation', *Communications in numerical methods in engineering* **23**(2), 121–134.
- Miller, T. D., Christian, T. F., Hopfenspirger, M. R., Hodge, D. O., Gersh, B. J. & Gibbons, R. J. (1995), 'Infarct size after acute myocardial infarction measured by quantitative tomographic 99mTc sestamibi imaging predicts subsequent mortality', *Circulation* **92**(3), 334–341.
- Miner, E. C. & Miller, W. L. (2006), A look between the cardiomyocytes: the extracellular matrix in heart failure, in 'Mayo Clinic Proceedings', Vol. 81, Elsevier, pp. 71–76.
- Mohan, D. & Melvin, J. W. (1983), 'Failure properties of passive human aortic tissue. ii—biaxial tension tests', *Journal of biomechanics* **16**(1), 31–44.
- Morse, J. M., Barrett, M., Mayan, M., Olson, K. & Spiers, J. (2002), 'Verification strategies for establishing reliability and validity in qualitative research', *International journal of qualitative methods* **1**(2), 13–22.
- Nagel, T. & Kelly, D. J. (2012), 'Remodelling of collagen fibre transition stretch and angular distribution in soft biological tissues and cell-seeded hydrogels', *Biomechanics and modeling in mechanobiology* **11**(3-4), 325–339.
- Nakamura, M., Ikezoe, T., Takeno, Y. & Ichihashi, N. (2012), 'Effects of a 4-week static stretch training program on passive stiffness of human gastrocnemius muscle-tendon unit in vivo', *European journal of applied physiology* **112**(7), 2749–2755.
- Nash, M. P. & Hunter, P. J. (2000), 'Computational mechanics of the heart - from tissue structure to ventricular function', *Journal of Elasticity*.
- Nikou, A., Dorsey, S. M., McGarvey, J. R., Gorman III, J. H., Burdick, J. A., Pilla, J. J., Gorman, R. C. & Wenk, J. F. (2016), 'Effects of using the unloaded configuration in predicting the in vivo diastolic properties of the heart', *Computer methods in biomechanics and biomedical engineering* **19**(16), 1714–1720.
- Nordez, A., Casari, P., Mariot, J. & Cornu, C. (2009), 'Modeling of the passive mechanical properties of the musculo-articular complex: acute effects of cyclic and static stretching', *Journal of biomechanics* **42**(6), 767–773.
- Oken, D. E. & Boucek, R. J. (1957), 'Quantitation of collagen in human myocardium', *Circulation research* **5**(4), 357–361.
- Olivetti, G., Cigola, E., Maestri, R., Corradi, D., Lagrasta, C., Gambert, S. R. & Anversa, P. (1996), 'Aging, cardiac hypertrophy and ischemic cardiomyopathy do not affect the proportion of mononucleated and multinucleated myocytes in the human heart', *Journal of molecular and cellular cardiology* **28**(7), 1463–1477.

- Olson, E. N. & Schneider, M. D. (2003), 'Sizing up the heart: development redux in disease', *Genes & development* **17**(16), 1937–1956.
- Omens, J. H., Miller, T. R. & Covell, J. W. (1997), 'Relationship between passive tissue strain and collagen uncoiling during healing of infarcted myocardium', *Cardiovascular research* **33**(2), 351–358.
- Oomen, P. J., Holland, M. A., Bouten, C. V., Kuhl, E. & Loerakker, S. (2018), 'Growth and remodeling play opposing roles during postnatal human heart valve development', *Scientific reports* **8**(1), 1235.
- Organisation, W. H. (2017), 'Cardiovascular diseases (CVDs)', [https://www.who.int/en/news-room/fact-sheets/detail/cardiovascular-diseases-\(cvds\)/](https://www.who.int/en/news-room/fact-sheets/detail/cardiovascular-diseases-(cvds)). [Online; accessed 30-July-2019].
- Pang, X., Wu, J.-P., Allison, G. T., Xu, J., Rubenson, J., Zheng, M.-H., Lloyd, D. G., Gardiner, B., Wang, A. & Kirk, T. B. (2017), 'Three dimensional microstructural network of elastin, collagen, and cells in achilles tendons', *Journal of Orthopaedic Research* **35**(6), 1203–1214.
- Paulus, W. J., Tschöpe, C., Sanderson, J. E., Rusconi, C., Flachskampf, F. A., Rademakers, F. E., Marino, P., Smiseth, O. A., De Keulenaer, G., Leite-Moreira, A. F. et al. (2007), 'How to diagnose diastolic heart failure: a consensus statement on the diagnosis of heart failure with normal left ventricular ejection fraction by the heart failure and echocardiography associations of the european society of cardiology', *European heart journal* **28**(20), 2539–2550.
- Pawlush, D. G., Moore, R. L., Musch, T. I. & Davidson Jr, W. (1993), 'Echocardiographic evaluation of size, function, and mass of normal and hypertrophied rat ventricles', *Journal of Applied Physiology* **74**(5), 2598–2605.
- Peterson, K., Tsuji, J., Johnson, A., DiDonna, J. & LeWinter, M. (1978), 'Diastolic left ventricular pressure-volume and stress-strain relations in patients with valvular aortic stenosis and left ventricular hypertrophy', *Circulation* **58**(1), 77–89.
- Pinkert, M. A., Hortensius, R. A., Ogle, B. M. & Eliceiri, K. W. (2018), 'Imaging the cardiac extracellular matrix', *Advances in experimental medicine and biology* **1098**, 21–44. 30238364[pmid].  
**URL:** <https://www.ncbi.nlm.nih.gov/pubmed/30238364>
- Pinto, A. R., Ilinykh, A., Ivey, M. J., Kuwabara, J. T., D'antoni, M. L., Debuque, R., Chandran, A., Wang, L., Arora, K., Rosenthal, N. A. et al. (2016), 'Revisiting cardiac cellular composition', *Circulation research* **118**(3), 400–409.
- Rachev, A. & Hayashi, K. (1999), 'Theoretical study of the effects of vascular smooth muscle contraction on strain and stress distributions in arteries', *Annals of biomedical engineering* **27**(4), 459–468.
- Robinson, T. F., Cohen-Gould, L. & Factor, S. M. (1983), 'Skeletal framework of mammalian

- heart muscle. arrangement of inter-and pericellular connective tissue structures.', *Laboratory investigation; a journal of technical methods and pathology* **49**(4), 482–498.
- Rodriguez, E. K., Hoger, A. & McCulloch, A. D. (1994), 'Stress-dependent finite growth in soft elastic tissues', *Journal of biomechanics* **27**(4), 455–467.
- Rohde, L. E., Aikawa, M., Cheng, G. C., Sukhova, G., Solomon, S. D., Libby, P., Pfeffer, J., Pfeffer, M. A. & Lee, R. T. (1999), 'Echocardiography-derived left ventricular end-systolic regional wall stress and matrix remodeling after experimental myocardial infarction', *Journal of the American College of Cardiology* **33**(3), 835–842.
- Roscoe, L. et al. (1988), 'Stereolithography interface specification', *America-3D Systems Inc* **27**.
- Rouillard, A. D. & Holmes, J. W. (2012), 'Mechanical regulation of fibroblast migration and collagen remodelling in healing myocardial infarcts', *The Journal of physiology* **590**(18), 4585–4602.
- Schrauwen, J., Vilanova, A., Rezakhaniha, R., Stergiopoulos, N., Van De Vosse, F. & Bovendeerd, P. (2012), 'A method for the quantification of the pressure dependent 3d collagen configuration in the arterial adventitia', *Journal of structural biology* **180**(2), 335–342.
- Schwer, L. E. (2009), 'Guide for verification and validation in computational solid mechanics'.
- Scollan, D. F., Holmes, A., Winslow, R. & Forder, J. (1998), 'Histological validation of myocardial microstructure obtained from diffusion tensor magnetic resonance imaging', *American Journal of Physiology-Heart and Circulatory Physiology* **275**(6), H2308–H2318.
- Seynnes, O. R., de Boer, M. & Narici, M. V. (2007), 'Early skeletal muscle hypertrophy and architectural changes in response to high-intensity resistance training', *Journal of applied physiology* **102**(1), 368–373.
- Shadwick, R. E. (1999a), 'Mechanical design in arteries', *Journal of Experimental Biology* **202**(23), 3305–3313.
- Shadwick, R. E. (1999b), 'Mechanical design in arteries', *J. Exp. Biol.* **202**(Pt 23), 3305–3313.
- Sphinx* (2019), <http://www.sphinx-doc.org/en/master/>. Accessed: 2019-08-28.
- STLA Files ASCII stereolithography files* (2014), <https://people.sc.fsu.edu/~jburkardt/data/stla/stla.html>. [Online; accessed 15-September-2019].
- Sugiura, S., Washio, T., Hatano, A., Okada, J., Watanabe, H. & Hisada, T. (2012), 'Multi-scale simulations of cardiac electrophysiology and mechanics using the university of tokyo heart simulator', *Progress in biophysics and molecular biology* **110**(2-3), 380–389.
- Sutton, M. G. S. J. & Sharpe, N. (2000), 'Left ventricular remodeling after myocardial infarction: pathophysiology and therapy', *Circulation* **101**(25), 2981–2988.

- Taber, L. A. (1998), 'Biomechanical growth laws for muscle tissue', *Journal of theoretical biology* **193**(2), 201–213.
- Talman, V. & Ruskoaho, H. (2016), 'Cardiac fibrosis in myocardial infarction—from repair and remodeling to regeneration', *Cell and tissue research* **365**(3), 563–581.
- Thygesen, K., Alpert, J. S., Jaffe, A. S., Simoons, M. L., Chaitman, B. R. & White, H. D. (2012), 'Third universal definition of myocardial infarction', *Circulation* **126**(16), 2020–2035.
- Tidball, J. G. (1992), 'Distribution of collagens and fibronectin in the subepicardium during avian cardiac development', *Anatomy and embryology* **185**(2), 155–162.
- Turillazzi, E., Di Paolo, M., Neri, M., Riezzo, I. & Fineschi, V. (2014), 'A theoretical timeline for myocardial infarction: immunohistochemical evaluation and western blot quantification for interleukin-15 and monocyte chemoattractant protein-1 as very early markers', *Journal of translational medicine* **12**(1), 188.
- van Empel, V. P. & De Windt, L. J. (2004), 'Myocyte hypertrophy and apoptosis: a balancing act', *Cardiovascular research* **63**(3), 487–499.
- Van Rossum, G. & Drake Jr, F. L. (1995), *Python tutorial*, Centrum voor Wiskunde en Informatica Amsterdam.
- Voorhees, A. P. & Han, H.-C. (2011), 'Biomechanics of cardiac function', *Comprehensive Physiology* **5**(4), 1623–1644.
- Wan, W., Hansen, L. & Gleason, R. L. (2010), 'A 3-d constrained mixture model for mechanically mediated vascular growth and remodeling', *Biomechanics and modeling in mechanobiology* **9**(4), 403–419.
- Watton, P., Hill, N. & Heil, M. (2004), 'A mathematical model for the growth of the abdominal aortic aneurysm', *Biomechanics and modeling in mechanobiology* **3**(2), 98–113.
- Watton, P. N., Ventikos, Y. & Holzapfel, G. A. (2009), 'Modelling the growth and stabilization of cerebral aneurysms', *Mathematical medicine and biology: a journal of the IMA* **26**(2), 133–164.
- Weber, K. T. (1989), 'Cardiac interstitium in health and disease: the fibrillar collagen network', *Journal of the American College of Cardiology* **13**(7), 1637–1652.
- Weber, K. T., Clark, W. A., Janicki, J. S. & Shroff, S. G. (1987), 'Physiologic versus pathologic hypertrophy and the pressure-overloaded myocardium.', *Journal of cardiovascular pharmacology* **10**, S37–50.
- Weber, K. T., Sun, Y., Tyagi, S. C. & Cleutjens, J. P. (1994), 'Collagen network of the myocardium: function, structural remodeling and regulatory mechanisms', *Journal of molecular and cellular cardiology* **26**(3), 279–292.

- Wenk, J. F., Sun, K., Zhang, Z., Soleimani, M., Ge, L., Saloner, D., Wallace, A. W., Ratcliffe, M. B. & Guccione, J. M. (2011), 'Regional left ventricular myocardial contractility and stress in a finite element model of posterobasal myocardial infarction', *Journal of biomechanical engineering* **133**(4), 044501.
- Wilcox, B. R., Cook, A. C. & Anderson, R. H. (2005), *Surgical anatomy of the heart*, Cambridge University Press.
- Wisdom, K. M., Delp, S. L. & Kuhl, E. (2015), 'Use it or lose it: multiscale skeletal muscle adaptation to mechanical stimuli', *Biomechanics and modeling in mechanobiology* **14**(2), 195–215.
- Woo, S.-Y., Lubock, P., Gomez, M., Jemmott, G., Kuei, S. & Akeson, W. (1979), 'Large deformation nonhomogeneous and directional properties of articular cartilage in uniaxial tension', *Journal of biomechanics* **12**(6), 437–446.
- Woodcock, E. A. & Matkovich, S. J. (2005), 'Cardiomyocytes structure, function and associated pathologies', *The international journal of biochemistry & cell biology* **37**(9), 1746–1751.
- Woods, R. H. (1892), 'A few applications of a physical theorem to membranes in the human body in a state of tension', *Transactions of the Royal Academy of Medicine in Ireland* **10**(1), 417–427.
- Zhuan, X., Luo, X., Gao, H. & Ogden, R. W. (2019), 'Coupled agent-based and hyperelastic modelling of the left ventricle post-myocardial infarction', *International journal for numerical methods in biomedical engineering* **35**(1), e3155.
- Zöllner, A. M., Abilez, O. J., Böhl, M. & Kuhl, E. (2012), 'Stretching skeletal muscle: chronic muscle lengthening through sarcomerogenesis', *PloS one* **7**(10), e45661.

# Appendix A

The code snippets presented here are supplementary to the descriptions provided in the sections for Chapter[4].

## A.1 Execution Files

### 1. *gr\_data\_setup\_controller.py*:

The file called into the main *gr\_hgo\_model.py* file, which executes the pertinent simulation based on the flag parameter. `flag = [cube, myocardium, gastrocnemius]`.

```
# -*- coding: utf-8 -*-
"""
Created on 24.08.2016
Edited on 17.12.2018
@Shaktidhar Dandapani – The University of Sheffield 2016
modified from the aneurysm library used in my masters thesis.
The current file writes an ANSYS .inp file for an exponential
hyperelastic material.
"""
import os

from collections import defaultdict

import ansys_total.ansyspreprocessing.ansys_file_reader as afr
import ansys_total.ansyspreprocessing.ansys_file_writer as afw
import ansys_total.genericoperations.centroid_fibre_gen as fg

# ----- #
# ANSYS .inp File GeneratorScript #
# ----- #

def write_inp_file(ansys_file_name=str,
                  data_directory=str,
```

## Appendix A

```
        fibre_dictionary=defaultdict(),
        parameters=defaultdict(),
        flag=STR,):

"""
The mesh information is formulated in this
method/ function to be used in writing out
various ANSYS apdl scripts for different simulations.
"""

# ----- #
#           Read in mesh information           #
# ----- #

mesh_data          = defaultdict()

# Associating data to different files from the data directory
nodes_file         = data_directory + "nlist.dat"
elements_file      = data_directory + "elist.dat"
materials_file     = data_directory + "materials.dat"

# Read in the mesh information to be passed onto the writer function file :)
v_file_reader      = afr.ListReader()
nodes_dictionary   = v_file_reader.read_nodes(nodes_file)
element_dictionary = v_file_reader.read_elements(elements_file)

# Basic data
# Creation of fibres with centroids :D
centroids_dictionary = fg.calculate_centroids(nodes_dictionary,
                                               element_dictionary)

# Structuring loose data into a neat dictionary
mesh_data['nodes']      = nodes_dictionary
mesh_data['elements']   = element_dictionary
mesh_data['centroids']  = centroids_dictionary
# All of this mesh_data can be encapsulated in the Mesh class

# Instead of mesh_data -> create a mesh class itself
if flag == "myocardium":
# Check if file exists, else either create a mat file manually
# or create a file with values to be read in
if os.path.isfile(materials_file):
materials_dictionary = afr.read_hgo_material(materials_file)
mesh_data['materials'] = materials_dictionary
```

## Appendix A

```
# To be executed if the flag is for a simulation involving myocardial tissue
inner_surface_file      = data_directory + "inner_surface.dat"
fixed_supp_file        = data_directory + "fixed_support.dat"
infarct_zone_file      = data_directory + "degradation_elements.dat"
inner_base_nodes_file  = data_directory + "base_inner.dat"

mesh_data['inner_surface']      = inner_surface_file
mesh_data['fixed_support']      = fixed_supp_file
mesh_data['infarct_zone']      = infarct_zone_file
mesh_data['base_inner']        = inner_base_nodes_file

o_writeFile = afw.AnsysInpWriter(ansys_file_name, mesh_data)
o_writeFile.inp_writer_lv_hgo_model(parameters)

elif flag == "cube":

# read material files from the csv for muscle format :)
if os.path.isfile(materials_file):
    materials_dictionary = afr.read_hgo_material_musc(materials_file)
    mesh_data['materials'] = materials_dictionary

o_write_file = afw.AnsysInpWriter(ansys_file_name, mesh_data)
o_write_file.write_cube_simulation(parameters)
```

## A.2 Preprocessing Code

### 1. *ansys\_file\_reader*

Python module containing methods for reading input files for STGRF.

```
# -*- coding: utf-8 -*-
"""
Created on 08.08.2016

Class file, containing methods/ functions to read in nodes and elements from
the nlist, elist exported from ANSYS APDL.

"""

import csv
from collections import defaultdict
import ansystotal.genericoperations.mesh_information_structures as mo
import re
```

## Appendix A

```
class ListReader:
    """
    \n
    Class for reading in nodes and elements. Individual objects for multiple files :)
    \n
    """

    def __init__(self, n_file_name = None, e_file_name = None):

        self.n_file_name = n_file_name
        self.e_file_name = e_file_name

    def read_nodes(self, n_file_name):
        """
        Reads the nodes in the file opened in a script.\n
        Returns a clean version of the node numbers with\n
        their co-ordinates

        Args:

        n_file_name (str): Name of the file containing ANSYS
        apdl formatted node description.

        Returns:

        node_coordinate_structure (dict): A dictionary
        containing the node numbers and node
        co-ordinates as follows - {node_no: [[x, y, z]]}
        """

        # Errors include - fileNotFound,
        # InvalidParameter to int/float, invalid array index.
        # Empty line given regex mismatch.
        if n_file_name:
            self.n_file_name = n_file_name
            self.n_file = open(self.n_file_name, "r+")
        else:
            self.n_file = open(n_file_name, "r+")

        content = self.n_file.readlines()

        node_coordinate_structure = defaultdict(list)

        expr_nodeLine = re.compile(r"\s*([0-9]+)")
```

## Appendix A

```
expr_text      = re.compile(r"\s+[A-Z]+\s+")

for line in content:
if re.match(expr_nodeLine, line) and not re.search(expr_text, line):

    line = line.rstrip()
    # strip away the end character on the line string
    line = line.split('_')
    clean_line = list(filter(None, line))

    node_number = clean_line[0] # .replace('.', '')
    node_number = float(node_number)

    # Create a Point class object to represent the node
    # and store in the dictionary using its label and coordinates
    point = mo.Point(float(clean_line[1]), float(clean_line[2]),
                    float(clean_line[3]), str(int(node_number)))
    node_coordinate_structure[int(point.get_label())].append(
    point)

self.n_file.close()
return node_coordinate_structure

def read_elements(self, e_file):
    """
    Reads in an ANSYS apdl output formatted element list text file.\n
    Provides a dictionary with the relevant element connectivity\n
    information.

    Example usage:

    .. code-block:: python

    read_elements("elist.dat")

    Args:

    filename (str): Enter the file name for the ansys elist input.

    Returns:

    element_dictionary (dict): an element dictionary for use and
    manipulation in python.
    co-ordinates as follows - {el_no: [[node_0, ....., node_n]]}
```

## Appendix A

```
"""
el_file = open(e_file, "r+")
el_line = el_file.readlines()
match_1 = r"\s+([0-9]+\s+"
expr_text = r"\s+[A-Z]+\s+"

regex = re.compile(match_1, re.MULTILINE)

element_dictionary = defaultdict(list)

clean_content = []
refined_content = []

for line in el_line:
    if re.match(regex, line) and not re.search(expr_text, line):
        line = line.rstrip()
        filtered_line = list(filter(None, line.split('_')))
        clean_content.append(filtered_line)

# can close the el_file here as all the rest is poured into clean_content
el_file.close()

# The code below needs refining
for index in range(len(clean_content)):
    # First check if 8 nodes exist in ansys output file for elist.
    if len(clean_content[index]) is 14:
        refined_content.append(clean_content[index])
    elif len(clean_content[index]) is 10:
        refined_content.append(clean_content[index])
    elif len(clean_content[index]) < 14:
        refined_content[-1].extend(clean_content[index])

for element_line in refined_content:
    nodes_list = []
    for i in range(6, len(element_line)):
        nodes_list.append(int(element_line[i]))
    element_dictionary[int(element_line[0])] = [nodes_list]

return element_dictionary

def read_hgo_material(filename):
    """
Reads in a csv file containing hgo material information about a mesh

```

## Appendix A

*and returns a dictionary to be further processed in a script.*

*Example usage:*

```
.. code-block:: python
```

```
read_hgo_material("material_values.csv")
```

*Args:*

*filename(str): a csv file containing material information*

*Returns:*

*material\_dictionary(dict): dictionary structure containing all material information in one neat variable.*

```
"""
```

```
material_dictionary = defaultdict(list)
```

```
with open(filename, 'rt') as csvfile:
```

```
reader = csv.reader(csvfile, delimiter=',')
```

```
# Cleanly instruct the csv reader to skip the header line
```

```
# this has been done in order to maintain a header line
```

```
# so as to be able to understand the csv file when opened
```

```
# manually
```

```
next(reader)
```

```
for row in reader:
```

```
element_number = int(row[0])
```

```
c1 = float(row[1])
```

```
k1 = float(row[2])
```

```
k2 = float(row[3])
```

```
k3 = float(row[4])
```

```
k4 = float(row[5])
```

```
av_x = float(row[6])
```

```
av_y = float(row[7])
```

```
av_z = float(row[8])
```

```
bv_x = float(row[9])
```

```
bv_y = float(row[10])
```

```
bv_z = float(row[11])
```

```
pvol = float(row[12])
```

```
m_gn = float(row[13])
```

```
m_c_i4 = float(row[14])
```

```
m_c_i6 = float(row[15])
```

```
material_dictionary[element_number] = [
```

## Appendix A

```
[c1, k1, k2, k3, k4], # c1, k1, k2
[av_x, av_y, av_z], # avector
[bv_x, bv_y, bv_z], # bvector
pvol,
[m_gm, m_c_i4, m_c_i6]
]

return material_dictionary

def read_strain_output(filename):
    """
    Reads in all the strain values from the Strain output file
    and provides an output of the Strain tensor.

    :param filename:
    :return:
    """
    input_file = open(filename, 'r')

    file_data = input_file.readlines()

    numerics_pattern = r"\s+[0-9]"
    element_number_line = r"^\s+ELEMENT"
    string_pattern = r"[A-Z]*E+"

    hencky_strain_dict = defaultdict(list)

    # Initialising variables to avoid errors
    node_counter = 0
    total_e_x = 0
    total_e_y = 0
    total_e_z = 0
    total_e_xy = 0
    total_e_yz = 0
    total_e_xz = 0
    element_number = 0

    for line in file_data:

        if re.match(element_number_line, line):
            element_line = line.rstrip()
            element_line = element_line.split('_')
            element_line = list(filter(None, element_line))
```

## Appendix A

```
element_number = int(element_line[1])
# Reset node variables
node_counter = 0

elif re.match( numerics_pattern, line) and not re.match( string_pattern, line):

# Here given the number of nodes -> calculate the average strain for
each strain component and set that up as a matrix
to be added to the strain dictionary per element

node_counter += 1
line_content = line.rstrip()
line_content = line_content.split('_')
line_content = list(filter(None, line_content))

e_x = float(line_content[1])
e_y = float(line_content[2])
e_z = float(line_content[3])

e_xy = float(line_content[4])
e_yz = float(line_content[5])
e_xz = float(line_content[6])

if node_counter == 1:
total_e_x = e_x
total_e_y = e_y
total_e_z = e_z

total_e_xy = e_xy
total_e_yz = e_yz
total_e_xz = e_xz
else:

total_e_x += e_x
total_e_y += e_y
total_e_z += e_z

total_e_xy += e_xy
total_e_yz += e_yz
total_e_xz += e_xz

avg_e_x = total_e_x / node_counter
avg_e_y = total_e_y / node_counter
avg_e_z = total_e_z / node_counter
```

## Appendix A

```
avg_e_xy    = total_e_xy / node_counter
avg_e_xz    = total_e_xz / node_counter
avg_e_yz    = total_e_yz / node_counter

avg_e_yx    = avg_e_xy
avg_e_zx    = avg_e_xz
avg_e_zy    = avg_e_yz

input_file.close()

# Return the green strain tensor, for further use.
return hencky_strain_dict

def read_fibroblast_stretch_file(filename):
    """
    Reads in a fibroblast file and provides a dictionary back as a
    data structure containing the information

    {e_no: lambda_f, lambda_f^R, lambda_tissue}

    :param filename:
    :return:
    """
    f_file = open(filename, 'r')

    fibro_stretch_dictionary = defaultdict(list)

    words_regex = re.compile(r'[A-Z]+')

    for line in f_file:
        if re.match(words_regex, line):
            pass
        else:
            line = line.rstrip()
            line = line.split(',')
            e_no = int(line[0])
            lambda_f_i4 = float(line[1])
            lambda_f_i6 = float(line[2])
            lambda_f__ri4 = float(line[3])
            lambda_f_r_i6 = float(line[4])
            lambda_t_i4 = float(line[5])
            lambda_t_i6 = float(line[6])
```

## Appendix A

```
fibro_stretch_dictionary[e_no] = [lambda_f_i4, lambda_f_i6,
lambda_f_ri4, lambda_f_r_i6, lambda_t_i4,
lambda_t_i6]

f_file.close()

return fibro_stretch_dictionary

def read_hgo_material_musc(filename):
    """
    Reads in a csv file containing hgo material information about a mesh
    and returns a dictionary to be further processed in a script.

    Example usage:

    .. code-block:: python

    read_hgo_material("material_values.csv")

    Args:
    filename(str): a csv file containing material information

    Returns:
    material_dictionary(dict): dictionary structure containing all material
    information in one neat variable.
    """
    material_dictionary = defaultdict(list)

    # Get the step number return it and update it !
    regex = r'^step.*'

    with open(filename, 'r') as csvfile:
        reader = csv.reader(csvfile, delimiter=',', quotechar='|')
        # Cleanly instruct the csv reader to skip the header line
        # this has been done in order to maintain a header line
        # so as to be able to understand the csv file when opened
        # manually
        next(reader)
        for row in reader:
            element_number = int(row[0])
            c1 = float(row[1])
            k1t = float(row[2])
            k2t = float(row[3])
```

## Appendix A

```
k1m = float(row[4])
k2m = float(row[5])
av_x = float(row[6])
av_y = float(row[7])
av_z = float(row[8])
bv_x = float(row[9])
bv_y = float(row[10])
bv_z = float(row[11])
pvol = float(row[12])
fx = float(row[13])

material_dictionary[element_number] = [
[c1, k1t, k2t, k1m, k2m, fx], # c1, k1, k2
[av_x, av_y, av_z], # avector
[bv_x, bv_y, bv_z], # bvector
pvol, # pvol,
fx
]

return material_dictionary

# Default hgo material reader without modifications for specific tissues !
def read_hgo_material_original(filename):
    """
    Reads in a csv file containing hgo material information about a mesh
    and returns a dictionary to be further processed in a script.

    Example usage:

    .. code-block:: python

    read_hgo_material("material_values.csv")

    Args:
    filename(str): a csv file containing material information

    Returns:
    material_dictionary(dict): dictionary structure containing all material
    information in one neat variable.
    """
    material_dictionary = defaultdict(list)

    with open(filename, 'rt') as csvfile:
        reader = csv.reader(csvfile, delimiter=',')
```

## Appendix A

```
# Cleanly instruct the csv reader to skip the header line
# this has been done in order to maintain a header line
# so as to be able to understand the csv file when opened
# manually
next(reader)

for row in reader:
    element_number = int(row[0])
    c1 = float(row[1])
    k1 = float(row[2])
    k2 = float(row[3])
    k3 = float(row[4])
    k4 = float(row[5])
    av_x = float(row[6])
    av_y = float(row[7])
    av_z = float(row[8])
    bv_x = float(row[9])
    bv_y = float(row[10])
    bv_z = float(row[11])
    pvol = float(row[12])
    material_dictionary[element_number] = [
    [c1, k1, k2, k3, k4], # c1, k1, k2
    [av_x, av_y, av_z], # avector
    [bv_x, bv_y, bv_z], # bvector
    pvol,
    ]

return material_dictionary
```

### 2. *ansys\_file\_writer*:

Python module containing writer functions to help produce output files readable by ANSYS® Mechanical for finite element analysis.

```
# -*- coding: utf-8 -*-
"""
Created on 08.08.2016

Class file containing methods to write ANSYS APDL .inp scripts for execution.
"""

from collections import defaultdict
```

## Appendix A

```
import ansys_total.ansys_preprocessing.ansys_component_writer as mw
import ansys_total.ansys_preprocessing.ansys_file_reader as afr
import ansys_total.generic_operations.calculate_displacement_function as cdf

class AnsysInpWriter:
    """
    ANSYS apdl script generator based on the material required. \n
    Current Implementation includes the neo-hookean material and \n
    the exponential form HGO material formulation.

    """

    def __init__(self,
                filename=None,
                mesh_data=None):

        self.filename      = filename
        self.mesh_data     = mesh_data

        if mesh_data != None:
            self.nodes      = mesh_data[ 'nodes' ]
            self.elements   = mesh_data[ 'elements' ]

    def write_cube_simulation(self, parameters):

        job_fname = self.filename

        prep_fname      = 'prep.inp'
        boundary_cond_fname = 'bcs.inp'
        nodes_fname     = 'nodes.inp'
        elements_fname  = 'elements.inp'
        materials_fname = 'materials.inp'
        solution_fname  = 'solution.inp'
        post_processing_fname = 'post.inp'

        # Create remaining files
        self.create_prep_file_cube(prep_fname)

        mat_values_file = 'material_values_0.csv'

        mat_writer = mw.DataWriter()

        mat_writer.write_nodes(nodes_fname,
                               self.nodes)
```

```

mat_writer.write_elements(elements_fname,
self.elements)

materials_dictionary = self.mesh_data['materials']
mat_writer.write_material_ahyper_expo_original(materials_fname,
mat_values_file,
materials_dictionary)

# Create Boundary Conditions
self.create_bcs_cube_incomp_extension(boundary_cond_fname)

disp_calculator = cdf.DisplacementCalculator(parameters=parameters)
displacement =
disp_calculator.calculate_displacement(str(parameters['step_function']))
self.create_solu_inp_file_tissue_cube(solution_fname, displacement)
post_directory = './libraries/ansysapdlscripts'
write_post_processes(post_processing_fname, post_directory)

# Create the ANSYS job file
with open(job_fname, 'w') as jfile:
jfile.write('\n/INPUT,prep,inp')
jfile.write('\nALLSEL')
jfile.write('\n/INPUT,nodes,inp')
jfile.write('\nALLSEL')
jfile.write('\n/INPUT,elements,inp')
jfile.write('\nALLSEL')
jfile.write('\n/INPUT,materials,inp')
jfile.write('\nALLSEL')
jfile.write('\n/INPUT,bcs,inp')
jfile.write('\nALLSEL')
jfile.write('\n/INPUT,solution,inp')
jfile.write('\nALLSEL')
jfile.write('\n/INPUT,post,inp')
jfile.write('\nALLSEL')

@staticmethod
def create_prep_file_cube(filename):
# Template for everything ?
with open(filename, 'w') as prep_file:
prep_file.write('\n/PREP7')
prep_file.write('\n/UNITS,MPA')
prep_file.write('\n/ET,1,SOLID185')

```

## Appendix A

```
prep_file.write("\nET,2,SOLID186") # 20 node solid element

@staticmethod
def create_solu_inp_file_tissue_cube(filename, displacement):

# Calculate displacements using parameters dictionary and proceed
# Read in the file for displacement !
with open(filename, 'w') as solu_file:
    solu_file.write('\n/SOLU')
    solu_file.write('\nNLGEOM,ON')
    solu_file.write('\nNSEL,S,LOC,X,10')
    solu_file.write('\nD,ALL,UX,{}'.format(displacement)) #
    solu_file.write('\nALLSEL')
    # solu_file.write('\nNSEL,S,LOC,Z,4')
    # solu_file.write('\nD,ALL,UZ,{}'.format(displacement))
    solu_file.write('\nALLSEL')
    solu_file.write("\nNSUBST,_10,_100,_10,_ON")
    solu_file.write('\nSOLVE')
    solu_file.write('\nFINISH')

@staticmethod
def create_solution_file(filename, displacement):

# Read in the file for displacement !
with open(filename, 'w') as solu_file:
    solu_file.write('\n/SOLU')
    solu_file.write('\nNLGEOM,ON')
    solu_file.write('\nNSEL,S,LOC,X,10')
    solu_file.write('\nD,ALL,UX,{}'.format(displacement))
    solu_file.write('\nALLSEL')
    solu_file.write('\nALLSEL')
    solu_file.write("\nNSUBST,_10,_100,_10,_ON")
    solu_file.write('\nSOLVE')
    solu_file.write('\nFINISH')

@staticmethod
def create_bcs_cube_incomp_extension(filename):

with open(filename, 'w') as bc_file:
    bc_file.write('\nNSEL,S,LOC,Y,0')
    bc_file.write('\nD,ALL,UY,0')
    bc_file.write('\nALLSEL')

bc_file.write('\nNSEL,S,LOC,X,0')
```

## Appendix A

```
bc_file.write('\nD,ALL,ALL,0')
bc_file.write('\nALLSEL')

bc_file.write('\nNSEL,S,LOC,Z,0')
bc_file.write('\nD,ALL,UZ,0')
bc_file.write('\nALLSEL')
"""
Writes the ANSYS input file for the HGO model.
"""
def inp_writer_lv_hgo_model(self, parameters):
    """
    This function/ method uses the other modules/ library
    to create a ansys simulation script for a hgo material.

    :param mat_constants:
    :param fibres:
    :return:
    """

    fs_file = self.mesh_data['fixed_support']
    base_inner_file = self.mesh_data['base_inner']
    pface_file = self.mesh_data['inner_surface']

    # ----- #
    #           Writing of the ANSYS inp File           #
    # ----- #
    input_file = open(self.filename, "w+")

    input_file.write("\n/PREP7\n")
    input_file.write("\n/UNITS,MPa\n")           # Set the units to MPa

    input_file.write("\nET,1,SOLID185")           # 8 node solid element
    input_file.write("\nET,2,SOLID186")           # 8 node solid element
    input_file.write("\nKEYOPT,1,6,1!Use_mixed_u-P_formulation_to_avoid_locking")
    input_file.write("KEYOPT,1,2,3!Use_Simplified_Enhanced_Strain_method")

    e_file = "elements"
    n_file = "nodes"
    m_file = "materials"

    e_file_inp = e_file + ".inp"
    n_file_inp = n_file + ".inp"
    m_file_inp = m_file + ".inp"
```

## Appendix A

```
# ----- #
#   Create Node, Elements, Materials Input Files   #
# ----- #

mat_writer = mw.DataWriter()

mat_writer.write_nodes(n_file_inp,
self.nodes)

mat_writer.write_elements(e_file_inp,
self.elements)

mat_values_file = 'material_values_0.csv'

materials_dictionary = self.mesh_data['materials']
mat_writer.write_material_ahyper_expo_lv(m_file_inp,
mat_values_file,
materials_dictionary)

input_file.write("\n\n/INPUT, {} , inp" .format(m_file))
input_file.write("\nALLSEL\n")
input_file.write("\n/INPUT, {} , inp" .format(n_file))
input_file.write("\nALLSEL\n")
input_file.write("\n/INPUT, {} , inp" .format(e_file))
input_file.write("\nALLSEL\n")

# Fixed Support
comp_fs_name      = "fixedsupp"
comp_fs_file      = comp_fs_name + ".inp"
comp_fs_nodes_file = fs_file

comp_base_inner_name      = "baseinner"
comp_base_inner_file      = comp_base_inner_name + ".inp"
comp_base_inner_nodes_file = base_inner_file

create_nodal_comp(comp_fs_file,
comp_fs_nodes_file,
comp_fs_name)

create_nodal_comp(comp_base_inner_file,
comp_base_inner_nodes_file,
comp_base_inner_name)
```

## Appendix A

```
# Set up pressure nodes
comp_pres_name      = "pface"
comp_pres_file      = comp_pres_name + ".inp"
comp_pres_nodes_file = pface_file

create_nodal_comp(comp_pres_file,
comp_pres_nodes_file,
comp_pres_name)

# get in the fixed support and pressure file
input_file.write("\n!Fixed_Support_Specification")
input_file.write("\n/INPUT,_%s,_%inp" % (comp_fs_name))
input_file.write("\nD,_%s,_%ALL,_%0" % (comp_fs_name))

# Inner base nodes rolling support file
input_file.write("\n\n!Inner_Base_Nodes_Specification")
input_file.write("\n/INPUT,_%s,_%inp" % (comp_base_inner_name))
input_file.write("\nD,_%s,_%UY,_%0" % (comp_base_inner_name))
# input_file.write("\nD, %s, ALL, 0" % (comp_base_inner_name))

input_file.write("\n\n!Application_of_pressure_to_inner_surfaces")
input_file.write("\n/INPUT,_%s,_%inp" % (comp_pres_name))

sol_f_name = "solu"
sol_file = sol_f_name + ".inp"
write_solution_file(sol_file, 1.33666e-3, comp_pres_name)
input_file.write("\n\n!Solutions_File")
input_file.write("\n/INPUT,_%s,_%inp" % (sol_f_name))

# Directory in which post processing scripts are stored.
post_directory = './libraries/ansysapdlscripts'

input_file.write("\n\n!Post_Processing_")
write_post_processes('post_p.inp', post_directory)

input_file.write("\n/INPUT,_%post_p,_%inp")
input_file.close()

# Methods outside the writer class.
def write_solution_file(file_name, pressure, region):
    """
    Writes out the solution section of the ansys apdl script.
```

## Appendix A

```
:param file_name:
:param pressure:
:param region:
:return:
"""

with open(file_name, 'w+') as sol_file:

sol_file.write("\n/SOLU")
sol_file.write("\nANTYPE,_STATIC")
sol_file.write("\nNLGEOM,_ON")
sol_file.write("\nPRED,ON, ,ON")
sol_file.write("\nNSUBST,_10,_100,_10,_ON")

sol_file.write("\n!Apply_pressure_to_all_nodes")
sol_file.write("\nSF,_%s,_PRES,_%f" % (region, pressure))

sol_file.write("\nALLSEL")
sol_file.write("\nSOLVE")
sol_file.write("\nFINISH")
sol_file.write("\n")

def write_post_processes(file_name, directory):
    """
    Writes the post processing commands for apdl script.

    :param file_name:
    :param directory:
    :return:
    """

    post_file = open(file_name, 'w')

    post_file.write("\n\n!Post_Processing_Commands_below:")
    post_file.write("\n!=====\n")
    post_file.write("\n/POST1\n")
    post_file.write("\n/INPUT,_get_disp_nodes,inp,{ }".format(directory))
    post_file.write("\n/INPUT,_get_stresses,inp,{ }".format(directory))
    post_file.write("\n/INPUT,_get_strains_comp,inp,{ }".format(directory))
    post_file.write("\n\nFINISH")

    post_file.close()

def create_nodal_comp(filename,
```

## Appendix A

```
nodes_file ,
component_name):
"""
A component is created, specifically a named selection in terms of ANSYS wb.

:param filename:
:param nodes_file:
:param component_name:
:return:
"""
# Opens file to write in components from filename
comp_file = open(filename, "w")

reader = afr.ListReader()

# Reads nodes from nodes_file
nodes = reader.read_nodes(nodes_file)
nodes_list = list(nodes.keys())

for i in range(0, len(nodes_list)):
if i == 0:
comp_file.write("\nNSEL,S,NODE,%d" %nodes_list[i])
else:
comp_file.write("\nNSEL,A,NODE,%d" % nodes_list[i])
comp_file.write("\nCM,_%s,_NODE" %(component_name))
comp_file.write("\nALLSEL")

comp_file.close()

def create_elem_comp(filename ,
nodes_file ,
component_name):
"""
A component is created, specifically a named selection in terms of ANSYS wb.

:param filename:
:param nodes_file:
:param component_name:
:return:
"""
# Opens file to write in components from filename
comp_file = open(filename, "w")

reader = afr.ListReader()
```

```

# Reads nodes from nodes_file
elems = reader.read_elements(nodes_file)
elems_list = list(elems.keys())

for i in range(0, len(elems_list)):
    if i == 0:
        comp_file.write("\nESEL,S,NODE,%d" %elems_list[i])
    else:
        comp_file.write("\nESEL,A,NODE,%d" % elems_list[i])

comp_file.write("\nCM,_%s,_ELEM" %(component_name))
comp_file.write("\nALLSEL")

comp_file.close()

```

### 3. *ansys\_component\_writer*:

An additional writer file complementing *ansys\_file\_writer* with supplementary functions.

```

from collections import defaultdict

# -*- coding: utf-8 -*-
"""
Created on 18.08.2017

Class file containing methods to write out nodes, elements and material model into
respective .inp files to be used by the ansysfilewriter script.

"""

class DataWriter:

    def __init__(self):
        pass

    @staticmethod
    def write_elements(filename, elements_dict=defaultdict(list)):

        # Supply the type here or write in the type before the number of nodes...
        """
        Reads in the file_name to output the elements file to, and the element dictionary.

        Dictionary Format:

```

## Appendix A

```
[Element_number: 'n1, n2 ..... nn']

:param filename:
:param elements_dict:
:return:
"""

e_file = open(filename, "w+")
# Element writing into the INP file
# For 8 Nodes
i = 1
for element, nodes in elements_dict.items():
# centroid = fg.centroidFinder()
# print 'Current Centroid: ', centroid
number_of_nodes = len(nodes[0])

if number_of_nodes is 2:
e_file.write("\nTYPE,5")          # BEAM188
e_file.write("MAT,%d\n" % i)
e_file.write("E,%d,%d\n\n" % (nodes[0][0], nodes[0][1]))
i += 1

if number_of_nodes is 4:
# write the element type here
e_file.write("\nTYPE,4\n")
e_file.write("MAT,%d\n" % i)
e_file.write("E,%d,%d,%d,%d\n\n"
% (nodes[0][0], nodes[0][1], nodes[0][2], nodes[0][3]))
i += 1

elif number_of_nodes is 8:
# write the element type here
e_file.write("\nTYPE,1\n")
e_file.write("MAT,%d\n" % i)
e_file.write("E,%d,%d,%d,%d,%d,%d,%d,%d\n\n"
% (
nodes[0][0], nodes[0][1], nodes[0][2], nodes[0][3],
nodes[0][4], nodes[0][5], nodes[0][6], nodes[0][7]))
i += 1

elif number_of_nodes is 10:
# write the element type here
e_file.write("\nTYPE,3\n")
e_file.write("MAT,%d\n" % i)
```

## Appendix A

```
e_file.write("E,_%d,_%d,_%d,_%d,_%d,_%d,_%d,_%d\n" % (
nodes[0][0], nodes[0][1], nodes[0][2], nodes[0][3],
nodes[0][4], nodes[0][5], nodes[0][6],
nodes[0][7]))
e_file.write("\nEMORE,_%d,_%d" %(nodes[0][8], nodes[0][9]))
i += 1

elif number_of_nodes is 20:
# write the element type here
e_file.write("\nTYPE,2\n")
e_file.write("MAT,_%d\n" % i)
e_file.write("\nE,_%d,_%d,_%d,_%d,_%d,_%d,_%d,_%d" % (
nodes[0][0], nodes[0][1], nodes[0][2], nodes[0][3],
nodes[0][4], nodes[0][5], nodes[0][6],
nodes[0][7]))
e_file.write("\nEMORE,_%d,_%d,_%d,_%d,_%d,_%d,_%d,_%d" %(
nodes[0][8], nodes[0][9], nodes[0][10], nodes[0][11],
nodes[0][12], nodes[0][13],
nodes[0][14], nodes[0][15]))
e_file.write("\nEMORE,_%d,_%d,_%d,_%d\n" %(nodes[0][16],
nodes[0][17], nodes[0][18], nodes[0][19]))
i += 1

e_file.close()

@staticmethod
def write_nodes(filename=str,
nodes_dict=DefaultDict(list)):
    """
    Read in the nodes information via a dictionary holding the information
    as nodes_dict = {node_number: Point(x, y, z)} and write out an input(.inp)
    file readable by the ANSYS MAPDL program.

    :param filename:
    :param nodes_dict:
    :return:
    """
    # Node Writing into the INP File
    # print(nodes_dict[1][0][0].get_x())

    with open(filename, 'w') as file:
for node, coords in nodes_dict.items():
file.write('\nN,_{number},_{x},_{y},_{z}\n'.format
(number=node, x=coords[0].get_x(), y=coords[0].get_y(), z=coords[0].get_z()))
```

```

@staticmethod
def write_material_ahyper_expo_lv(filename, mat_values_csv_file,
material_dictionary):
"""
:param filename:
:param mat_values_csv_file:
:param material_dictionary:
:return:
"""
text_file = open(mat_values_csv_file, "w+")
text_file.write(
"ElementxNumber, _c, _k1, _k2, _k3, _k4,
avec_x, _avec_y, _avec_z, _bvec_x, _bvec_y,
bvec_z, _volume, _m_ground_matrix, _m_collagen_i4,
m_collagen_i6\n")

for element_number, m_values in material_dictionary.items():
c1 = m_values[0][0]
k1 = m_values[0][1]
k2 = m_values[0][2]
k3 = m_values[0][3]
k4 = m_values[0][4]
avec_x = m_values[1][0]
avec_y = m_values[1][1]
avec_z = m_values[1][2]
bvec_x = m_values[2][0]
bvec_y = m_values[2][1]
bvec_z = m_values[2][2]
vol = m_values[3]
m_gm = m_values[4][0]
m_c_i4 = m_values[4][1]
m_c_i6 = m_values[4][2]

text_file.write("{el_no}, _{c1}, _{k1}, _{k2}, _{k3}, _{k4}, _{avec_x}, _{avec_y}, _"
"{avec_z}, _{bvec_x}, _{bvec_y}, _{bvec_z}, _{vol}, _{m_gm}, _{m_c_i4}, _{m_c_i6}\n" \
.format(el_no=element_number, c1=c1, k1=k1, k2=k2, k3=k3, k4=k4,
avec_x=avec_x, avec_y=avec_y, avec_z=avec_z, bvec_x=bvec_x,
bvec_y=bvec_y, bvec_z=bvec_z, vol=vol, m_gm=m_gm, m_c_i4=m_c_i4, m_c_i6=m_c_i6))

text_file.close()

f_file = open(filename, "w+")

```

## Appendix A

```
for element_number, m_values in material_dictionary.items():

    c1 = m_values[0][0]
    k1 = m_values[0][1]
    k2 = m_values[0][2]
    k3 = m_values[0][3]
    k4 = m_values[0][4]

    avec_x = m_values[1][0]
    avec_y = m_values[1][1]
    avec_z = m_values[1][2]

    bvec_x = m_values[2][0]
    bvec_y = m_values[2][1]
    bvec_z = m_values[2][2]

    vol = m_values[3]

    f_file.write('\nTB,_AHYPER,_%d,_,_EXPO_\n' % element_number)
    f_file.write('TBDATA,_1,_%f,_0,_0,_0,_0_\n' % c1)
    f_file.write('TBDATA,_7,_%f,_%f,_%s,_%f\n' % (k1, k2, k3, k4))
    f_file.write('TB,_AHYPER,_%d,_,_PVOL_\n' % element_number)
    f_file.write('TBDATA,_,_%f_\n' % vol)

    f_file.write('TB,_AHYPER,_%d,_,_AVEC_\n' % element_number)
    f_file.write('TBDATA,_,_%f,_%f,_%f_\n' % (avec_x, avec_y, avec_z))
    f_file.write('TB,_AHYPER,_%d,_,_BVEC_\n' % element_number)
    f_file.write('TBDATA,_,_%f,_%f,_%f_\n' % (bvec_x, bvec_y, bvec_z))

f_file.close()

@staticmethod
def write_material_ahyper_expo_musc(filename, mat_values_csv_file, material_dictionary):
    """

    :param filename:          'materials.inp'
    :param mat_values_csv_file: 'material_values_*.csv'
    :param material_dictionary: new_materials
    :return:
    """

    text_file = open(mat_values_csv_file, "w+")
```

## Appendix A

```
text_file.write("e_no,c,k1t,k2t,klm,k2m,ax,ay,az,bx,by,bz,pvol,fx\n")

for element_number, m_values in material_dictionary.items():
    c1      = m_values[0][0]
    k1t     = m_values[0][1]
    k2t     = m_values[0][2]
    klm     = m_values[0][3]
    k2m     = m_values[0][4]
    avec_x  = m_values[1][0]
    avec_y  = m_values[1][1]
    avec_z  = m_values[1][2]
    bvec_x  = m_values[2][0]
    bvec_y  = m_values[2][1]
    bvec_z  = m_values[2][2]
    vol     = m_values[3]
    fx      = m_values[4]

    text_file.write("%d,%f,%f,%f,%f,%f,%f,%f,%f,%f,%f,%f,%f,%f\n"
% (element_number, c1, k1t, k2t, klm, k2m,
avec_x, avec_y, avec_z, bvec_x, bvec_y, bvec_z,
vol, fx))

text_file.close()

f_file = open(filename, "w+")
for element_number, m_values in material_dictionary.items():

    c1      = m_values[0][0]
    k1t     = m_values[0][1]
    k2t     = m_values[0][2]
    klm     = m_values[0][3]
    k2m     = m_values[0][4]
    avec_x  = m_values[1][0]
    avec_y  = m_values[1][1]
    avec_z  = m_values[1][2]
    bvec_x  = m_values[2][0]
    bvec_y  = m_values[2][1]
    bvec_z  = m_values[2][2]
    # vol   = m_values[3]
    fx      = m_values[4]

    if fx == 0:

        f_file.write('\nTB,_AHYPER,%s,%s,%s,_EXPO_\n' % element_number)
```

## Appendix A

```
f_file.write('TBDATA,1,%f,0,0,0,0\n' % (c1))
f_file.write('TBDATA,7,%f,%f,%f,%f\n' % (k1t, k2t, k1m, k2m))

f_file.write('TB,AHYPER,%s,%s,PVOL\n' % element_number)
f_file.write('TBDATA,1\n')

f_file.write('TB,AHYPER,%s,%s,AVEC\n' % element_number)
f_file.write('TBDATA,%f,%f,%f\n' % (avec_x, avec_y, avec_z))

f_file.write('TB,AHYPER,%s,%s,BVEC\n' % element_number)
f_file.write('TBDATA,%f,%f,%f\n' % (bvec_x, bvec_y, bvec_z))

elif 0 < fx < 1:

f_file.write('\nTB,AHYPER,%s,%s,EXPO\n' % element_number)
f_file.write('TBDATA,1,%f,0,0,0,0\n' % (c1))
f_file.write('TBDATA,7,%f,%f,%f,%f\n' % (k1t, k2t, k1m, k2m))

f_file.write('TB,AHYPER,%s,%s,PVOL\n' % element_number)
f_file.write('TBDATA,1\n')

f_file.write('TB,AHYPER,%s,%s,AVEC\n' % element_number)
f_file.write('TBDATA,%f,%f,%f\n' % (avec_x, avec_y, avec_z))

f_file.write('TB,AHYPER,%s,%s,BVEC\n' % element_number)
f_file.write('TBDATA,%f,%f,%f\n' % (bvec_x, bvec_y, bvec_z))

elif fx == 1:

f_file.write('\nTB,AHYPER,%s,%s,EXPO\n' % element_number)
f_file.write('TBDATA,1,%f,0,0,0,0\n' % (c1))
f_file.write('TBDATA,7,%f,%f,%f,%f\n' % (k1t, k2t, k1m, k2m))

f_file.write('TB,AHYPER,%s,%s,PVOL\n' % element_number)
f_file.write('TBDATA,1\n')

f_file.write('TB,AHYPER,%s,%s,AVEC\n' % element_number)
f_file.write('TBDATA,%f,%f,%f\n' % (avec_x, avec_y, avec_z))

f_file.write('TB,AHYPER,%s,%s,BVEC\n' % element_number)
f_file.write('TBDATA,%f,%f,%f\n' % (bvec_x, bvec_y, bvec_z))

f_file.close()
```

## Appendix A

```
@staticmethod
def write_material_ahyper_expo_original(filename,
mat_values_csv_file, material_dictionary):
    """

    :param filename:
    :param mat_values_csv_file:
    :param material_dictionary:
    :return:
    """

    text_file = open(mat_values_csv_file, "w+")
    text_file.write(
    "ElementxNumber, c, k1, k2, k3, k4,
    avec_x, avec_y, avec_z, bvec_x, bvec_y, bvec_z,
    volume\n")

    for element_number, m_values in material_dictionary.items():
        c1 = m_values[0][0]
        k1 = m_values[0][1]
        k2 = m_values[0][2]
        k3 = m_values[0][3]
        k4 = m_values[0][4]
        avec_x = m_values[1][0]
        avec_y = m_values[1][1]
        avec_z = m_values[1][2]
        bvec_x = m_values[2][0]
        bvec_y = m_values[2][1]
        bvec_z = m_values[2][2]
        vol = m_values[3]

        text_file.write("{el_no}, {c1}, {k1}, {k2}, {k3}, {k4}, {avec_x}, {avec_y}, {
        {avec_z}, {bvec_x}, {bvec_y}, {bvec_z}, {vol}\n" \
        .format(el_no=element_number, c1=c1, k1=k1, k2=k2, k3=k3, k4=k4,
        avec_x=avec_x, avec_y=avec_y, avec_z=avec_z, bvec_x=bvec_x,
        bvec_y=bvec_y, bvec_z=bvec_z, vol=vol))

    text_file.close()

    f_file = open(filename, "w+")

    for element_number, m_values in material_dictionary.items():
        c1 = m_values[0][0]
        k1 = m_values[0][1]
```

## Appendix A

```
k2 = m_values[0][2]
k3 = m_values[0][3]
k4 = m_values[0][4]
avec_x = m_values[1][0]
avec_y = m_values[1][1]
avec_z = m_values[1][2]
bvec_x = m_values[2][0]
bvec_y = m_values[2][1]
bvec_z = m_values[2][2]
vol = m_values[3]

f_file.write('\nTB,_AHYPER,_%d,_,_,_EXPO_\n' % element_number)
f_file.write('TBDATA,_%d,_%f,_%d,_%d,_%d,_%d_\n' % c1)
f_file.write('TBDATA,_%d,_%f,_%f,_%f,_%f_\n' % (k1, k2, k3, k4))
f_file.write('TB,_AHYPER,_%d,_,_,_PVOL_\n' % element_number)
f_file.write('TBDATA,_,_%f_\n' % vol)

f_file.write('TB,_AHYPER,_%d,_,_,_AVEC_\n' % element_number)
f_file.write('TBDATA,_,_%f,_%f,_%f_\n' % (avec_x, avec_y, avec_z))
f_file.write('TB,_AHYPER,_%d,_,_,_BVEC_\n' % element_number)
f_file.write('TBDATA,_,_%f,_%f,_%f_\n' % (bvec_x, bvec_y, bvec_z))

f_file.close()
```

### A.3 Postprocessing Files

#### 1. *vtk\_file\_writer*:

```
class VTKFileWriter:

def __init__(self, mesh_data):
    # Filename, optional argument for what
    # functions described below need to be used
    self.mesh_data = mesh_data
    self.nodes     = self.mesh_data['nodes']
    self.elements  = self.mesh_data['elements']
    # self.fibres   = self.mesh_data['fibres']

def create_tetrahedral_mesh(self, filename, results):

    total_nodes = len(self.nodes.keys())
    total_elems = len(self.elements.keys())
```







```

from scipy.linalg import expm

import ansystotal.ansyspreprocessing.ansys_file_reader as afr

def create_invariant_dictionaries(mat_props=defaultdict,
hencky_strain_dict=defaultdict):
    """
    Calculate i4 for each element provided the green strain dictionary as the input.
    The resultant dictionary contains the values for i4 for each individual element.

    Example usage:

    .. code-block:: python

    create_I_4_tensor_dict(gs_dictionary)

    Args:

    mat_props (defaultdict): provide the dictionary with material values
    hencky_strain_dict (defaultdict) : Dictionary containing
    average hencky strain tensor for each element.

    Returns:

    i4_dictionary (defaultdict): the value of i4 for each element
    is returned as a dictionary data structure
    as follows - {el_no: i4_value}

    """
    # Read in the material properties from the excel sheet

    I_4_dictionary = defaultdict()
    I_6_dictionary = defaultdict()

    for element_number, g_strain_tensor in hencky_strain_dict.items():
        a_0_1 = mat_props[element_number][1]
        a_0_2 = mat_props[element_number][2]

        # Calculate the Cauchy Stress tensor.
        u_tensor, c_tensor = hencky_strain_transformations(g_strain_tensor)

        I_4 = calculate_invariants(c_tensor, a_0_1)
        I_6 = calculate_invariants(c_tensor, a_0_2)
        I_4_dictionary[element_number] = I_4

```

## Appendix A

```
I_6_dictionary[element_number] = I_6

return I_4_dictionary, I_6_dictionary

def create_i4_dictionary_musc(filename, hencky_strain_dict):
    """
    Calculate i4 for each element provided the green strain dictionary as the input.
    The resultant dictionary contains the values for i4 for each individual element.

    Example usage:

    .. code-block:: python

    create_I_4_tensor_dict(gs_dictionary)

    Args:

    filename (str): Provide the file containing the material
    properties for a current geometry.
    hencky_strain_dict (defaultdict) : Dictionary containing
    average hencky strain tensor for each element.

    Returns:

    i4_dictionary (defaultdict): the value of i4 for each element
    is returned as a dictionary data structure
    as follows - {el_no: i4_value}

    """
    # Read in the material properties from the excel sheet
    mat_props = afr.read_hgo_material_musc(filename)
    I_4_dictionary = defaultdict()
    I_6_dictionary = defaultdict()

    for element_number, g_strain_tensor in hencky_strain_dict.items():

    #
    a_0_1 = mat_props[element_number][1]
    a_0_2 = mat_props[element_number][2]

    # Calculate the Cauchy Stress tensor.
    u_tensor, c_tensor = hencky_strain_transformations(g_strain_tensor)
    I_4 = calculate_invariants(c_tensor, a_0_1)
    I_6 = calculate_invariants(c_tensor, a_0_2)
```

## Appendix A

```
I_4_dictionary[element_number] = I_4
I_6_dictionary[element_number] = I_6

return I_4_dictionary, I_6_dictionary

def hencky_strain_transformations(hencky_strain_tensor):
    """
    Transform hencky strain tensor into required quantities.

    :param hencky_strain_tensor:
    :return u_tensor, c_tensor:
    """
    # Hencky strain is defined as:
    #  $h = \ln(U)$ 
    # therefore,  $U = \exp(h)$ 

    u_tensor = expm(np.matrix(hencky_strain_tensor))

    c_tensor = np.linalg.matrix_power(u_tensor, 2) #  $U^2$ 

    return u_tensor, c_tensor

def calculate_invariants(cauchy_green_tensor, a_0_x):

    np_a_0_x = np.matrix(a_0_x)

    A = np.outer(np_a_0_x, np_a_0_x)

    np_cauchy_green_tensor = np.matrix(cauchy_green_tensor)

    invariant = np.tensordot(np_cauchy_green_tensor, A)

    return invariant

def calculate_aniso_stresses(k_num, k_den, invariant):

    if invariant > 1:

        cauchy_stress = 2 * invariant * k_num * (invariant - 1) *
            (math.exp(k_den * (invariant - 1) ** 2))
        pk_stress = cauchy_stress / math.sqrt(invariant)

    else:
        cauchy_stress = 0
```

```
pk_stress = 0

return pk_stress, cauchy_stress
```

## A.4 Custom Workflow Creation

### 1. Main execution script (PERL)

This particular script serves as the start point to execute the customised workflow, by executing the scripts within the STGRE, external remodelling python script and executing the ANSYS® Mechanical solver as well as managing the loop back to set up the next iteration/step in the simulation till the desired time limit.

```
#!/usr/bin/perl
use warnings;
use strict;
use Cwd;
use libraries::RemodellingRoutines::check_file;
use libraries::RemodellingRoutines::execute_ansys;
use libraries::RemodellingRoutines::read_file_to_hash;
use File::Copy;

# Read in the parameters file and calculate the time etc automatically here !
# using python dictionary approach
my %param_data;
my $param_fname = "./parameters/parameters_myocardium.dat";

# Include a command to print out the time stamp and calculate
# the time taken for the simulation to finish

my $datestring = localtime();
print "Start_Time:_", $datestring;

# 1. Declare the name of the file and store into a variable

my $file_name_python = "gr_hgo_model.py";
# my $dir = getcwd;

# Read n system argument for stress_evo
my $evo_flag = $ARGV[0];
print($evo_flag);
# 2. Run a command using the file name and run the file

if (!-e $file_name_python) {
```

## Appendix A

```
print "no_python_script_generator_file_found.";
# die "\nNeed a python file to run\n";
} else {
# my $shear_modulus = 2e06;
system("python", $file_name_python, "myocardium");
}

# 3. Only monitor the creation/ modification of .inp file
print "\n_____ (ctrl+c_to_halt) _____\n";

my $input_file = 'ansys_job.inp';

check_file_existence({filename => $input_file});

# 4. Once the .inp file is created execute ansys
# Place a check on job name and create new jobname for each iteration
my $step_counter = 0;
my $job_name_clean = 'gr_step_';
my $job_name = $job_name_clean. $step_counter;

execute({
input_file => $input_file,
job_name => $job_name
});

print "\n_end_ansys_job";

# ----- #
# 5.b. if nlist and elist are found, use them to run through the
#      script for building fibres..... and proceed to initiate the .inp file
#      to the next step.
my $file_stress = 'stress_list.txt';
my $file_strain = 'strain_list.txt';

my $exists_file_stress = check_file_existence({filename => $file_stress});

my $file_homeo_stress = 'stress_list_0.txt';
my $file_homeo_strain = 'strain_list_0.txt';

if ($exists_file_stress){
rename $file_stress, $file_homeo_stress;
rename $file_strain, $file_homeo_strain;
print "\n_Homeostatic_state_Saved";
}
```

## Appendix A

```
# Run fibroblast script to create recruitment field
system("python", "./workflows/write_fibroblast_file.py");
my $fibroblast_homeo_fname = "fibroblast_info_0.csv";

# Growth And Remodelling Loop

my $homeostatic_material_values = "material_values_0.csv";
rename "material_values.csv", $homeostatic_material_values; # dont need this line

%param_data = read_parameters_file({
filename => $param_fname,
});
# print $param_data{'time_period'};
my $time_period_param = $param_data{'time_period'};
my $no_of_steps_param = $param_data{'number_of_iterations'};
my $step_param = $param_data{'iteration'};

my $file_time = "./parameters/parameters_myocardium.dat";
my $material_ansys = "materials.inp";
my $rem_script = "./workflows/remodelling_mod_hgo.py";
my $gr_steps_limit = int($no_of_steps_param) - 1;
my $old_material_values = "_"; # initialise variable
my $remodelled_material_values = "_";
my $prev_strain_list = "strain_list_0.txt";
my $prev_stress_list = "stress_list_0.txt";
my $prev_material_list = "material_values_0.csv";
my $new_job_name = "";
my $old_fibro_file = "";
my $remodelled_fibro_file = "";
my $new_rem_strain_list = "";
my $homeo_counter = 0;

for (my $i = $step_counter; $i <= $gr_steps_limit; $i++){
%param_data = read_parameters_file({
filename => $param_fname,
});
my $time_period_param = $param_data{'time_period'};
my $no_of_steps_param = $param_data{'number_of_iterations'};
my $step_param = $param_data{'iteration'};
print "\n_Curr_Step:_", $step_param;
print "\n_Curr_Time:_", $step_param * ($time_period_param/$no_of_steps_param);
# Evolve the homeostatic state if evo_flag is active
if ($evo_flag == 1){
```

## Appendix A

```
$homeo_counter = int($i/4);
}
if ($i == 0){
$prev_material_list = $homeostatic_material_values;
$old_fibro_file     = $fibroblast_homeo_fname;
}
else{
$old_fibro_file     = $remodelled_fibro_file;
}

if ($i < 2){
$file_homeo_strain  = "strain_list_". $homeo_counter. ".txt";
}
else{
$file_homeo_strain  = "strain_list_rem_". $homeo_counter. ".txt";
}
$new_job_name       = $job_name_clean. "rem_". $i;

$remodelled_fibro_file       = "fibroblast_info_rem_". $i. ".csv";

$remodelled_material_values  = "material_values_rem_". $i. ".csv";

# Execute Growth & Remodelling Script
print "\n_Remodelling_Script_Running...";
system("python",
$rem_script,
$prev_strain_list,
$file_homeo_strain,
$prev_material_list,
$homeostatic_material_values,
$remodelled_material_values,
$material_ansys,
$fibroblast_homeo_fname,
$old_fibro_file,
$remodelled_fibro_file,
$file_time,
$evo_flag);

# Execute ansys simulation for remodelled materials list
execute({
input_file => $input_file,
job_name => $new_job_name
});
```

## Appendix A

```
# save a copy of the stresses for the degraded simulation
my $exists_file_stress      = check_file_existence({filename => $file_stress});
my $exists_file_strain     = check_file_existence({filename => $file_strain});

# This will come when deg stops and remodelling kicks in
my $new_rem_stress_list    = "stress_list_rem_".$.i.".txt";
$new_rem_strain_list       = "strain_list_rem_".$.i.".txt";

# Save the output files in the names of the current step and phase.
if ($exists_file_stress){
copy($file_stress , $new_rem_stress_list);
}

if ($exists_file_strain){
copy($file_strain , $new_rem_strain_list);
}

$prev_material_list = $remodelled_material_values;
$prev_strain_list   = $new_rem_strain_list;
$prev_stress_list   = $new_rem_strain_list;
my $datestring_2 = localtime ();
print "\n_System_Time:_", $datestring_2;
}

my $datestring_3 = localtime ();
print "\nEnd_Time:_", $datestring_3;
```

2. External Python Script: The external customised remodelling scripts are shown below:

a. For left ventricle with a myocardial infarction.

```
import math
import sys
from collections import defaultdict
import csv

from ansystotal.ansyspreprocessing import
ansys_component_writer as acr
from ansystotal.ansyspreprocessing import
ansys_file_reader as afr
from ansystotal.genericoperations import
generic_commands as gc, gr_commands as grc
from ansystotal.ansyspostprocessing import
vtk_file_writer as vfw, tensor_operations as to
import ansystotal.genericoperations.mesh_information_structures as mis
```

```

def read_updated_homeo_file(filename):

curr_homeo_value_dict = defaultdict()

with open(filename, 'rt') as uphome_file:
reader = csv.reader(uphome_file, delimiter=',')

# Cleanly instruct the csv reader to skip the header line
# this has been done in order to maintain a header line
# so as to be able to understand the csv file when opened
# manually
next(reader)
for row in reader:
el_no = int(row[0])
sigma_h_i4 = float(row[1])
sigma_h_i6 = float(row[2])
curr_homeo_value_dict[el_no] = [sigma_h_i4, sigma_h_i6]

return curr_homeo_value_dict

def write_updated_homeo_file(filename, home_stress_dict):

# with open(filename)
with open(filename, 'w') as uph_file:
uph_file.write("e_no, _sigma_ch_i4, _sigma_ch_i6\n")
for e_no, values in home_stress_dict.items():
sigma_ch_i4 = values[0]
sigma_ch_i6 = values[1]
uph_file.write("{} , {} , {} \n".format(e_no, sigma_ch_i4, sigma_ch_i6))

def write_result_sheet_files(results_dictionary, c_curr_iteration):
# Write it out
for keys, values in results_dictionary.items():

# keys -> name of the file
# values -> {e_no: quantity_pair}
new_fname = './results/' + str(keys) +
'_step_rem_' + str(c_curr_iteration) + '.csv'
with open(new_fname, 'w') as wfile:
for e_no, quantity in values.items():

```

## Appendix A

```
wfile.write("{} ,_{}\n".format(int(e_no), float(quantity)))

def write_vtk_file(materials_dictionary, results_dictionary, curr_step):

    if curr_step < 10:
        vtk_file = 'results_vtk_0' + str(curr_step) + '.vtk'
        vtk_file_materials = 'materials_vtk_0' + str(curr_step) + '.vtk'
    else:
        vtk_file = 'results_vtk_' + str(curr_step) + '.vtk'
        vtk_file_materials = 'materials_vtk_' + str(curr_step) + '.vtk'

    # Mesh data to pass onto the vtk file writer function
    root_dir = gc.return_read_root_directory_name(
        './parameters/directories_information.dat')
    # Gives us the directory
    data_directory = root_dir['myocardium']

    nodes_fname = data_directory + "nlist.dat"
    elems_fname = data_directory + "elist.dat"
    disp_nodes_fname = "./disp_nodes.txt"

    disp_nodes_reader = afr.ListReader()
    disp_nodes = disp_nodes_reader.read_nodes(disp_nodes_fname)

    # Read in the mesh data using STGRF functions
    mesh_reader = afr.ListReader()

    nodes = mesh_reader.read_nodes(nodes_fname)
    elems = mesh_reader.read_elements(elems_fname)

    new_nodes = defaultdict()

    for node, coords in disp_nodes.items():
        x_coord = coords[0].get_x() + nodes[node][0].get_x()
        y_coord = coords[0].get_y() + nodes[node][0].get_y()
        z_coord = coords[0].get_z() + nodes[node][0].get_z()
        new_nodes[node] = [mis.Point(x_coord, y_coord, z_coord, str(int(node)))]

    mesh_data = defaultdict()

    mesh_data['nodes'] = new_nodes
    mesh_data['elements'] = elems
```

## Appendix A

```
# Write VTK file
vtk_writer = vfw.VTKFileWriter(mesh_data)
# same for I4, I6
vtk_writer.create_results_vtk_hexahedral(vtk_file, results_dictionary)
vtk_writer.create_material_value_tables_myocardium_hexahedral(
vtk_file_materials, materials_dictionary)

# vtk_writer for stresses (change in the core file :) )

def remodelling_routine(strain_curr_step_file,
strain_homeostatic_step_file,
material_curr_step_file,
material_homeostatic_step_file,
material_values_new_step_fname,
material_inp_fname,
fibroblast_info_homeo_fname,
fibroblast_info__curr_fname,
fibroblast_info_new_fname,
parameters_file,
evo_flag):

# a. Read in the output from ANSYS (log strains)
# b. Calculate i4, i6
# c. In turn calculate Cauchy Stresses in respective fibre directions
# d. Growth based on fibroblast stretch changes
# e. Remodelling based on Cauchy Stresses.
# f. Update files for the next step

parameters = grc.read_params_file(parameters_file)

# data directory reader
data_directory =
gc.return_read_root_directory_name('./parameters/directories_information.dat')

time_period = int(parameters['time_period'])
steps = int(parameters['number_of_iterations'])
alpha = float(parameters['alpha'])
beta = float(parameters['beta'])
gamma = float(parameters['gamma'])
curr_step = int(parameters['iteration'])

c_delta_t = float(time_period/steps)

# Read infarcted tissue zone
```

## Appendix A

```
infarct_reader = afr.ListReader()
infarct_file = data_directory['myocardium'] + "degradation_elements.dat"
infarct_zone = infarct_reader.read_elements(infarct_file)

# Read in the strain files
hencky_strains_curr = afr.read_strain_output(strain_curr_step_file)
hencky_strains_home = afr.read_strain_output(strain_homeostatic_step_file)

material_values_dict_curr =
afr.read_hgo_material(material_curr_step_file)
material_values_dict_home = afr.read_hgo_material(material_homeostatic_step_file)

i4_dict_curr, i6_dict_curr =
to.create_invariant_dictionaries(material_values_dict_curr, hencky_strains_curr)
i4_dict_home, i6_dict_home =
to.create_invariant_dictionaries(material_values_dict_home, hencky_strains_home)

# Read in the fibroblast stretch files
fibroblast_info_dict_curr =
afr.read_fibroblast_stretch_file(fibroblast_info__curr_fname)
fibroblast_info_dict_home =
afr.read_fibroblast_stretch_file(fibroblast_info_homeo_fname)

# Storing new values and dictionaries for the next step and vtk files
new_materials_dict = material_values_dict_curr

fibroblast_info_dict_new = defaultdict()

sigma_aniso_i4_h = defaultdict()
sigma_aniso_i4_curr = defaultdict()
sigma_aniso_i4_difference = defaultdict()

sigma_aniso_i6_h = defaultdict()
sigma_aniso_i6_curr = defaultdict()
sigma_aniso_i6_difference = defaultdict()

fibroblast_stretch_i4 = defaultdict()
fibroblast_stretch_i6 = defaultdict()

# Homeo Update
homeo_file_name_updated = "updated_homeo.csv"

updated_homeo_stress = defaultdict()
inp_up_homeo_stress = read_updated_homeo_file(homeo_file_name_updated)
```

## Appendix A

```
results_dictionary = defaultdict()
results_dictionary['sigma_aniso_i4_h'] = sigma_aniso_i4_h
results_dictionary['sigma_aniso_i4_curr'] = sigma_aniso_i4_curr
results_dictionary['sigma_aniso_i4_difference'] = sigma_aniso_i4_difference

results_dictionary['sigma_aniso_i6_h'] = sigma_aniso_i6_h
results_dictionary['sigma_aniso_i6_curr'] = sigma_aniso_i6_curr
results_dictionary['sigma_aniso_i6_difference'] = sigma_aniso_i6_difference

results_dictionary['i4'] = i4_dict_curr
results_dictionary['i6'] = i6_dict_curr

results_dictionary['stretch_fibroblast_i4'] = fibroblast_stretch_i4
results_dictionary['stretch_fibroblast_i6'] = fibroblast_stretch_i6

# Extra constants
d_time = 14 * (steps / time_period)
d_time_coll = 5 * (steps / time_period)

for e_no, values in material_values_dict_curr.items():

    _alpha = 1.0 * alpha
    _gamma = 1.0 * gamma
    _beta = 1.0 * beta

# Read in the values for the homeostatic step file
c_homeo = material_values_dict_home[e_no][0][0]
k1_home = material_values_dict_home[e_no][0][1]
k2_home = material_values_dict_home[e_no][0][2]
k3_home = material_values_dict_home[e_no][0][3]
k4_home = material_values_dict_home[e_no][0][4]

# Read in the values for the current step file
c_curr = values[0][0]
k1_curr = values[0][1]
k2_curr = values[0][2]
k3_curr = values[0][3]
k4_curr = values[0][4]

avec = values[1]
bvec = values[2]
```

## Appendix A

```
vol = values[3]
m_gm = values[4][0]
v_m_c_i4 = float(values[4][1])
v_m_c_i6 = float(values[4][2])
c_new = c_curr

# Degrade
if e_no in infarct_zone.keys():

    if curr_step <= d_time:
m_gm = 0.001**(curr_step / d_time)
c_new = c_homeo * m_gm
    if c_new <= 0.001 * c_homeo:
c_new = 0.001 * c_homeo # be careful how you degrade !
    else:
c_new = 0.001 * c_homeo

# Now proceed with the cauchy stress calculations
i4_homeo = i4_dict_home[e_no]
i6_homeo = i6_dict_home[e_no]

i4_curr = i4_dict_curr[e_no]
i6_curr = i6_dict_curr[e_no]

an_pk_home_i4, an_cauchy_home_i4 =
    to.calculate_aniso_stresses(k1_home, k2_home, i4_homeo)
an_pk_home_i6, an_cauchy_home_i6 =
    to.calculate_aniso_stresses(k3_home, k4_home, i6_homeo)
up_homeo_cauchy_i4 = inp_up_homeo_stress[e_no][0]
up_homeo_cauchy_i6 = inp_up_homeo_stress[e_no][1]

an_pk_curr_i4, an_cauchy_curr_i4 =
    to.calculate_aniso_stresses(k1_curr, k2_curr, i4_curr)
an_pk_curr_i6, an_cauchy_curr_i6 =
    to.calculate_aniso_stresses(k3_curr, k4_curr, i6_curr)

# ----- Fibroblast update ----- #

fibro_stretch_homeo_i4 = fibroblast_info_dict_home[e_no][0]
fibro_stretch_homeo_i6 = fibroblast_info_dict_home[e_no][1]
```

## Appendix A

```
fibro_stretch_rec_i4 = fibroblast_info_dict_curr[e_no][2]
fibro_stretch_rec_i6 = fibroblast_info_dict_curr[e_no][3]

tissue_stretch_i4 = math.sqrt(i4_curr)
tissue_stretch_i6 = math.sqrt(i6_curr)

fibro_stretch_curr_i4 = tissue_stretch_i4 / fibro_stretch_rec_i4
fibro_stretch_curr_i6 = tissue_stretch_i6 / fibro_stretch_rec_i6

fibro_rec_new_i4 = fibro_stretch_rec_i4 + _gamma * c_delta_t *
fibro_stretch_rec_i4 * \
((fibro_stretch_curr_i4 - fibro_stretch_homeo_i4) /
fibro_stretch_homeo_i4)

fibro_rec_new_i6 = fibro_stretch_rec_i6 + _gamma * c_delta_t *
fibro_stretch_rec_i6 * \
((fibro_stretch_curr_i6 - fibro_stretch_homeo_i6) /
fibro_stretch_homeo_i6)

fibroblast_info_dict_new[e_no] = [fibro_stretch_curr_i4, fibro_stretch_curr_i6,
fibro_rec_new_i4, fibro_rec_new_i6,
tissue_stretch_i4, tissue_stretch_i6]

# Update the values in the new materials dictionary to be fed
# into the next simulation

m_c_new_i4 = v_m_c_i4 + _beta * v_m_c_i4 * c_delta_t * \
((fibro_stretch_curr_i4 - fibro_stretch_homeo_i4) / fibro_stretch_homeo_i4)

m_c_new_i6 = v_m_c_i6 + _beta * v_m_c_i6 * c_delta_t * \
((fibro_stretch_curr_i6 - fibro_stretch_homeo_i6) / fibro_stretch_homeo_i6)

# ----- Fibroblast update end ----- #

# Evolution of homoeostatic stress for collagen fibres.
if int(evo_flag) == 1 and curr_step <= d_time - (1 * (steps / time_period)):
an_cauchy_home_i4_temp = (an_cauchy_home_i4 + an_cauchy_curr_i4) / 2
an_cauchy_home_i6_temp = (an_cauchy_home_i6 + an_cauchy_curr_i6) / 2
```

## Appendix A

```
if an_cauchy_home_i6_temp < up_homeo_cauchy_i6:
an_cauchy_home_i6 = up_homeo_cauchy_i6
else:
an_cauchy_home_i6 = an_cauchy_home_i6_temp

if an_cauchy_home_i4_temp < up_homeo_cauchy_i4:
an_cauchy_home_i4 = up_homeo_cauchy_i4
else:
an_cauchy_home_i4 = an_cauchy_home_i4_temp
else:
an_cauchy_home_i4 = up_homeo_cauchy_i4
an_cauchy_home_i6 = up_homeo_cauchy_i6

updated_homeo_stress[e_no] = [an_cauchy_home_i4, an_cauchy_home_i6]

if an_cauchy_curr_i4 > 0 and an_cauchy_home_i4 > 0:
k2_new = k2_curr - _alpha * k2_curr * c_delta_t * \
(v_m_c_i4 * an_cauchy_curr_i4 - an_cauchy_home_i4) / an_cauchy_home_i4

if k2_new <= 0.01 * k2_home:
k2_new = 0.01 * k2_home

else:
k2_new = k2_curr

if an_cauchy_curr_i6 > 0 and an_cauchy_home_i6 > 0:
k4_new = k4_curr - _alpha * k4_curr * c_delta_t * \
(v_m_c_i6 * an_cauchy_curr_i6 - an_cauchy_home_i6) / an_cauchy_home_i6

if k4_new < 0.01 * k4_home:
k4_new = 0.01 * k4_home
else:
k4_new = k4_curr

k1_new = k1_home * (k2_new / k2_home)
k3_new = k3_home * (k4_new / k4_home)

if k1_new < 0.01 * k1_home:
k1_new = 0.01 * k1_home

if k3_new < 0.01 * k3_home:
k3_new = 0.01 * k3_home
```

## Appendix A

```
# if e_no in infarct_zone.keys():
new_materials_dict[e_no][0][0] = c_new
new_materials_dict[e_no][0][1] = k1_new * m_c_new_i4
new_materials_dict[e_no][0][2] = k2_new
new_materials_dict[e_no][0][3] = k3_new * m_c_new_i6
new_materials_dict[e_no][0][4] = k4_new
# Mass density updates
new_materials_dict[e_no][4][1] = m_c_new_i4
new_materials_dict[e_no][4][2] = m_c_new_i6

# Storing values
# Store values
sigma_aniso_i4_curr[e_no] = an_cauchy_curr_i4
sigma_aniso_i4_h[e_no] = an_cauchy_home_i4
sigma_aniso_i4_difference[e_no] =
(an_cauchy_curr_i4 - an_cauchy_home_i4) #/ an_cauchy_home_i4
#
sigma_aniso_i6_curr[e_no] = an_cauchy_curr_i6
sigma_aniso_i6_h[e_no] = an_cauchy_home_i6
sigma_aniso_i6_difference[e_no] =
(an_cauchy_curr_i6 - an_cauchy_home_i6) #/ an_cauchy_home_i6

fibroblast_stretch_i4[e_no] = fibro_stretch_curr_i4
fibroblast_stretch_i6[e_no] = fibro_stretch_curr_i6

# Write Updated Homeostatic File
write_updated_homeo_file(homeo_file_name_updated, updated_homeo_stress)

# Write in the new materials
mat_writer = acr.DataWriter()

mat_writer.write_material_ahyper_expo_lv(
material_inp_fname, material_values_new_step_fname, new_materials_dict)

grc.write_params_file(parameters_file,
time_period,
steps,
curr_step + 1,
alpha,
beta,
gamma)

# Write out the fibroblast recruitment field file
grc.write_fibroblast_file(fibroblast_info_new_fname,
```

## Appendix A

```
fibroblast_info_dict_new)
write_vtk_file(new_materials_dict, results_dictionary, curr_step)
# write_result_sheet_files(results_dictionary, curr_step)

def exec_remodelling():

    strain_curr_step_file = sys.argv[1]
    strain_homeostatic_step_file = sys.argv[2]
    material_curr_step_file = sys.argv[3]
    material_homeostatic_step_file = sys.argv[4]
    material_values_new_step_fname = sys.argv[5]
    material_inp_fname = sys.argv[6]
    fibroblast_info_homeo_fname = sys.argv[7]
    fibroblast_info__curr_fname = sys.argv[8]
    fibroblast_info_new_fname = sys.argv[9]
    parameters_file = sys.argv[10]
    evo_flag = sys.argv[11]

    remodelling_routine(
    strain_curr_step_file ,
    strain_homeostatic_step_file ,
    material_curr_step_file ,
    material_homeostatic_step_file ,
    material_values_new_step_fname ,
    material_inp_fname ,
    fibroblast_info_homeo_fname ,
    fibroblast_info__curr_fname ,
    fibroblast_info_new_fname ,
    parameters_file ,
    evo_flag)

if __name__ == '__main__':
    exec_remodelling()
```

b. For over-stretch of gastrocnemius skeletal muscle *remodelling\_tissue\_strip.py*

```

import sys

from collections import defaultdict

import ansys_total.generic_operations.gr_commands as grc
import ansys_total.ansys_preprocessing.ansys_file_reader as afr
import ansys_total.ansys_preprocessing.ansys_component_writer as acw
import ansys_total.ansys_preprocessing.ansys_file_writer as afw
import ansys_total.ansys_postprocessing.tensor_operations as to
import ansys_total.generic_operations.calculate_displacement_function as cdf
import ansys_total.ansys_postprocessing.vtk_file_writer as vfw
import ansys_total.generic_operations.mesh_information_structures as mis
from ansys_total.generic_operations import generic_commands as gc

def remodel_material(strain_curr_file,
                    strain_homeo_file,      # Homeostatic step - strain file
                    stress_curr_file,       # Current Step - Stress File
                    stress_homeo_file,      # Homeostatic step - stress file
                    material_curr_csv,      # Current Step - Materials File
                    materials_inp_fname,    # 'materials.inp'
                    material_new_csv,       # New File_name - next_step
                    # materials_values_*.csv
                    material_homeo_csv,     # Homeostatic Step - Materials File
                    parameters_file):      # Parameters file

    """
    Algorithm:

    1. read in the old material values file into a dictionary (read_hgo_material)
    2. read in old stress file and current stress file
    3. calculate tissue_stress_grad of the stresses
    4. remodel k2m, k2t
    5. Write in a new materials file and material value file
    6. Create the input for next simulation
    """

    # Read time info for rates and step info
    parameter_info = grc.read_params_file(parameters_file)
    beta_t = float(parameter_info['beta_t'])
    beta_m = float(parameter_info['beta_m'])

```

## Appendix A

```
time_period          = int(parameter_info['time_period'])
number_of_iterations = int(parameter_info['number_of_iterations'])
curr_step            = int(parameter_info['iteration'])

init_time = int(parameter_info['init_time'])
max_time  = int(parameter_info['max_time'])
init_disp = float(parameter_info['init_disp'])
max_disp  = float(parameter_info['max_disp'])

c_delta_t = time_period / number_of_iterations

# ----- #
#           Remodelling of k2           #
# ----- #

# Remodelling

# Reading in files and calculating new material values based on
# what information we have from the previous steps.
# 1. Read in homeostatic strains
# 2. Read in current strain values
# 3. calculate the Cauchy stresses in collagen via I_4
# 4. This will help us in the remodelling equations

# Reading in the strains
hencky_strains_current = afr.read_strain_output(strain_curr_file)
hencky_strains_homeo   = afr.read_strain_output(strain_homeo_file)

i4_dict_curr, i6_dict_curr =
    to.create_i4_dictionary_musc(material_curr_csv, hencky_strains_current)
i4_dict_homeo, i6_dict_homeo =
    to.create_i4_dictionary_musc(material_homeo_csv, hencky_strains_homeo)

# Read in the materials file to get a materials
# dictionary to be used in the calculation of stresses
material_values_curr = afr.read_hgo_material_musc(material_curr_csv)
material_values_homeo = afr.read_hgo_material_musc(material_homeo_csv)

new_materials = material_values_curr

# Tendon
sigma_aniso_h_t = defaultdict()
sigma_aniso_curr_t = defaultdict()
sigma_aniso_difference_t = defaultdict()
```

## Appendix A

```
# Muscle
sigma_aniso_h_m      = defaultdict()
sigma_aniso_curr_m   = defaultdict()
sigma_aniso_difference_m = defaultdict()

sv_c_curr = defaultdict()
sv_k1t_curr = defaultdict()
sv_k1m_curr = defaultdict()
sv_k2t_curr = defaultdict()
sv_k2m_curr = defaultdict()

for e_no in hencky_strains_homeo.keys():

c1_homeo = material_values_homeo[e_no][0][0]
k1t_homeo = material_values_homeo[e_no][0][1]
k2t_homeo = material_values_homeo[e_no][0][2]
k1m_homeo = material_values_homeo[e_no][0][3]
k2m_homeo = material_values_homeo[e_no][0][4]
# av_x      = material_values_homeo[e_no][1][0]
# av_y      = material_values_homeo[e_no][1][1]
# av_z      = material_values_homeo[e_no][1][2]
# bv_x      = material_values_homeo[e_no][2][0]
# bv_y      = material_values_homeo[e_no][2][1]
# bv_z      = material_values_homeo[e_no][2][2]
# pvol      = material_values_homeo[e_no][3]
# fx_homeo  = material_values_homeo[e_no][4]

# need all values from current iteration so
# that materials can be set up for next run
c1_curr   = material_values_curr[e_no][0][0]
k1t_curr  = material_values_curr[e_no][0][1]
k2t_curr  = material_values_curr[e_no][0][2]
k1m_curr  = material_values_curr[e_no][0][3]
k2m_curr  = material_values_curr[e_no][0][4]
av_x_curr = material_values_curr[e_no][1][0]
av_y_curr = material_values_curr[e_no][1][1]
av_z_curr = material_values_curr[e_no][1][2]
bv_x_curr = material_values_curr[e_no][2][0]
bv_y_curr = material_values_curr[e_no][2][1]
bv_z_curr = material_values_curr[e_no][2][2]
pvol_curr = material_values_curr[e_no][3]
```

## Appendix A

```
fx_curr      = material_values_curr[e_no][4]

# Remodelling values

if fx_curr == 0:

pk_stress_musc_homeo, cau_stress_muscle_homeo =
to.calculate_aniso_stresses(k1m_homeo, k2m_homeo,
i4_dict_homeo[e_no])
pk_stress_muscle_curr, cau_stress_muscle_curr =
to.calculate_aniso_stresses(k1m_curr, k2m_curr,
i4_dict_curr[e_no])
if cau_stress_muscle_homeo > 0:
cau_stress_muscle_gradient = float(
(cau_stress_muscle_curr - cau_stress_muscle_homeo) / cau_stress_muscle_homeo)
else:
cau_stress_muscle_gradient = 0

# Store stresses
sigma_aniso_curr_m[e_no] = cau_stress_muscle_curr
sigma_aniso_h_m[e_no]     = cau_stress_muscle_homeo

sigma_aniso_difference_m[e_no] = cau_stress_muscle_gradient

sigma_aniso_curr_t[e_no] = 0
sigma_aniso_h_t[e_no]     = 0

sigma_aniso_difference_t[e_no] = 0

new_k2m = k2m_curr - k2m_curr * ((beta_m *
cau_stress_muscle_gradient) * c_delta_t)

if new_k2m <= 0.01:
new_k2m = 0.01

new_k1m = new_k2m * (k1m_homeo/k2m_homeo)
if new_k1m <= 0.1 * k1m_homeo:
new_k1m = 0.1 * k1m_homeo

new_materials[e_no] = [
[c1_curr, k1t_curr, k2t_curr, new_k1m, new_k2m],
[av_x_curr, av_y_curr, av_z_curr],
[bv_x_curr, bv_y_curr, bv_z_curr],
pvol_curr,
```

## Appendix A

```
fx_curr
]

sv_k1m_curr[e_no] = round(new_k1m, 4)
sv_k2m_curr[e_no] = round(new_k2m, 4)
sv_k1t_curr[e_no] = round(k1t_curr, 4)
sv_k2t_curr[e_no] = round(k2t_curr, 4)

elif fx_curr == 1:

pk_stress_tendon_homeo, cau_stress_tendon_homeo =
    to.calculate_aniso_stresses(k1t_homeo, k2t_homeo,
i6_dict_homeo[e_no]) # Tendon
pk_stress_tendon_curr, cau_stress_tendon_curr =
    to.calculate_aniso_stresses(k1t_curr, k2t_curr,
i6_dict_curr[e_no])
if cau_stress_tendon_homeo > 0:
cau_stress_tendon_gradient = float(
(cau_stress_tendon_curr - cau_stress_tendon_homeo) / cau_stress_tendon_homeo)
else:
cau_stress_tendon_gradient = 0

# Store stresses
sigma_aniso_curr_m[e_no] = 0
sigma_aniso_h_m[e_no] = 0

sigma_aniso_difference_m[e_no] = 0

sigma_aniso_curr_t[e_no] = cau_stress_tendon_curr
sigma_aniso_h_t[e_no] = cau_stress_tendon_homeo

sigma_aniso_difference_t[e_no] = cau_stress_tendon_gradient

new_k2t =
    k2t_curr - k2t_curr * ((beta_t * cau_stress_tendon_gradient) * c_delta_t)

if new_k2t <= 0.01:
new_k2t=0.01

new_k1t = new_k2t * (k1t_homeo / k2t_homeo)
if new_k1t < 0.1 * k1t_homeo:
new_k1t = 0.1 * k1t_homeo

new_materials[e_no] = [
```

## Appendix A

```
[c1_curr, new_k1t, new_k2t, k1m_curr, k2m_curr],
[av_x_curr, av_y_curr, av_z_curr],
[bv_x_curr, bv_y_curr, bv_z_curr],
pvol_curr,
fx_curr
]

sv_k1m_curr[e_no] = round(k1m_curr, 4)
sv_k2m_curr[e_no] = round(k2m_curr, 4)
sv_k1t_curr[e_no] = round(new_k1t, 4)
sv_k2t_curr[e_no] = round(new_k2t, 4)

elif 0 < fx_curr < 1:

pk_stress_tendon_homeo, cau_stress_tendon_homeo =
    to.calculate_aniso_stresses(k1t_homeo, k2t_homeo,
i4_dict_homeo[e_no]) # Tendon
pk_stress_tendon_curr, cau_stress_tendon_curr =
    to.calculate_aniso_stresses(k1t_curr, k2t_curr,
i4_dict_curr[e_no])

pk_stress_musc_homeo, cau_stress_muscle_homeo =
    to.calculate_aniso_stresses(k1m_homeo, k2m_homeo,
i6_dict_homeo[e_no])
pk_stress_muscle_curr, cau_stress_muscle_curr =
    to.calculate_aniso_stresses(k1m_curr, k2m_curr,
i6_dict_curr[e_no])

if cau_stress_muscle_homeo > 0:
cau_stress_muscle_gradient =
float(
(cau_stress_muscle_curr - cau_stress_muscle_homeo) / cau_stress_muscle_homeo)
else:
cau_stress_muscle_gradient = 0

if cau_stress_tendon_homeo > 0:
cau_stress_tendon_gradient = float(
(cau_stress_tendon_curr - cau_stress_tendon_homeo) / cau_stress_tendon_homeo)
else:
cau_stress_tendon_gradient = 0

# Store stresses
sigma_aniso_curr_m[e_no] = cau_stress_muscle_curr
```

## Appendix A

```
sigma_aniso_h_m[e_no] = cau_stress_muscle_homeo

sigma_aniso_difference_m[e_no] = cau_stress_muscle_gradient

sigma_aniso_curr_t[e_no] = cau_stress_tendon_curr
sigma_aniso_h_t[e_no] = cau_stress_tendon_homeo

sigma_aniso_difference_t[e_no] = cau_stress_tendon_gradient

# Remodelling

new_k2t = k2t_curr - k2t_curr * ((beta_t *
cau_stress_tendon_gradient) * c_delta_t)
new_k2m = k2m_curr - k2m_curr * ((beta_m *
cau_stress_muscle_gradient) * c_delta_t)

if new_k2t <= 0.01:
new_k2t = 0.01

if new_k2m <= 0.01:
new_k2m = 0.01

new_k1t = new_k2t * (k1t_homeo / k2t_homeo)
if new_k1t < 0.01 * k1t_homeo:
new_k1t = 0.01 * k1t_homeo

new_k1m = new_k2m * (k1m_homeo/k2m_homeo)
if new_k1m <= 0.01 * k1m_homeo:
new_k1m = 0.01 * k1m_homeo

new_materials[e_no] = [
[c1_curr, new_k1t, new_k2t, new_k1m, new_k2m],
[av_x_curr, av_y_curr, av_z_curr],
[bv_x_curr, bv_y_curr, bv_z_curr],
pvol_curr,
fx_curr
]

sv_k1m_curr[e_no] = round(new_k1m, 4)
sv_k2m_curr[e_no] = round(new_k2m, 4)
sv_k1t_curr[e_no] = round(new_k1t, 4)
sv_k2t_curr[e_no] = round(new_k2t, 4)
```

## Appendix A

```
results_dictionary = defaultdict()
material_results_dict = defaultdict()

results_dictionary['sigma_aniso_h_t'] = sigma_aniso_h_t
results_dictionary['sigma_aniso_curr_t'] = sigma_aniso_curr_t
results_dictionary['sigma_aniso_difference_t'] = sigma_aniso_difference_t

results_dictionary['sigma_aniso_h_m'] = sigma_aniso_h_m
results_dictionary['sigma_aniso_curr_m'] = sigma_aniso_curr_m
results_dictionary['sigma_aniso_difference_m'] = sigma_aniso_difference_m
results_dictionary['i4_values'] = i4_dict_curr
results_dictionary['i6_values'] = i6_dict_curr

material_results_dict['k1m_values'] = sv_k1m_curr
material_results_dict['k2m_values'] = sv_k2m_curr

material_results_dict['k1t_values'] = sv_k1t_curr
material_results_dict['k2t_values'] = sv_k2t_curr

writer_object = acw.DataWriter()
writer_object.write_material_ahyper_expo_musc(
    materials_inp_fname, material_new_csv, new_materials)

# 3. update the parameters file\
parameters = parameter_info # unnecessary dummy variable
step_function = str(parameters['step_function'])

grc.write_params_muscle(parameters_file,
    time_period,
    number_of_iterations,
    curr_step + 1,
    beta_t,
    beta_m,
    init_time,
    max_time,
    init_disp,
    max_disp,
    step_function)

# Calculate displacement for the next step
displacement_calc = cdf.DisplacementCalculator(parameters=parameters)

displacement = displacement_calc.calculate_displacement(flag=step_function)
```

```

print ("\ncurrent_Displacement:{}".format(displacement))

sol_file_writer = afw.AnsysInpWriter()
sol_file_writer.create_solution_file("solution.inp", displacement)

write_vtk_file(material_results_dict, results_dictionary, curr_step)

def write_result_sheet_files(results_dictionary, c_curr_iteration):
for keys, values in results_dictionary.items():
new_fname = './results/' + str(keys) + '_step_rem_' + str(c_curr_iteration) + '.csv'
with open(new_fname, 'w') as wfile:
for e_no, quantity in values.items():
wfile.write("{} ,_{} \n".format(int(e_no), float(quantity)))

# Create a tetrahedral one !
def write_vtk_file(material_results_dictionary,
                  results_dictionary, curr_step):

if curr_step < 10:
    vtk_file = 'results_vtk_0' + str(curr_step) + '.vtk'
    vtk_file_mat = 'material_' + vtk_file
    else:
    vtk_file = 'results_vtk_' + str(curr_step) + '.vtk'
    vtk_file_mat = 'material_' + vtk_file

# Mesh data to pass onto the vtk file writer function
root_dir = gc.return_read_root_directory_name(
    './parameters/directories_information.dat')
# Gives us the directory
data_directory = root_dir['gastro']

nodes_fname = data_directory + "nlist.dat"
elems_fname = data_directory + "elist.dat"
disp_nodes_fname = "./disp_nodes.txt"

disp_nodes_reader = afr.ListReader()
disp_nodes = disp_nodes_reader.read_nodes(disp_nodes_fname)

# Read in the mesh data using STGRF functions
mesh_reader = afr.ListReader()

```

## Appendix A

```
nodes = mesh_reader.read_nodes(nodes_fname)
elems = mesh_reader.read_elements(elems_fname)

new_nodes = defaultdict()

for node, coords in disp_nodes.items():
    x_coord = coords[0].get_x() + nodes[node][0].get_x()
    y_coord = coords[0].get_y() + nodes[node][0].get_y()
    z_coord = coords[0].get_z() + nodes[node][0].get_z()
    new_nodes[node] = [mis.Point(x_coord, y_coord, z_coord, str(int(node)))]

mesh_data = defaultdict()

mesh_data['nodes'] = new_nodes
mesh_data['elements'] = elems

# Write VTK file
vtk_writer = vfw.VTKFileWriter(mesh_data)
vtk_writer.create_tetrahedral_mesh(vtk_file, results_dictionary)
# vtk_writer.create_hexahedral_mesh("muscle_surface.vtk")
vtk_writer.create_tetrahedral_mesh_only("surface_"+vtk_file)
vtk_writer.create_tetrahedral_mesh(vtk_file_mat, material_results_dictionary)

def exec_remodelling():

    strain_curr_file           = sys.argv[1]
    strain_homeo_file          = sys.argv[2]
    stress_curr_file           = sys.argv[3]
    stress_homeo_file          = sys.argv[4]
    material_old_csv           = sys.argv[5]
    material_new_csv           = sys.argv[6]
    materials_inp_file         = sys.argv[7]
    material_homeo_csv         = sys.argv[8]
    parameters_file            = sys.argv[9]

    remodel_material(strain_curr_file,
                     strain_homeo_file,
                     stress_curr_file,
                     stress_homeo_file,
                     material_old_csv,
                     material_new_csv,
                     materials_inp_file,
                     material_homeo_csv,
                     parameters_file)
```

## Appendix A

```
if __name__ == '__main__':  
    exec_remodelling()
```

# Appendix B

## B.1 STL file

The file extension stl is an abbreviation for "stereolithography", where a surface for a geometry is created using computer graphics by triangulation of points or vertices making up said geometry. An example is shown in Figure [B.1], where a cubic object is represented using stl ([STLA Files ASCII stereolithography files \(2014\)](#)).

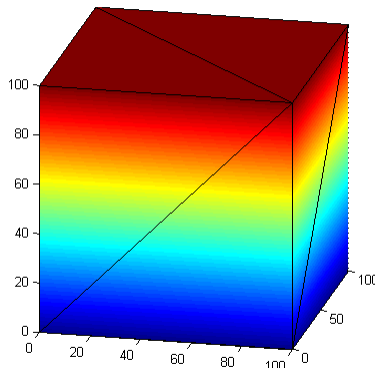


**Figure B.1:** A block or cube, represented as an stl file where each surface comprises of two triangles providing an idea about how stl surface geometries are generated.

## B.2 Code For Volume Fraction Assignment Algorithm

The MATLAB script for projecting surfaces inwards and partitioning, along with the assignment of volume fractions via interpolation in tecplot are shown below.

```

clear all

%% File reading *****

read = fopen('ranges.txt','r');
if ( read==-1 )
error('Can''t open the file. ');
end
% read case id
C1 = textscan(read, '%s', 'delimiter', '\n');
pattern1 = 'Case: ';
idx1 = find(~cellfun(@isempty, regexp(C1{1}, pattern1)));
frewind(read)
textscan(read, '%s', idx1, 'Delimiter', '\n');
c1 = textscan(read, '%d', 'delimiter', '\n');

% make sure the user type in the correct case number
if c1{1} == 0 || c1{1} == 1
caseId = str2num(string(c1));
else
error('Case_number_should_be_either_0_or_1');
end

frewind(read)

% read aponeurosis case
C2 = textscan(read, '%s', 'delimiter', '\n');
pattern2 = 'Aponeurosis_case_id: ';
idx = find(~cellfun(@isempty, regexp(C2{1}, pattern2)));
frewind(read)
textscan(read, '%s', idx, 'Delimiter', '\n');
c2 = textscan(read, '%d', 'delimiter', '\n');
apo_caseId = str2num(string(c2));
frewind(read)

% read cylinder height
C3 = textscan(read, '%s', 'delimiter', '\n');
pattern3 = 'length: ';
idx3 = find(~cellfun(@isempty, regexp(C3{1}, pattern3)));
frewind(read)

```

## Appendix B

```
textscan(read, '%s', idx3, 'Delimiter', '\n');
c3 = textscan(read, '%f', 'delimiter', '\n');
cylinder_length = str2num(string(c3));

% Check the variables
% if isnumeric(c2{1}) == 1
%     cylinder_length = str2num(string(c2));
% else
%     error('Length should be declared as an integer or a double');
% end
frewind(read)

% read cylinder radius
C4 = textscan(read, '%s', 'delimiter', '\n');
pattern4 = 'radius: ';
idx4 = find(~ cellfun(@isempty, regexp(C4{1}, pattern4)));
frewind(read)
textscan(read, '%s', idx4, 'Delimiter', '\n');
c4 = textscan(read, '%f', 'delimiter', '\n');
cylinder_radius = str2num(string(c4));
frewind(read)

fclose(read);

%% Initial decisions *****

cylinder = caseId; % make a cylinder=1, else import data=0
aponeurosiscase = apo_caseId; % illustrative testcases
%for aponeurosis models
reversenormal = 0
apothick = 1; % aponeurosis thickness
transthick = 1; % transition thickness

%% Setting up the matrices *****

if cylinder == 1

cyllength = cylinder_length;
radius = cylinder_radius;
nelem_l = 50;
nelem_c = 60;

% Coordinate matrices
count = 0;
```

## Appendix B

```
for i = 1:nelem_l+1;
for j = 1:nelem_c
count=count+1
x(count) = cyllength*(i-1)/nelem_l;
y(count) = radius*cos(2*pi*(j-1)/nelem_c);
z(count) = radius*sin(2*pi*(j-1)/nelem_c);
end
end

% Connectivity matrix
count2 = 0;
for i = 1:nelem_l;
for j = 1:nelem_c-1
count2=count2+1;
connect(count2,2) = nelem_c*(i-1)+j ;
connect(count2,3) = nelem_c*i+j+1;
connect(count2,4) = nelem_c*(i-1)+j+1;

count2=count2+1;
connect(count2,2) = nelem_c*(i-1)+j ;
connect(count2,3) = nelem_c*i+j ;
connect(count2,4) = nelem_c*i+j+1;
end
end

for i = 1:nelem_l;
j= nelem_c
count2=count2+1;
connect(count2,2) = nelem_c*(i-1)+j ;
connect(count2,3) = nelem_c*i+1;
connect(count2,4) = nelem_c*(i-1)+1;
count2=count2+1;
connect(count2,2) = nelem_c*(i-1)+j ;
connect(count2,3) = nelem_c*i+j ;
connect(count2,4) = nelem_c*i+1;
end

lp = count;
lc = count2;

c(:,1) = connect(:,2);
c(:,2) = connect(:,3);
c(:,3) = connect(:,4);
```

## Appendix B

```
else

load('points.dat')
load('connect.dat')

lp = length(points); % length of points array (nodes)
lc = length(connect);% length of elements array

count = 0;

for i=1:lp
for j=1:3
count=count+1;
x(count) = points(i,3*(j-1)+1);
y(count) = points(i,3*(j-1)+2);
z(count) = points(i,3*(j-1)+3);
end
end

c(:,1) = connect(:,2)+1;
c(:,2) = connect(:,3)+1;
c(:,3) = connect(:,4)+1;

end

%*****

% Coordinates matrix v
v(:,1) = x;
v(:,2) = y;
v(:,3) = z;
lx=length(x);

% Define a theta variable [0,2*pi] as a function of x and y
% Here based relative to 0,0 but maybe better defined relative to
% centreline if the long axis does not go through muscle.
for i = 1:lx
locy = v(i,2);
locz = v(i,3);
if (locy >= 0) & (locz >= 0)
theta(i) = atan(locz/locy);
elseif (locy < 0) & (locz >= 0)
theta(i) = pi/2+ atan(-locy/locz);
elseif (locy < 0) & (locz < 0)
```

## Appendix B

```
theta(i) = pi+ atan(locz/locy);
elseif (locy >= 0) & (locz < 0)
theta(i) = 3*pi/2+ atan(locy/(-locz));
%else
% theta(i)=0;
end
end

col = z';

% Calculation of unit normals
% First unit normals for elements
for i = 1:lc
%Create two vectors in each element (consistent on orientation)
vec1(1)= x(c(i,3))-x(c(i,2));
vec1(2)= y(c(i,3))-y(c(i,2));
vec1(3)= z(c(i,3))-z(c(i,2));

vec2(1)= x(c(i,1))-x(c(i,2));
vec2(2)= y(c(i,1))-y(c(i,2));
vec2(3)= z(c(i,1))-z(c(i,2));

%compute the cross product
crossvec = cross(vec1,vec2);
normcrossvec = (crossvec(:,1)^2+crossvec(:,2)^2+crossvec(:,2)^2)^0.5;
scrossvec = crossvec/normcrossvec;
normvec(i,:)= scrossvec;
end

% Then unit normals for vertices
for i = 1:lx
store=[];
for j=1:lc
if c(j,1) == i
store(end+1) = j;
end

if c(j,2) == i
store(end+1) = j;
end

if c(j,3) == i
store(end+1) = j;
end
```

## Appendix B

```
end

lstore=length(store);
vertvex(i,1)= 0;
vertvex(i,2)= 0;
vertvex(i,3)= 0;

for k=1:lstore
for s=1:3
vertvex(i,s) = vertvex(i,s)+normvec(store(k),s);
end
end

avertvex(i,:)=vertvex(i,:)/lstore;
end

% Reversenormal
for i = 1:lx
mag = (avertvex(i,1)^2+avertvex(i,2)^2+avertvex(i,3)^2)^0.5;
if reversenormal ==1
vecmorph(i,:) = - avertvex(i,:)/mag;
else
vecmorph(i,:) = avertvex(i,:)/mag;
end
end

%% Boundaries *****

% Define z-locations (or read in from file)
% These are critical z-regions for aponeurosis
xmax = max(v(:,1));
xmin = min(v(:,1));

% Boundaries for cases 1-6 & 8-9 (z-boundaries, propotions of length)

xupper1 = 0.9*xmax;
xupper2 = 0.8*xmax;
xupper3 = 0.75*xmax;
xlower3 = 0.25*xmax;
xlower2 = 0.2*xmax;
xlower1 = 0.1*xmax;

if aponeurosiscase == 7
% Boundaries for case 7
```

## Appendix B

```
xupper1 = 0.9*xmax;
xupper2 = 0.9*xmax;
xupper3 = 0.7*xmax;
xlower3 = 0.3*xmax;
xlower2 = 0.1*xmax;
xlower1 = 0.1*xmax;
end

%% Cases *****

%*****
%
%
%
%
%*****

% 1. Initial case, all layers are symmetric
if aponeurosiscase == 1
% Create the inner boundaries for aponeurosis
for i = 1:lx
vapothonk(i) = apothick;
vtranthick(i) = transthick;
end

% 2. Function of z without theta
elseif aponeurosiscase == 2

for i = 1:lx
height = v(i,1);
if (height >= xupper1)
vapothonk(i) = apothick;
vtranthick(i) = transthick;
elseif (height > xupper2) & (height < xupper1)
vapothonk(i) = apothick;
vtranthick(i) = transthick;
elseif (height >= xupper3) & (height <= xupper2)
vapothonk(i) = 0;
vtranthick(i) = 0;
elseif (height <= xlower1)
vapothonk(i) = apothick;
vtranthick(i) = transthick;
elseif (height > xlower1) & (height <= xlower2)
vapothonk(i) = apothick;
vtranthick(i) = transthick;
```

## Appendix B

```
elseif (height <= xlower3) & (height > xlower2)
vapothick(i) = 0;
vtransthick(i) = 0;
else
vapothick(i) = 0;
vtransthick(i) = 0;
end

end

% 3. Function of z and theta
elseif aponeurosiscase == 3

for i = 1:lx
height = v(i,1);
angle = theta(i);

%Initialise to 0
vapothick(i)=0;
vtransthick(i)=0;

if (height>=xupper1) % uppermost tendon
vapothick(i)=apothick;
vtransthick(i)=transthick;
elseif (height<=xlower1)
vapothick(i)=apothick;
vtransthick(i)=transthick;
end

if (angle>=0) & (angle < 3*pi/2)

if (height>xupper2) & (height < xupper1)
vapothick(i)=apothick;
vtransthick(i)=transthick;
elseif (height>=xupper3) & (height <= xupper2)
vapothick(i)=apothick; % this could be linear transition region
vtransthick(i)=transthick; %
elseif (height>=xlower2) & (height <= xlower3)
vapothick(i)=apothick; %this could be linear transition region
vtransthick(i)=transthick;
elseif (height>xlower1) & (height < xlower2)
vapothick(i)=apothick;
vtransthick(i)=transthick;
```

```

end
end
end

% 4.
elseif aponeurosiscase == 4
for i = 1:lx
height = v(i,1);
angle = theta(i);

%Initialise to 0
vapothickness(i,1)=0;
vtranstickness(i,1)=0;
if (angle>=pi) & (angle < 2*pi) % on the lower half of
% the cylinder tendon is across the right side
if (height>=xupper1)
vapothickness(i)=apothickness;
vtranstickness(i)=transtickness;
elseif (height<=xlower1)
vapothickness(i)=apothickness;
vtranstickness(i)=transtickness;
elseif (height>=xupper2) & (height < xupper1)
vapothickness(i)=0;
vtranstickness(i)=0;
elseif (height>=xupper3) & (height < xupper2) % linear transition region
vapothickness(i)=apothickness;
vtranstickness(i)=transtickness;
elseif (height>=xlower3) & (height < xupper3) % muscle region
vapothickness(i)=0;
vtranstickness(i)=0;
elseif (height>=xlower2) & (height < xlower3) % linear transition region
vapothickness(i)=transtickness/2;
vtranstickness(i)=transtickness/2;
elseif (height>xlower1) & (height < xlower2)
vapothickness(i)=apothickness;
vtranstickness(i)=transtickness;
end
elseif (angle>=0) & (angle < pi) % on the upper half of
% the cylinder tendon is across the left side
if (height>=xupper1)
vapothickness(i)=apothickness;
vtranstickness(i)=transtickness;
elseif (height<=xlower1)

```

## Appendix B

```
vapothick(i)=apothick;
vtransthick(i)=transthick;
elseif (height>xupper2) & (height <= xupper1)
vapothick(i)=apothick;
vtransthick(i)=transthick;
elseif (height>xupper3) & (height <= xupper2) % linear transition region
vapothick(i)=apothick/2;
vtransthick(i)=transthick/2;
elseif (height>xlower3) & (height <= xupper3) % muscle region
vapothick(i)=0;
vtransthick(i)=0;
elseif (height>xlower2) & (height <= xlower3) % linear transition region
vapothick(i)=apothick;
vtransthick(i)=transthick;
elseif (height>xlower1) & (height <= xlower2)
vapothick(i)=apothick;
vtransthick(i)=transthick;
end
end
end

% 5.
elseif aponeurosis == 5
for i = 1:lx
height = v(i,1);
vapothick(i,1) = 0;
vtransthick(i,1) = 0;
angle = theta(i)

if (height >= xupper1)
vapothick(i) = apothick;
vtransthick(i) = transthick;
elseif (height > xupper2) & (height < xupper1)
vapothick(i) = 2*apothick*(cos(angle)+1)/2;
vtransthick(i) = 2*transthick*(cos(angle)+1)/2;
elseif (height >= xupper3) & (height <= xupper2)
vapothick(i) = 0;
vtransthick(i) = 0;
elseif (height <= xlower1)
vapothick(i) = apothick;
vtransthick(i) = transthick;
elseif (height > xlower1) & (height <= xlower2)
vapothick(i) = 2*apothick*(cos(angle)+1)/2;
vtransthick(i) = 2*transthick*(cos(angle)+1)/2;
```

## Appendix B

```
elseif (height <= xlower3) & (height > xlower2)
vapothonk(i) = 0;
vtranthick(i) = 0;
end
end

% 6.
elseif aponeurosiscase == 6
for i = 1:lx
height = v(i,1);
vapothonk(i,1) = 0;
vtranthick(i,1) = 0;
angle = theta(i);
normangle = angle/2;

if (height >= xupper1)
vapothonk(i) = apothick;
vtranthick(i) = transtheick;
elseif (height > xupper2) & (height < xupper1)
vapothonk(i) = apothick*normangle;
vtranthick(i) = transtheick*normangle;
elseif (height >= xupper3) & (height <= xupper2)
vapothonk(i) = 0;
vtranthick(i) = 0;
elseif (height <= xlower1)
vapothonk(i) = apothick;
vtranthick(i) = transtheick;
elseif (height > xlower1) & (height < xlower2)
vapothonk(i) = apothick*normangle;
vtranthick(i) = transtheick*normangle;
elseif (height <= xlower3) & (height >= xlower2)
vapothonk(i) = 0;
vtranthick(i) = 0;
end
end

% 7.
elseif aponeurosiscase == 7
for i = 1:lx
height = v(i,1);
angle = theta(i);
vapothonk(i,1) = 0;
vtranthick(i,1) = 0;
if (height >= xupper1)
```

## Appendix B

```
vapothick(i) = apothick;
vtransthick(i) = transthick;
elseif (height > xupper2) & (height < xupper1)
vapothick(i) = sin(angle^2/2) + apothick;
vtransthick(i) = sin(angle^2) + transthick;
elseif (height >= xupper3) & (height <= xupper2)
vapothick(i) = 0;
vtransthick(i) = 0;
elseif (height <= xlower1)
vapothick(i) = apothick;
vtransthick(i) = transthick;
elseif (height > xlower1) & (height < xlower2)
vapothick(i) = sin(angle^2/2) + apothick;
vtransthick(i) = sin(angle^2) + transthick;
elseif (height <= xlower3) & (height >= xlower2)
vapothick(i) = 0;
vtransthick(i) = 0;
end
end

% 8.
elseif aponeurosiscase == 8
for i = 1:lx
height = v(i,1);
vapothick(i,1) = 0;
vtransthick(i,1) = 0;
angle = theta(i)
if (height >= xupper1)
vapothick(i) = apothick;
vtransthick(i) = transthick;
elseif (height > xupper2) & (height < xupper1)
vapothick(i) = 2*apothick*(cos(angle)+1)/2;
vtransthick(i) = 2*transthick*(cos(angle)+1)/2;
elseif (height >= xupper3) & (height <= xupper2)
vapothick(i) = 0;
vtransthick(i) = 0;
elseif (height <= xlower1)
vapothick(i) = apothick;
vtransthick(i) = transthick;
elseif (height > xlower1) & (height <= xlower2)
vapothick(i) = 2*apothick*((-1)*cos(angle)+1)/2;
vtransthick(i) = 2*transthick*((-1)*cos(angle)+1)/2;
elseif (height <= xlower3) & (height > xlower2)
vapothick(i) = 0;
```

## Appendix B

```
vtransthick(i) = 0;
end

end

% 9.
elseif aponeurosiscase == 9
for i = 1:lx
height = v(i,1);
vapothonk(i,1) = 0;
vtransthick(i,1) = 0;
angle = theta(i);
exweight=2;
anglexponent_bottom =
1+(exweight*((height-xlower1)/(xlower2-xlower1)));
anglexponent_top =
1+(exweight*(1-((height-xupper2)/(xupper1-xupper2))));
aeb=anglexponent_bottom;
aet=anglexponent_top;

if (height >= xupper1)
vapothonk(i) = apothonk;
vtransthick(i) = transthick;
elseif (height > xupper2) & (height < xupper1)
vapothonk(i) = apothonk*((cos(pi+angle)+1)/2)^aet;
vtransthick(i) = transthick*((cos(pi+angle)+1)/2)^aet;
elseif (height >= xupper3) & (height <= xupper2)
vapothonk(i) = 0;
vtransthick(i) = 0;
elseif (height <= xlower1)
vapothonk(i) = apothonk;
vtransthick(i) = transthick;
elseif (height > xlower1) & (height <= xlower2)
vapothonk(i) = apothonk*((cos(angle)+1)/2)^aeb;
vtransthick(i) = transthick*((cos(angle)+1)/2)^aeb;
elseif (height <= xlower3) & (height > xlower2)
vapothonk(i) = 0;
vtransthick(i) = 0;
end
end
end

%% Patching *****
```

## Appendix B

```
% Create the inner boundary of aponeurosis
for i = 1:lx
exv1(i,1) = v(i,1)+vapothickness(i)*vecmorph(i,1);
exv1(i,2) = v(i,2)+vapothickness(i)*vecmorph(i,2);
exv1(i,3) = v(i,3)+vapothickness(i)*vecmorph(i,3);
end

% the region between inner boundary
% of aponeurosis and the inner boundary of
% muscle is a transition region

% create the inner boundary of muscle
for i = 1:lx
exv2(i,1) = exv1(i,1)+vtranstickness(i)*vecmorph(i,1);
exv2(i,2) = exv1(i,2)+vtranstickness(i)*vecmorph(i,2);
exv2(i,3) = exv1(i,3)+vtranstickness(i)*vecmorph(i,3);
end

% outermost to innermost
patch_handle1 =
patch('Faces',c,'Vertices',v,'EdgeColor',
'k','Edgealpha',1,
'FaceColor','red','FaceAlpha',.1,
'facelighting','phong')
hold on
patch_handle2 = patch('Faces',c,'Vertices',exv1,'EdgeColor',
'k','Edgealpha',1,
'FaceColor','red','FaceAlpha',.2,
'facelighting','phong')
hold on
patch_handle3 = patch('Faces',c,'Vertices',exv2,'EdgeColor',
'k','Edgealpha',1,
'FaceColor','red','FaceAlpha',.5,
'facelighting','phong')

daspect([1 1 1]);
set(patch_handle1,'AmbientStrength',0.8,
'DiffuseStrength',0.5,'SpecularStrength',0.5);
set(patch_handle2,'AmbientStrength',0.8,
'DiffuseStrength',0.5,'SpecularStrength',0.5);
set(patch_handle3,'AmbientStrength',0.8,
'DiffuseStrength',0.5,'SpecularStrength',0.5);
light('Position',[1 1 1]);
view(45,45);
```

## Appendix B

```
axis equal off

%% Association *****

% Innermost surface associated with zeros
exv2(end-1:end,:)=[];
exv2_zeros = zeros(length(exv2),1);

%Conditional statement to replace zeros with 1's if in tendon region.
for i=1:length(exv2)
if (v(i,1)<xlower1) | (v(i,1)>xupper1)
exv2_zeros(i) = 1;
end
end

new_exv2 = [exv2, exv2_zeros];
wox = new_exv2.';

% Middle surface associated with ones
exv1(end-1:end,:)=[];
exv1_ones = ones(length(exv1),1);
new_exv1 = [exv1, exv1_ones];
wux = new_exv1.';

wconnect=connect';

% Get directory paths dynamically
curr_dir = pwd;
idcs = strfind(curr_dir, '\');
upper_dir = curr_dir(1:idcs(end)-1);

%% Writing to output file *****

%Create another cloud of points to represent that anything in this region
%is tendon
%use cuboids

%Find dimensions of a cuboid to enclose the muscle
ymax1 = max(v(:,2));
ymax2 = -min(v(:,2));
zmax1 = max(v(:,3));
zmax2 = -min(v(:,3));
cubemaxxy = max(ymax1,ymax2)
```

## Appendix B

```
cubemaxz = max(zmax1, zmax2)
cubemax = max(cubemaxxy, cubemaxz)

cubeymin = -cubemax;
cubeymax = cubemax;
cubezmin = -cubemax;
cubezmax = cubemax;

%increments
N_cube = 20;
%Beginning tendon region
%Lower tendon (achilies)

cubexmin = 0-0.1*xmax ;
cubexmax = xlower1;
cubexinc = (cubexmax - cubexmin)/N_cube;
cubeyinc = (cubeymax - cubeymin)/N_cube;
cubezinc = (cubezmax - cubezmin)/N_cube;

i=0; %initialise counter
for xvalue = cubexmin:cubexinc:cubexmax
for yvalue= cubeymin:cubeyinc:cubeymax
for zvalue=cubezmin:cubezinc:cubezmax
i=i+1;
x_cube(i) = xvalue;
y_cube(i) = yvalue;
z_cube(i) = zvalue;
cube_tendon(i) = 1;
end
end
end
%upper tendon (achilies)

cubexmin = xupper1 ;
cubexmax = xmax+0.1*xmax;
cubexinc = (cubexmax - cubexmin)/N_cube;
cubeyinc = (cubeymax - cubeymin)/N_cube;
cubezinc = (cubezmax - cubezmin)/N_cube;

for xvalue = cubexmin:cubexinc:cubexmax
for yvalue= cubeymin:cubeyinc:cubeymax
for zvalue =cubezmin:cubezinc:cubezmax
i=i+1;
```

## Appendix B

```
x_cube(i) = xvalue;
y_cube(i) = yvalue;
z_cube(i) = zvalue;
cube_tendon(i) = 1.00;
end
end
end

%Construct cuboid matrix for output
cube_matrix = [ x_cube ; y_cube ; z_cube ; cube_tendon];
%cube_matrix_output = cube_matrix';

% Write output .dat file

filename = fullfile(upper_dir, 'OutputFiles', 'analyzed_model.dat');
fid = fopen(filename, 'wt');
fprintf(fid, 'TITLE===== "ANALYZED_MODEL"\n');
fprintf(fid, 'VARIABLES= "X", "Y", "Z", "C"\n');
fprintf(fid, 'ZONE_T="STEP_0_Incr_0"\n');
fprintf(fid, 'F= POINT\n');
fprintf(fid, '%f%f%f%f\n', wox);
fprintf(fid, '%f%f%f%f\n', wux);
fprintf(fid, '%f%f%f%f\n', cube_matrix);
fclose(fid);

%% Additional file output tests *****

% For my testing purposes
%dlmwrite('v.txt', v, '\t');
%dlmwrite('exv1.txt', exv1, '\t');
%dlmwrite('exv2.txt', exv2, '\t');
```

### B.3 Tecplot Macro

The tecplot macro employed to produce a volume fraction file for defining the muscle, tendon and aponeurosis region is shown here:

```
#!MC 1200
# Created by Tecplot 360 build 12.2.0.9077
# Here for the MFBD -> need to set the directory
# to the directory in which the .dat files are
# present in.
```

## Appendix B

```

$!VarSet |MFB| = '..\OutputFiles'
$!READDATASET '"|MFB|\analyzed_model.dat" '
READDATAOPTION = NEW
RESETSTYLE = YES
INCLUDETEXT = NO
INCLUDEGEOM = NO
INCLUDECUSTOMLABELS = NO
VARLOADMODE = BYNAME
ASSIGNSTRANDIDS = YES
INITIALPLOTTYPE = CARTESIAN3D
VARIABLELIST = '"X" "Y" "Z" "C"'
$!READDATASET '"|MFB|\new_centroids_file.dat" '
READDATAOPTION = APPEND
RESETSTYLE = NO
INCLUDETEXT = NO
INCLUDEGEOM = NO
INCLUDECUSTOMLABELS = NO
VARLOADMODE = BYNAME
ASSIGNSTRANDIDS = YES
INITIALPLOTTYPE = CARTESIAN3D
VARIABLELIST = '"X" "Y" "Z" "C"'
$!INVERSEDISTINTERPOLATE
SOURCEZONES = [1]
DESTINATIONZONE = 2
VARLIST = [4]
INVDISTEXPONENT = 1
INVDISTMINRADIUS = 0
INTERPPTSELECTION = OCTANTPOINTS
INTERPNPOINTS = 8
$!WRITEDATASET '"|MFB|\new_centroids_file_C.dat"
INCLUDETEXT = NO
INCLUDEGEOM = NO
INCLUDECUSTOMLABELS = NO
INCLUDEAUTOGENFACENEIGHBORS = YES
ASSOCIATELAYOUTWITHDATAFILE = NO
ZONELIST = [2]
VARPOSITIONLIST = [4]
BINARY = NO
USEPOINTFORMAT = YES
PRECISION = 9
TECPLOTVERSIONTOWRITE = TECPLOTCURRENT
$!RemoveVar |MFB|
$!QUIT

```

This page has been intentionally left blank.

# Appendix C

## C.1 Modification of Material Model

The modification of anisotropic term for strain energy function of a collagen fibre in the HGO material model is formulated as below:

$$\begin{aligned}\tilde{\Psi}_{C,I_4} &= \frac{k_1}{2k_2} \{\exp[k_2(I_4 - 1)^2] - 1\} \rightarrow \tilde{\Psi}_C^{mod} = \tilde{k} \{\exp[k_2(I_4 - 1)^2] - 1\} \\ \tilde{\Psi}_{C,I_6} &= \frac{k_3}{2k_4} \{\exp[k_4(I_6 - 1)^2] - 1\} \rightarrow \tilde{\Psi}_C^{mod} = \hat{k} \{\exp[k_4(I_6 - 1)^2] - 1\}\end{aligned}\quad (C.1)$$

This particular form has been chosen due to its effect on the stress-stretch profile of the collagen fibre. In the original HGO model, the effect of remodelling non-dimensional material parameter values ( $k_2, k_4$ ) results in a right ward shift of the curve. However, the shift is quite limited based on the Cauchy stress values expected for the myocardial model i.e. strain stiffening effect is observed between a stretch of 2.0 to 2.5 thereby restricting the deformation of the finite element model. The modified parameters  $\tilde{k}$ , has an effect on this curve as seen in Figure [C.1], allowing for deformation stretches to reach values of 2.5 before the strain-stiffening effect comes into play for the collagen fibre. The desired effect of the remodelling ties in with Equations[6.6, 6.7] where in for the same level of stretch with a change in the  $k_2, k_4$  material parameter for collagen family of fibres in the  $I_4, I_6$  direction, a reduction in Cauchy stress is observed in an effort to maintain a preferred state of Cauchy stress (homoeostatic Cauchy stress as assumed in our model ( $\sigma_{CH,I_4}, \sigma_{CH,I_6}$ )).

## Appendix C

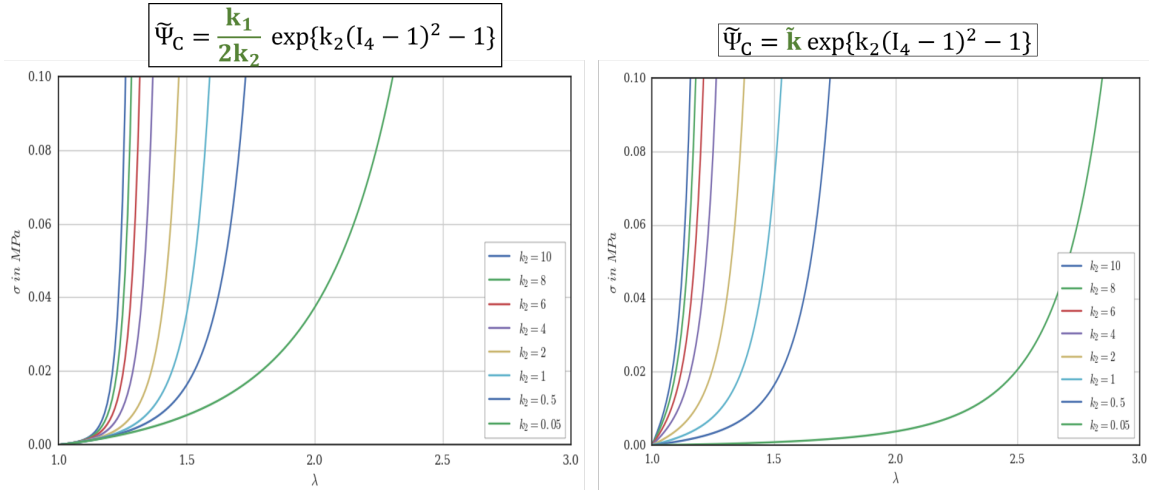


**Figure C.1:** A right-ward shift is observed based on the remodelling of  $k_2$  material parameter (**left**) For the original HGO model, adapted in an ANSYS ® hyperelastic fibre-reinforced material subroutine. (**right**) Modified HGO model, based on post-processed material parameters after each simulation step to mimic the changes as would be obtained in an analytical solution for the strain energy function considered. The right-ward shift is greater in the modified HGO model and therefore, allowing the soft tissue model to dilate further than would be possible with the original strain energy formulation. The same applies for the collagen fibre strain energy with  $k_4$  remodelling.

The formulation allows for the remodelling of the collagen fibre to help maintain a preferred homeostatic stress level whilst allowing larger dilatations of the collagen fibres. This implementation needs to be done externally as ANSYS ® Mechanical requires a custom user material subroutine to employ a modified material model. Therefore, we introduce a work around drawing equivalence between the strain energy formulations of the modified material parameter and after every simulation modify the input to the  $k_1, k_3$  parameters are follows:

$$k_1(\mathbf{X}, t) = m^{C, I_4}(t) k_1(\mathbf{X}, t=0) \frac{k_2(\mathbf{X}, t)}{k_2(\mathbf{X}, t=0)}; \quad k_3(\mathbf{X}, t) = m^{C, I_6} k_3(\mathbf{X}, t=0) \frac{k_4(\mathbf{X}, t)}{k_4(\mathbf{X}, t=0)} \quad (C.2)$$

This ensures the value input for  $k_1, k_3$  produces a behaviour similar to the modified HGO model formulation, by utilising the material model available within the FE software, without resorting to the development of complex user material subroutines.